

Robust Wearable UHF Antennas for Security Applications

THÈSE N° 6569 (2015)

PRÉSENTÉE LE 1^{ER} MAI 2015

À LA FACULTÉ DES SCIENCES ET TECHNIQUES DE L'INGÉNIEUR
LABORATOIRE D'ÉLECTROMAGNÉTISME ET ACOUSTIQUE
PROGRAMME DOCTORAL EN GÉNIE ÉLECTRIQUE

ÉCOLE POLYTECHNIQUE FÉDÉRALE DE LAUSANNE

POUR L'OBTENTION DU GRADE DE DOCTEUR ÈS SCIENCES

PAR

Jovanche TRAJKOVIKJ

acceptée sur proposition du jury:

Dr F. Fleuret, président du jury
Prof. A. Skrivervik, directrice de thèse
Prof. C. Dehollain, rapporteuse
Prof. M. Ammann, rapporteur
Prof. Z. Sipus, rapporteur



ÉCOLE POLYTECHNIQUE
FÉDÉRALE DE LAUSANNE

Suisse
2015

Волим буку, бука је стварање.

I love noise since noise is creation.

— Nikola Tesla

To my parents...

Abstract

Wearable electronics are occupying an increasing portion of our daily activities. The span of wearable applications extends from purely medical, over different security services to various sports and fashion devices.

Antennas play one of the most important roles in wearable networks as they have a key contribution to the overall efficiency of a wearable wireless link. This work focuses on the design and practical realization of robust wearable antennas intended for voice communication inside the Ultra High Frequency (UHF) band. The proposed antennas are mainly envisioned for security services such as military, police or rescue services. To this aim, several questions have been addressed while analyzing and designing the proposed antennas.

The on-body environment significantly affects the characteristics of an antenna. The coupling between the antenna and the host body influences both the antenna and the body characteristics. On one hand, the complex lossy nature of the hosting body tends to deteriorate the radiation performances of the wearable antenna, while on the other hand, the radiation from the antenna can cause an increase of the temperature of the wearer's body (locally and/or of the entire body).

The wearability aspect also requires that the size and the profile of the antenna are appropriate so that it can be easily integrated into the wearer's garment. The size of the wearable antennas becomes more critical at lower frequencies (for instance UHF), where the wavelengths become comparable with the size of the body, thus adding an additional limitation while selecting the type of the antenna. A Planar Inverted F Antenna (PIFA) was selected as an appropriate antenna candidate addressing the introduced specifications. In parallel with the antenna prototype, a suitable technology, combining flexible conductors and stretchable substrates, has been proposed. The suggested technology also enables an adjustment of the electric properties of the designated substrate materials. Several antenna prototypes were successfully designed, fabricated and characterized.

Finally, a set of tests in realistic everyday conditions were performed, thus validating the performance of the proposed antenna concepts along with the proposed technology and assessing their potential of being used for commercial purposes. We believe that the obtained results provide useful guidelines for future design of robust flexible wearable antennas.

Key words: Wearable antennas, security services, Ultra High Frequency (UHF), Planar Inverted F Antenna (PIFA), polydimethylsiloxane (PDMS), copper meshes, robustness, flexibility, waterproof, Specific Absorption Rate (SAR).

Kurzfassung

Tragbare Elektronik findet sich immer häufiger in Anwendungen unseres täglichen Lebens. Die Spannweite reicht von rein medizinischen über verschiedene Sicherheitsdienste bis hin zu Sport- und Modeaccessoires.

Antennen spielen dabei eine entscheidende Rolle, da sie einen wichtigen Beitrag zur Effizienz der tragbaren und drahtlosen Übertragungssysteme leisten. Diese Dissertation konzentriert sich daher auf die Entwicklung und die praktische Realisierung von robusten tragbaren Antennen für die Sprachübertragung im UHF-Band. Die vorgeschlagenen Lösungen sind hauptsächlich für Sicherheitsdienste wie Militär, Polizei und Rettungsdienste gedacht. Zu diesem Zweck wurden verschiedene Aspekte während der Analyse und der Entwicklung der Antennen betrachtet.

Der menschliche Körper beeinflusst sehr stark die Antennencharakteristik. Die Koppelung zwischen der Antenne und dem Körper beeinträchtigt dabei die Eigenschaften von beiden. Einerseits verschlechtert die komplexe, verlustbehaftete Natur des menschlichen Körpers die Abstrahleigenschaften der Antenne während andererseits die Antennenstrahlung zu einer Temperaturerhöhung lokal oder im gesamten Körper führen kann.

Um die Antennen am Körper tragen zu können, muß ihre Größe und ihr Profil geeignet gewählt werden, damit sie in die Kleidungsstücke ihres Trägers integriert werden können. Die Antennengröße ist jedoch bei niedrigen Frequenzen (z. B. im UHF-Band) ein kritischer Faktor, weil die Wellenlänge in der Größenordnung des menschlichen Körpers liegt. Dies führt zu weiteren Einschränkungen bei der Wahl des Antennentyps. Als möglicher Kandidat für eine Antenne wurde eine PIFA ausgewählt, um die gegebenen Spezifikationen zu erfüllen. Zusammen mit dem Antennenprototyp wurde eine geeignete Technologie gesucht, die flexible Leiter und dehnbare Substrate miteinander verbindet. Die gewählte Technologie erlaubt darüberhinaus eine Anpassung der elektrischen Eigenschaften der entwickelten Substrate. Mehrere Antennenprototypen wurden erfolgreich entwickelt, hergestellt und charakterisiert.

Abschließend wurden mehrere Tests unter Alltagsbedingungen durchgeführt, um einerseits die Leistungsfähigkeit der vorgeschlagenen Antennenkonzepte und der gewählten Technologie zu verifizieren und um andererseits die Möglichkeiten einer Vermarktung abzuschätzen. Die gewonnenen Erkenntnisse liefern wertvolle Richtlinien für zukünftige Lösungen von robusten und flexiblen tragbaren Antennen.

Schlagworte: tragbare Antennen, UHF, PIFA, polydimethylsiloxane (PDMS), Kupfergitter

Résumé

Les dispositifs électroniques intégrés à nos vêtements occupent une partie grandissante de nos activités quotidiennes. La panoplie d'applications liées aux dispositifs portatifs, intégrés aux textiles s'étend du domaine purement médical, aux différents systèmes de sécurité, jusqu'au monde du sport et de la mode.

Dans le concept "wearable" les antennes jouent un rôle déterminant puisque la communication s'effectue sans fil pour des dispositifs à même le corps. Plus précisément, cette étude se focalise sur la conception et la réalisation pratique d'une antenne robuste intégrée aux habits, pour une communication vocale dans la bande des Ultra Hautes Fréquences (UHF). Les antennes proposées ici sont conçues principalement pour des applications de défense et sécurité, typiquement des systèmes militaires, policiers ou encore de secours. Dans cette perspective, l'analyse et le design de l'antenne proposée a soulevé un nombre de questions pertinentes auxquelles ce travail se veut de répondre.

L'environnement proche ou même au contact du corps humain apporte des changements significatifs au fonctionnement propre de l'antenne. Les influences qui existent entre le corps porteur et l'antenne entraînent une relation bidirectionnelle corps-antenne. D'un côté, la nature complexe et dissipative du corps humain a tendance à détériorer les performances de la propagation d'onde, de l'autre côté une propagation d'onde excessive de l'antenne peut causer une augmentation néfaste de la température du corps de l'utilisateur (localement et/ou de l'ensemble du corps). La forme ainsi que la taille sont sujettes aux contraintes qu'impose le vêtement de l'utilisateur. La taille de ces dispositifs est d'autant plus critique aux fréquences "basses" (typiquement les UHF) pour lesquelles la longueur d'onde est comparable à la taille du corps, ce qui est un critère additionnel à prendre en compte lors du choix de l'antenne. L'antenne planaire F inversée (PIFA) satisfait les contraintes mentionnées ci-dessus.

En parallèle avec la conception de cette antenne, une nouvelle technologie alliant un conducteur flexible et un substrat extensible a été développée. Cette technologie permet un ajustement des propriétés diélectriques du substrat. Plusieurs prototypes ont été conçus, fabriqués et caractérisés avec succès.

Finalement, un ensemble de tests a été mené dans des conditions réalistes de la vie quotidienne, qui valident la performance de l'antenne présentée et de la technologie en vue d'un réel potentiel de commercialisation. Nous croyons que le résultat de ce travail servira de cadre utile à la future conception d'antennes flexibles robustes.

Mots clefs: antennes intégrées aux vêtements, systèmes de sécurité, Ultra Hautes Fréquences (UHF), Antenna Planaire F Inversée (PIFA), PDMS, maillage de cuivre, robustesse, flexibilité, étanchéité, densité d'absorption spécifique (DAS).

Сажетак

Wearable electronics (електронски уређаји који се носе у близини људског тела или на самом телу) заузимају све важније место у нашој свакодневници. *Wearable* апликације налазе се у најразличитијим уређајима, почевши од чисто медицинскиких, преко различитих безбедносних служби, па све до спортских и модних уређаја.

Антене играју значајну улогу у *wearable* мрежама, пре свега због њихове кључне улоге у обезбеђивању ефикасних *wearable* бежичних линкова. Овај рад се усредсређује на дизајн и практичну израду робусних *wearable* антена, намењених за говорну комуникацију унутар ултрависоких фреквенцијских (UHF) опсега. Предложене антене су углавном намењене безбедносним службама, као што су војска, полиција или спасилачке службе. У то име, нуди се одговор на неколико питања подстрекнутих током анализе и дизајна предложених антена.

Присуство људског тела значајно утиче на особине саме антене. Спрега која се јавља између антене и тела на коме је она постављена утиче не само на антену, него и на само тело. С једне стране, сложени састав људског тела, по карактеру склон производњи електричних губитака услед присуства различитих ткива, погоршава радијацијске особине *wearable* антене, док с друге стране, зрачење које долази од антене може значајно да повећа телесну температуру тела (локално и/или по целом телу).

Wearable аспект такође изискује да величина и профил антене буду одговарајући како би се антена лако уградила у униформу носиоца. Величина *wearable* антене постаје још критичнија на нижим фреквенцијама (на пр. UHF), где таласна дужина постаје упоредива са величином људског тела, додајући додатна ограничења при избору типа антене. *Planar Inverted F Antenna (PIFA)* одабрана је као одговарајући кандидат који одговара задатим спецификацијама.

Истовремено са одабиром типа антене, предложена је и одговарајућа технологија којом се комбинују савитљиви (флексибилни) проводници и растегљиви (еластични) субстрати. Понуђена технологија такође омогућава подешавање електричних особина одабраних субстратних материјала. Неколико прототипова антена успешно је дизајнирано, произведено и измерено.

На самом крају, опсежна мерења у реалним околностима спроведена су у различитим свакодневним околностима, потврђујући још једном одабир антена заједно са предложеном технологијом и нудећи их за потенцијалну тржишну

употребу. Верујемо да остварени резултати обезбеђују утабану путању за даљи развој робусних флексибилних *wearable* антена.

Кључне речи: *Wearable* антене, безбедносне службе, ултрависоке фреквенције (UHF), *Planar Inverted F Antenna (PIFA)*, *polydimethylsiloxane (PDMS)*, бакарне мреже, робусност, флексибилност, водоотпорност, *Specific Absorption Rate (SAR)*.

Резиме

Wearable electronics (електорнски уреди кои се носат во близина на човековото тело или на самото тело) заземаат сè поважно место во нашето секојдневие. *Wearable* апликации се наоѓаат во најразлични уреди, почнувајќи од чисто медицински, преку различни безбедносни служби, па се до спортски и модни уреди.

Аntenите играат значајна улога во *wearable* мрежите, пред се поради нивната клучна улога во обезбедување на ефикасни *wearable* безжични линкови. Овој труд се всредоточува на дизајн и практична изработка на робусни *wearable* антени, наменети за говорна комуникација во рамките на ултрависоки фреквенциски (UHF) појаси. Предложените антени главно се наменети за безбедносните служби, како што се војската, полицијата или спасувачките служби. Во тоа име, се нуди одговор на неколку прашања поттикнати во текот на анализите и дизајнот на предложените антени.

Присуството на човековото тело значајно влијае на особеностите на самата антена. Спрегата што се јавува помеѓу антената и човековото тело на кое што е поставена влијае не само на антената туку и на самото тело. Од една страна, сложениот состав на човечкото тело, по природа склоно кон создавање електрични губитоци поради присуството на различни ткива, ги влошува радиациските особености на *wearable* антената, додека од друга страна, зрачењето кое доаѓа од антената може да доведе до значајно зголемување на телесната температура на телото (локално и/или по целото тело).

Wearable аспектот исто така бара големината и профилот на самата антена да бидат соодветни така што антената лесно би се вградила во униформата на носителот. Величината на *wearable* антена станува уште покритична на ниски фреквенции (на пр. UHF), каде што брановата должина станува споредлива со големината на човечкото тело, додавајќи дополнителни ограничувања при изборот на типот на антена. *Planar Inverted F Antenna (PIFA)* е избрана како соодветен кандидат кој одговара на зададените спецификации.

Истовремено со одборот на типот на антена, предложена е и соодветна технологија која што комбинира совитливи (флексибилни) проводници и растегливи (еластични) субстрати. Понудената технологија исто така овозможува подесување на електричните карактеристики на избраните субстратни мате-

ријали. Неколку прототипови на антени успешно се дизајнирани, произведени и измерени.

За крај, направени се темелни мерења во реални околности покривајќи различни секојдневни ситуации, потврдувајќи го уште еднаш изборот на селектираните антени заедно со предложената технологија и нудејќи ги истите за потенцијална пазарна употреба. Веруваме дека остварените резултати го попложуваат патот за понатамошен развој на робусни флексибилни *wearable* антени.

Клучни зборови: *Wearable* антени, безбедносни служби, ултрависоки фреквенции (UHF), *Planar Inverted F Antenna (PIFA)*, *polydimethylsiloxane (PDMS)*, бакарни мрежи, робусност, флексибилност, водоотпорност, *Specific Absorption Rate (SAR)*.

Acknowledgements

Doing a PhD is like sailing. Without the support of the crew behind, this thesis would not have been anchored where it is now. First and foremost, my deepest and the most sincere thanks to my supervisor, Prof. Anja Skrivervik. Her professional guidance and human qualities made me to feel free and confident over my entire PhD adventure. *Merci beaucoup Anja, c'était vraiment un énorme plaisir de réaliser ma thèse avec toi.*

A good crew needs a good captain behind. Indeed, LEMA has an extraordinary captain, Prof. Juan Mosig, a person of extraordinary qualities, who always knows how and where to guide his LEMA kids. Thank you Juan for making LEMA such a pleasant place to work.

Many of my antenna prototypes wouldn't have seen the light of the day without the expertise and knowledge of Jean-François Zürcher. Another expert, to whom I am really grateful is Tomislav, responsible for many useful discussions, comments and efforts to measure my "specific" antennas. I would also like to acknowledge the members of my thesis jury, Prof. Zvonimir Sipus, Prof. Max Ammann, Prof. Catherine Dehollain and Dr. François Fleuret for having examined my work and provided constructive comments.

Special thanks to Michael Mattes for his constant willingness to help whatsoever, from "trivial" computer issues to shortening excessive abstracts in English, *Vielen Dank!* ELB 030, "le bureau" where all the nice things start and all the problems are gone. *Un grand merci pour le tandem Eulalia & Mercedes, toujours disponibles pour quoi que ça soit.* ELB 011, an office of "cool" people as one of them would say. Starting from Francesco to whom I am abundantly grateful for introducing me into the football story at EPFL to continue with the two prominent warriors who gave a real flavor to my stay in LEMA. Marc, always ready for an action in Thun or Memphis, always helpful, always cheerful and Anton, a person with wide interests and even wider soul. My deep bow to both of you.

Huge thanks to "my" post-docs Roberto, Santiago, Vick and Benji for all the useful advices and help they provided me with during my research time. A special thank to Mina, an extraordinary friend and inexhaustible source for various matlab advices, French translations and SAT beers. None of the LEMA skiings, hikings or underwater performances wouldn't have been possible without Joana, Apo, Michele, Pietro, Maria, Hamed, Pedro and all former and current LEMA members. Special thanks to my office mates, Ioannis and Baptiste for sharing not only the office but overall the life at LEMA. *Un grand merci à "la bande" de Lisek, Sami, Etienne merci beaucoup pour toutes les performances magnifique.* Many thanks to my "Balkan crew" for all

the "social" outings, Mihajlo, Marija, Ana, Gorica, Nevena, Ivan and many many others. Thank you all for making my PhD time pleasant and enjoyable.

Since the really beginning of my stay in Lausanne, football became and still it is my great passion. Having Martin around, ⚽ becomes more than a game, it becomes a *philosophy*, intertwining playing, friends, beer, playing, friends, beer ... a periodical phenomenon. Huge thanks to the rest of the Lausanne Galaxy warriors, Cedric, Iuli, Fra ... for many many non-forgettable, but even more for many "forgettable" nights in Great Escape, Jagers...

One person in particular was supporting my idea to start the PhD and now I feel it is the time to tell him that I am there, done. Вуче хвала ти на неизмерној подршци и вери коју си имао у мене када сам кретао у ову авантуру. My day-to-day (non-)PhD activities were fully enriched by the discussions with my freind Spase, with whom all the topics were getting different dimension. Благодарам!

A colossal Хвала goes to a "giant" man/person/friend, (једном речју људина). Bogdane I am extremely lucky person having you as a friend and as my PhD fellow traveler. There are still many books, trips, experiences to be shared ...

I am so happy that during the most of my PhD sailing I had a person next to me who became substantial part of my life and was always there to overcome together, one new wave, one new obstacle ... my girlfriend Lucy. I think one cannot ask for more love or understanding than what you are giving to me. I am immensely thankful for everything you have done for me.

Finally, I would like to thank my family, for everything they have done for me and they are still doing. If you find some language mistakes in this thesis please address them to my sister Roza (the official "*lector*" of this thesis), while me, I will address only one enormous Хвала for everything we have passed through. I cannot even find appropriate words to express all my gratitude and respect to my parents for offering me all their love, support and understanding during all my adventures, in particular the last one. Мама, неизмерно сам ти захваљан на свему што си ми пружила, а пре свега љубав и пажњу и на све корз шта смо прошли заједно. Ова дисертација је у неку руку потврда тога.

I dedicate this thesis to all of you, but still to one special person in particular, to my father Stojan, for whom I really hoped to see this achievement one day... Although physically not among us, his spiritual presence will remain forever with me ... Тата хвала ти што си био мој најкориснији критичар. Без тебе ја данас не бих био где јесам. Од свег срца ову дисертацију посвећујем теби...

Lausanne, 08 April 2015



Contents

Acronyms and Abbreviations	xvii
1 Introduction	1
1.1 Context of the Work	4
1.2 Challenges and Motivation	6
1.3 Thesis Outline and Original Contribution	7
2 Wearable Antennas Background and Overview	11
2.1 Applications	11
2.1.1 Security (Military and Police) and Rescue Service Applications	11
2.1.2 Medical Applications	13
2.1.3 Sport, Entertainment and Fashion Applications	16
2.2 Antenna Families	17
2.2.1 Introduction into Miniaturization Techniques	17
2.2.2 The Dipole and Related Antennas	18
2.2.3 Monopole Antennas	20
2.2.4 Patch Antennas	22
2.2.5 Planar Inverted F Antennas (PIFAs)	24
2.2.6 Commercially Available UHF Wearable Antennas	28
2.3 Materials and Fabrication Methods	29
2.3.1 Textiles	30
2.3.2 Printed Technology	33
2.3.3 Substrate Integrated Waveguide (SIW) Technology	34
2.3.4 Polymer Substrates	35
2.4 Frequency Band Selection	36
2.4.1 Wave Propagation Characteristics	37
2.4.2 Frequency Bands Suitable for Wearable Antennas for Security and Rescue Service Applications	38
2.4.3 Tetrapol Communication Band	41
2.5 Conclusions	42

3	Materials, Characterization and Technology	45
3.1	Dielectric Materials	46
3.1.1	Polymers	46
3.1.2	Polydimethylsyloxane - PDMS	46
3.2	Adjusting the EM Properties of PDMS	47
3.3	Conductive Materials	51
3.3.1	Copper Mesh Structures as Conductors	51
3.3.2	Perforated Conductive Sheets	52
3.4	Technology	53
3.5	Realized Patch Antenna	59
3.6	Conclusions	62
4	Antenna Prototypes	63
4.1	PIFA (Copper-Mesh) Operating at 365 MHz	64
4.1.1	Antenna Model and Geometrical Parameters	64
4.1.2	Fabrication of the Antenna Prototype	65
4.1.3	Comparison of $ S_{11}(f) $ Responses for Different Situations	68
4.1.4	Radiation Pattern and Gain	72
4.1.5	Conclusions	77
4.2	PIFA (Hexagon) Operating at 385 MHz	78
4.2.1	Antenna Model and Geometrical Parameters	79
4.2.2	Fabrication of the Antenna Prototype	82
4.2.3	Comparison of $ S_{11}(f) $ Responses for Different Situations	85
4.2.4	Radiation Pattern and Gain	88
4.2.5	Conclusions	92
4.3	PIFA with an Air Gap Operating at 380 MHz	93
4.3.1	Antenna Model and Geometrical Parameters	93
4.3.2	Fabrication of the Antenna Prototype	95
4.3.3	Comparison of $ S_{11}(f) $ Responses for Different Situations	98
4.3.4	Radiation Pattern and Gain	99
4.3.5	Conclusions	103
4.4	Summary on the Results	104
5	System Measurements and Comparison with the Commercial Antennas	109
5.1	Measurements in a Controlled Environment	111
5.1.1	Measured ($ S_{21}(f) $) in a Controlled Environment (Anechoic Chamber)	112
5.1.2	Stability, Free Space vs. On-body	114
5.2	Measurements in a Realistic Environment	116
5.2.1	Equipment Used for Quantitative Measurements	116
5.2.2	Equipment Used for Qualitative Measurements	117
5.2.3	Measurements Inside the Laboratory (Corridors+Offices)	118
5.2.4	Measurements Inside the University Building	121
5.2.5	Measurements on the Campus (Outdoor)	123

5.2.6	Extended Outdoor Scenario (on the Campus)	125
5.2.7	Outdoor, Open-Field Scenario (Aarberg Area)	129
5.2.8	Rotating Scenario (Outdoor)	132
5.3	Conclusions	136
6	Specific Absorption Rate (SAR),	
	Near-field Effects and Radiation Efficiency	137
6.1	Models and Methods	140
6.2	SAR Comparison, PIFA vs. Dipole	142
6.3	Results	144
6.3.1	Near-fields Triggered by the High Density Current Regions	144
6.3.2	Role of the Substrate Material in SAR Evaluation	146
6.4	Conclusions	148
7	Conclusions and Perspectives	149
7.1	Conclusions	149
7.2	Perspectives	151
	Bibliography	153
	CV	167
	List of Publications	169

Acronyms and Abbreviations

2D	Two Dimensional
3D	Three Dimensional
AMF	Asymmetric Meandered Flare
AUT	Antenna Under Test
BW	Bandwidth
CAD	Computer-Aided Design
CNC	Computerized Numerical Control
EHF	Extremely High Frequency
EM	Electromagnetic
EMC	Electromagnetic Compatibility
ETSI	European Telecommunications Standards Institute
FCC	Federal Communications Commission
FDMA	Frequency Division Multiple Access
GEOSAR	Geostationary-Orbit Search and Rescue
GMSK	Gaussian Minimum Shift Keying
GPS	Global Positioning System
HF	High Frequency
HMSIW	Half-Mode Substrate Integrated Waveguide
ICNIRP	International Commission on Non-Ionizing Radiation Protection
ICT	Information and Communication Technology
IEEE	Institute of Electrical and Electronics Engineers
IFA	Inverted F Antenna
ISM	Industrial Scientific Medical
ITU	International Telecommunication Union

LCP	Liquid Crystal Polymers
LF	Low Frequency
LoS	Line of Sight
NLoS	Non-Line of Sight
MedRadio	Medical Device Radio Communications Service
MF	Medium Frequency
MICS	Medical Implant Communication Service
NATO	North Atlantic Treaty Organization
OFCOM	Federal Office of Communications
PAMR	Public Access Mobile Radio
PCPTF	Plain Copper Polyester Taffeta Fabric
PCS	Personal Communication System
PDMS	Polydimethylsyloxane
PEI	Polyetherimide
PET	Polyethyleneterephthalate
PICA	Planar Inverted Conical Antenna
PIFA	Planar Inverted F Antenna
PLC	Power Line Communication
PMR	Private Mobile Radio
PPDR	Public Protection and Disaster Relief
PSS	Public Safety and Security
PTFE	Polytetrafluoroethylene
PVC	Polyvinyl Chloride
RF	Radio Frequency
R&S	Rohde & Schwarz
RLAN	Radio Local Area Network
SAR	Specific Absorption Rate
SHF	Super High Frequency
SIW	Substrate Integrated Waveguide
SMA	SubMiniature version A (connector)
SMILA	Smart Monobloc-Integrated L-Antenna
SRD	Short Range Distance
TETRA	Terrestrial Trunked Radio

UAV	Unmanned Aerial Vehicle
UHF	Ultra High Frequency
UMTS	Universal Mobile Telecommunications System
UV	Ultraviolet
UWB	Ultra Wideband
VHF	Very High Frequency
VLF	Very Low Frequency
VNA	Vector Network Analyzer
WAS	Wireless Access Systems
WBAN	Wireless Body Area Network
WG	Waveguide
WLAN	Wireless Local Area Network
WPAN	Wireless Personal Area Network

1 Introduction

*Таман си научио да будеш дијете, а постајеш
младић. Кад научиш да будеш младић,
постајеш зрео човек. Схватићеш увек смо
почетници у овом животу.*

*As soon as you have learned to be a child, you become a
young man. Once you have learned to be a young man,
you turn into a mature person. Then you learn that we
are eternal beginners in this world.*

—Nikola Tesla's father, Milutin Tesla

The general trend in today's communications is achieving the highest possible level of portability. Voice communication, data transfer, positioning and entertainment are just some of the many applications that are covered by modern communication systems. Specific needs of different population groups lead to different requirements, varying from purely medical, through practical and efficient performance of different rescue and security services, to sports, entertainment or even fashion applications [1].

In recent years mobility is often equalized with wearability, where having all the devices and gadgets integrated in the clothes or mounted on the body offer the wearers' freedom in their daily activities. One of the last example of wearable electronics are smart watches [2]. To undertake the classification and understanding of different wearable aspects, the Institute of Electrical and Electronics Engineers (IEEE), IEEE 802, established in December 2006 a task group, entitled IEEE 802.15.6, for the standardization of Wireless Body Area Network (WBAN) applications [3]. A general idea about the WBAN concept [4] is illustrated in Fig. 1.1.

Depending on the type of communication, WBANs can be divided in three different categories: **On-body**, communication within the same body (wearer), **Off-body**, communication between

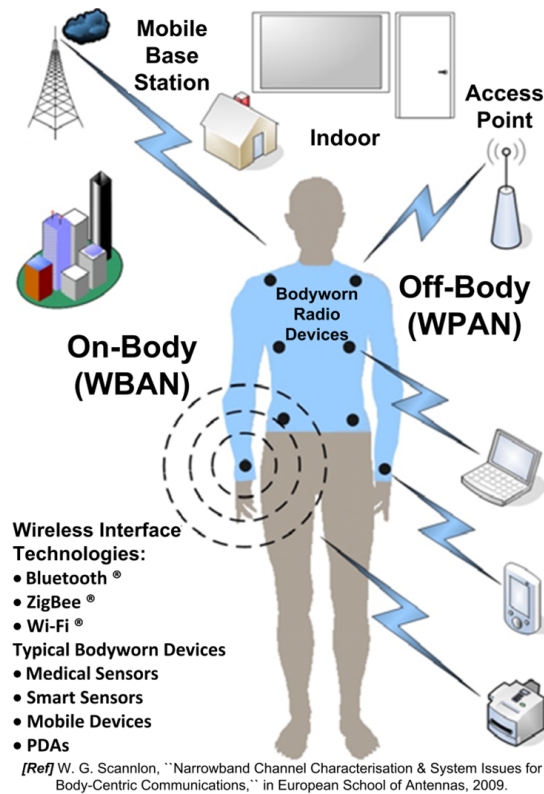


Fig. 1.1: Wireless Body Area Network (WBAN) concept [4].

the body (wearer) and an external unit, and **In-body**, communication between the implanted device in the body and device mounted on the body [5–7].

On-body communication describes the case when different wearable devices are mounted on the same body. The devices can communicate between themselves and all the data can be forwarded and collected in one point (device), which is usually called central master device. This device is often considered as a hub and all the gathered data can be further proceeded to an external unit. Today on-body communication is mainly intended for health monitoring and sport. Communication between the hub device and the external unit is an example of Off-body communication.

The communication link between any of the body mounted devices and an external unit is defined as an **Off-body** communication. External units can be computers, smart phones, base stations or other wearable devices mounted on a different wearer, which actually introduces a separate sub-group of off-body communication, known as **Body-to-Body** communication. Body-to-Body communication is widely spread in different security and rescue service applications, where in some situation the wearers communicate directly between themselves, without using base stations or other intermediate points.

The third category of WBANs is the **In-body** communication. In-body links provide a link between an implant and a device mounted on the wearer. Instead of communicating with an external unit, as defined in the off-body concept, the In-body concept shortens the path and establishes a link with the device mounted on the wearer, thus overcoming the problem of the strong attenuation caused by the lossy nature of the human body. In-body communication is mainly used for medical purposes [8, 9]. An example presented in Fig. 1.2 shows a modern hospital environment, where the three different networks are represented, In-, On- and Off-Body communication [8].

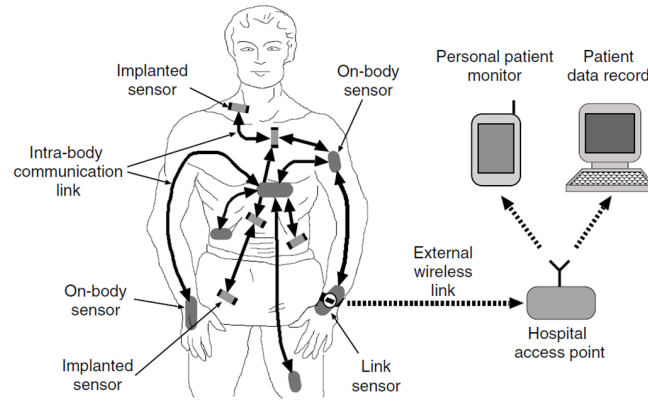


Fig. 1.2: Intra body concept [8].

Off-body communication is the wider research interest of this thesis. More precisely, a voice communication link in the Ultra High Frequency (UHF) band, 380-400 MHz, within the existing voice communication platforms will be a subject of consideration. The communication is intended for security and rescue services, where links between a wearer and a base station or between two wearers are needed. In both scenarios, off-body communication is required.

The main scope of the thesis is the development and design of robust wearable antennas for voice communication at UHF frequencies. The proposed wearable antennas must have good performances in various scenarios. The antennas need to maintain robust and reliable communication links in everyday security activities (e.g. police and military) or rescue operation scenarios, in urban and rural environment.

The proposed wearable antennas should be suitable for the integration in the wearer's uniform, provide stable links and be resilient to different environmental and weather conditions (e.g. water, rain, humid, snow, ice, etc.). In some situations, the wearers need to maintain different types of communication, thus requiring multiband or separate antennas for services like Global Positioning System (GPS) or satellite communication, raising the question of interoperability.

1.1 Context of the Work

The research carried out in this thesis has been accomplished in the framework of a collaboration between Armasuisse¹ and the Laboratory of Electromagnetics and Acoustics (LEMA) at École Polytechnique Fédérale de Lausanne (EPFL).

The aim of this collaboration was the design and development of a robust wearable antenna intended for a voice communication for security service purposes. The proposed antenna should work at UHF frequencies or more specifically inside the Tetrapol communication band [10]. Tetrapol communication band is a frequency range exclusively dedicated for voice communication for different security services such as army, police, rescue services etc. In Switzerland this band is defined between 380-430 MHz [11].

Among the project requirements, a list of the most relevant ones is presented here:

- The antenna should operate inside the 380-430 MHz frequency band (Tetrapol).
- Indoor and outdoor communication.
- Robustness of the antennas:
 - Robustness against the body influence.
 - Robustness against different mechanical (e.g. bending, twisting, etc.) or environmental influences (e.g. different weather conditions like rain, snow, ice, etc.).
- Suitable antenna size for easy integration within the wearers' uniform.
- Fulfilling the potential hazard health regulations (Specific Absorption Rate (SAR)).

In the second part of this project, an additional collaboration was established with a branch of a Swiss based company, the RUAG Network Enabled Operations - NEO Services department [12]. They already had an existing commercially available communication platform intended for the Tetrapol band, "POLYCOM Radio portable COVERT700" [13]. Since they did not have their own antennas, their goal was to find appropriate wearable antennas which can be an alternative to the limited choice of the existing commercial antennas.

At this point, additional requirements were established in agreement with RUAG. The goal was to test the wearable antennas developed in the first part of this project in different realistic everyday conditions like indoor, in urban, in rural and in an open-field environment and at the same time to compare our antennas with the commercial ones. Thanks to this initiative and the communication equipment provided by RUAG, interesting measurements and results

¹Project: *Study on Wearable Antennas*, contract Nr 041-18, Swiss Science and Technology Federal Department of Defense, Civil Protection and Sport (DDPS), armasuisse.

were obtained and they are mainly addressed in Chapter 5. This collaboration is still active and future goals have been already set beyond the duration of this PhD. The main target is to improve the existing antenna prototypes making them suitable for serial production and further commercial use.

The wider context of the performed work underlines the importance and the need for development of new wearable antennas intended for the security services. Nowadays, in Europe and worldwide, there are two main players in the field of Public Safety and Security (PSS) networks and Public Access Mobile Radio (PAMR) operators, Terrestrial Trunked Radio (TETRA) [14] and Tetrapol [10], communication platforms. The span of the potential customers spreads over different groups and services like police, fire and rescue services. This type of communication is also widely exploited by sectors like transportation, oil & gas and industry networks who are either privately owned or run by network operators who invest in the network and sell their communications services [14].

If we look closer at the numbers related to the above mentioned communication system, a real potential and need can be seen. Namely, today more than 1 850 000 users are covered by Tetrapol, with 85 networks in more than 30 countries [15]. On the other side, TETRA radio is also on a constant increase since its beginning in 1997, when the first TETRA voice network in the world was implemented at Gardermoen Airport in Norway, until today, with more than 250 TETRA networks being used by governments for public safety, military and defense, and other public services [16].

Up to date, the largest TETRA network, is the Airwave network in Great Britain, which has 3600 base stations and approximately 350 000 users. Germany's network, nearing completion, will become the largest in the world, with more than 500 000 users, while the North American market has just been opened up to TETRA technology [16]. Therefore, there is a constant need for wearable antennas that are able to provide robust and reliable communications within the TETRA and Tetrapol systems.

Although the research carried out in this thesis deals mainly with the antennas intended for UHF frequency range, the technology proposed here can be easily extended to any type of tailored wearable antenna solutions, where robustness against the mechanical influences and environmental conditions is one of the highest priority.

1.2 Challenges and Motivation

Any wearable antenna design faces many challenges during the development process. If we look into the design of robust wearable antennas intended for the UHF range, being our particular case of interest, some of the initial challenges can be even more emphasized. Several of them are listed below:

- Antenna \Leftrightarrow Human body interaction (coupling).
- Technology and used materials (flexibility and waterproof).
- Integration within the wearers' uniform (size, shape, conformation).
- SAR reduction.

In the design of a wearable antenna, the interaction between the antenna and the wearer is one of the main challenges and is thus central to this research. Translated into electromagnetic language, this interaction can be defined as coupling.

Several strategies can be chosen in order to mitigate the coupling effects. Selecting an antenna with an appropriate structure (e.g. presence of a ground plane and/or polarization perpendicular to the wearer) and an adequate radiation pattern can reduce the coupling effects. The selection of the antenna type at the same time intertwines with the integration problem, as we require an antenna that can be integrated in the wearer's uniform. It should thus be of suitable size and low profile, while fulfilling the requirements of coupling and radiation.

Another approach for the coupling mitigation can be the use of substrate materials with higher relative permittivities, able to confine certain portion of the EM radiation, thus reducing the coupling towards the body. Yet, one should be careful because high permittivity may worsen the antenna's performance. Therefore, there is a trade-off between the coupling reduction and the overall antenna characteristics.

The choice of materials, substrate and conductive, determines the mechanical characteristics of the wearable antennas in terms of their robustness and resilience against bending, twisting or being repellent to water. The selection of materials along with compatible manufacturing processes is of particular interest for this work. This is the key to our final goal of creating a robust and resilient structure, i.e. wearable antenna.

Recently, hazard health issues and their influence are becoming more emphasized in the wearable antennas context. With a constant and everyday exposure of the wearers to a various EM radiation, the regulatory offices are becoming more strict, while requiring the reduction of the human body exposures to the EM radiation. This raises the question of SAR, which is directly related to the coupling level. SAR is the way to monitor human body exposure to the

electromagnetic (EM) radiation and it is defined as a ratio between the transferred power and the mass of the body where the SAR values are evaluated [17].

The motivation of this PhD thesis is to link the context of the proposed project with the challenges which have arose. In other words, the goal is to develop a robust wearable antenna for UHF band that can be easily integrated into the wearer's uniform, ensuring at the same time a minimal coupling to the body. The proposed concepts and solutions can provide a solid guideline for the future design of robust wearable antennas.

1.3 Thesis Outline and Original Contribution

This thesis concerns the design, optimization and characterization of robust wearable antennas intended to operate in harsh environment. Fig. 1.3 depicts the thesis flow in an illustrative manner. Descriptions and the original contributions are addressed in the following sections.

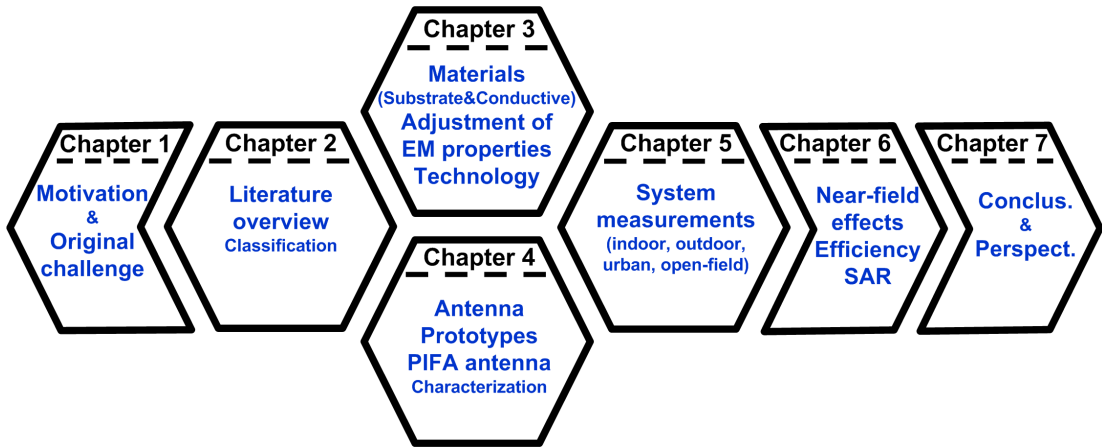


Fig. 1.3: Thesis outline.

Chapter 2 - Wearable Antennas Background and Overview

Description: Although the concept of wearable antennas is relatively recent, there exist many publications on the topic. Publications found in literature cover different types of antennas, various operating frequency bands, different conductive and substrate materials, different technologies etc. Therefore, in order to have a clear starting point for the design and development of wearable antennas, some overview is needed.

Original contribution: A summary and classification of the literature on wearable antennas is performed. The classification is done according to the application groups they belong to, different antenna families, different technologies and materials and the appropriate frequency bands.

Chapter 3 - Materials, Characterization and Technology

Description: Wearable antennas can be built from different conductive and substrate materials. Variable mechanical (bending, crumpling, etc.) and weather conditions (rain, snow, ice, etc.) require appropriate materials with suitable electromagnetic (EM) and mechanical properties. A set of fabrication processes and materials combinations are found among different technologies.

Original contribution: A theoretical study over a range of possible materials is performed. A silicone based elastomer, polydimethylsyloxane (PDMS), is selected as a base material for the substrates. The initial liquid state of the PDMS is loaded with preselected inclusions, thus changing the final EM properties like permittivity and losses. Perforated or mesh structured conductive sheets are completely embedded inside the liquid elastomer, resulting in a final waterproof antenna. This technology was selected to continue with the design of the foreseen robust wearable antenna.

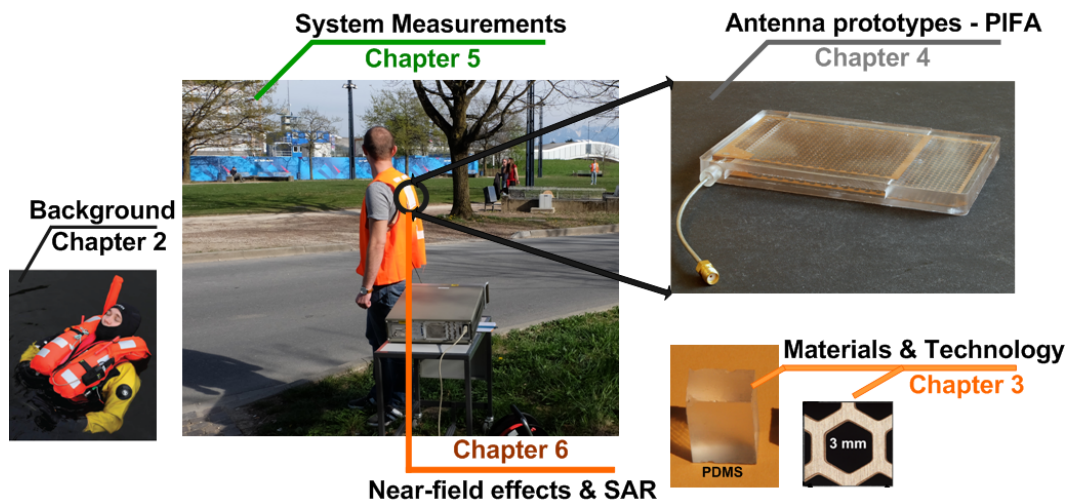


Fig. 1.4: System.

Chapter 4 - Antenna Prototypes

Description: The choice of the antenna type is mainly determined by the factors defined in the application's specification like required communication (e.g. Off-body), allocated frequency bands and available space for placement. A low profile of the antenna and a minimal coupling to the wearer ensure easy integration and reliable communication links when mounted on the body.

Original contribution: A Planar Inverted F Antenna (PIFA) is proposed as an antenna solution for UHF frequencies. The optimized antenna design with a height of 11 mm, $\lambda_0/70$, (rather low with respect to the operating frequency of 385 MHz), makes it suitable for integration into

the wearer's uniform. The optimization of the ground plane and the feeding structure leads to a minimum coupling to the wearer and thus better radiation performances. A complete encapsulation of all the conductive parts inside the PDMS results in a flexible and waterproof antenna.

Chapter 5 - System Measurements and Comparison with the Commercial Antennas

Description: Performance of antennas in various everyday situations and different environmental conditions, both urban and rural, provides the full picture of their behavior.

Original contribution: A set of measurements performed on body and in free space shows that the antennas operate stably, without being affected by the environment. Additional tests performed with an operational voice communication equipment report steady and reliable functioning in various realistic conditions. Moreover, in most of the comparisons with the antennas found on the market, PIFAs exhibit better performances.

Chapter 6 - Specific Absorption Rate (SAR), Near-field Effects and Radiation Efficiency

Description: Near-field effects should be taken into account when dealing with wearable antennas. The presence of the human body in the antenna's near-field region affects the overall performance. The coupling between the antenna and the wearer reduces the radiation efficiency and increases the SAR values. In some cases by applying some simple modifications within the antenna's structure, the unwanted effects can be mitigated.

Original contribution: The selection of the PIFA (presence of a ground plane + part of the feeding structure perpendicularly oriented with respect to the wearer), already mitigates the coupling effects. The introduction of an air-gap (lossless medium) in the antenna's near-field region, improves the radiation efficiency of the PIFA. Reduction of the SAR is achieved by reducing the high current density regions (e.g. ground plane extension) and by using substrates with higher permittivity.

Chapter 7 - Conclusions and Perspectives

The last part summarizes the work performed during this PhD thesis, emphasizing the most important conclusions and original contributions. Perspectives for future work are proposed based on the topics covered in the thesis.

The original contributions of this thesis have been validated via two journal publications and several presentations in international peer reviewed conferences. The link between thesis chapters and publications is summarized in Table 1.1. The complete list of publications can be found at the end of this document, on page 169.

Chapter 1. Introduction

Chapter	Topic	Publications
3	Flexible copper-mesh conductors & Adjusting the EM properties of PDMS	[18, 19]
	Perforated (hexagonal shape) copper-bronze conductive sheets & pure PDMS	[19]
4	Antenna prototypes - PIFA antennas	[19, 20]
5	Stability of the proposed antennas (On-body vs. Free space)	[21]
	System measurements	[22]
6	Near-field effects & SAR	[23]

Tab. 1.1: Link between the thesis chapters, topics and publications.

2 Wearable Antennas Background and Overview

Wearable antennas have been a topic of interest for more than the past decade, and hundreds of scientific papers can be found on the subject. This large number of publications asks for some classification in order to get an overview of the trends and challenges. To this aim an overview of wearable antennas according to the applications, antenna families, materials and technology and allowed frequency bands, is proposed.

2.1 Applications

2.1.1 Security (Military and Police) and Rescue Service Applications

Our main focus will be orientated towards wearable robust antennas intended to operate in various harsh environments. These antennas are mainly used for security and defense applications [24] and within different rescue services like firefighters [25], mountain and water rescue workers [26,27].



(a)



(b)

Fig. 2.1: Illustrative examples of wearable antennas applications: (a) Army forces and (b) Firefighters.

Frequency bands intended for security and rescue applications are regulated by special government regulatory offices. In our case we will mainly consider the regulations and frequency allocations of the Swiss authorities [11], which are overlapping with the International Telecommunication Union (ITU) regulations [28]. A band of interest is the Tetrapol communication band, 380-430 MHz, widely used by different security and emergency services within the Private Mobile Radio (PMR) applications [10].

There are two common requirements for most of the wearable antennas used in security and rescue service applications: the size miniaturization and the resilience of the antenna to the environment.

The wavelength of the antennas operating inside the Tetrapol band, if observed in a free space, is rather large. For example, for an antenna operating at 400 MHz, the wavelength is around 80 cm, which will lead to physically large antennas not suited to be mounted on a wearer. Therefore, miniaturization is required to overcome the size problem. Antennas proposed for these applications should be small, non-protrusive, low profile and conformable so that can be easily mounted inside the uniform and placed around the wearer's body.

Apart from the antenna size, another important aspect is the environment and weather conditions where wearable antennas operate. As most of the wearers from the indicated groups operate outdoor, robustness against water, rain, moisture, mud, etc., is among the antenna requirements. Moreover, taking into account that the uniforms need to be washed an integrated antenna should withstand this process.

Several antenna prototypes exist in literature and on the market [24, 25, 29–33]. All the reported antennas have a size suitable for placement on the wearer. Some of the antennas are waterproof and most of them are too specific and customized and cannot be widely used for different situations. For example, the antenna presented in [24] is exclusively designed for armor vests used by the military and law enforcement agencies. It is an asymmetric dipole antenna that can be integrated only in the specified vests. Another dipole wearable antenna type is presented by the same authors in [29], a conformal Asymmetric Meandered Flare (AMF) dipole antenna. The antenna's conductive surface is fabricated by using precise embroidering techniques in order to produce fully flexible antenna conformal to the wearer and his clothes, see Fig. 2.2. More wearable antenna prototypes operating between 0.1-1 GHz, mainly for military applications, are presented in [30], exploiting different conductive and textile materials.

A set of textile wearable antennas intended for firefighter services have been introduced by Hertleer *et al.* A textile GPS wearable antenna is presented in [31], and the antenna intended for voice communication between the firefighters is shown in [25]. Same authors

have reported a multiband circularly polarized patch antenna for positioning and satellite communication [32].



Fig. 2.2: Asymmetric Meandered Flare (AMF) wearable dipole antenna [29].

Importance of the wearable devices in the everyday operations of modern security and rescue services is reported in [33]. Different parameters can be monitored with the units integrated in their garments like psychological parameters, actual position or the conditions on the field where they operate.

In summary, all the concerned applications mentioned above, such as military, fire fighters or rescue services, require an involvement of different electronic devices and equipment in their daily activities. Depending on the type of application and activities they perform, different wearable antennas are needed. Therefore, wearable antennas play an important role in ensuring robust and reliable communication links and thus performance of these services.

2.1.2 Medical Applications

Medical applications consume large portion of the WBANs [34]. These applications are mainly used for health monitoring of different categories of patients and elderly people. They can monitor 24 hours a day different parameters and detect changes, for instance blood pressure, heart rate or body temperature [35]. With the more emphasized use of smart phones, collected data from the medical applications can be directly sent to the hospital or responsible medical doctors [36,37]. An illustrative example of wearable medical applications [38] is presented in Fig. 2.3.

Before showing some of the typical wearable antenna prototypes found among the medical applications, a short overview of their dedicated standards and frequency bands will be

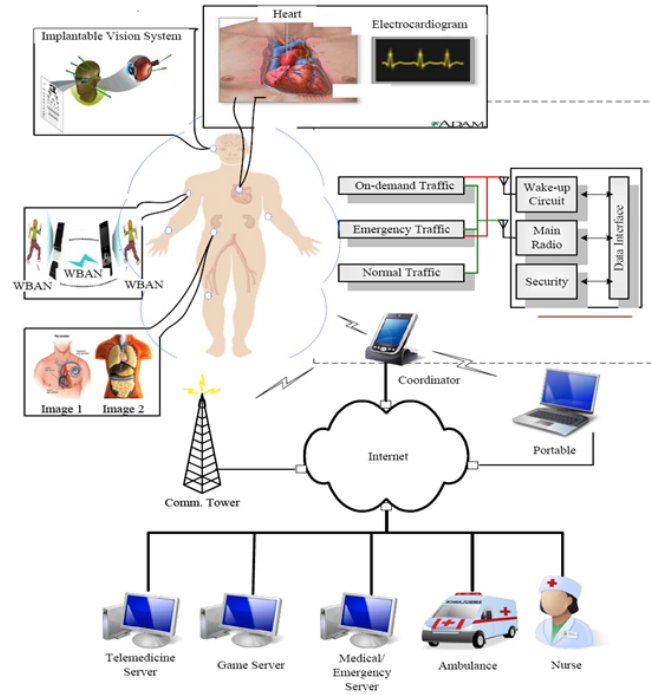


Fig. 2.3: Wireless Body Area Network for Ubiquitous Health Monitoring [38].

presented. The large number of bands indicates how widely these applications are spread, emphasizing their importance.

Depending on the type of devices (implanted or on body) and the required communication (In-, On- or Off-body) different standards have been defined. The Federal Communications Commission (FCC) has established a Medical Implant Communication Service (MICS) like the band for communication with medical implants [39], while in Europe the same standard is regulated by the European Telecommunications Standards Institute (ETSI) [40]. In 2009, the Medical Device Radio Communications Service (MedRadio) range, 401-406 MHz, has been created by the FCC for diagnostic and therapeutic purposes in implanted medical devices and devices worn on the body [41].

Large number of wearable applications operate inside one of the FCC proposed Industrial Scientific Medical (ISM) bands, 902-928¹ MHz, 2.4-2.4835 GHz and 5.725-5.875 GHz. Some of the bands are used on a secondary basis because they are already utilized in other applications. These ISM bands are submitted to certain restrictions, like short distance operation or low emitted power, in order to allow their co-existence in the spectrum with minimal interference [39, 41].

¹Applies only for Region 2 according to the International Telecommunication Union (ITU) [28].

In 2002, a spectrum from 3.1-10.6 GHz has been allocated by the FCC for Ultra Wideband (UWB) applications [42]. A lot of research and different types of wearable medical applications can be found in this band, making it one of the most exploited frequency ranges for WBAN applications [5].

The most recent frequency band with a potential to be used for wearable applications is the millimeter wave range between 57-64 GHz, or also known as a 60 GHz band [43]. Some research about the propagation characteristics at 60 GHz for WBAN has been done in [44, 45] while antenna designs are proposed in [46, 47] giving promising results.

The large choice of frequency bands used for medical WBAN applications leads to various wearable antenna families. Several implantable and wearable antennas are presented within the following subsection.

Implantable antennas are a specific group challenging to design, fabricate and package and implant. The antenna and the accompanying electronic components need to be implanted into the human or animal body, leading to a complex procedure. The antenna needs to be small, compact, built out of appropriate bio-compatible materials and when implanted providing a reliable communication link towards the external units and devices [48]. An overview and analysis on the development and implantation of these antennas is presented in [49]. Several other implantable antenna designs are shown in [50–53].

Wearable antennas on the other side, offer more freedom in terms of size, shape and communication link, because they are placed on the wearer's body. Different antenna types used for medical purposes are found in the literature, e.g. patch antenna [54], monopole type antenna [55], PIFA [56], Planar Inverted Conical Antenna (PICA) [57], printed strip antenna [58], classical dual-band patch antenna [59], etc. Each of the antenna types will be overviewed in more details in the antenna families section 2.2.

Medical applications will remain one of the main consumers of various wearable devices. Constant progress of the wearables allows monitoring of various health activities and parameters. The fact that nowadays smart phones and other wireless devices (e.g. tablets, lap tops, etc.) can act as reliable hubs and transceivers, make the wearable applications even more favorable. Wearable antennas will continue to be the crucial connection between the on-body devices and the external units, providing reliable and on time communication.

2.1.3 Sport, Entertainment and Fashion Applications

Another attractive market for wearables is sport, entertainment and fashion applications. Nowadays consumers enjoy keeping track of performances in any kind of sports activity they do. Different wearable applications are able to track and record speed, elevation, distance and other similar parameters. Most of the tracking can be performed with the currently existing smart phones, but some separate wearable devices also exist. Several wrist watches with built-in GPS antennas, that can measure time, distance, position of the wearer or even the heart rate, can be found on the market [60, 61]. Wearable GPS antennas [62–64] play important role in performance of such systems. Furthermore, for the purposes of professional sportsmen, wearable devices are used in a more extensive manner. All the collected data from different wearable sensors are analyzed and used for further improvement for the sportspeople performances [65].

Interesting examples of wearable antennas intended for integration into the shoes and thus potential use for sports applications are presented in [66, 67]. In [66], two different UWB wearable antenna prototypes, (a monopole and a Vivaldi type) are proposed in order to provide a link between the footwear sensors and the rest of the body centric network, while in [67], mainly the channel aspects and the influence of the rapid and repetitive movement of the foot on the overall communication are considered.



Fig. 2.4: Illustrative examples of wearable antennas applications in Sports, Entertainment and Fashion: (a) Skiing [68], (b) Swimming and (c) Intelligent shoes [69].

Entertainment applications is also a market for the wearable technologies. They offer a lot of possibilities to this industry. Some examples of entertainment wearables present on the market, include a bluetooth jacket [70], intelligent shoes [69] or a ski monitoring system, *flaik* [68]. The list of wearable applications used in sports, entertainment and fashion is growing rapidly, occupying significant part of the market [71].

2.2 Antenna Families

Different types (families) of antennas are used in different situations. Wearable antennas follow similar trends and thus wide number of various antenna types can be found in the literature. The following four antenna families are considered for the purposes of this thesis:

- Dipole antennas.
- Monopole antennas.
- Patch antennas.
- Planar Inverted F Antennas (PIFAs).

The antennas' size plays an important role for their placement on the wearer. The gain and effective area are directly proportional to the antenna's size measured in wavelengths [72]. Usually, antennas that are smaller than quarter a free space wavelength are considered to be electrically small or miniature antennas [73]. Before considering each of the indicated antenna family, a short overview of the miniaturization techniques will be presented.

2.2.1 Introduction into Miniaturization Techniques

In order to be practical, wearable antennas should often be small in size, which can be problematic for the designs especially in the UHF band. Therefore, a short overview of miniaturization techniques will be presented. Antenna miniaturization is always a matter of compromise between size and radiation characteristics [73].

The fundamental physical limits on antenna EM performance related to size are well known since the early days of wireless communication [74–76]. The study of these limits regained a huge interest in the nineties with the boom of mobile phones (see for instance [77]). Lately, these limits have been refined taking into account antennas shape [78].

Apart from restrictions in bandwidth², gain, efficiency and polarization purity [79], the process of miniaturization brings to the surface problem of feeding a small antenna efficiently. In general, antennas are either balanced or unbalanced, and their feeding should be in accordance to this. The majority of small antennas are of unbalanced character and the reduction of their size is always followed by the reduction of their ground (often a plane). A reduced ground cannot absorb the charge flow as proper ground would, leading to spurious ground currents altering the radiation characteristics of the antenna [80]. Electrically small antennas require thus specific measurement techniques.

²Industrial standard bandwidth (-10 dB bandwidth in the $|S_{11}|$).

The main techniques available for antenna miniaturization are presented in [73]:

- Material or lumped element loading, usually at the expense of the bandwidth of the antenna.
- Geometrical loading, by using bends and slots.
- Using grounds and short circuits.
- Using the antenna's environment to enhance the radiation.

Examples of miniaturization techniques [73], are illustrated in Fig. 2.5, and Fig. 2.6, [81, 82], where an environment (human body) is used for the miniaturization.

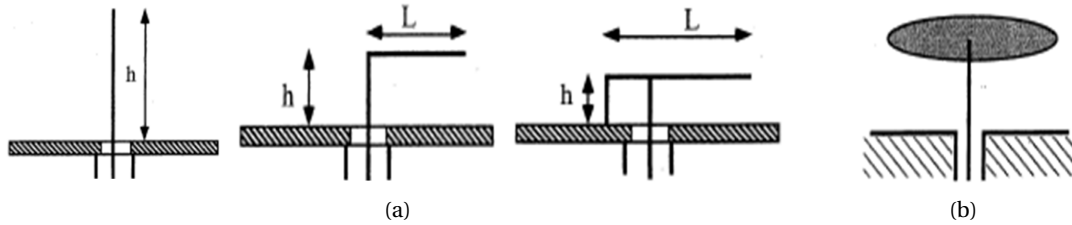


Fig. 2.5: Miniaturization techniques [73]: (a) Geometrical transformation steps (bending) of a monopole into Inverted F Antenna (IFA) and (b) A capacitor-plate antenna (loaded monopole).

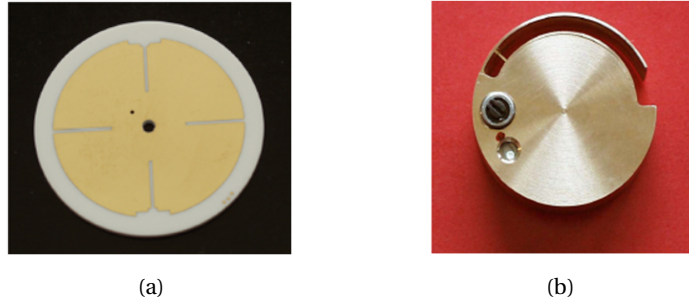


Fig. 2.6: (a) Printed patch antenna for GPS for watch application [81] and (b) SMILA (Smart Monobloc-Integrated L-Antenna) [82].

2.2.2 The Dipole and Related Antennas

Let us first consider the dipole as a candidate for a body-worn antenna. The dipole is the most basic design of an antenna, it is a symmetric structure, consisting of a straight thin wire conductor of a certain length and a center feeding, see for instance Fig. 2.7. The maximal radiation power is achieved in the plane perpendicular to the dipole. The typical radiation pattern is therefore in the shape of a torus. The dipole is a typical resonant antenna, having well defined resonances precisely located in frequency.

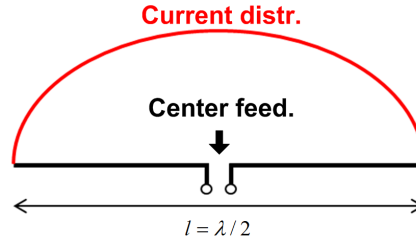


Fig. 2.7: Dipole antenna.

Dipole antennas are widely used for wearable applications and several antenna designs are presented in the literature. In [24], a wearable asymmetric dipole antenna was introduced for military applications. Compared to the conventional center-fed dipole, asymmetry provides a broader frequency band and a slightly smaller size. The model is designed to be placed on the armor vest, and miniaturization techniques are applied (bending) to reduce the size. The main limitation of this antenna is that it has to be placed on flat surfaces, see Fig. 2.8. Similar wearable antennas, exclusively dedicated for armor vests, are presented in [83].

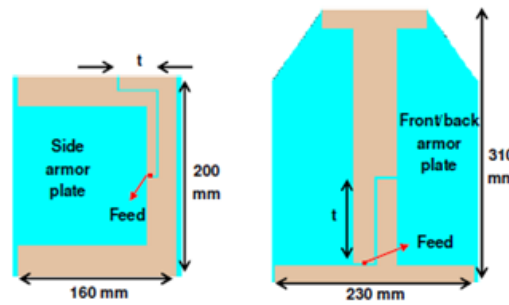


Fig. 2.8: Asymmetric wearable dipole antenna for armor vests [24].

Volakis *et al.* [29, 84] have investigated more conventional models of dipole antennas that can be used in a larger field of applications as they are conformable. Their mounting around the wearer's body is more convenient compared to the previous examples. The presented antennas are based on a printed wide dipole, with slight differences between them. The first is the so called bow-tie dipole, the second a flare dipole, while the last one is an Asymmetric Meandered Flare (AMF), and they are all shown in Fig. 2.9. Apart from being conformal, the dimensions of those antennas, $305 \times 38 \text{ mm}^2$, allow to place several of them on the same wearer. Their overall size makes them suitable for placing at different positions of the human body like chest, back, shoulders, etc.

Table 2.1 gives an overview of the advantages and disadvantages of dipole antennas while placed on the wearer's body.

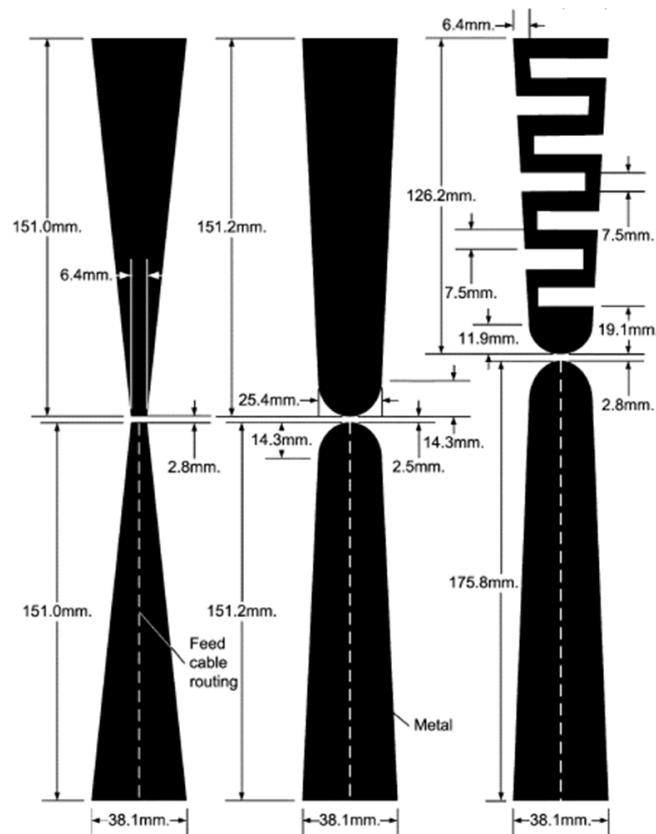


Fig. 2.9: Wide printed dipole antennas for wearable applications, from left to right: Bow-Tie, Flare and Asymmetric Meandered Flare (AMF) dipole [84].

Advantages ☺	Disadvantages ☹
Single and sharp resonant behavior, good for filtering input signal	Due to the lossy body nature the antenna requires wider operating frequency bandwidth
Radiation pattern - "Torus shape" perpendicular to the wearer's body	Radiation pattern - "Torus shape" part of the energy still penetrates into the body
Most of the models are flexible and conformal for mounting	Narrow fractional bandwidth, up to 10%
Miniaturization - bending or meandering the antenna structure	Balanced feeding, need for baluns in some cases
	The lack of the ground plane and polarization parallel to the wearer increases the penetration of the radiation inside the body

Tab. 2.1: A summary of the positive and negative aspects for dipole antennas when used for wearable applications [85].

2.2.3 Monopole Antennas

The monopole antenna can be near-resonant (length is approximately a quarter-wavelength) or electrically short (length is much shorter than a quarter-wavelength). Compared to the

dipole, the monopole requires a ground plane in its structure. The dimensions of the ground plane may vary from a fraction of a wavelength to many wavelengths [86]. The monopole has many variations, see for instance Fig. 2.5.

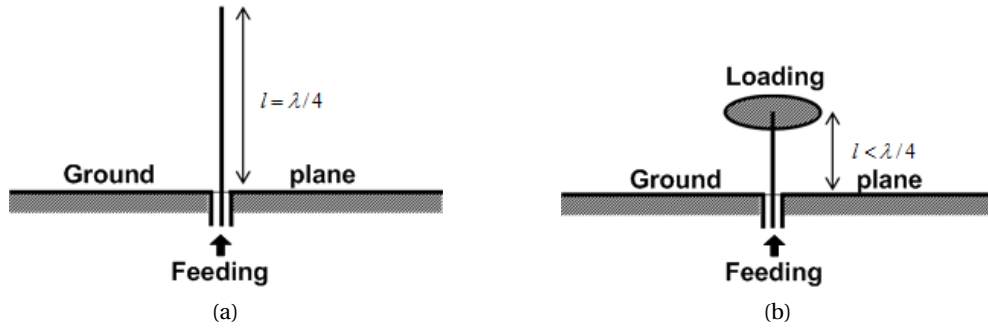


Fig. 2.10: Monopole antenna: (a) Quarter-wavelength monopole and (b) Electrically short monopole.

In the case of wearable applications, the presence of the ground is an advantage, since it allows some shielding of the body. The protrusion of the antenna orthogonally to the body however is a serious disadvantage and miniaturization is required to make the monopole low profile. Most of the monopole antennas found in the literature have planar characteristics, because it is much easier to integrate planar structure into the garment or any kind of uniform [55, 87].

Button Antenna as a Special Monopole Antenna Case

An especially interesting sub-group of monopole antennas is the button antenna. It is designed by loading the monopole antenna with a certain load, composed of metal in most of the cases, leading to a decrease of its height. This loading method is successfully applied in many button antennas, as it will be seen from the examples shown in this section.

The existing literature gives some examples of button antennas integrated into wearable applications. For example in [88], a dual-band metallic button antenna is shown for body area network applications, for covering both Off- and On-body communications. The operating frequencies of this antenna are 2.45 GHz and 5.5 GHz. For the specified frequencies the dimensions of the antenna are the following: ground plane size of 50 x 50 mm², top disc diameter 16 mm, and total height of 8.3 mm. The 3D model of the antenna is presented in Fig. 2.11 (a).

More complex loading shapes are also present in literature. An antenna loaded with a G-shaped metallic structure has been reported in [90]. This antenna operates at ISM bands and it is a dual band antenna with overall size of 40 x 40 mm² of the ground plane and 10 mm in the height. The geometrical shape of the loading can be adapted to the desired feature of the antenna. Another monopole loaded antenna has been introduced by Koohestani *et al.*,



Fig. 2.11: (a) Monopole button antenna loaded with a disc [88] and (b) Monopole antenna loaded with a cross shape structure (Swiss flag cross) [89].

where a cross (Swiss flag symbol) is used as a shape for loading a vertically polarized UWB antenna [89], see Fig. 2.11 (b).

Most of these antennas operate inside the ISM or UWB bands. Communication distance is aimed for a short range, from a few centimeters up to 10 meters [57], where the majority of applications using button antennas are for indoor communication. Button antennas remain good candidates for applications where a compact antenna integrated in different parts of the clothes is needed for short range communication.

Advantages ☺	Disadvantages ☺
Presence of a ground plane	Protrusive structure
Polarization perpendicular to the wearer	
<i>Printed monopole</i> planar structure	Polarization perpendicular to the wearer
<i>Button antenna</i> compact → easy integration	Mostly for <i>ISM & UWB</i> bands short distance communic.

Tab. 2.2: A summary of the positive and negative aspects for the monopole and button antennas when used for wearable applications [85].

2.2.4 Patch Antennas

The microstrip patch is a planar antenna, consisting of a radiating patch on one side of a dielectric substrate, and the ground plane on the other. The radiating elements are made of conducting materials (e.g. copper, usually photo-etched). Patches can be found in any geometrical shape, but the most common have some regular shapes as square, rectangular, circular, triangular, elliptical, etc. They radiate primarily because of the fringing fields between the patch and the ground plane, see for instance Fig. 2.12. The radiation pattern of these antennas is perpendicular to the plane of the patch [72].

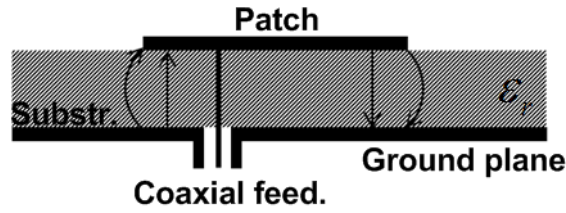


Fig. 2.12: Cross section of a microstrip patch antenna.

Different structures can be used for feeding the patch antennas, such as microstrip line, coaxial probe, aperture coupling or proximity coupling [72]. The variety of the feeding techniques provides some degrees of freedom in the design phase, as well as in later stages while mounting them on the wearer's body. The microstrip patch is a candidate for any narrowband wearable application, as it has a low profile and can be made conformal for integration into the clothing. The presence of the ground plane is an additional advantage when these antennas are used in wearable applications, preventing the radiation into the wearer's body.

Patch antennas are mainly used in GPS and ISM bands. Hertleer *et al.* have introduced several patch based antennas operating inside the ISM and GPS bands, intended for wearable applications [25, 31, 91]. All the proposed antennas are built out of specific textile materials, conductive and dielectric, and are mainly used for fire fighter service applications.

An alternative shape to the conventional rectangular patch antenna can be a circular disk microstrip antenna. The main advantage of circular configuration, compared to the rectangular geometry, is that the circular disk occupies less physical area, leading to an easier integration in arrays for instance. In [92] circular disk microstrip Wireless Local Area Network (WLAN) wearable antenna is presented, operating at 2.45 GHz. Using a copper as a conducting layer, this antenna achieves a gain of 5.7 dBi, slightly lower than its rectangular counterpart which has a gain of 5.9 dBi.

A complete textile patch antenna is shown in [93], where both the substrate and the patch are textile materials with good conductive and dielectric characteristics respectively. Zelt³ material is used for building the patch and the ground plane, while Felt⁴ is used as a substrate material. Both materials will be considered in more details in the section considering the materials. Fig. 2.13 depicts the top view of the discussed antenna. The dimensions of this patch are: 13.5 x 13.3 cm², i.e. half wavelength at 920 MHz.

A summary about the suitability of patch antennas when used in wearable applications is shown as an overview of advantages and disadvantages, Table 2.3.

³Zelt is a widely known material for building tents.

⁴Felt is a type of textile material.

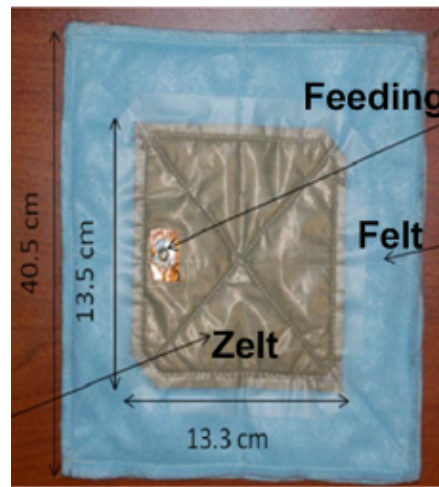


Fig. 2.13: Patch antenna using Zelt fabric as conductor and Felt as a substrate [93].

Advantages ☺	Disadvantages ☹
Light weight and low volume	Narrow bandwidth
Conformability	Low efficiency
Low cost of fabrication	Low gain
Supports linear and circular polarization	Extraneous radiation from feeds and junctions
High level of integrability	Low power handling capacity
Capable of multiband operations	Surface wave excitation
Mechanically robust	

Tab. 2.3: A summary of the positive and negative aspects for patch antennas when used for wearable applications [85].

2.2.5 Planar Inverted F Antennas (PIFAs)

A Planar Inverted-F Antenna (PIFA) is the last family of antennas enclosed in this overview which is a subject of consideration. Basically, PIFA is a kind of inverted F antenna (IFA) with the wire radiator element replaced by a plate to expand the bandwidth. On one hand, the PIFA is derived from the monopole antenna, where by bending and shortening, its characteristic shape is achieved [94], while on the other hand, it can also be considered as a short circuited patch antenna [95]. The addition of the shorting strip allows a good impedance match to be achieved with a top plate, which is typically less than $\lambda/4$ long [73]. The PIFA consists of a ground plane, a top plate element, a feed wire attached between the ground plane and the top plate, and a shorting wire or strip that is connected between the ground plane and the top plate. Fig. 2.14 illustrates a typical PIFA configuration.

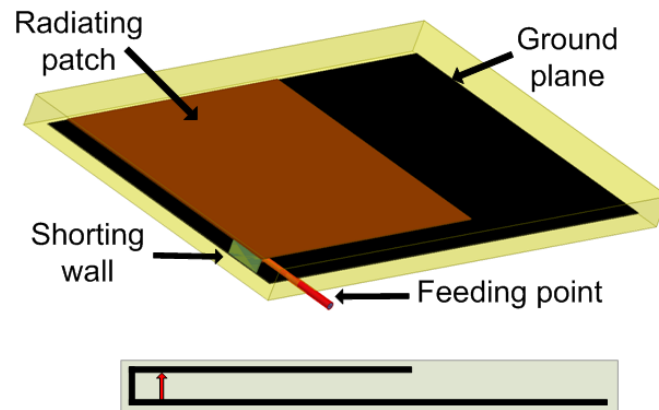


Fig. 2.14: Configuration of PIFA.

PIFA is a widely deployed antenna among many Personal Communication System (PCS) devices because of its characteristics. PIFAs have many advantages that make them very good candidates for the hand-held and mobile devices [96]. They are highly integrable into a casing or other components of the environment and have a reduced backward radiation towards the users' body. In this way, the SAR is significantly reduced, which is an important aspect when it comes to the body-worn antennas [97]. They exhibit moderate to medium gain in both vertical and horizontal states of polarization. This feature is very useful in certain situations where the antenna does not have a fixed position and different reflections are present in its environment. For the applications where larger bandwidth is required, several different techniques can be used for its enhancement [98]:

- Varying the size of the ground plane.
- Use of a thick air substrate.
- Use of parasitic resonators with resonant lengths close to main resonant frequency.
- Adjusting the location and spacing between the shorting posts.
- Use of stacked elements.

PIFAs have two main advantages making them suitable for wearable applications:

- Presence of the ground plane in its structure which insulates the antenna from the wearer, thus reducing the coupling (favorable for off-body communications).
- Antennas low profile allows easy integration within the wearer's garments.

As an interesting candidate for UHF wearable applications, an overview of PIFAs used in WBANs is presented. A simple PIFA prototype, built out of textile materials, intended for wearable applications is presented in [99]. The antenna operates at 2.45 GHz, with the overall

dimensions $50 \times 24 \times 10 \text{ mm}^3$, see Fig. 2.15. The presented antenna is characterized in free space and when placed in the vicinity of the human body.

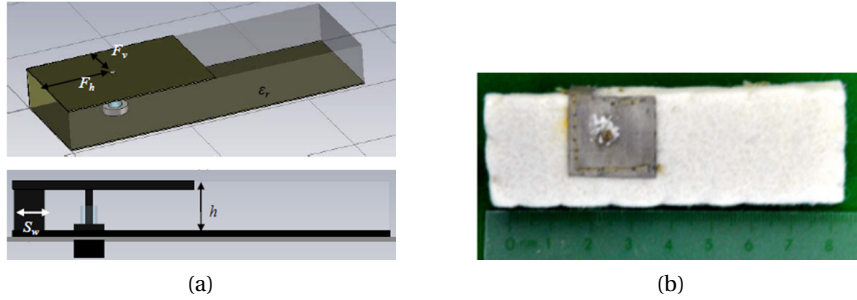


Fig. 2.15: PIFA wearable antenna [99]: (a) A 3-D model and (b) Fabricated PIFAs using ShieldIt conductive textiles.

Simulated and experimental results indicated that the textile PIFAs are able to operate with a reflection coefficient below -10 dB, and fractional bandwidth of around 27%. On average the measured gain is 1.6 dBi, while the efficiency ranges between 77-85% (measurements obtained in free space, not on body or phantom).

Two more antennas based on the PIFA concept, operating at 2.45 GHz and 5.2 GHz, are presented in the literature, the dual-band Sierpinski fractal textile PIFA [100], and a broadband all-textile slotted PIFA [101]. Sierpinski fractal antenna incorporates a triangular Sierpinski radiator at the top and a standard rectangular ground plane at the bottom. It operates in dual-band mode, at 2.45 and 5.2 GHz, respectively, and has a volume of $44 \times 34 \times 6 \text{ mm}^3$. The measured gain and efficiency of this antenna are 3.1 dBi and 70%, respectively (measurements obtained in free space). The slotted PIFA provides increased bandwidth because of the introduced slot in the radiating patch of the antenna and a fractional bandwidth of more than 46%.

A wearable PIFA shown in [102] is based on the same concept of multiband operation, but with a tuning function. A variable capacitance is used for tuning the antenna frequency without changing the dimensions of the antenna. The proposed antenna can cover three bands at higher frequencies, the ISM band (2.40-2.48 GHz), Wireless Broadband (2.30-2.40 GHz) and Universal Mobile Telecommunications System (UMTS, Rx 2.1-2.17 GHz) band. The slot structure in the patch covers also the lower band (950-956 MHz). The overall antenna's dimensions are $40 \times 20 \times 6 \text{ mm}^3$.

In the frame of this work, the PIFA wearable antennas operating inside the UHF frequency band are of particular interest and are described bellow. A modified E-shaped PIFA (see Fig. 2.16) introduced in 2004, [103], has been one of the pioneering antennas in the frame of this thesis project. It has been intended to operate inside the Tetrapol communication band, 380-400 MHz. The antenna exhibits -12 dBi gain while mounted on the body, which is better

than the conventional half-wavelength dipoles. The proposed antenna has overall dimensions of $30 \times 30 \times 2 \text{ cm}^3$, which makes it suitable for mounting, but the area occupied is still fairly large. However this antenna can be seen as a good starting example for development of UHF wearable antennas.

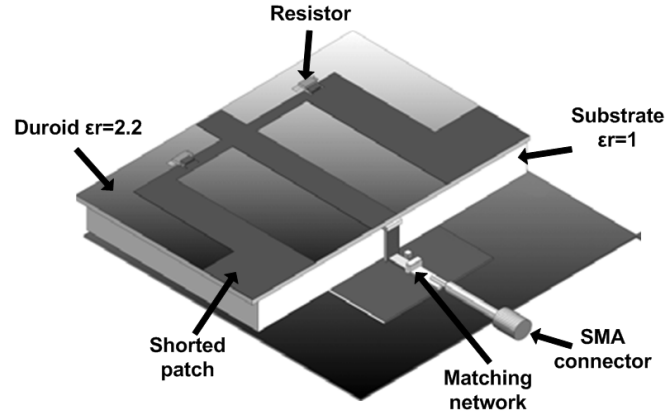


Fig. 2.16: Modified E-PIFA structure [103].

Lilja *et al.* have developed a body-worn antenna integrated into the life-jacket for rescue satellite systems [27]. The proposed antenna is a PIFA operating at 406 MHz. Light-weight and low-loss foam is used as a substrate while the conductive layers are implemented by using inkjet-printing. Additional protective layers for mechanical-abrasion and salty environment are added. The used technology makes the antenna waterproof and resilient to the salty water. The antenna has a rather large fractional bandwidth of more than 30%. Large bandwidth is achieved by making the antenna large and thick enough, $28.3 \times 6.5 \times 1.75 \text{ cm}^3$.

PIFAs exhibit good performance when used for wearable applications. The antenna's structure, and the low coupling to the wearer provides stable and reliable performance. The low profile of the antenna makes it a suitable candidate for integration into the wearer's uniform. Overall, PIFAs are very good candidates for wearable UHF voice communication applications like Tetrapol or Polycom. Table 2.4 summarizes the most relevant advantages and disadvantages of the PIFAs when used for wearable applications.

Advantages ☺	Disadvantages ☹
<i>PIFA structure:</i> good compromise f_c vs. size (low profile) vs. on-body placement	<i>PIFA structure:</i> at UHF frequencies the size still fairly large
Moderate to medium gain	Moderate to medium efficiency
Reduced coupling to the wearer (low SAR)	

Tab. 2.4: A summary of the positive and negative aspects for the PIFAs when used for wearable applications [85].

2.2.6 Commercially Available UHF Wearable Antennas

In addition to the antennas found in the literature, there are also wearable antennas available on the market. Our interest will be narrowed to the antennas operating at UHF frequencies. Due to the specificity of the band and government regulations, to our knowledge there are not many UHF wearable antennas offered on the market.

Wearable UHF antennas are mainly provided by Pharad [104], a United States (US) based company and British aerospace and defense (BAE Systems) [105] and Panorama [106], both located in the United Kingdom (UK). There are probably other companies providing wearable antennas for UHF band, but no sufficient information is accessible. Two commercially available antennas, from Pharad and Panorama, are presented in this section. The antenna prototypes are shown in Fig. 2.17.



Fig. 2.17: Commercial TETRAPOL wearable antennas: (a) Tetra Wearable Antenna [104] and (b) Covert dipole antenna [106].

The wearable antenna developed by Pharad is mainly aimed for soldiers engaged in urban and combat missions. The antenna is fabricated out of thin flexible material that conforms to the body or tactical vest. Since the antenna is completely sealed inside the waterproof material it

is not known what type of antenna is used. According to the radiation pattern (please refer to the antenna data sheet [107]) and non-stable behavior of the antenna when placed on the wearer (our personal experience while measuring it), the antenna is most probably a patch antenna with a very small ground plane. Additional non-stability comes from the feeding cable that also contributes to the overall radiation. Since the antenna is rather small for the given frequency, the feeding cable helps in order to achieve the desired frequency, 380-430 MHz.

The second commercial antenna is the one offered by Panorama. It is a body worn dipole antenna mainly intended for undercover operations. Since the dipole legs consist of flexible conductor surrounded by soft insulation, this antenna can be easily mounted around the wearer's body. This antenna operates inside the Tetrapol communication band 380-430 MHz. Some of the basic characteristics of the presented antenna are found in the corresponding data sheet [108]. Yet, the optimum performance of the antenna is obtained when the dipole legs are vertically oriented on the wearer's back, thus requiring custom tailored sleeves for their placement (information obtained from an internal police report [109]). As in the case of the Pharad wearable antenna, the coaxial cable contributes to the final radiation, thus making this antenna also non-stable. The presented commercial antennas were used for comparing purposes with the antennas proposed by the author. The obtained results will be presented in Chapter 5.

As has been shown, most commercial antennas couple energy to the feeding cable making it non-robust and sensitive to the surroundings. As previously mentioned, one of the most important contributions of this thesis has been to propose an antenna design which overcomes/alleviates this problem.

2.3 Materials and Fabrication Methods

Materials play an important role in the design and fabrication of wearable antennas. The integration of the antennas into the wearers' clothes indirectly imposes the potential choice of conductive and substrate materials. A wide range of materials can be found in the literature: textiles, specially treated yarns, printed conductors, polymers, etc. [110–112].

Selected materials need to be combined through the set of technological and fabrication processes in order to build the final antenna structures. Several different technologies found in the literature are presented. A set of embroidering techniques, ink-jet printing, Substrate Integrated Waveguide (SIW) technology and a combination of polymers and different conductive materials [113, 114].

The operating environment also influences the performance of the antenna. Apart from the body's influence on the antennas, they can be also exposed to different harsh environment, manifested through different weather conditions like rain, humidity, snow, mud, ice, etc. This is an additional reason why a careful selection of the materials should be considered [115].

2.3.1 Textiles

Textile materials are among the most deployed materials for building wearable antennas. They are light weight and can be easily integrated in the wearer's garments. The proposed textiles need to satisfy certain electromagnetic, mechanical and environmental conditions.

Starting from the EM properties, we will consider a simple patch antenna in order to understand the role of the different materials. The materials used for the radiating patch and the ground plane need to have good conducting characteristics and low losses, while the dielectric material should have constant thickness and low loss dielectric permittivity [116].

On one hand, wearable antennas need to be conformable and when mounted on the wearer should remain stable and to provide reliable radiation. On the other hand, by bending and crumpling the textile, being the two most frequent situations, the features of the antenna can be deteriorated. Therefore, precaution should be taken in the design procedure and material selection [117].

Textile materials used for fabrication of wearable antennas are divided in two major groups, conductive and dielectric materials. An overview of the conductive materials is reported in [30]:

- *Conducting Ribbon*. This is a commercially available product consisting of typically 3-6 tracks of conductive thread woven into a non-conductive backing ribbon fabric.
- *Insulated wire*. This is a standard flexible insulated wire which is an ideal candidate for the broadband dipole.
- *Conducting Paint*. These materials are consisting of high silver content to produce a low electrical resistance.
- *Conducting Nylon*. Material available from a variety of manufacturers.
- *Conducting Thread*. Material suitable for spiral antennas.
- *Screen Print*. Easy way to write a pattern on some textile.
- *Coated copper fabric*. There are a variety of commercial processes available to coat fabric with copper.

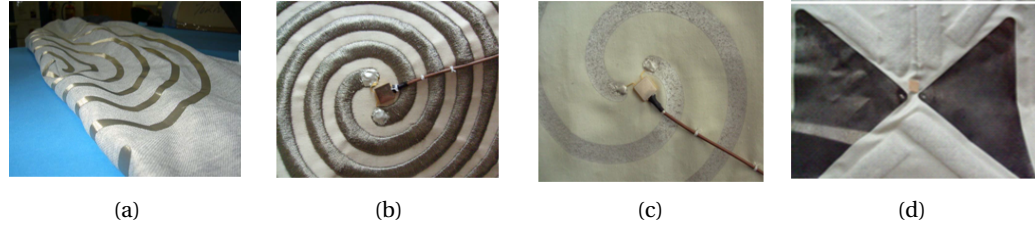


Fig. 2.18: Different textile materials used for wearable antennas' design [30]: (a) Conducting nylon spiral antenna, (b) Embroidered conducting thread spiral, (c) Conducting paint spiral and (d) Copper coated fabric bow-tie antenna.

Some of the materials and technologies presented in [30] are shown in Fig. 2.18.

More conductive materials are found in [116, 118], and they are presented in Table 2.5, showing their thickness and surface sheet resistance.

Material	Thickness [mm]	Sheet resistance [Ω/\square]
Silver-Copper-Nickel plated woven fabric	0.15	0.02
FlecTron	0.15	0.1
Zelt	0.06	0.01
Nora (Nylon fabric)	0.15	0.02
Knitted P130	0.55	<1

Tab. 2.5: Conductive materials used for wearable antennas [25, 116–118].

Preparation of the textile conductive materials requires certain procedures and techniques. As an example, we will consider plating of the textile yarns when used as conductors, presented in [118].

Nickel-Plated fabric is one possible solution. This material shows excellent resistance against corrosion, but since the plating is applied after the weaving process, woven fibers are not entirely plated where they cross each other. As a result, a single fiber is not continuously conductive. The electrical current cannot flow along a single fiber, but instead must “hop” over the small overlapping plating or crossing fibers. These transitions over the fibers are the main reason for high sheet resistance of about $5 \Omega/\square$. Another drawback of these structures is the inhomogeneous sheet resistance [118]. Fig. 2.19 (a) depicts the structure of the Nickel-Plated fabric and its cross section.

The inhomogeneity problem is overcome by plating the fibers of the fabrics before knitting and weaving, Fig. 2.19 (b) and (c), respectively, thus resulting in a lower electrical resistance, $< 1 \Omega/\square$. Their shapes can be manufactured precisely, but the bending of such antenna becomes limited. The edges of the knitted fabric tend to fray easily due to the nature of the

knitting process. Overall, the woven fabric possesses good electrical properties for building well-behaved and geometrically accurate antennas [118].

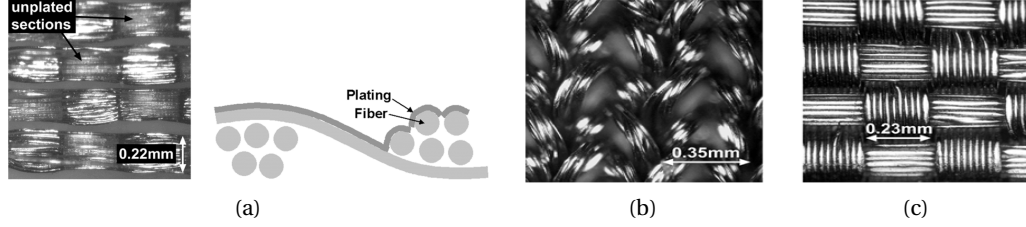


Fig. 2.19: Conductive fabrics [118]: (a) Nickel-Plated fabric and cross section drawing, (b) Platted-knitted (P130) and (c) Platted-woven (Nora fabric).

Another solution is Silver-Plated Knitted Fabric. This fabric has very good mechanical properties and the antenna composed of it is bendable and can comfortably be integrated into the clothing. The manufacturing process is however not easy because precise shaping and assembly of the antenna is required [118]. Different techniques and fabrication steps have been presented by Ukkonen *et al.* [119], where analysis of the sheet resistance from different structures are reported.

In order to give an idea of how these materials behave and perform when concrete antenna prototypes are built, a comparison of gain [dBi], efficiency [%], and bandwidth [%] of reference copper patch antenna, electro-textile patch antenna (metallic), and electro-textile patch antenna (fabric) is shown, Table 2.6. All the antennas radiate in free space (no presence of body or phantom). It can be seen that some of the features like gain and efficiency are deteriorated compared to the reference copper patch antenna, while the bandwidth is improved. This shows that textiles and fabrics can successfully replace conventional conducting materials [116].

Material	Gain [dBi]	Efficiency [%]	Bandwidth [%]
Reference copper patch antenna	7.4	95	2.2
Electro-textile patch antenna (metallic)	7.1	88	2.6
Electro-textile patch antenna (fabric)	6.6	79	2.9

Tab. 2.6: Performance of electro-textile patch antennas compared with the conventional copper patch antennas(@ 2.44 GHz) [116].

The choice of dielectric materials is larger compared to the conductive ones. Simply, most of the textiles have low relative permittivity and relatively low loss tangent angle, thus making them suitable substrates for wearable antennas. Since no additional fabrication treatments are required, theoretically most of the textiles can be used as substrate materials. Table 2.7

presents the different dielectric materials found among the wearable applications, showing their thicknesses and the electrical characteristics (relative permittivity and loss tangent).

Material	Single layer thickness [mm]	ϵ_r	$\tan \delta$
Felt	1.1	1.38	0.023
Woolen felt	3.5	1.45	0.02
Polyamide fabric	6	1.14	Negligible
Fleece	2.56	1.25	Negligible
Closed-cell foam	3.94	1.52	0.012
Silk	0.58	1.75	0.012
Tween	0.68	1.69	0.008
Panama	0.437	2.12	0.018
Moleskin	1.17	1.45	0.05
PTFE	11.66	2.05	0.0017
Cordura	NA	1.90	0.0098
Cotton	NA	1.60	0.04
100% polyester	NA	1.90	0.0045
Quartzel fabric	NA	1.95	0.0004
Cordura/lycra	NA	1.50	0.0093
Jeans textile	1	1.7	0.025
Acrylic textile	0.5	2.6	NA

Tab. 2.7: Dielectric materials used for wearable antennas [25, 116, 116–118].

2.3.2 Printed Technology

Printing is an alternative method for deploying conductive layers on the substrates. Printing technology can easily shape the required pattern of the conductive paste since it is fast, it consumes the minimum required material and it does not require masks. In majority of the cases silver and copper nanoparticles are used for creating the conducting lines. Carbon nanotube inks are also considered as potential solution, but due to the low conductivity they are used less compared to the silver and copper particles [120].

Printing is considered as more ecological compared to etching, because no waste is created. Namely, with etching the unwanted metal from the substrate's surface is removed, while the printing delivers only the required ink droplet to the desired area. One of the main disadvantages of the printed technology is the low efficiency of the fabricated antennas, being around 70% [121, 122].

Whittow *et al.* in [121, 122], have presented an overview of various wearable antennas fabricated with printing technology. The antennas can be printed on different substrate materials like paper [120], Polyethylene Terephthalate (PET) [123] or Kapton [124]. For example in [125] a stretchable PIFA is fabricated by depositing a nanoscale thin (50-100 nm) gold film on a silicone elastomer, polydimethylsyloxane (PDMS).

Most of the printed antennas found in the literature work between 2-5 GHz, suggesting that printed technology is more convenient for smaller and more compact antennas, where precision is important, rather than for larger antennas operating for instance at 400 MHz. However, with the constant advance of the materials and machines for different printings, this technology can be successfully used for wearable antennas fabrication.

2.3.3 Substrate Integrated Waveguide (SIW) Technology

Substrate integrated waveguide (SIW) is a relatively young technology, which appeared in 2001 [126]. The possibility to integrate passive components and active elements on the same substrate makes this technology favorable for different types of applications. Filters, couplers or oscillators, amplifiers as well as antennas can be combined and fabricated on the same substrate [127]. The first traces of SIW technology used for wearable antennas date back to 2010, when Langley *et al.* [128], introduced SIW for channeling the EM signals between two wearable antennas mounted on the same wearer. The textile material was used as a common substrate where the SIW waveguide was designed in order to maximize the communication between the two antennas. When an off-body communication was needed, the SIW waveguide was switched off.

By then, the potential of SIW technology was also recognized for off-body communications. Different designs of miniaturized half mode cavities appeared as wearable antennas [129]. Bozzi *et al.* introduced the SIW technology for different substrates. In [130] they present plastic-based SIW components and antennas, where the SIW is implemented on polyethylene terephthalate (PET) substrate. An inkjet-printed SIW structure on low-cost material was presented in [131], where low-cost and eco-friendly interconnects and components were fabricated and tested on multilayer paper substrates.

Wearable antennas based on the fundamental half-mode SIW cavities are presented in [132–134]. Cavity based antennas are popular for wearable applications because of their stable performance in the vicinity of the human body. They radiate only in one hemisphere [133]. There are different approaches for fabricating SIW structures. In [132], vias for the integrated waveguide are realized by passing the conductive yarns through the low-loss foam, using computer steered embroidery, while in [133, 134], copper tube eyelets are utilized for the SIW realization. Some of the structures built with the SIW technology are shown in Fig. 2.20.

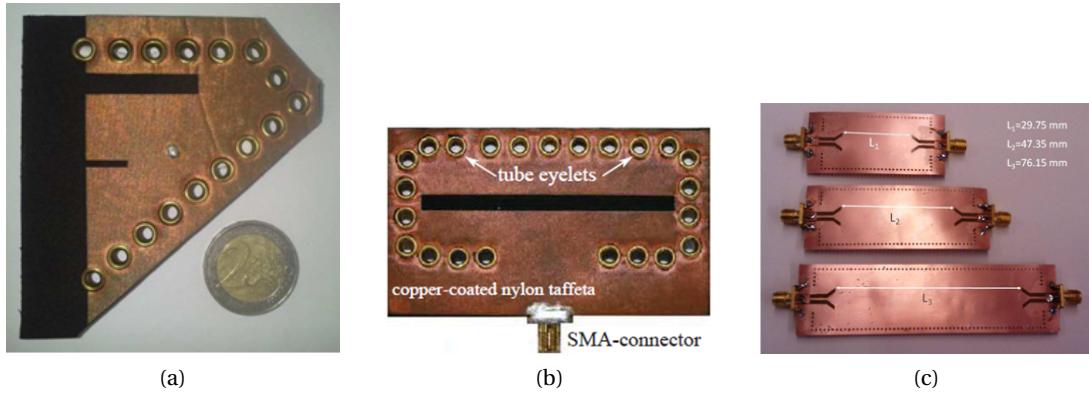


Fig. 2.20: Illustrative examples of wearable antennas and interconnection structures built in SIW technology: (a) Dual-band Half-Mode Substrate Integrated Waveguide (HMSIW) on-body antenna [134], (b) UWB SIW textile antenna [133] and (c) SIW interconnects [130].

SIW technology is a good candidate for building robust and stable wearable antennas for on-body performance. With modern computer embroidery machines different shapes and structures can be realized. However, all the presented antennas in the literature are for frequencies above 2.4 GHz, so it would be interesting to design and study the behavior of wearable SIW antennas at lower frequencies, for instance in UHF band.

2.3.4 Polymer Substrates

In recent years, flexible and stretchable electronics built on flexible polymer substrates have received an increasing attention due to their wide use in different types of applications. Stretchable sensors, bio-integrated electronics, or flexible displays are some of the possible applications where they find their use. A comprehensive overview of the different applications, materials and their physical and chemical characteristics is presented in [135]. Following the similar trends, many wearable antennas are built on different polymer substrates.

In [136], several polymer based materials are introduced as potential candidates for flexible antenna's substrates, Liquid Crystal Polymers (LCP), Polyetherimide (PEI) or Polyethylene terephthalate (PET). Nevertheless, one particular elastomer recently has been extensively used in micro-fabrication and flexible electronics, the so-called PDMS [137]. The most deployed type of PDMS is the Sylgard RTV 184, from Dow Corning [138]. PDMS is chemically inert, thermally stable, permeable to gases, simple to handle and manipulate, and exhibits isotropic and homogenous properties [139], which make it a suitable candidate for flexible and stretchable antennas. There are also different variations of the PDMS appearing on the market [139]. For example, there are more PDMS based materials like the ultraviolet (UV) light cured PDMS, X-34-4184-A/B Liquid Silicone Rubber UV Cure Type (PDMS) [140], which essentially has

similar characteristics with the Sylgard 184, but the only difference is the possibility of the fast curing by using the UV light.

In [141–143], PDMS was used as a silicone elastomer for the design of stretchable microfluidic antennas: Microfluidic channels were created inside the PDMS where fluid metal alloys were injected. In [144, 145], micro-machined PDMS membranes for ultra-flexible planar antennas obtained through complex technological operations were presented. Using elastic membranes instead of bulk substrates improves the overall radiation efficiency of the antennas. Other examples of flexible antennas based on PDMS were presented in [125], where a PIFA was fabricated by depositing nanoscale gold (Au) film on PDMS, see Fig. 2.21 (a). Wang *et al.* [146], reported conformal antennas based on embroidered conductive metal-polymer fibers (E-fiber) on polymer-ceramic composites (PDMS), see Fig. 2.21 (b).

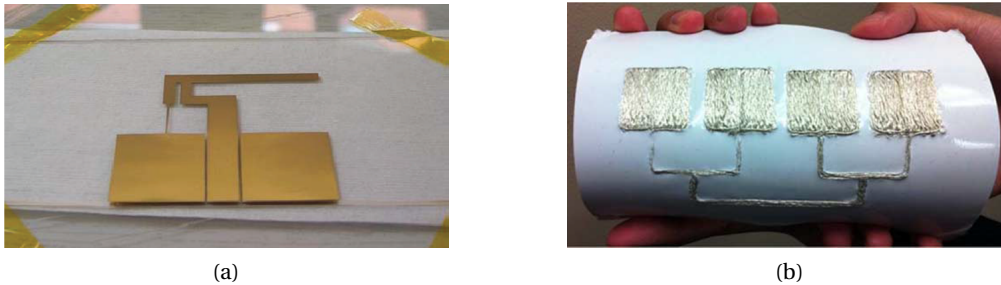


Fig. 2.21: Antenna prototypes built on PDMS substrates: (a) Stretchable PIFA based on a new metallization technique of depositing nanoscale thin Au film on a PDMS elastomer [125] and (b) Antenna array built on embroidered E-fibers and polymer composites (PDMS) [146].

2.4 Frequency Band Selection

The selection of the available frequency bands are regulated by the frequency allocation plans published by government offices. Specific frequency bands indirectly can determine the size of the antenna and influence the choice of the antenna type. Too low frequencies would result in large antenna structures that would be hard to integrate on the user's body, whereas too high frequencies would result in very small structures sensitive to fabrication tolerances, leading to the increase of the fabrication costs. Moreover, as the frequency increases, so does the complexity of the embedded electronics and the antenna feeding, which again increases the fabrication costs.

The International Telecommunication Union (ITU), which is the United Nations (UN) specialized agency for information and communication technologies (ICTs), allocates the global radio spectrum and develops different technical standards [147]. Each country regulates its own frequency spectrum, but in most of the cases in accordance with the ITU regulations

and recommendations. In Switzerland these regulations are regulated by the Swiss National Frequency Allocation Plan and Specific Assignments governed by the Federal Office of Communications, OFCOM, Frequency Management Division [11]. Swiss frequency allocation plan is in accordance with the ITU regulations.

This section provides information on some of the general characteristics on wave propagation, and frequency bands suitable for wearable antenna's applications.

2.4.1 Wave Propagation Characteristics

Electromagnetic wave propagation is strongly linked to the frequency, where the wavelength determines the size of the obstacles or transmission medium that will mostly influence the wave and its propagation [148]. For frequency ranges from a few Hz up to several GHz, THz or higher, the size of the wavelength goes from several km down to a few nm, respectively. Table 2.8 shows several radio wave bands and their corresponding propagation phenomena, as well as the considered wavelength.

Band	Frequency	Wavelength	Propagation
Very Low Frequency (VLF)	3-30 kHz	100-10 km	Ionosphere refraction
Low Frequency (LF)	30-300 kHz	10-1 km	Ionosphere refraction
Medium Frequency (MF)	300-3000 kHz	1-0.1 km	Ionosphere refraction
High Frequency (HF)	3-30 MHz	100-10 m	Ionosphere refraction
Very High Frequency (VHF)	30-300 MHz	10-1 m	Direct waves
Ultra High Frequency (UHF)	300-3000 MHz	100-10 cm	Direct waves
Super High Frequency (SHF)	3-30 GHz	10-1 cm	Direct waves
Extremely High Frequency (EHF)	30-300 GHz	10-1 mm	Direct waves high absorption

Tab. 2.8: Radio Spectrum [149].

According to this table and previously introduced limitations, three frequency bands are possibly seen as appropriate solutions for Body-Worn antennas, VHF, UHF and SHF band. The sizes of the antennas operating at those three bands are convenient so that they can be easily placed on the wearer's body.

Frequency bands lower than VHF are not good since their wavelengths are longer than 10 m and they are usually used for very long distances. On the other end of the frequency spectrum, EHF band faces the problem of traveling of such waves across most of the obstacles like walls, trees, buildings, and even the atmosphere. The smaller the wavelength is, the more interference with small objects appears, at some point even interfering with molecules.

Fig. 2.22 shows the absorption characteristics of the atmosphere in dB/km as a function of frequency [148].

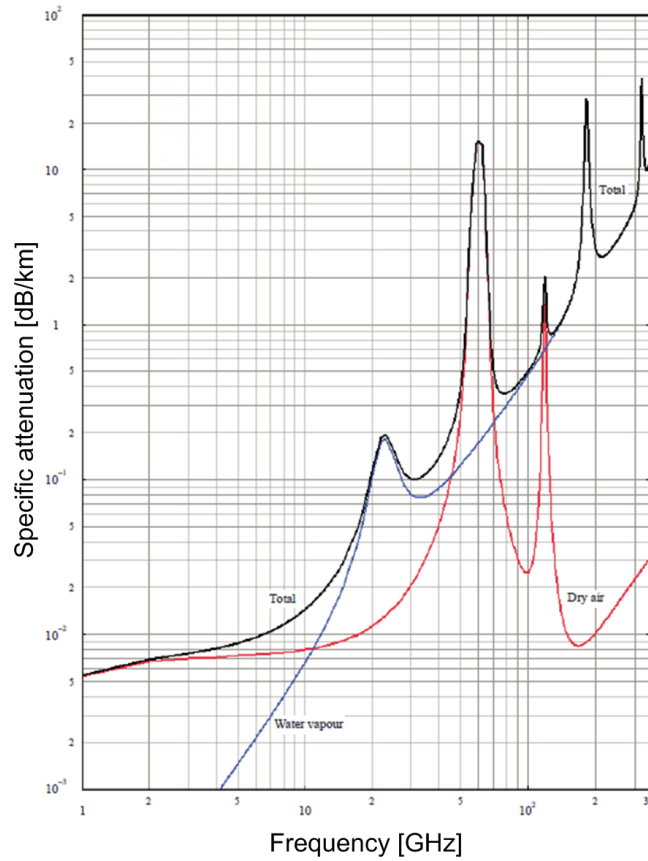


Fig. 2.22: Specific attenuation due to atmospheric gases [148].

The majority of the signal absorption is caused by two compounds, oxygen (O_2) and water vapor (H_2O). As can be seen from Fig. 2.22, the first peak occurs at 22 GHz due to the water and the second at 63 GHz due to the oxygen. These graphs apply from a sea level to around 1 km of altitude.

2.4.2 Frequency Bands Suitable for Wearable Antennas for Security and Rescue Service Applications

An overview of the frequency bands that can be used for security and rescue applications defined by the OFCOM and ITU regulations is shown. Apart from the exclusively dedicated bands, some adjacent or even overlapping civilian bands are included for allowing a polyvalent use of the bands.

30.500–87.500 MHz

As a result of the migration from analogue to digital broadcasting, the analogue TV transmitters in band I, 47 – 68 MHz, were shut down at the end of 2008. This band is therefore available for military use, except the sub-band 50 – 52 MHz that is assigned to the amateur radio service. Tactical mobile systems for voice and data communications are planned in this frequency range.

The wavelengths at these frequencies are between 3.5-10 m, respectively, and long distance communication could be achieved. The higher the antenna is mounted above the ground, the longer the distances that can be covered. The size of the antenna at these frequencies is fairly large for placing it around the body. One of the solutions can be applying some of the mentioned miniaturization techniques, but in that case antenna's performances will deteriorate. Another issue appearing with this frequency band is the existence of Electromagnetic Compatibility (EMC) problem due to the emergence of Power Line Communication (PLC) devices. After all, this frequency band does not seem as a convenient solution for wearable antennas due to its narrow bandwidth, fairly large antennas, and the appearance of the EMC problem⁵.

230–400 MHz

This range is fully coordinated with the North Atlantic Treaty Organization (NATO) and is used for tactical Unmanned Aerial Vehicle (UAV) systems and for national crisis management (e.g. emergency organizations). This is a very important band for military use. No major changes are foreseen in the use of these frequencies. A special emphasis can be put on the ranges 380-385 MHz and 390-395 MHz that are intended for Digital Land Mobile System for Emergency Services in Switzerland⁶.

380–470 MHz

This frequency band has been designated as a “tuning range” for future narrow band Public Protection and Disaster Relief (PPDR) systems⁷. Inside this band there are two sub-bands that can be of particular interest regarding the security and rescue service applications. Both 418-420 MHz and 428-430 MHz are exclusively dedicated only for military use. No major changes are foreseen in the use of these frequencies⁸.

⁵See page 41-44 [11].

⁶See page 55 [11].

⁷See page 9 [11].

⁸See page 55-62 [11].

2.4–2.5 GHz

This range is also known as a Short Range Distance (SRD) and it is allocated for the civil administration. It is also part of the ISM band that was originally internationally dedicated for RF electromagnetic fields for industrial, scientific and medical purposes. Wireless network equipment compatible with IEEE 802.11b, and 802.11g standards operates at 2.4 GHz.

4.4–5 GHz

Military fixed link systems are operating in this frequency range. The band is of great significance to the military because future broadband requirements can be implemented with new technologies in this range⁹.

5.250–5.725 GHz

This band is dedicated for the new sensor systems that will be used by Swiss army and NATO. It has a broadband radio characteristics which are expected to be very important for the new broadband technologies used by the military. Since this band is not exclusively dedicated to military use, it is also used by some civilian broadband systems¹⁰.

Ultra Wideband (UWB)

According to the FCC, ultra wideband (UWB) is defined as any system having a bandwidth of at least 500 MHz or a fractional bandwidth larger than 0.2. In 2002 FCC allowed the frequency band between 3.1-10.6 GHz for unlicensed UWB transmission [42]. The transmitted power is spread over the entire spectrum by using short time pulses (impulse radio) which ensures good EMC with the various devices (Military and Civil) using the wide frequency range of this technology. There is a positive trend of using the UWB band for wearable applications. This is mainly due to the suitability of the impulse radio technology for wearable communication, as it can help mitigate the problems caused by fading and environmental changes [150].

15.700–17.300 GHz

This band is dedicated exclusively to military applications, and it is mostly used for sensors systems, both in Switzerland and in NATO. Its broadband radio nature makes it a good can-

⁹See page 92 [11].

¹⁰See page 94-96 [11].

didate for the future broadband military applications. It is to be widely deployed in Wireless Access Systems (WAS), and Radio Local Area Networks (RLANs)¹¹.

Other Frequency Bands

There are also other available bands above 20 GHz, but as was presented in Fig. 2.22, wavelengths of the electromagnetic waves higher than 20 GHz suffer the high atmospheric absorption. These bands are predominantly used for the satellite applications or extremely short terrestrial communication. For example, 19.700 GHz – 21.200 GHz band is allocated for fixed and mobile satellite space-to-Earth military communications¹².

In summary, security and rescue services, and in particular military applications, have the advantage of using wide span of bands in the whole frequency spectrum. On the other hand, considering all these bands from the wearable antenna point of view, not all of them can compete as convenient candidates. While for the lower frequencies the main problem is the size of the antenna for a chosen frequency, for the higher frequencies the difficulties are mainly due to the high atmospheric absorption of the signals.

2.4.3 Tetrapol Communication Band

Tetrapol is a digital cellular trunked radio for voice and data communication. Originally it has been developed by the French company, *Matra Communication*. This radio system is intended for private and public radio applications and for emergency services. Two groups are mainly using Tetrapol system, Private Mobile Radio (PMR) and Public Access Mobile Radio (PAMR) [10].

Tetrapol is used by various groups of customers like safety agencies, utility transport or emergency services like rescue, police or military. Nowadays there are almost 2 000 000 users in more than 30 countries worldwide. In most of the cases it is used by security forces [15].

In Switzerland, Tetrapol digital trunked radio has been chosen as a national radio network for rescue and security services, Polycom [151]. This network should serve the needs of different services across the country like border guards, police, firefighters, first aid, civil protection and military formations.

Among the several services provided by Tetrapol, the two main ones are the network mode and direct mode communication. The network mode establishes a communication always through a base station, and all the services are monitored by this station. In the direct mode,

¹¹ See page 109 [11].

¹² See page 112 [11].

two or more mobile stations communicate directly, without using the base station. This mode is also known as walkie-talkie mode. The big advantage of the direct mode is its usage in the areas where no infrastructure exists or when there is no radio coverage (e.g. tunnels, mountain areas, etc.) [10]. Direct mode communication is one of the favorable choice for rescue services.

The dedicated operating frequency for the Swiss national emergency and radio network is between 380-400 MHz. Wearable antennas proposed in this thesis are intended for the UHF band and to be incorporated among the existing communication security systems, for instance Polycom system [13]. Some of the major Tetrapol parameters are presented in Table 2.9. More detailed study and analysis on the Tetrapol system are reported in [152].

Parameter	Value
Channel spacing	12.5 kHz
Transmission power of base station per carrier frequency (typically)	25 W ERP
Transmission power of mobile equipment	1 W, 2 W, 10W
Receiver sensitivity, dynamic	Mobile Station (MS): -119 dBm Base Station (BS): -113 dBm
Mode	Semi-duplex
Channel access method	Frequency Division Multiple Access (FDMA)
Modulation	Gaussian Minimum Shift Keying (GMSK)
Range	Rural: ca. 20 km Suburban: ca. 6 km

Tab. 2.9: Tetrapol parameters [10].

2.5 Conclusions

An overview of different wearable antennas found in the literature and on the market was presented in this chapter. We have selected four categories in order to simplify their classification: applications, antenna types and families, materials and technology and the available allocated frequency bands.

The classification based on the four categories gives a picture of published work and a starting point for the design and development of wearable antennas. In order to provide a better overview of the performed classification, some of the characteristics, linked with several different parameters are shown in Table 2.10. This table classifies the antennas according to their operating frequency linking the latter with the communication range, data rates and size and materials the antennas are built of.

2.5. Conclusions

Operating frequency <i>Wavelength</i>	400 MHz <i>0.75 m</i>	868 MHz <i>0.345 m</i>	2.45 GHz <i>0.12 m</i>	3-10.6 GHz <i>0.1 - 0.003 m</i>
Range	up to several km	up to 9 m	2 -10 m	1 -10 m
Indoor	✓	✓	✓	✓
Outdoor	up to several km	mainly indoor RFID	ZigBee as an extreme case up to 100 m	mainly indoor
Fractional Bandwidth (%)	10 %	2 %	4 - 8 %	50 - 60 %
Data Rates	10-20 Kbps	32 Kbps	up to 150 Mbps	0.1 - 1 Gbps
Dimensions (Typical)	30 x 20 cm ²	10 x 6 cm ²	4 x 4 cm ²	From: 6 x 6 cm ² To: 1.5 x 1.5 cm ²
Diversity Space	occupies large area (VESTS)	easy placement on the body	easy placement on the body	easy placement on the body
Choice of materials	conventional conduct. & subst. + textiles	wide range of textiles	wide range of textiles	wide range of textiles

Tab. 2.10: Antenna characteristics overview over the four frequency ranges [85].

The main focus of the thesis research is on the short to medium range coverage and medium data throughput. Depending on the application requirements and the band characteristics, the proposed antennas should be designed for some of the available frequency bands between 300 MHz and 10.6 GHz.

3 Materials, Characterization and Technology

Materials, characterization of their properties and a technology proposed for building robust and flexible wearable antennas are reported in this chapter. In the first part, the main emphasis is put on the choice of dielectric and conductive materials, while the second part provides more details regarding the proposed technology and the built antenna prototypes.

During the selection process of dielectric and conductive materials, a set of criteria have been introduced, considered and followed, emphasizing the three most important ones:

- Electromagnetic (EM) properties - Permittivity and Losses.
- Mechanical properties - Flexibility and Softness.
- Chemical properties - Bio-compatibility and Waterproof aspects.

The overview performed in Section 2.3 (Materials and Fabrication methods) provided a good starting point for selection of the appropriate materials. Among the considered ones, polymer based dielectrics and mesh/perforated conductors are good candidates according to the defined criteria. Polydimethylsyloxane (PDMS) is selected as a substrate material, while copper mesh and perforated copper-bronze sheets are used as conductors. The initial viscous condition of the PDMS has two advantages. First, it enables embedding the conductors inside the substrate, thus avoiding the adhesion problem between the polymers and classical solid-sheet conductors and second, since the conductive parts are encapsulated inside the substrate, it is enough that only the substrate material is waterproof or bio-compatible.

This chapter is organized as follows: in the first part PDMS is investigated from the EM and mechanical point of view, and ways to adjust its EM properties are proposed. Copper mesh structures and custom perforated copper-bronze conductive sheets are considered in the second part. Finally, a complete fabrication process is shown by fabricating a real antenna prototype.

3.1 Dielectric Materials

Different types of dielectrics can be used as antenna substrates. From the EM point of view, two important characteristics matter: low permittivity and low losses improve the antenna's radiation characteristics, i.e. bandwidth and radiation efficiency [72]. Therefore, the efforts will be concentrated on lowering the permittivity and losses of the selected dielectric materials.

3.1.1 Polymers

The word *polymer* comes from the classical Greek words *poly*, which means "many" and *meros* meaning "parts". In other words, polymers are long-chain molecules composed by repeating a large number of units of an identical structure [137]. Polymers can be found in nature like cellulose, proteins or silk or can be synthetically produced like nylon or the polymer we are looking at, PDMS. Polymers that are able to change their initial size are also known as elastomers [153].

Elastomers are rubber-like polymers with low elastic modulus and high yield strain. Simply stated, an elastomer is resistive to the external applied forces and has a tendency to return to its original shape. These characteristics come from their molecular structure, where each chain behaves as a spring, thus resulting in overall elastic structure [135].

3.1.2 Polydimethylsyloxane - PDMS

Polydimethylsiloxane (PDMS) is a silicone-based elastomer widely used in different types of applications like microsystems, bioMEMS, microfluidic chips, actuators or stretchable electronics [135]. PDMS serves also as a base material for transfer printing and soft lithography. Initially it was developed as a high-voltage outdoor insulator material [135]. PDMS is chemically inert, thermally stable, permeable to gases, simple to handle and manipulate, and exhibits isotropic and homogenous properties [139]. It is an excellent water isolator thus enabling a long-term, stable device operation (e.g. antenna). It has good radio frequency (RF) and mechanical characteristics, low dielectric constant and good chemical stability [154].

The initial fluid state of PDMS allows the preparation of composite substrates of various concentrations, thus controlling the range of dielectric constants and the flexibility that can be obtained. Moreover, the fluid state of the elastomer also offers control over the substrate thickness as well as the possibility of immersing the antenna inside the substrate. Based on the presented criteria and characteristics, PDMS was selected as a basic material for the antenna substrate.

3.2 Adjusting the EM Properties of PDMS

As already stated, PDMS has been used as a substrate in various electronic and antenna applications [125, 135, 141, 142, 144, 146]. In most of the cases, Sylgard RTV 184, a silicone elastomer kit, produced by the Dow Corning Corporation, has been used as PDMS [155]. The only available data from the producer, regarding the relative permittivity of the Sylgard PDMS are for frequencies at 100 Hz and 100 KHz, 2.72 and 2.68, respectively [138].

On the other hand, there are reported measured values for the relative permittivity and loss tangent for a similar polymer, Sylgard RTV 182, between 0.1-40 GHz, in [156]. The measured values are $\epsilon_r=2.77$ and $\tan \delta=0.012$. Ideally, for the purposes of wearable antenna design, we would like to have lower relative permittivity and loss tangent in order to improve the radiation performance of the antenna like bandwidth and antenna's radiation efficiency [72].

Nevertheless, up to the author's knowledge the possibility of doping the PDMS with different inclusions to tune its mechanical and EM properties has not been reported yet. For that reason, a method of loading PDMS with different materials is presented. Several potential fillers were investigated, sample prototypes built and permittivity and loss values measured and compared. Finally, the combination of PDMS+filler with the lowest permittivity and the lowest losses was selected for the design of a wearable antenna prototype. Substrates with a higher relative permittivity are useful for the design of electronic circuits, while most of the antenna designs require substrates with lower permittivity.

Sylgard RTV 184, a silicone elastomer kit, produced by the Dow Corning Corporation, was selected for PDMS [155]. Sylgard RTV 184 is liquid in its initial stage and solidifies when the proper polymerizer is added. Depending on the polymerization conditions, cured in the oven or at room temperature, the process can last from 2-3 hours to one or two days [138].

Three types of micro-spheres were tested as inclusions suitable to lower the permittivity: hollow glass, phenolic and silicate micro-spheres, with diameters between 20-50 μm [157]. Liquid PDMS was mixed with the polymerizer as indicated in [155], and then for each case different inclusions were added. For each of the inclusions the amount of the added micro-spheres was determined through a set of trials and tests [158]. The mixture of the PDMS+inclusions is mixed until certain homogeneity is achieved. All the mixing procedures are done by hand and in non-controlled laboratory conditions, leading to some side effects like appearance of air-bubbles inside the mixture. In order to prevent excessive air, before curing the samples are exposed to a degassing procedure with a simple vacuum pump. More details on the degassing process are given in the section 3.4. Four different combinations of PDMS+inclusions were poured in customized molds and left to polymerize at room temperature for 48 hours. The four polymerized samples are depicted in Fig. 3.1.



Fig. 3.1: PDMS loaded with different inclusions, from left to right: pure PDMS (no inclusions), hollow glass, phenolic, and silicate micro-spheres.

Characterization of the Built Samples

The samples were characterized with two different methods, using a waveguide (WG) as a probe holder and a network analyzer for characterization in X-band (9.5-11.3 GHz) and a commercial probe station at lower frequencies (0.2-5 GHz) [159]. Since the dimension of the inclusions is several orders of magnitude smaller than the wavelength at the desired frequencies, the built samples can be considered as homogeneous dielectrics.

The WG method measures both reflection and transmission, with the dielectric sample completely filling the cross-section of the waveguide, $22 \times 10 \text{ mm}^2$. A detailed description of the used method is reported in [160]. In order to minimize the potential measurement errors, one sample was measured several times and the obtained values were averaged. There were no significant discrepancies between the measured values for the same sample.

A second method used for characterization of the built samples, is a probe method based on the reflection measurements only. A commercial APC-7 coaxial probe and the Agilent 85070E probing kit were used for the measurements at lower frequencies. Both, the equipment and the method are fully described in the Agilent application note *Basics of measuring the dielectric properties of the materials* [159]. Since the probe comes in direct contact with the sample, and the pressure applied by the probe is determined by the human factor, some measurement uncertainties can appear. The samples need to be as flat as possible, thus avoiding the presence of air between the probe and the material. Therefore, if the pressure is too low, some air might appear between the probe and the sample, thus influencing the measured values. On the other hand, a too high pressure might modify the structure of the sample, again leading towards incorrect measured values. At the end, a moderate pressure

was defined. The samples were measured from four different sides and the obtained values were averaged. A situation where one of the samples was measured is shown in Fig. 3.2.

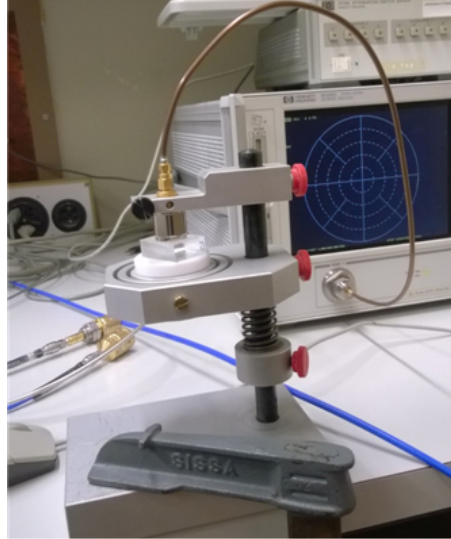


Fig. 3.2: A sample of PDMS measured with the Agilent probe set-up.

The acquired results from both methods are presented in Table 3.1. The last two columns in this table report the volume [%] of the inclusions with the respect to the volume of the PDMS and the relative permittivities of the inclusive materials themselves (glass, phenol and silica), respectively. Since the Sylgard RTV 182 PDMS was already investigated and characterized in some previous works, we compared the obtained results for pure PDMS with the results reported in [156]. There is a slight discrepancy in the obtained values, for relative permittivity 2.75 vs. 2.65 (ours) and 0.015 vs. 0.02 (ours) for the loss tangent. One of the reasons for the slight discrepancy and uncertainties might lay in the difference of the used PDMS, Sylgard RTV 182 vs. Sylgard RTV 184 (ours).

The lowest permittivity and the lowest losses were obtained by using the hollow glass micro-spheres as fillers. The spheres are made of glass and filled with air (relative permittivity close to 1). Both, permittivity and losses, were reduced for the case of the loaded PDMS, compared to the non-loaded one. However, since the glass micro-spheres are fragile and while mixing the materials manually, certain number of spheres can brake, full control over the final permittivity and losses cannot be guaranteed.

Fig. 3.3 and 3.4 report the performed measurements for the relative permittivity and loss tangent for the pure PDMS and PDMS loaded with glass micro-spheres. The measurements were done with the WG method in X-band (9.5-11.3 GHz).

Silgard - 184 RTV <i>mixed with:</i>	WG method 9.5 – 11.3 GHz		Probe method 0.2 – 5 GHz		Volume [%]	ϵ_r ^a
	ϵ_r	$\tan \delta$	ϵ_r	$\tan \delta$	incl. vs. Sylgard	incl. material
No inclusions	2.65	0.02	2.76	0.03		
Glass micro-spheres	1.85	0.014	2.00	0.03	12.7%	4-10
Phenolic micro-spheres	2.24	0.022	2.58	0.04	12.7%	8
Silicate micro-spheres	2.45	0.02	2.62	0.04	45%	2.5-3.5

Tab. 3.1: Measurement results.

^aThis column reports the values for the relative permittivity of the basic materials like glass, phenol and silica.

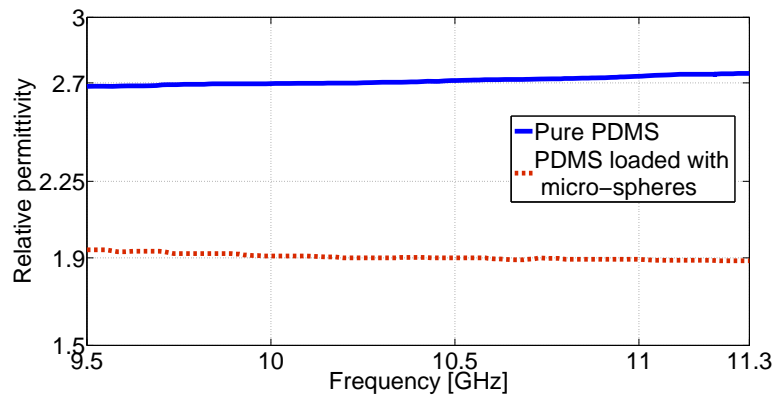


Fig. 3.3: Measured values for the relative permittivity, for pure PDMS and PDMS loaded with glass micro-spheres, with the WG method.

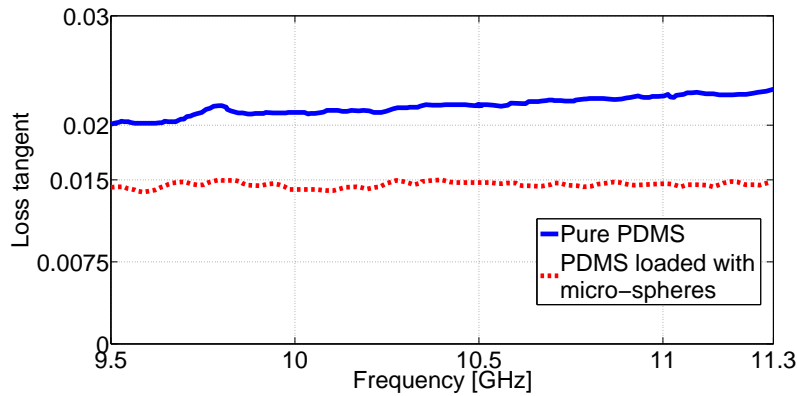


Fig. 3.4: Measured values for the loss tangent, for pure PDMS and PDMS loaded with glass micro-spheres, with the WG method.

3.3 Conductive Materials

For testing purposes, the first selected material was a thin copper-beryllium (Cu-Be) conductive sheet. Cu-Be sheet was attached to the PDMS in the initial liquid phase and cured in an oven at 80°C for 3 hours. Once the PDMS was polymerized, the structure was twisted and bended in order to assess its mechanical properties. As can be seen from Fig. 3.5 (a), the copper-beryllium sheet detached from the PDMS substrate, first on the corners then over the entire structure, thus illustrating the adhesion problem as one of the main issues when dealing with PDMS and conventional conductive sheets. Moreover, the flexibility of the final structure is not sufficient. Therefore, it was decided that another approach will be used in order to obtain better adhesion and flexibility. The selection of the conductive materials was partially influenced by the choice of PDMS as a substrate. Indeed, the liquid state of PDMS can be used to pass through the perforated or mesh structures, resulting in an encapsulated conductor.

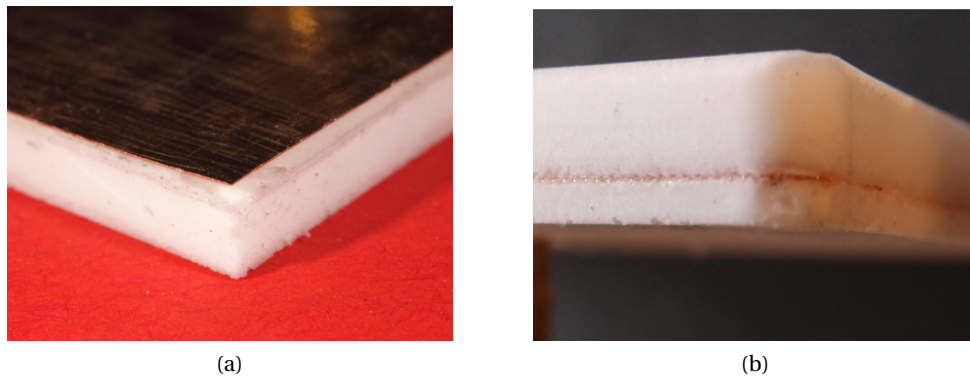


Fig. 3.5: PDMS cross-sections: (a) Copper-Beryllium sheet attached to the PDMS – poor adhesion and (b) Copper mesh sheet “sandwiched” between the PDMS layers – excellent adhesion.

3.3.1 Copper Mesh Structures as Conductors

Mesh structures are flexible, they have good conductivity (as already seen for plated and intertwined structure in section 2.3.1, silver-plated woven/knitted yarns), and they allow an easy flow of the PDMS through the mesh, thus mitigating the adhesion issue. Once the PDMS is polymerized, the conductive mesh is completely encapsulated and sandwiched between the PDMS layers, resulting in a robust and flexible structure, see for instance Fig. 3.5 (b).

Two different mesh structures were considered, a structure with a finer mesh, having a wire diameter of 0.1143 mm, an opening size 0.14 mm and a thickness of 0.2286 mm [161], and a structure with coarser mesh having a wire diameter of 0.3810 mm, an opening size of 0.76 mm and an overall thickness of 0.762 mm [162]. Fine mesh structures are mainly used for

the fabrication of antennas where the precision is important, especially at higher frequencies, (2.45 GHz or in UWB band, 3.1-10.6 GHz). The coarse mesh structures can be used for cases where precision is not that critical, for instance at UHF frequencies and for the ground planes.

PDMS loaded with glass micro-spheres was used to test the flow of the mixture through the fine mesh structure. Microscopic pictures shown in Fig. 3.6 (a) and (b), depict the pure copper mesh and penetration of the loaded PDMS through the mesh, respectively. It can be seen that the loaded PDMS easily passes through the mesh, although the size of the spheres is in a similar range as the size of the apertures.

Copper mesh structures are good candidates for building robust and flexible antennas. On one hand, they increase the flexibility, while on the other hand, by letting the PDMS or any other liquid dielectric, flow through the mesh ensures the robustness of the final product. However, due to the intertwined and non-soldered assembly, mesh structures are not sufficiently precise for some applications.

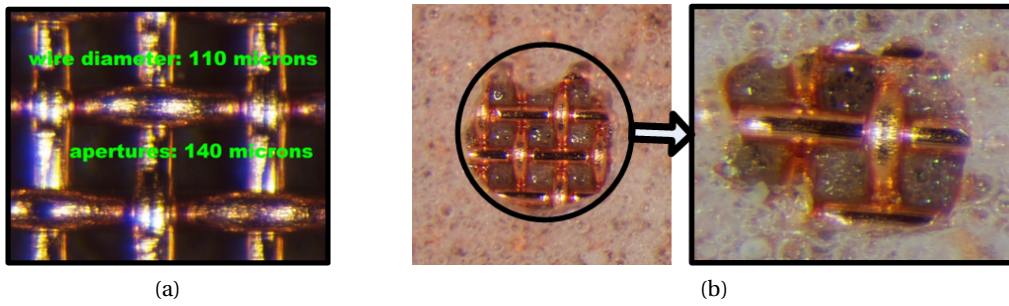


Fig. 3.6: Microscopic pictures of: (a) Pure copper mesh and (b) Penetration of PDMS mixed with the hollow glass micro-spheres (20-50 μm) through the copper mesh structure.

3.3.2 Perforated Conductive Sheets

In order to overcome the imprecision issue, perforated thin conductive sheets, for instance copper-bronze, were also considered for the fabrication of flexible antennas. The perforations increase the overall flexibility and allow the free flow of PDMS through the conductive sheet. Compared to the mesh structures, the perforated structures provide higher fabrication precision, but at the same time increase the overall production complexity, as the conducting plate has to be etched or laser cut.

Different arrangements can be used for the perforation process and optimizing the position and shape of the "holes" can bring some advantages to the final structure. For example, hexagon shaped perforations ensure the optimal deployment of the holes over the conductive sheet and at the same time contribute to some miniaturization of the antenna design. Indeed,

hexagon patterns enlarge the current path on the antenna, thus making the antenna electrically larger. A hexagon perforated copper-bronze conductive sheet is presented in Fig. 3.7. The proposed sheet has a thickness of $300\text{ }\mu\text{m}$, while the perforation was done using a classic photo-lithographic etching process. Details regarding the size and spacing of the hexagon perforations will be reported in Chapter 4 along with the concerned antenna prototypes.

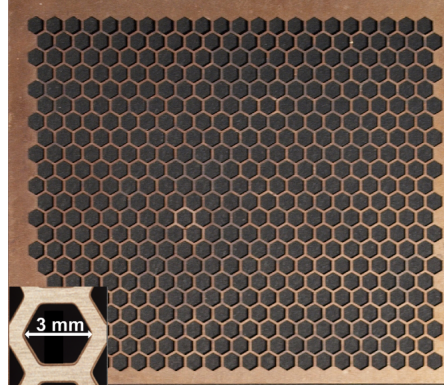


Fig. 3.7: Copper-bronze conductive sheet perforated with hexagonal shapes.

3.4 Technology

This section describes all the steps performed during the fabrication process of a robust flexible antenna built using pure and/or loaded PDMS and copper mesh and/or perforated copper sheets. A simple patch antenna operating at 2.5 GHz is used as an example for the demonstration purposes. For this particular case, fine copper mesh structure was used as a conductor and PDMS loaded with glass micro-spheres as a substrate material.

Simulations and Tailoring - Copper-mesh structures - The antenna was designed and simulated with the commercially available 3D EM full wave software *HFSS* [163]. Once the optimal performance was obtained the dimensions of the antenna were extracted and used for tailoring the fine copper mesh conductive sheet¹. HFSS model of the patch antenna and the 2D sketches with all the dimensions are shown in Fig. 3.8, while Table 3.3 reports the values of all the geometrical parameters.

Since the mesh structure is rather soft, it can be cut with scissors. However, the non-soldered intertwined structure tend to fray on the edges, thus not allowing a full control over the dimensions and shape. One of the solutions can be soldering the edges, as shown in Fig. 3.13 (a), but it is time consuming. Therefore, in order to achieve certain precision, etching is considered as an alternative.

¹For the simulation purposes no mesh structure was used. Instead, just a copper conductive sheet with the same thickness as the mesh and characteristics as indicated in the HFSS materials library. The structure of the mesh is dense enough so that can be considered as a solid conductor.

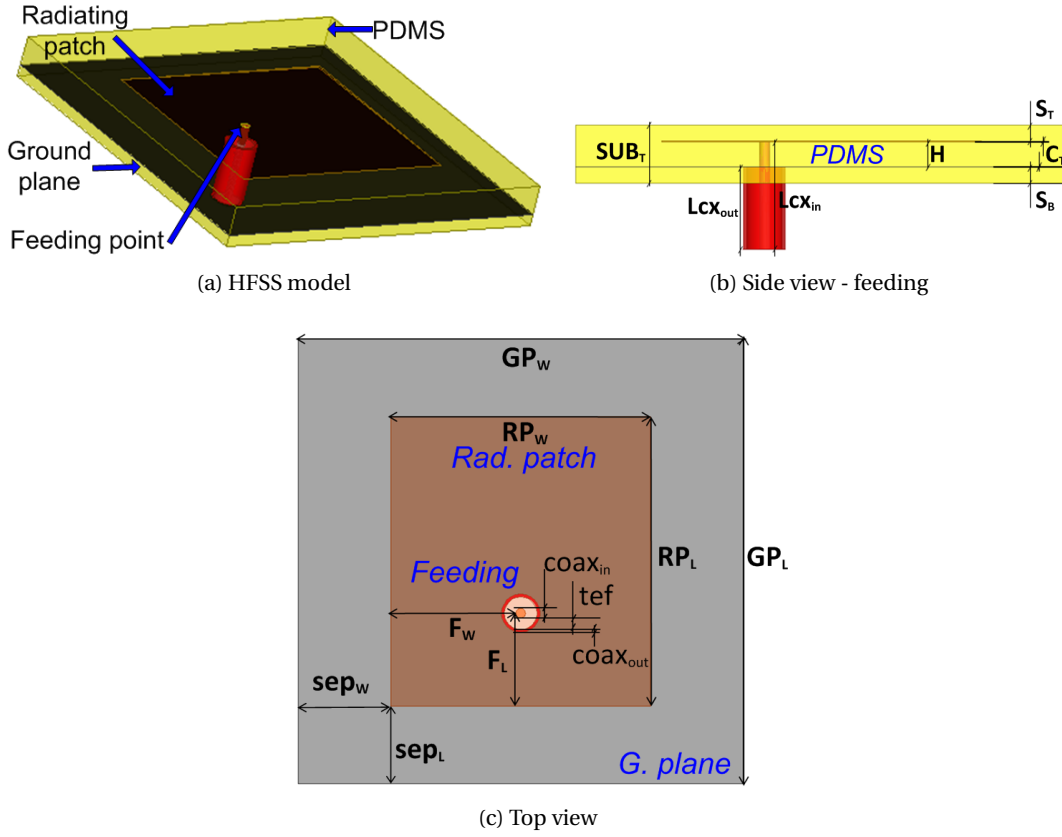


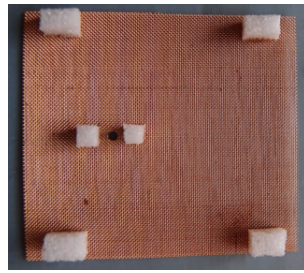
Fig. 3.8: A patch antenna model and 2D sketches of the designed antenna prototype: (a) HFSS model, (b) Side view - coaxial cable feeding and (c) Top view - PDMS, ground plane, patch and position of the feeding.

Parameter	Value [mm]	Parameter	Value [mm]	Parameter	Value [mm]
GP_L	60	F_L	12.5	SUB_T	7
GP_W	60	F_W	17.5	Lcx_{in}	13
RP_L	39	S_B	2	Lcx_{out}	10
RP_W	35	S_T	1	$coaX_{in}$	0.65
sep_L	10.5	C_T	0.035	$coaX_{out}$	2.2
sep_W	12.5	H	3	tef	2.6

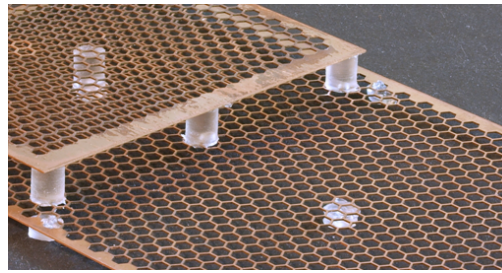
Tab. 3.2: Values of the designed parameters indicated in Fig 3.8.

Simulations and Tailoring - Perforated conductive sheets - For the antennas where the conductors are perforated with etching, preparation and extraction of the file formats require some additional intermediate processing steps. After the design and optimization of the antenna in HFSS, the obtained shapes are further processed in order to produce the etching mask, needed for the photo-lithographic procedure.

Spacing - Both proposed conductors, copper mesh and etched copper-bronze sheet, are thin and flexible. For the antennas that have a ground plane and radiating part, the distance between them should remain constant all the time. For that reason, foam spacers can be used in order to assure the parallelism between the sheets, Fig. 3.9 (a). From the EM point of view, the foam spacers do not affect much the performance of the antenna. Still, since their permittivity and losses are different from the filling materials (i.e. PDMS), certain imprecision might appear. A solution can be found in making the spacers from the same material as the substrate itself, thus avoiding the non-controlled effects. In Fig. 3.9 (b) spacers in a shape of cylinder are produced from the same material as the substrate itself, in this case pure PDMS.



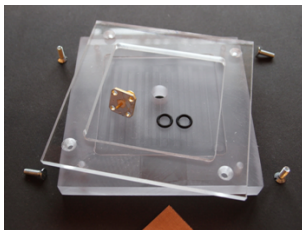
(a) Foam spacers



(b) Spacers in the shape of cylinder fabricated from the same material as the substrate, PDMS

Fig. 3.9: Spacing with different materials.

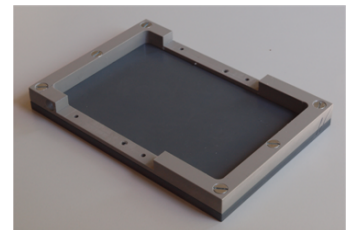
Molds - The initial liquid state of the PDMS requires custom fabricated molds, where all the conductive parts are fixed before they are sprinkled with the elastomer. All the molds are prepared in-house, using a 3D computer-aided design (CAD) software, *Solidworks* [164], for modeling and computerized numerical control (CNC) machines for fabrication. All the molds are fabricated from polyvinyl chloride (PVC). In Fig. 3.10 three different molds, for antennas operating at different frequencies, are presented. For easier extraction of the polymerized antennas, some of the molds are built in modular way, while all the inner parts of the molds are lubricated with vaseline.



(a)



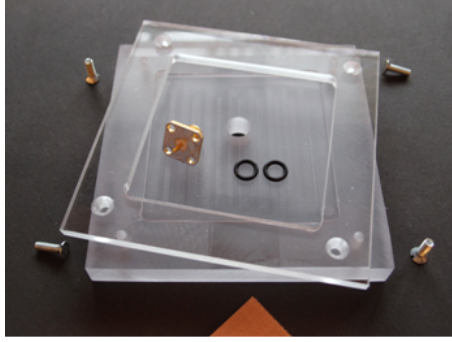
(b)



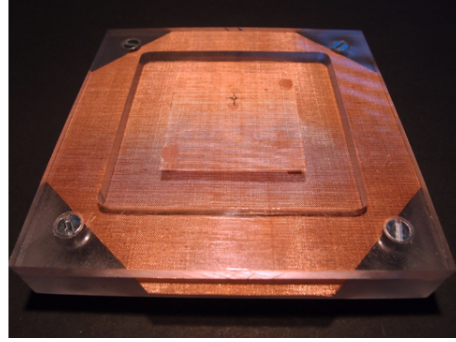
(c)

Fig. 3.10: Custom fabricated molds from PVC for different antenna types operating at different frequencies (a) Patch antenna @ 2.45 GHz, (b) PIFA @ 363 MHz and (c) PIFA @ 385 MHz.

For the concrete design of patch antenna, the mold prototype and the conductive parts of the antenna placed inside the mold are shown in Fig. 3.11, while the 2D sketches and all the dimensions are shown in Fig. 3.12 and Table 3.3, respectively.



(a) Custom in-house designed mold



(b) Conductive parts + connector fixed inside the mold

Fig. 3.11: In-house custom designed mold.

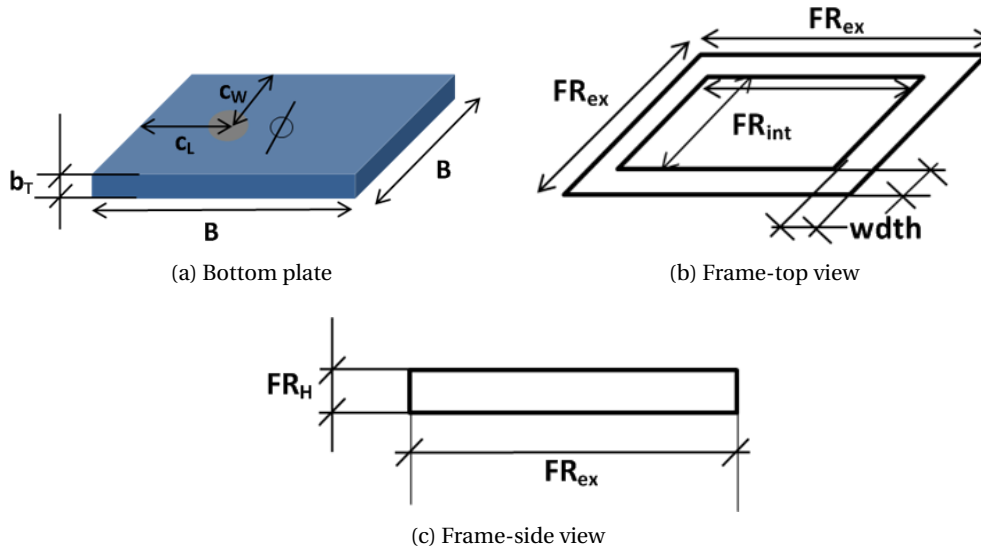


Fig. 3.12: 2D sketches of the designed mold: (a) Bottom plate, (b) Frame - top view and (c) Frame - side view.

One shot sprinkling - It is important that the PDMS is sprinkled at the same time over the entire mold, thus guaranteeing a uniform distribution of the material through the conductors and the mold. Consequently, whenever the antenna type allows, all the conductive parts and the connectors should be soldered and fixed inside the mold before the PDMS is sprinkled, thus providing a stable and uniform distribution, as shown in Fig. 3.11 (c).

Parameter	Value [mm]	Parameter	Value [mm]
B	90	FR_{ex}	90
b_T	10	FR_{int}	60
c_W	45	FR_H	6.7
c_L	38	$width$	15
\varnothing	8		

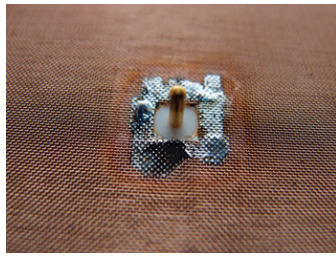
Tab. 3.3: Values of the designed parameters indicated in Fig 3.12.

PDMS preparation - The used PDMS is the Sylgard RTV 184 produced by Dow Corning, which is delivered with precise instructions on how it should be prepared [155]. The kit consists of a base and a curing agent (polymerizer), that need to be mixed in a defined ratio. All the preparations are performed manually in a standard lab environment. Mixing of the base, polymerizer and the fillers was done by hand. Unfortunately, hand mixing process introduces uncontrolled amount of air-bubbles inside the material, that changes the final values of the permittivity and losses. For that reason, degassing is applied.

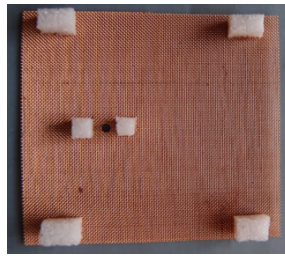
Degassing - The captured air-bubbles were removed by a vacuum pump. Five to six degassing cycles (10 min per cycle) are enough to remove the excessive air. The degassing was applied in two phases, first after the preparation of the PDMS and then once everything was placed and the PDMS was sprinkled inside the mold, see Fig. 3.13 (f) and (h), respectively.

Polymerization - Polymerization of the used PDMS can be done either by exposing the mixture in an oven at temperatures around 80°C, for 3-4 hours or leaving it at a room temperature for two or three days. It should be mentioned that when the mold is placed in the oven, due to the thermal expansion of the PVC, the shape can be slightly changed, resulting in modified antenna's shape and dimensions. For the majority of antennas reported in these thesis, room temperature was used for curing. For the patch antenna presented in this section, oven was used during the curing process.

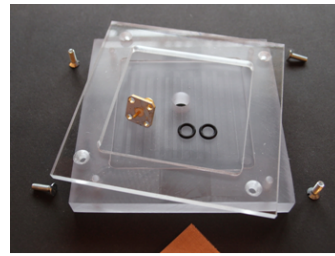
Fig. 3.13 shows all the performed steps during the fabrication procedure of a patch antenna operating at 2.5 GHz.



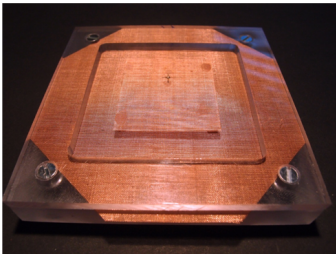
(a) Mesh structure with soldered pin



(b) Foam spacers



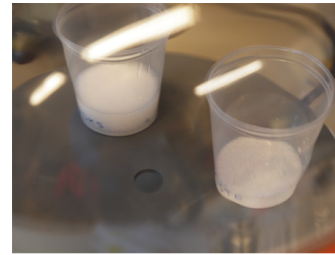
(c) Custom in-house designed mold



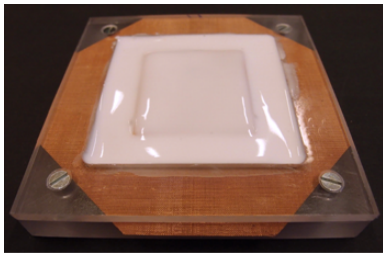
(d) Conductive parts + connector fixed inside the mold



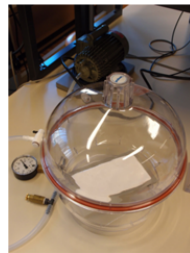
(e) Preparation of PDMS



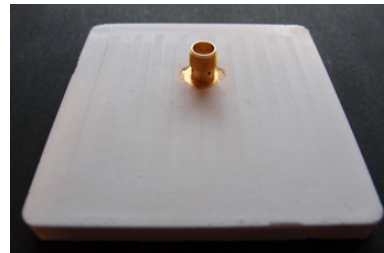
(f) Degassing the PDMS



(g) Sprinkling the PDMS



(h) Degassing the trapped air inside the mold



(i) Final structure, antenna prototype

Fig. 3.13: Fabrication processes, step by step.

3.5 Realized Patch Antenna

After applying all the indicated fabrication steps, the final antenna prototype was extracted from the mold and was ready for measurements. The antenna prototype is shown in Fig. 3.14, from both sides, top and bottom.

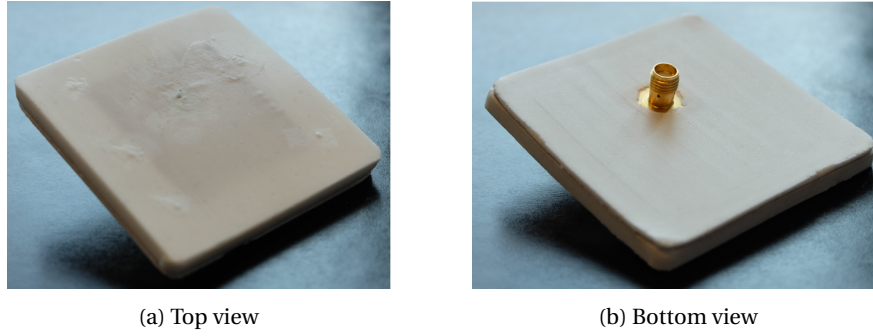


Fig. 3.14: Final patch antenna prototype.

Fig. 3.15 shows a comparison between the predictions (simul.) and experiment (meas.) of $|S_{11}(f)|$ response.

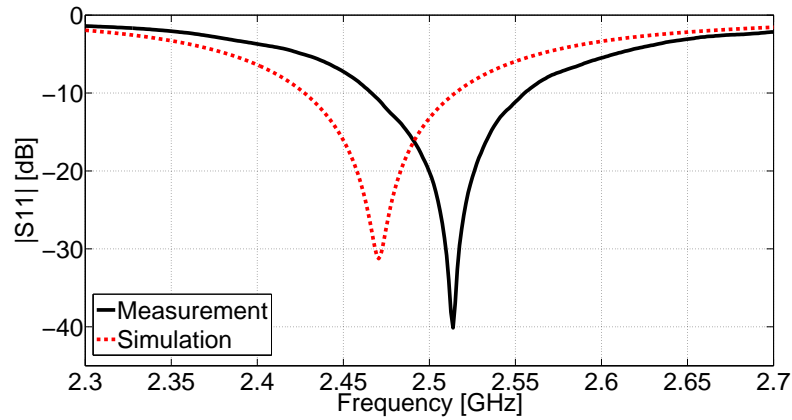


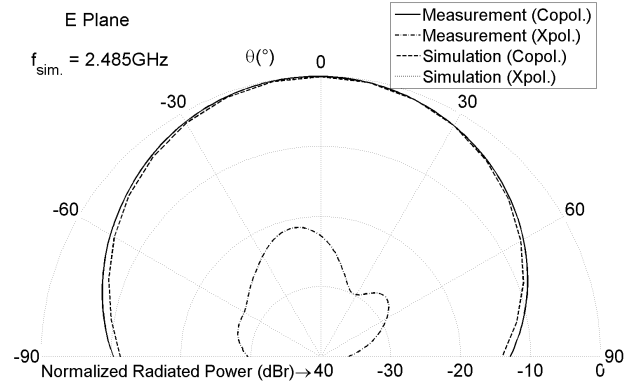
Fig. 3.15: Comparison of simulated and measured $|S_{11}(f)|$ of the patch antenna.

It can be seen from the graph that there is a discrepancy of 40 MHz between the simulation and the experiment. Several reasons can be identified as sources of the observed discrepancy:

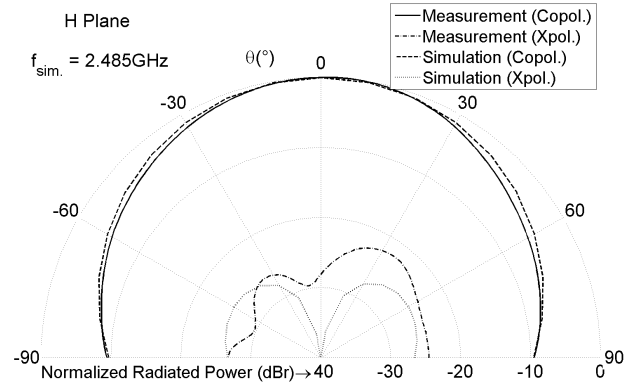
- Difference between the simulated structure (solid conductors used) and actual measured structure (copper-mesh structure used).
- Imprecision due to the copper mesh fraying and soldering.

- Imprecision in the permittivity of the substrate due to the brake of glass micro-spheres.
- Thermal expansion of the mold while curing, resulting in changed final antenna's dimensions.

A second comparison was performed by analyzing the measured and simulated radiation pattern of the proposed antenna. The radiation patterns are represented in two different planes, E-plane and H-plane, by showing the co-polar and cross-polar cuts, see for instance Fig. 3.16. The differences between the prediction and experiment are almost negligible.



(a) E-plane



(b) H-plane

Fig. 3.16: Measured and simulated radiation patterns for the patch antenna: (a) E-plane and (b) H-plane.

As the proposed technology is intended for robust antenna for security applications, we decided to assess the waterproofness and durability of the built prototype by washing it in a washing machine at 60° C for a complete cycle. The antenna placed inside the washing machine is depicted in Fig. 3.17. The visible red cap at the bottom side of the antenna is a protection for the SMA connector. The antenna was washed five times and $|S_{11}(f)|$ were measured after each washing. As can be seen from Fig. 3.18, the deviation between any response is almost negligible, thus validating the waterproof aspect of the proposed technology.



Fig. 3.17: Patch antenna inside the washing machine.

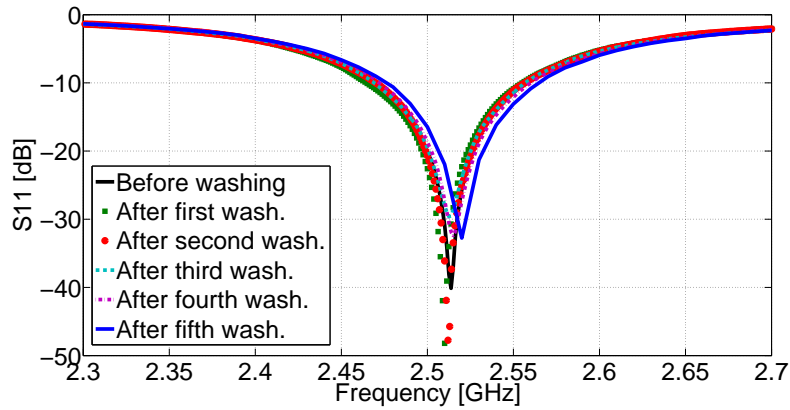


Fig. 3.18: Comparison of the measured $|S_{11}(f)|$ responses of the patch antenna after 5 consecutive washings.

After the fifth washing we observed small abrasions at the antenna's corners and a crack from the top side, see for instance Fig. 3.19. The occurred crack happened because of the thin layer of PDMS above the patch mesh, 1 mm, which was not enough to withstand the fast centrifugal rotations in the five washings. For all the next prototypes, we increased this layer to 2 mm, having from both sides, bottom and top, 2 mm layer of PDMS used as shielding. The abrasions appeared due to the high rotation speed of the washing machine (1200 rpm), thus damaging the edges of the PDMS and the ground plane mesh structure. In order to prevent

this malfunctioning for all the future antenna prototypes we also used 2-4 mm shielding of substrate material around the antenna conductors. In other words, each antenna was at least 2 mm immersed inside the substrate material from any side.



(a) PDMS crack - top side



(b) PDMS abrasions

Fig. 3.19: Condition of the patch antenna after five washing cycles.

3.6 Conclusions

A combination of substrate and conductive materials was presented, analyzed and for demonstration purposes a simple patch antenna prototype was built. The initial liquid phase of PDMS was used for adjustment of its EM properties by adding inclusions with permittivity and losses different from the base substrate. The use of thin, flexible and perforated and/or mesh conductive sheets reinforced the overall flexibility and stability of the structure. Full encapsulation of the conductive sheets resulted in a stable waterproof structure.

A simple patch antenna prototype was built using the proposed technology, reporting the measured $|S_{11}(f)|$ and radiation pattern. Moreover, since the PDMS itself is waterproof, the final prototype was washed and $|S_{11}(f)|$ were measured and compared after each washing. No significant discrepancies were observed in the measured responses. Although some imprecision appeared at certain stages, it should be taken into account that all the performed steps were done in a standard laboratory environment, using standard laboratory equipment. In case of an automatized production, under controlled conditions, the proposed technology can provide sufficiently precise manufacturing, thus making this technology a good candidate for the design and development of robust wearable antennas.

4 Antenna Prototypes

After a successful implementation of the proposed technology and the design of a functional patch antenna, the suggested method was used for further wearable antenna designs. According to the thesis project specifications, the aim was to develop and design robust wearable antenna, operating in ultra high frequency (UHF) range for voice communication intended for security applications. The proposed antennas should have a suitable size, a low profile and be easily integrated into the wearer's garment. From the radiation point of view, the antennas should provide hemispherical like radiation pattern (away from the body) and be minimally coupled to the wearer's body.

Based on the overview and analysis of different antenna families reported in section 2.2 (Antenna families), a Planar Inverted F Antenna (PIFA) was selected as a suitable antenna candidate for the specified requirements. PIFAs are relatively small with the respect to their operating frequency, which make them an appropriate solution for wearable applications. The presence of the ground plane in their structure decouples the antenna from the human body, resulting in improved overall radiation characteristics.

In this Chapter three different antenna prototypes are presented. All the prototypes are intended for voice communication inside the UHF range and they are PIFA based antennas. The antennas are built with the technology introduced in Chapter 3, with slight variations for the different prototypes. An inspiration for the initial antenna's structure was found in [165], while in [166] some further analysis and enhancements were performed. The first built prototype operates at 365 MHz and it was built using a copper-mesh structure as a conductor and PDMS loaded with glass micro-spheres as a substrate. For the second prototype the copper-mesh conductor was replaced by an etched copper-bronze conductive sheet and as a substrate pure PDMS was used instead of the loaded one. The operating frequency of this antenna is 383 MHz. Materials used for fabrication of the third prototype are identical with the second one, whereas the structure of the PIFA is modified by introducing an air gap between

the ground plane and the radiation patch. The role of the air gap is mainly to improve the radiation characteristics of the antenna and by overcoming the near-field effect issues. This antenna also operates around 380 MHz.

For all the three prototypes, a detailed description is provided. Each of the prototypes is explained from the modeling and technological point of view, defining the introduced concepts and providing the dimensions of the modeled and built prototypes. A set of simulations and measurements are shown and compared under different circumstances like free space, on a body phantom, on a chunk of pork meat (mimicking real human muscle) and on a wearer. Additional robustness tests, such as bending of the antennas are performed for the first two prototypes.

4.1 PIFA (Copper-Mesh) Operating at 365 MHz

4.1.1 Antenna Model and Geometrical Parameters

The first built prototype was a PIFA fabricated using a copper-mesh structure as conductor and loaded PDMS as a substrate material. The proposed antenna was modeled and designed in HFSS. For simulation purposes, the ground plane, the radiating patch and the shorting wall were modeled as solid copper conductive sheets, with a thickness of $300\text{ }\mu\text{m}$ and material properties as suggested from the HFSS material library for copper, relative permittivity $\epsilon_r=1$ and bulk conductivity $\sigma=2\cdot 10^7\text{ S/m}$. The substrate was additionally defined in the HFSS material library, using the values obtained from the characterization of the loaded PDMS reported in section 3.2, relative permittivity $\epsilon_r=2.15$ and loss tangent $\tan\delta=0.01$. A full 3D model and detailed 2D sketches of the designed antenna are illustrated in Fig. 4.1 and Fig. 4.2, respectively, while Table 4.1 reports the values of all the geometrical parameters. Position and modeling of the coaxial feeding was done as depicted in Fig. 4.2 (a) and (b), where copper material (HFSS) was used for creating the inner and outer conductor and Teflon having $\epsilon_r=2.1$ and $\tan\delta=0.001$ as a dielectric in between.

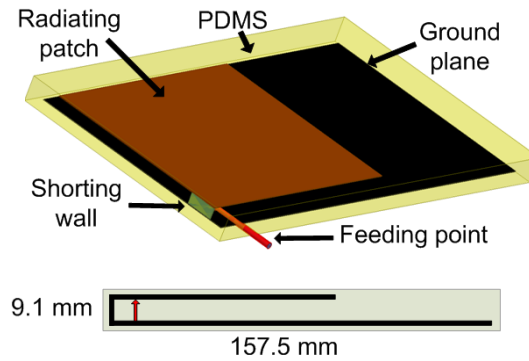


Fig. 4.1: Model of the PIFA modeled in HFSS.

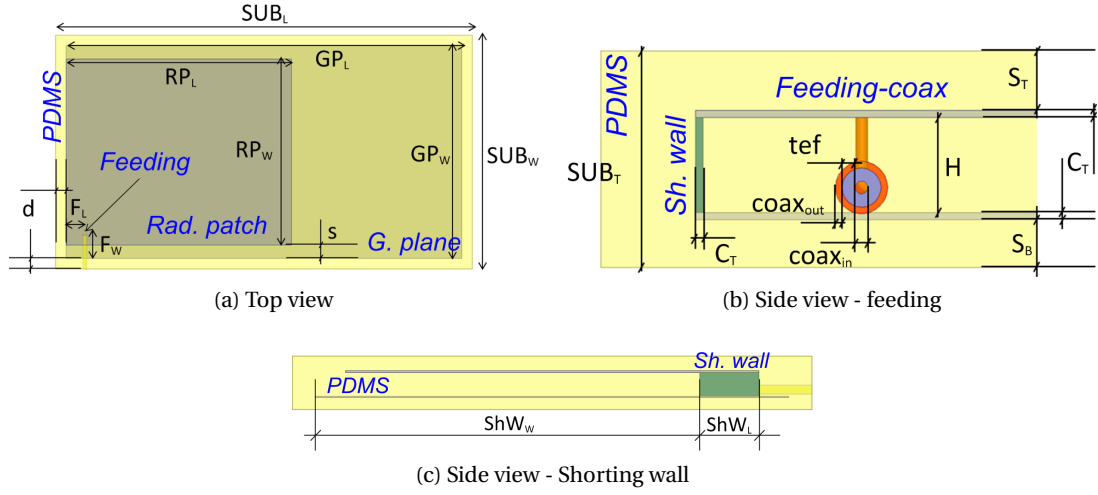


Fig. 4.2: 2D sketches of the designed antenna prototype: (a) Top view - PDMS, ground plane, patch and position of the feeding, (b) Side view - coaxial cable feeding and (c) Side view - Shorting wall.

Parameter	Value [mm]	Parameter	Value [mm]
GP_L	149.4	s	5
GP_W	80	C_T	0.3
RP_L	85	S_T	2
RP_W	70	S_B	2
SUB_L	157.4	H	4
SUB_W	88	$coax_{in}$	0.53
SUB_T	9.1	$coax_{out}$	0.275
F_L	7	tef	1.65
F_W	10.5	ShW_L	10
d	4	ShW_W	65

Tab. 4.1: Values of the designed parameters indicated in Fig 4.2.

4.1.2 Fabrication of the Antenna Prototype

For fabrication purposes, a coarse copper-mesh structure was used as a conductor [162], and PDMS loaded with glass micro-spheres, $\epsilon_r = 2.15$ and $\tan \delta = 0.01$, as a substrate material (already introduced in sections 3.3.1 and 3.2, respectively). The final antenna prototype was built following the fabrication guideline introduced in Fig. 3.13 in Chapter 3. However, several fabrication details can be considered as typical for the considered antenna prototype: soldering of the edges of the selected mesh in order to avoid fraying of the copper strings, introduction and gluing of foam spacers for ensuring the parallelism between the two plates and fixation of the coaxial feeding within the mesh structure (before introducing it inside

the mold). The size and position of the spacers were provisionally determined, placing them mainly on the edges of the radiating patch. All the introduced details are depicted in Fig. 4.3 (a) and (b), respectively.

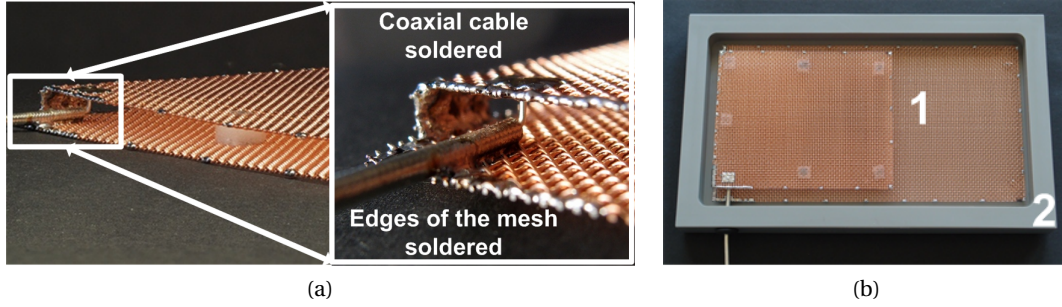


Fig. 4.3: Conductive parts of the copper-mesh PIFA prototype: (a) With introduced spacers and soldered coaxial cable and (b) Placed inside the mold.

The mold used for this antenna prototype was built from PVC material. Details for the designed and fabricated mold are shown in Fig. 4.4, while Table 4.2 reports the values of all the geometrical parameters.

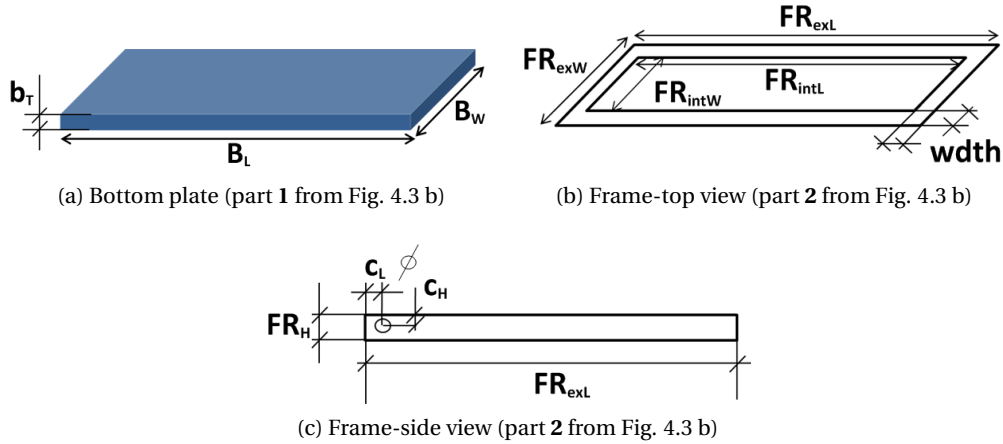


Fig. 4.4: 2D sketches of the designed mold: (a) Bottom plate, (b) Frame - top view, (c) Frame - side view.

The final antenna prototype, having dimensions $157.4 \times 88 \times 9.1 \text{ mm}^3$, is shown in Fig. 4.5. Since the antenna was built of copper-mesh structure, in the continuation of this manuscript it will be referred to as a copper-mesh PIFA. Fig. 4.6 reports a comparison between the predictions (simul.) and experiment (meas.) at the desired frequency. A slight discrepancy (2-3 MHz) that appears between the simulated and measured $|S_{11}(f)|$ of the HFSS model and fabricated antenna prototype is mainly due to the non-complete control over the mesh conductor tailoring and soldering processes and the difference between the dielectric properties of simulated

4.1. PIFA (Copper-Mesh) Operating at 365 MHz

Parameter	Value [mm]	Parameter	Value [mm]
B_L	178	FR_{intW}	88
B_W	108	FR_H	9.1
B_T	5.9	$width$	10
FR_{exW}	178	c_L	14
FR_{exL}	108	c_H	6
FR_{intL}	157.4	\varnothing	8

Tab. 4.2: Values of the designed parameters indicated in Fig 4.4.

and actually used materials. Nevertheless, these initial results provided a good starting point for additional measurements and analysis.

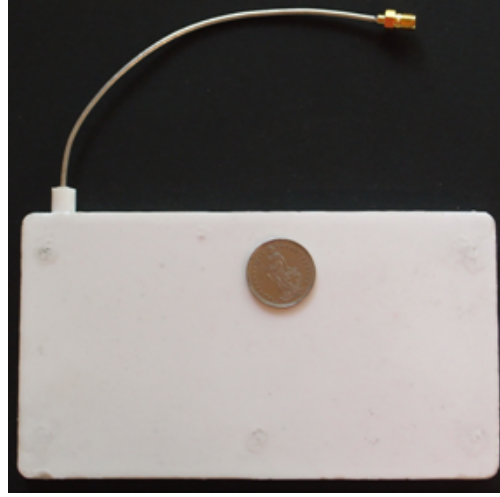


Fig. 4.5: Manufactured copper-mesh PIFA prototype.

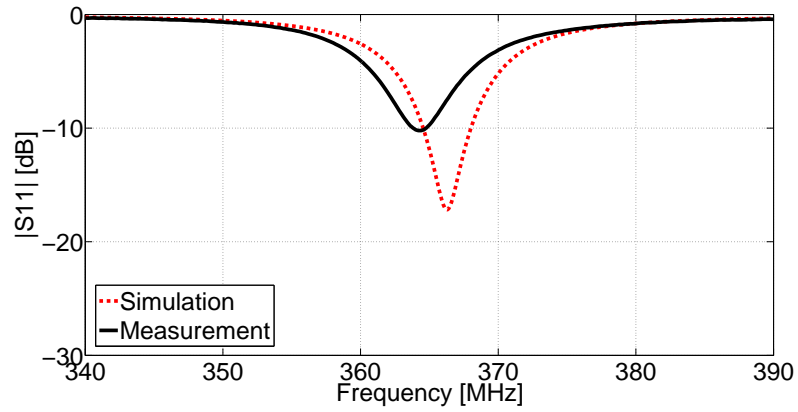


Fig. 4.6: Comparison of simulated and measured $|S_{11}(f)|$ of the copper-mesh PIFA.

4.1.3 Comparison of $|S_{11}(f)|$ Responses for Different Situations

In order to assess the antennas' performance when brought in the vicinity of the human body, a simplified single layer muscle phantom was used for simulation purposes, a chunk of pork meat, mimicking the muscle tissue, for measuring purposes and measurements done directly on a wearer. The phantom used for the simulation mimics the human muscle electric properties at 400 MHz, $\epsilon_r = 56$ and $\tan \delta = 0.6$ [167]. It is a single layer phantom allowing sufficient precision [29, 168], in estimating the proposed antennas' behavior at the defined frequencies. The size of the phantom is $488 \times 566 \times 80 \text{ mm}^3$, large enough to ensure a quarter wavelength margin between the antenna and the phantom edges. The antenna is simulated with 1 mm thick textile material, $\epsilon_r = 1$ and $\tan \delta = 0$, introduced between the phantom and the antenna. The model of the used phantom with the antenna placed on it is depicted in Fig. 4.7. In the continuation of this manuscript, it will be simply referred only as a phantom. The same phantom is used for all the reported antenna prototypes.

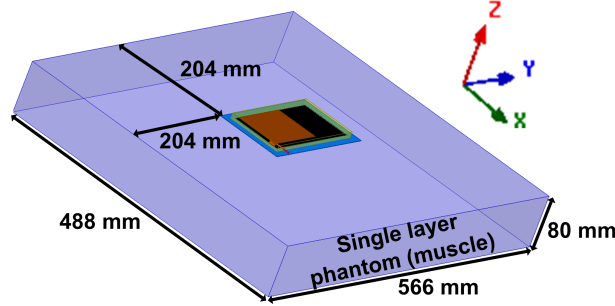


Fig. 4.7: Simplified single layer phantom model designed in HFSS.

For the measurement purposes, 1 kg of pork meat was cut and prepared as shown in Fig. 4.8 (a). The meat was packed in a nylon bag and then placed in a plastic (PVC) box with the following dimensions: $195 \times 110 \times 30 \text{ mm}^3$, Fig.4.8 (b). It can be seen that the size of the meat used for measurement does not correspond to the size of the phantom used for simulation. This is due to the technical limitations of using bulky objects inside the anechoic chamber.



Fig. 4.8: Pork meat used for measurement purposes: (a) Two chunks of pork meat with a layer of fat on the top and (b) Meat packed in a nylon bag and then in a plastic (PVC) box.

In order to evaluate the wearability aspect of the proposed antenna, two measurements were performed for two different scenarios. In the first scenario the antenna was measured while placed on the human arm, whereas in the second scenario the antenna was measured while it was placed on the wearer's chest. For both cases, textile (sweater) was separating the antenna from the human skin. As it can be seen from Fig. 4.9, the antenna remains tuned all the time, without being dependent on the environment where it operates, in a free space or on the wearer. This behavior clearly demonstrates the role of the ground plane in decoupling the antenna from the wearer. Only the matching level changes, which is expected due to the lossy nature of the human body.

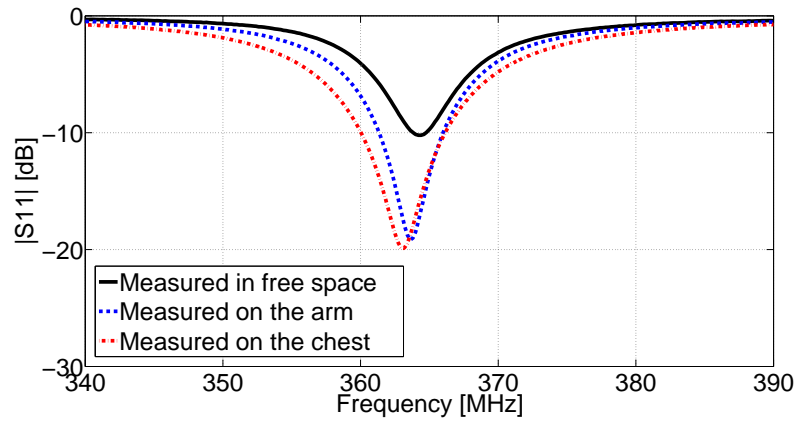


Fig. 4.9: Comparison of measured $|S_{11}(f)|$ of the copper-mesh PIFA in a free space and when placed on the human body.

Additional comparison, where simulations (free space & phantom) and measurements (in free space, on a chunk of pork meat and on-body (Fig. 4.10)) of $|S_{11}(f)|$ is reported in Fig. 4.11. As an illustration, two measurement scenarios, with the antenna placed on the chunk of pork meat and on the human arm, are depicted in Fig. 4.10. The aim of this comparison is to present in the same plot all the possible scenarios that wearable antenna can occur in and to observe its response under the different circumstances. As it can be seen, all five responses remain stable within the defined frequency band, confirming one more time the stable behavior of the tested antenna when exposed in different environments.



Fig. 4.10: Antenna measured on: (a) A chunk of pork meat and (b) On-body, on a human arm.

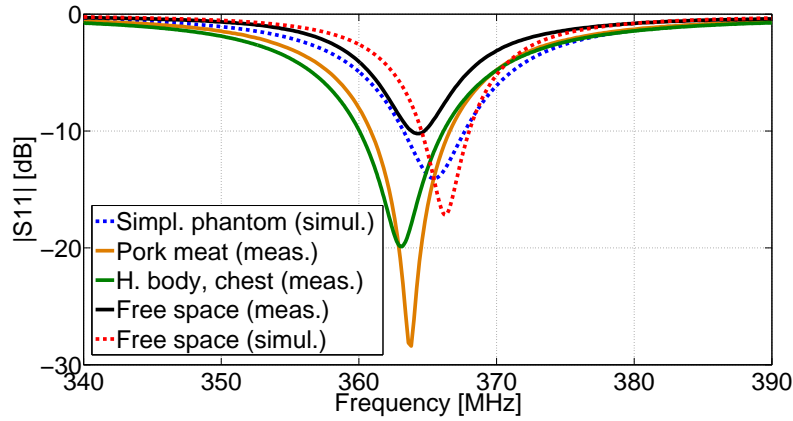


Fig. 4.11: Comparison of simulated and measured $|S_{11}(f)|$ of the copper-mesh PIFA in a free space, on a simplified single layer muscle phantom, on a chunk of pork meat and when placed on the human body.

Flexibility and Bending Characteristics

Both materials used for fabrication of the reported antenna, coarse copper mesh and loaded PDMS, have a certain flexibility. In order to test the flexibility of the final antenna prototype, a set of bending measurements were performed with an in-house designed bending set-up, shown in Fig. 4.12 (a). The set-up consists of two fixed supports at the ends, the antenna is introduced in between, while the bending curvature is changed by introducing a foam spacers with different height in order to achieve different radii. With simple mathematical manipulations and the model proposed in Fig. 4.12 (b), values for the obtained radii, R , can be extracted. A comparison of the measured $|S_{11}(f)|$ when the antenna is bended under different radii is reported in Fig. 4.13. As it can be seen, the maximum frequency deviation is not larger than 2 MHz. Taking into account the length of the antenna (157.4 mm) we have assumed that the tested antenna will not be bended more than a curvature defined by $R=230$ mm.

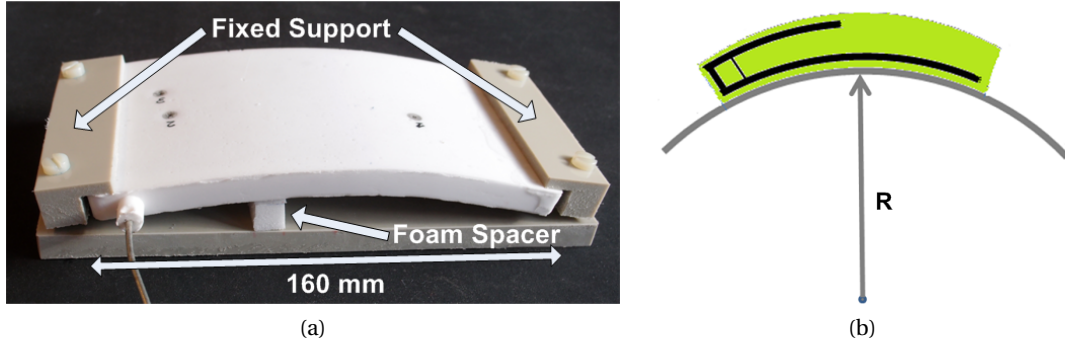


Fig. 4.12: Bending of the PIFA: (a) In-house custom designed bending set-up and (b) Bending skim for determining the radius of the bended curvature.

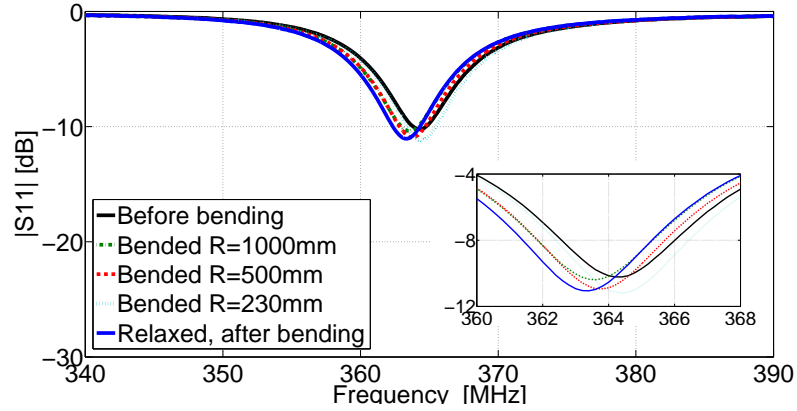


Fig. 4.13: Comparison of measured $|S_{11}(f)|$ of the copper-mesh PIFA when bended under different radii.

Washing

Washing tests were repeated and for the copper-mesh PIFA. In the case of the patch antenna, the antenna was washed four times in a washing machine at 60° C for a complete cycle. The antenna placed inside the washing machine is depicted in Fig. 4.14. The only difference from the patch antenna was the presence of the coaxial cable, instead of the SMA connector. In order to protect the cable and thus the connector on its end from the mechanical damages due to the rotations, the antenna was folded in a tissue and washed like that. The antenna was washed four times and $|S_{11}(f)|$ were measured after each washing. As can be seen from Fig. 4.15, the deviation between any response is almost negligible, thus validating the waterproof aspect of the proposed technology.

Since the layer of PDMS around the conductors was increased by 1 mm from the top side compared to the patch antenna, all the conductive parts were completely immersed inside the PDMS, 2 mm from top and bottom and 4 mm from all the other sides, thus preventing the antenna from mechanical damages like breaking and abrasions.

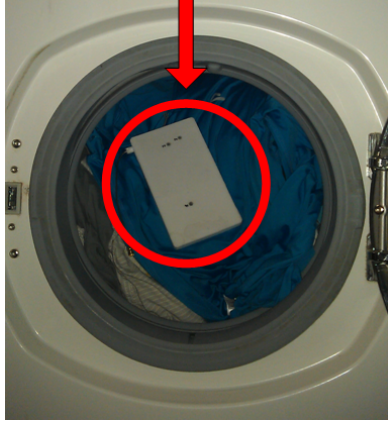


Fig. 4.14: Copper-mesh PIFA inside the washing machine.

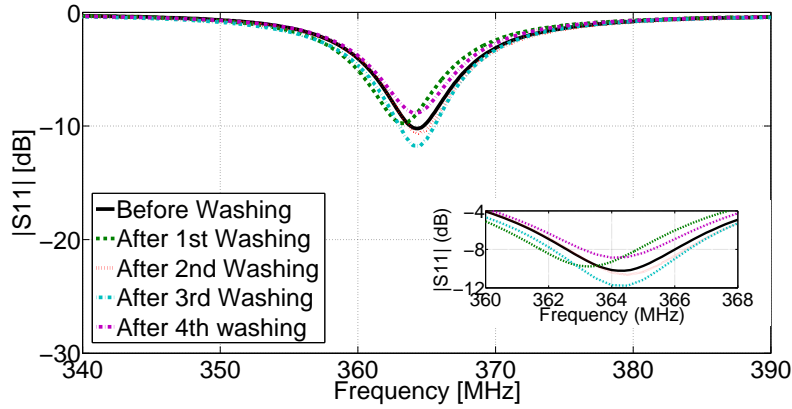


Fig. 4.15: Comparison of the measured $|S_{11}(f)|$ responses of the copper-mesh PIFA after 4 consecutive washings.

4.1.4 Radiation Pattern and Gain

This section reports the computed and measured radiation patterns and gain of the copper-mesh PIFA. Computed radiation patterns are done with HFSS, for two different scenarios, antenna in free space and antenna placed on the phantom. The measurement of the radiation patterns was performed in the laboratory's anechoic chamber, depicted in Fig. 4.16. The size of the chamber, $4 \times 2.5 \times 3 \text{ m}^3$ is at the lower limits for characterizing antennas around 400 MHz. Also, the used pyramid absorbers (45 cm) inside the chamber are not providing an optimal attenuation at the considered frequency. Yet, as it can be further seen in this section, simulated and measured patterns fairly correspond. Measurements of the radiation patterns were also performed for two different scenarios, the antenna under test (AUT) characterized in free space and the AUT characterized when placed on a chunk of pork meat placed inside a plastic box (Fig. 4.8).

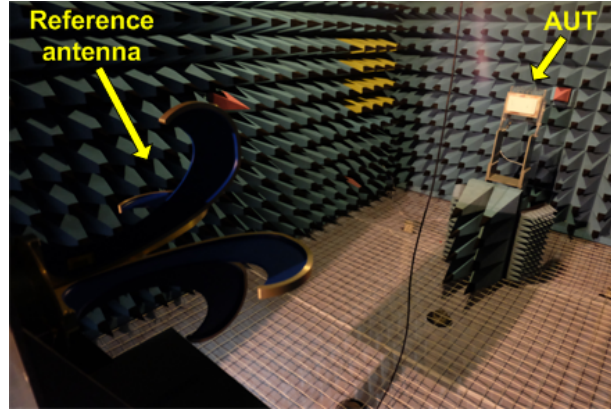


Fig. 4.16: Inside the anechoic chamber.

The simulated radiation patterns and the computed gain for an antenna in free space and antenna placed on a simplified phantom are depicted in Fig. 4.17 (a) and (b), respectively. As can be seen from the reported patterns, when the antenna is in a free space, the simulated radiation pattern is similar to the one of a dipole antenna, indicating that certain radiation appears because of the contribution from the ground plane. For the case when the antenna is placed on the phantom, the back radiation is significantly suppressed and the antenna exhibits a hemispherical like radiation pattern. This is a desirable radiation pattern for the situations when the antenna is placed on the wearer's chest or back, thus providing wide radiation coverage away from the wearer. The simulated gain values and radiation efficiencies (@ 365 MHz), as computed by HFSS, for the antenna placed in free space and placed on the phantom, are -6.99 dBi and -9.19 dBi for the gain and 15% and 4.7% for the efficiency, respectively.

The simulated values for the gain are rather low, which is actually due to the used loaded PDMS as a substrate. The latter has non-negligible losses, $\tan \delta = 0.01$ and the losses from the solid conductor, copper in our case, also contribute to lowering the gain. For the case with the phantom, additional losses are introduced from the phantom itself, resulting in even lower gain and efficiency.

Inside the anechoic chamber the AUTs were characterized and measured under two different scenarios. For the first scenario, the AUT is in a free space, while for the second the AUT is placed on a chunk of meat. Fig. 4.18 illustrates the described scenarios. For each scenario the antennas were characterized for two different orientations, orientation marked as a $\Phi=0^\circ$ and orientation marked as a $\Phi=90^\circ$, see for instance Fig. 4.19. For each orientation two different cuts were measured, $\Phi=0^\circ$ cut (XZ-plane) and $\Phi=90^\circ$ cut (YZ-plane). Simulated and measured radiation patterns for the copper-mesh PIFA are reported in Fig. 4.20.

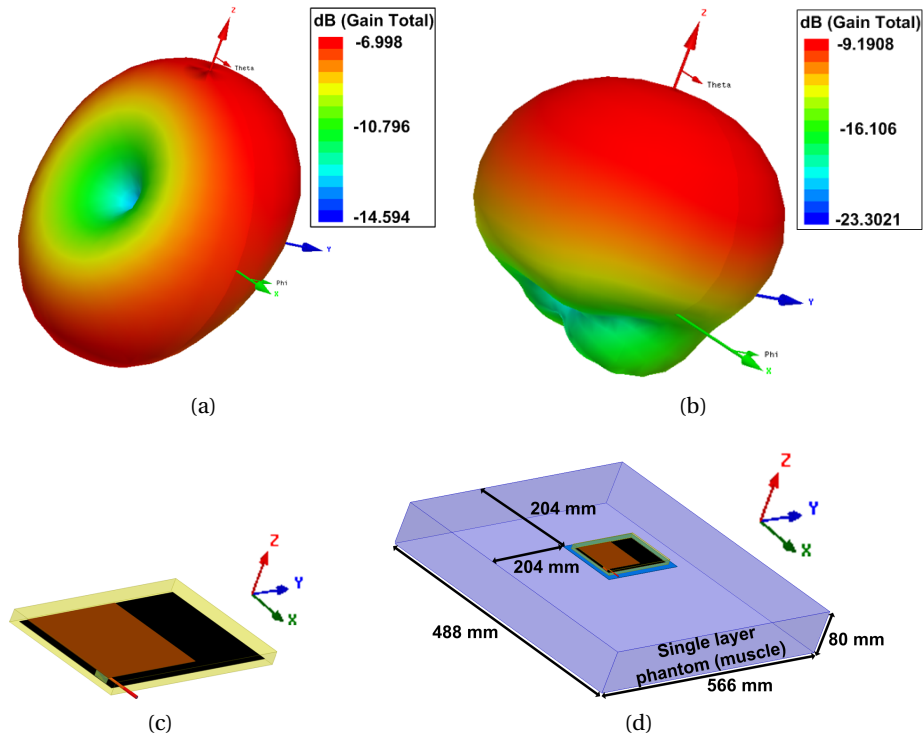


Fig. 4.17: Simulated radiation pattern and computed gain of the copper-mesh PIFA (with HFSS @365 MHz): (a) In free space, (b) On a simplified phantom, (c) Antenna orientation and (d) Orientation of the antenna when placed on the phantom.

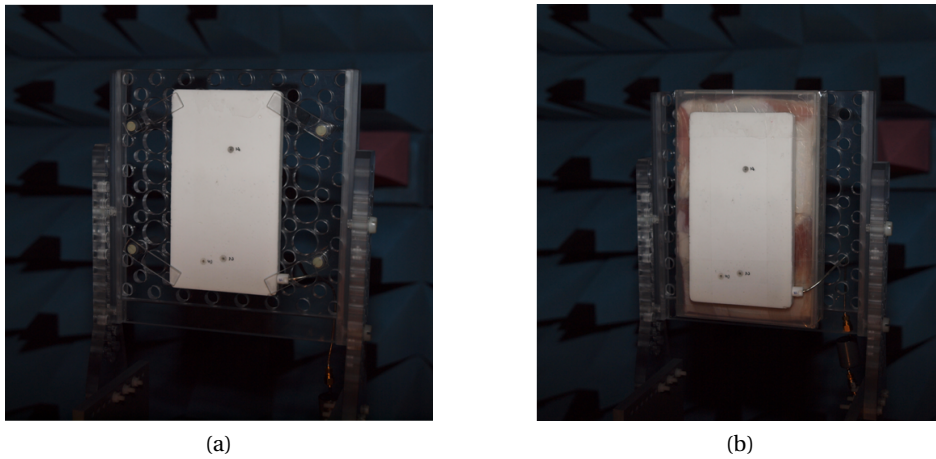


Fig. 4.18: AUT inside the anechoic chamber: (a) In free space and (b) On a chunk of pork meat placed inside the plastic box.

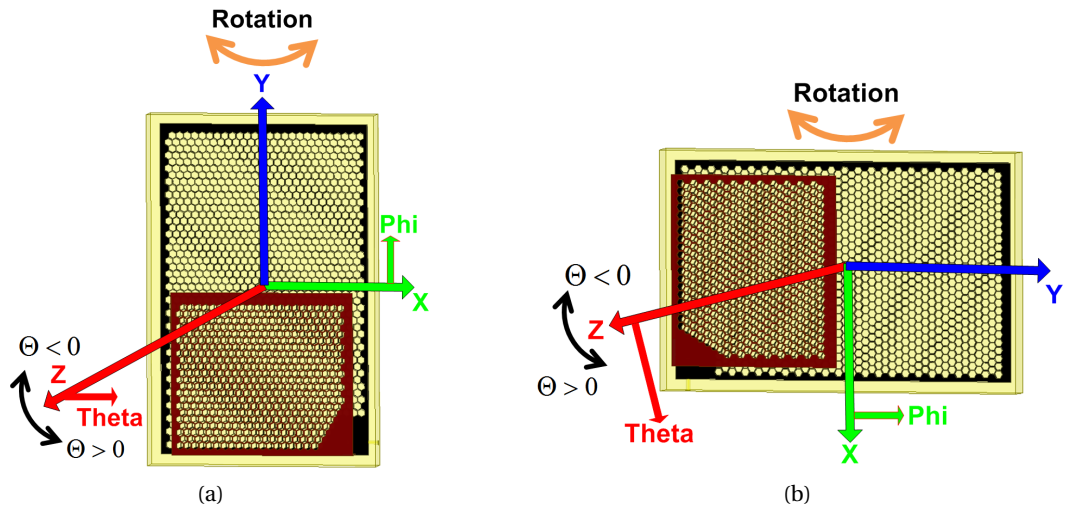


Fig. 4.19: Orientation of the AUT while measuring the radiation pattern inside the anechoic chamber:
 (a) Orientation of the antenna for the case $\Phi=0^\circ$ and (b) Orientation of the antenna for the case $\Phi=90^\circ$.

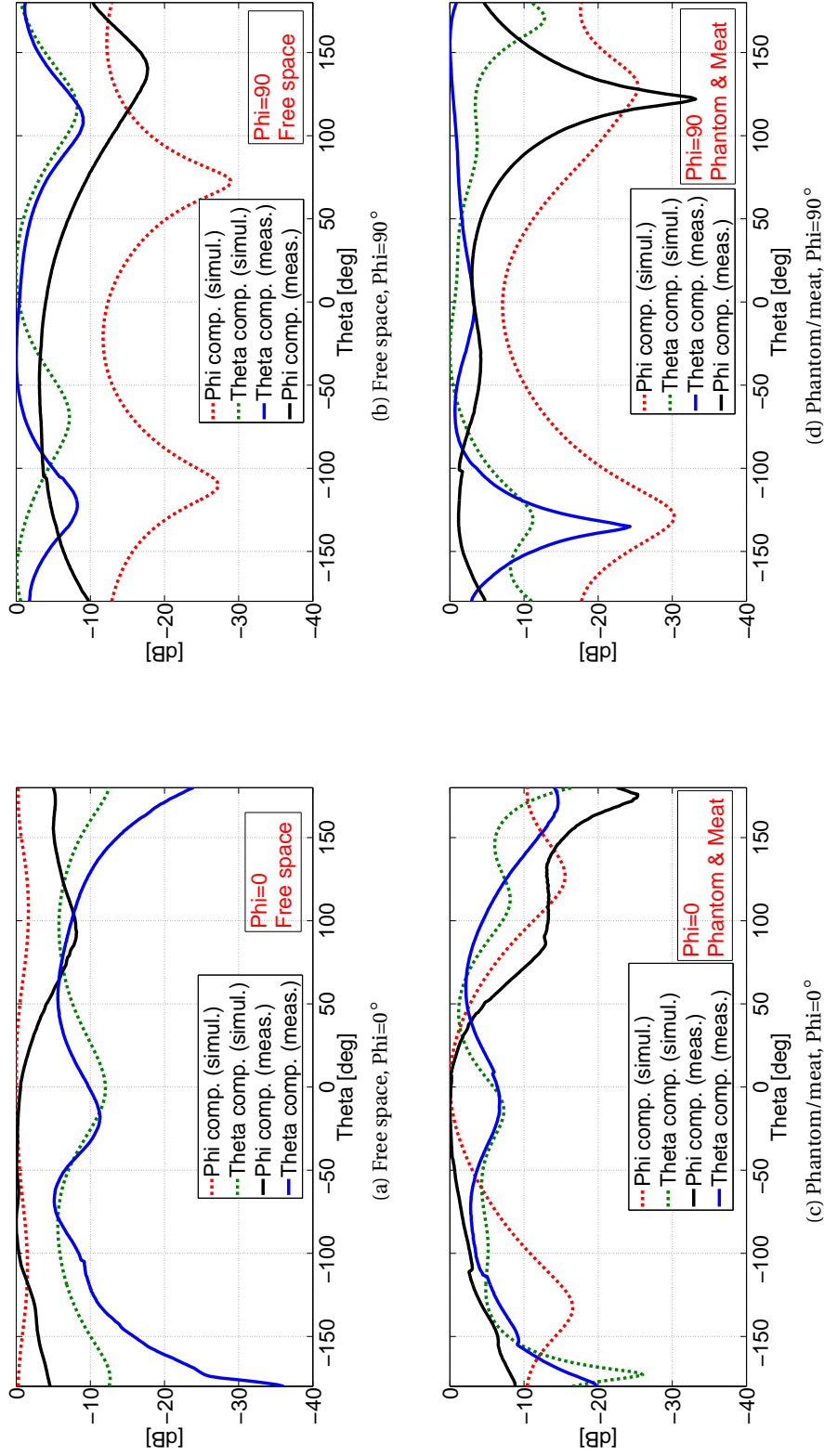


Fig. 4.20: Measured and simulated radiation patterns for the copper-mesh PIFA (@365 MHz): (a) AUT in free space, $\Phi=0^\circ$, (b) AUT in free space, $\Phi=90^\circ$, (c) AUT on a phantom/meat, $\Phi=0^\circ$ and (d) AUT on a phantom/meat, $\Phi=90^\circ$.

After analyzing the simulated and measured radiation pattern cuts, one can notice that the antenna does not have a pure polarization, as co- and cross-polar components have similar levels.

Although the measured and simulated radiation patterns fairly match, some discrepancies still appear. Due to the low directivity of the AUT, the smallest objects inside the anechoic chamber contribute to the overall radiation pattern. During the performed measurements a ferrite choke was used in order to prevent the unwanted currents on the connecting cables. Still, some reflections occurred from the cable and they contributed to the measured radiation pattern.

For the case where the AUT is measured on a chunk of pork meat placed inside the plastic box, this phenomena is less emphasized because the antenna is becoming more directive and small objects do not have such a big influence. Another important remark is that the size of the simplified phantom used for simulation and the chunk of pork meat used for measurement are not identical, thus resulting in some differences when comparing the radiation patterns.

Maximum Measured Gain

The analysis performed for the radiation patterns helped us to calculate the measured gain of the antenna. The obtained gain values for the both scenarios are reported below:

- Antenna in free space, Gain=-8.42 dBi
- Antenna placed on a chunk of pork meat, Gain=-12.7 dBi

4.1.5 Conclusions

The copper-mesh PIFA was the first realized antenna prototype, intended for the UHF band. The antenna was realized by combining flexible copper-mesh conductive sheets and loaded PDMS as a substrate. All the performed tests and measurements in different environments and under different circumstances confirmed the robust nature of the proposed antenna. The robustness of the antenna against the mechanical deformations was tested by bending it and observing the deviations of the $|S_{11}(f)|$ response. The antenna remained stable, with only 2 MHz of the frequency deviation at the desired band.

Communication robustness of the antenna was tested through the measurements performed on a chunk of a pork meat and directly on the body. In both cases the $|S_{11}(f)|$ response of the antenna remained stable in terms of operating frequency, while only the level of the input matching changed, which was expected due to the lossy nature of the meat and the human

body. A hemispherical radiation pattern validates the suitability of this antenna for wearable applications, allowing for the antenna to be mounted either on wearer's chest and/or back.

Two main drawbacks were identified while dealing with the reported antenna, the imprecision appearing due to the nature of the copper-mesh structures and a rather low antenna's efficiency and gain. These are actually the two directions in which the attention was focused for the next two antenna prototypes.

Table 4.3 summarizes the simulated and measured gain and radiation efficiency of the copper-mesh PIFA.

Copper-mesh PIFA @ 365 MHz	Free Space		Phantom/Meat	
	Gain [dBi]	η [%]	Gain [dBi]	η [%]
Simulation	-6.99	15	-9.19	4.7
Measurement ^a	-8.42	NA	-12.7	NA

Tab. 4.3: A summary of the simulated and measured gain and radiation efficiency of the copper-mesh PIFA (@365 MHz).

^aThere are no available measured values for the radiation efficiency.

4.2 PIFA (Hexagon) Operating at 385 MHz

The results reported from the performance of the copper-mesh PIFA provided a good base for further development and enhancement of the proposed technology and antenna prototypes. The main focus of the future research was directed towards resolving the issue of the imprecision (copper mesh and substrate permittivity and losses) and improving the overall antenna's radiation characteristics. An alternative solution was provided for fabricating the conductive parts, while the improvement of the radiation characteristics was approached by modifying the antenna structure and changing some parameters.

Instead of the copper-mesh structures, perforation of conventional conductive sheets was considered. The perforation process is fast and precise because it can be automatized, both for laser cut or for a classic photo-lithographic etching process. Still, this automatized process also increases the price of the product. Details about the shapes used for perforation and how it was done were already introduced in section 3.3.2. In our case copper-bronze sheet, with a thickness of 300 μm was used as a base for fabricating the conductive parts.

The choice of the substrate material was also reconsidered. Instead of a PDMS loaded with glass micro-spheres, pure PDMS was used. There were several reasons for this. Among them we found that the loaded PDMS resulted in a reduced flexibility and that also introduced some

uncertainties in the final permittivity and loss tangent values (non-controlled standard lab environment), which was an additional reason to try different alternatives for the substrate material. Moreover, since the PDMS is fully transparent, it allows one to see the interaction between the conductive parts and the substrate. The entire structure can be observed from any side.

In order to improve the overall radiation characteristics, some modifications were applied to the antenna's structure. The distance between the ground plane and the radiating patch was increased by 2 mm, compared to the copper-mesh antenna, thus enlarging the high density near-field region of the antenna, which on the other side resulted in improved radiation efficiency and gain.

4.2.1 Antenna Model and Geometrical Parameters

The second built antenna prototype was the PIFA intended to operate around 385 MHz (Tetrapol band [10]). The proposed antenna was modeled and designed in HFSS. For simulation purposes, the ground plane, radiating patch and the shorting wall were modeled from solid copper conductive sheets perforated with hexagons, with a thickness of 300 μm and material properties as suggested from the HFSS materials library for copper, relative permittivity $\epsilon_r=1$ and bulk conductivity $\sigma=2 \cdot 10^7$ S/m. The substrate material, intended to be a pure PDMS, was defined as an external material in HFSS material library with the following electric properties, relative permittivity $\epsilon_r=2.8$ and loss tangent $\tan \delta=0.006^1$.

A full 3D model and detailed 2D sketches are illustrated in Fig. 4.21 and Fig. 4.22, respectively, while Table 4.4 reports the values of all the geometrical parameters. Detailed dimensions of the hexagon shapes used for the perforation are depicted in Fig. 4.22 (d). The size of the hexagons, 3 mm in diameter, is very small compared to the wavelength ($\lambda_0/250$), thus not affecting performance of the antenna from the EM point of view. Positioning and modeling of the coaxial feeding was done as shown in Fig. 4.22 (a) and (b), where copper was used for modeling the inner and outer conductor and Teflon, $\epsilon_r=2.1$ and $\tan \delta=0.001$ as a dielectric in between.

¹The used value for the loss tangent slightly differs from the value measured in Chapter 3, mainly due to the fact that we were not able to characterize the material at the desired frequencies, but slightly above.

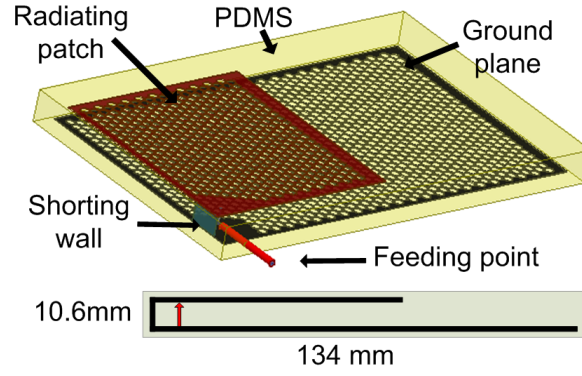


Fig. 4.21: Model of the PIFA modeled in HFSS.

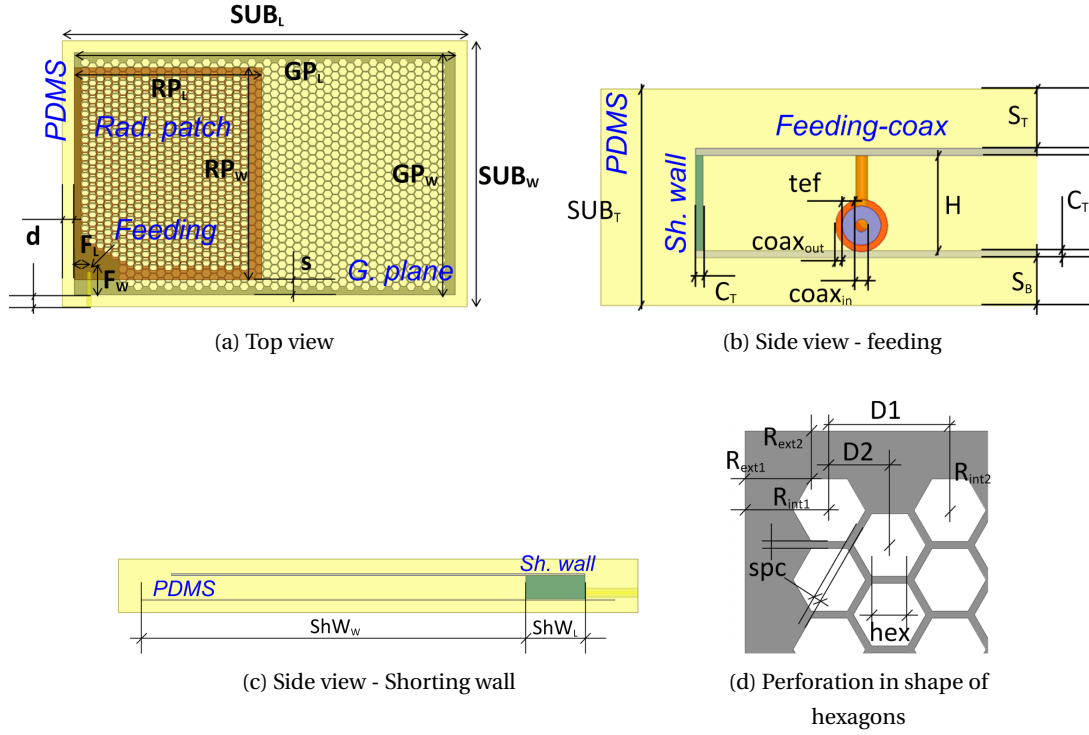


Fig. 4.22: 2D sketches of the designed antenna prototype: (a) Top view: PDMS, ground plane, patch and position of the feeding, (b) Side view - coaxial cable feeding, (c) Side view - Shorting wall and (d) Perforations applied on the ground plane and radiating patch.

4.2. PIFA (Hexagon) Operating at 385 MHz

Parameter	Value [mm]	Parameter	Value [mm]	Parameter	Value [mm]
GP_L	126	s	5	R_{ext1}	2.75
GP_W	80	C_T	0.3	R_{ext2}	2
RP_L	62	S_T	2	R_{int1}	3.5
RP_W	70	S_B	2	R_{int2}	3.3
SUB_L	134	H	6	D_1	5.02
SUB_W	88	$coax_{in}$	0.53	D_2	2.51
SUB_T	10.6	$coax_{out}$	0.275	hex	1.5
F_L	4.8	tef	1.65	spc	0.3
F_W	9.5	ShW_L	10		
d	4	ShW_W	65		

Tab. 4.4: Values of the designed parameters indicated in Fig 4.22.

Simulating the Perforated Conductive Sheets

At first glance, the choice of the hexagon shape for perforation might seem complex and time consuming for the analysis and simulation in HFSS. After comparing the time needed for simulating an antenna with solid conductors and antenna with hexagon perforated conductors, the difference was 3-4 hours longer for the hexagon structure ². As an illustration, the mesh generated by HFSS for the radiating patch at the frequency of interest, 383 MHz, is depicted in Fig. 4.23. Three different areas are emphasized, around the feeding (1), in the center of the patch (2) and at the upper right corner (3). As expected, the regions around the feeding (1) and at the edges (3) are the most dense ones, while the region (2) shows a rather regular mesh.

²HFSS ver. 14, Windows 64-bit operating system, processor i7 and 16 GB RAM.

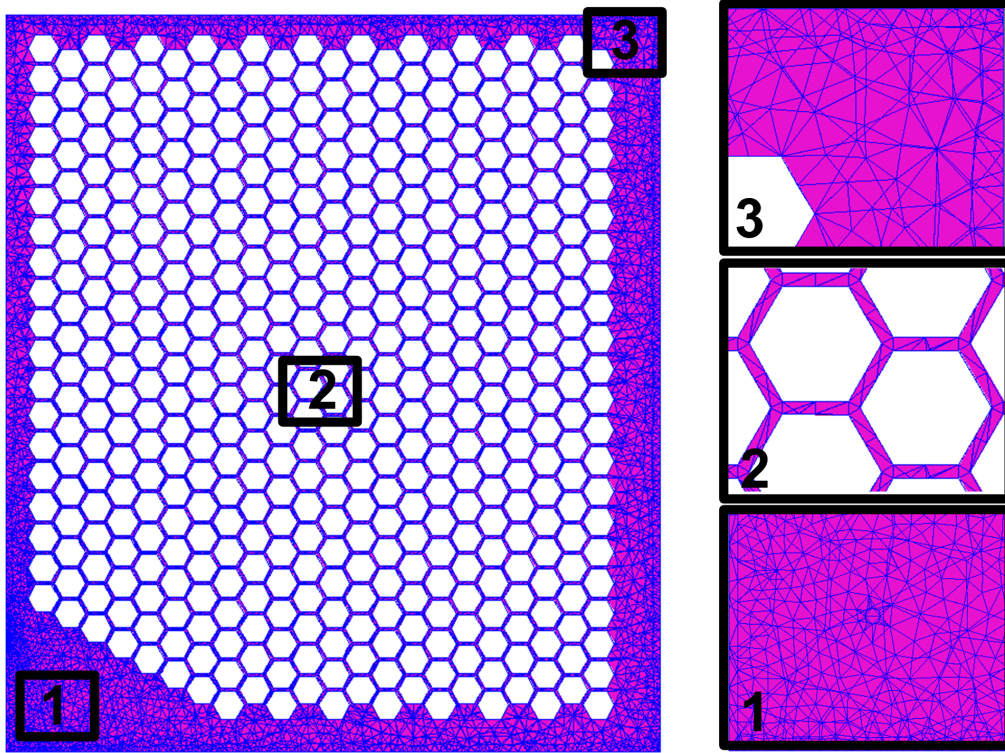


Fig. 4.23: Mesh generated by HFSS on the radiating patch at 383 MHz.

4.2.2 Fabrication of the Antenna Prototype

A copper-bronze sheet with a thickness of $300\ \mu\text{m}$ perforated by a classic photo-lithographic etching process and a pure PDMS (Sylgard RTV 184 [155]), $\epsilon_r = 2.8$ and $\tan \delta = 0.006$, as a substrate material were selected for the fabrication of the antenna prototype. The process of the production followed the same fabrication guideline introduced in Fig. 3.13 in Chapter 3.

A brief explanation on the classic photo-lithographic etching process follows. Based on the final antenna model in HFSS, with all the dimensions and characteristics, an etching mask was created. In order to create the mask, and to make the whole etching process more straightforward, all the conductive parts of the antenna were "opened", as depicted in Fig. 4.24 (a). Since we have used solid copper-bronze conductive sheet, two almost identical masks were created, and the sheet was sandwiched between them. With this kind of constellation the acid corroded the sheet from both sides equally, and reduced the time needed for the etching at half.

Another advantage of the double sided etching was the possibility of creating the bending grooves, as shown in Fig. 4.24 (a). For the proposed antenna, the size of the shorting wall and thus the bending are very sensitive and precise execution was needed. By using the double

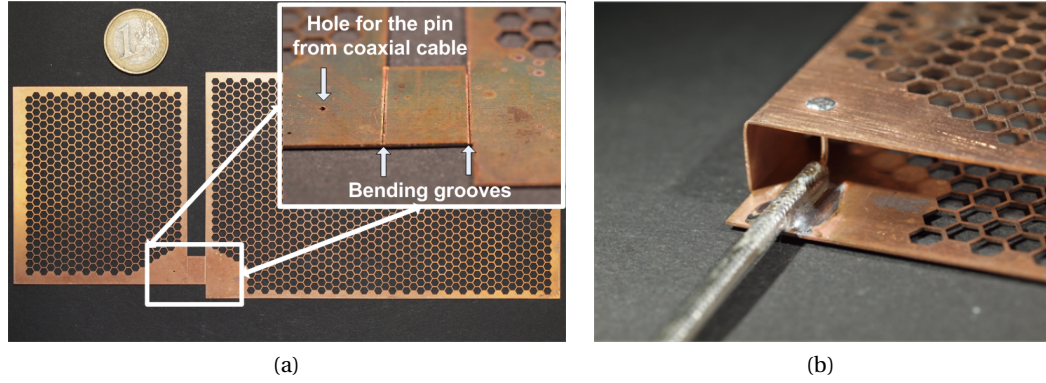


Fig. 4.24: Conductive parts of the wearable PIFA prototype: (a) Conductive parts after the etching process and (b) Coaxial cable fixed and soldered.

side etching, on one of the masks we left the gaps for the bending grooves, so that during the etching process (double side exposure), the grooves were etched only until the half of the copper-bronze sheet thickness, thus allowing easy and precise bending.

The position of the feeding is also very sensitive for the proposed antenna type. In order to fix the inner coaxial pin at the desired position, in the etching mask we defined the hole for the pin, so that the fixation and soldering of the pin would not create additional uncertainties.

Fig. 4.24 (b) shows all the conductive parts bended and the semi-flexible coaxial cable fixed and soldered before introducing the full structure inside the custom prepared mold. Compared to the copper-mesh antenna, the spacers used for this antenna prototype were produced using pure PDMS. The spacer have a cylindrical shape, 6 mm in height and 3 mm in diameter, they were placed and glued mainly on the edges of the antenna and one in the center of the radiating patch, as depicted in Fig. 4.25 (a).

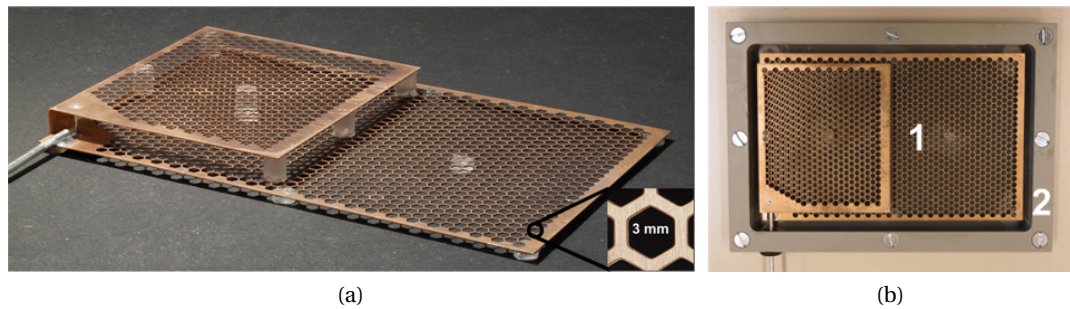


Fig. 4.25: Conductive parts of the hexagon PIFA prototype: (a) Conductive parts bended, coaxial feeding soldered and spacers introduced and (b) Placed inside the mold.

Chapter 4. Antenna Prototypes

The mold used for this antenna prototype was also built from the PVC material with all the detailed sketches and values of the geometrical parameters reported in Fig. 4.26 and in Table 4.5, respectively.

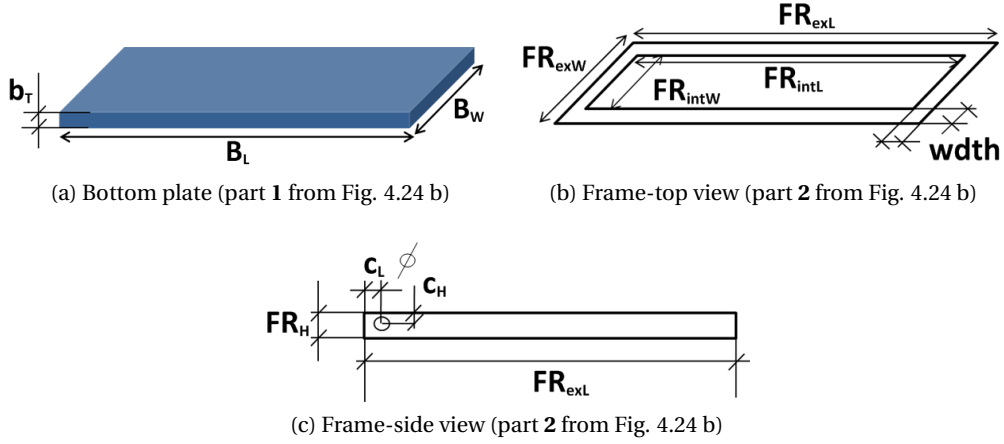


Fig. 4.26: 2D sketches of the designed mold: (a) Bottom plate, (b) Frame - top view and (c) Frame - side view.

Parameter	Value [mm]	Parameter	Value [mm]
B_L	154	FR_{intW}	88
B_W	107	FR_H	10.6
B_T	6	$width$	10
FR_{exW}	154	c_L	9
FR_{exL}	107	c_H	5
FR_{intL}	134	\varnothing	8

Tab. 4.5: Values of the designed parameters indicated in Fig 4.26.

The final antenna prototype, with the size $134.4 \times 88 \times 10.6 \text{ mm}^3$, is depicted in Fig. 4.27 (b). Since the antenna was built out of conductors perforated by hexagonal shapes, in the continuation of this manuscript it will be referred to as a hexagon PIFA. A comparison of the predictions (simul.) and experiment (meas.) of $|S_{11}(f)|$ is reported in Fig. 4.28. One can see that the discrepancy between the simulated and measured responses is significantly reduced compared to the copper-mesh PIFA and it is within 1 MHz, thus justifying the proposed technology both in terms of simulation and fabrication precision for the considered antenna design.

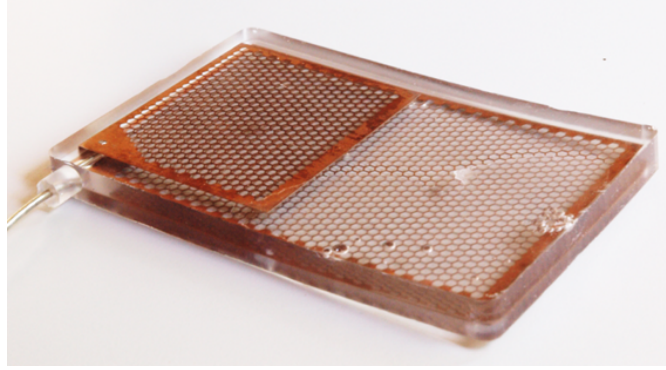


Fig. 4.27: Manufactured hexagon PIFA prototype.

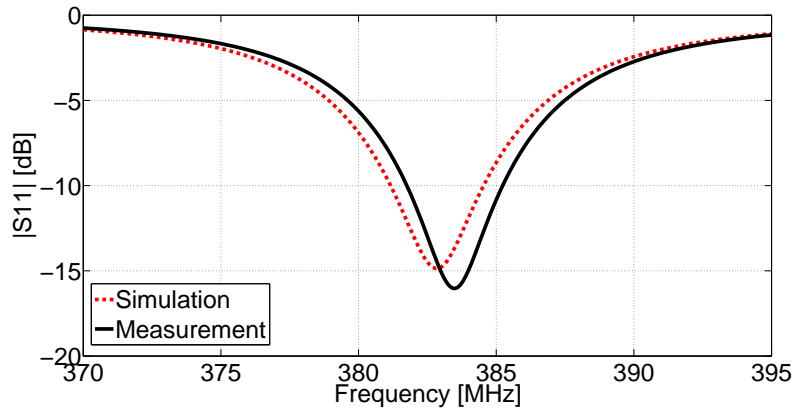


Fig. 4.28: Comparison of simulated and measured $|S_{11}(f)|$ of the hexagon PIFA.

4.2.3 Comparison of $|S_{11}(f)|$ Responses for Different Situations

All the simulated and measured results for the hexagon PIFA will be presented in a similar manner to the copper-mesh PIFA. The phantom model and the chunk of pork meat described in section 4.1.3 were used for the simulation and measurement purposes and for the hexagon PIFA.

A set of $|S_{11}(f)|$ simulations and measurements were performed when the antenna was in free space (simul. & meas.), placed on the phantom (simul.), placed on the chunk of pork meat (meas.), and placed on a wearer (meas.). As an illustration, two measurement scenarios, with the antenna placed on the chunk of pork meat and on the human arm are depicted in Fig. 4.29.

It can be seen in Fig. 4.30 that the antenna stays tuned all the time, no matter whether it is in free space or at any part of the body, thus demonstrating again the effect of the ground plane in decoupling the antenna from the wearer. One should notice that although the hexagonal perforations are larger compared to the apertures of the coarse mesh structure,

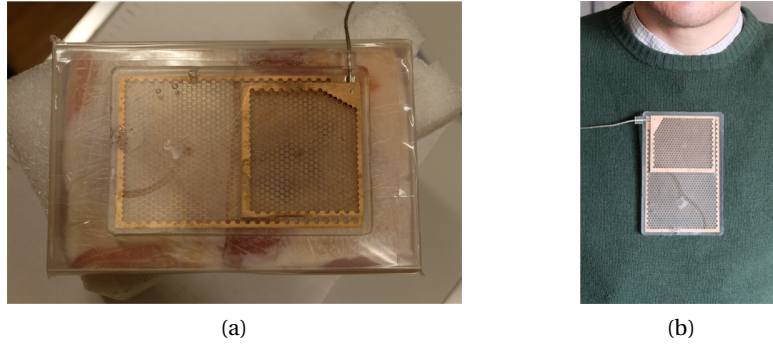


Fig. 4.29: Antenna measured on: (a) A chunk of pork meat and (b) On-body, on a human chest.

the stability of the antenna is not affected. Therefore, one can draw the conclusion that, not the perforation shapes or mesh structure, but the entire antenna structure determines the stability of the antenna when placed on the wearer, as long as the holes are relatively smaller than the wavelength.

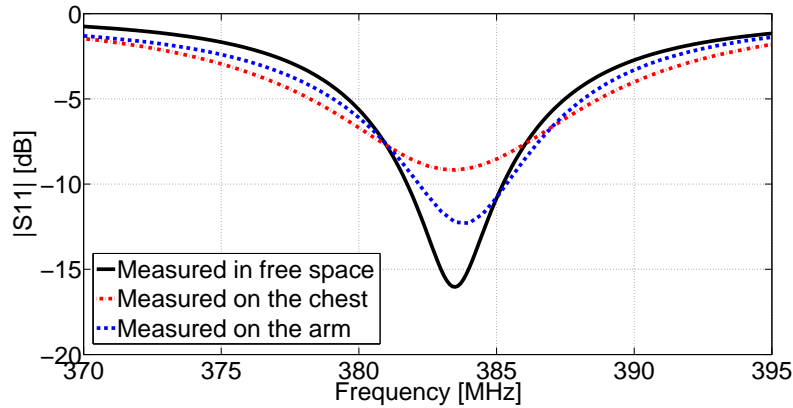


Fig. 4.30: Comparison of measured $|S_{11}(f)|$ of the hexagon PIFA in a free space and when placed on the human body.

A comparison of simulations (free space & phantom) and measurements (Free space, chunk of pork meat and human body) of $|S_{11}(f)|$ is shown in Fig. 4.31. As can be seen, all the responses remain stable within the defined frequency band except the measurements on the chunk of pork meat. This kind of deviation is not present when the antenna is placed on the human body, because the distance between the antenna and the body is larger compared to the case with meat placed inside the box. The discrepancy could also come from some surface wave diffraction at the borders of the meat in the case of the pork phantom. It should be mentioned that in the case of copper-mesh PIFA, this kind of deviation was not observed.

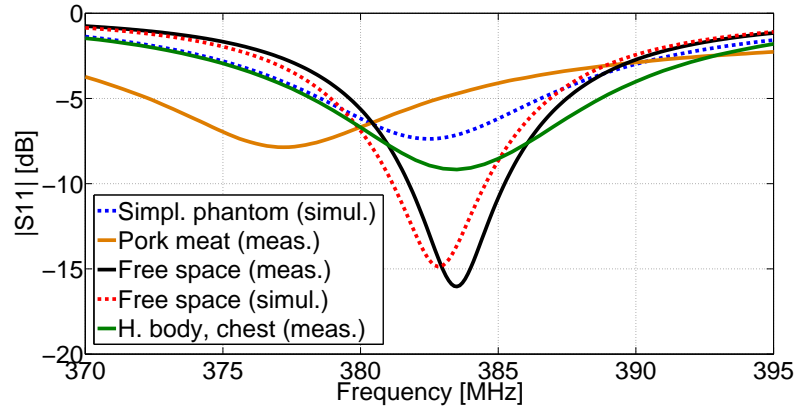


Fig. 4.31: Comparison of simulated and measured $|S_{11}(f)|$ of the hexagon PIFA in a free space, on a simplified single layer muscle phantom, on a chunk of pork meat and when placed on the human body.

Flexibility and Bending Characteristics

The same set-up used for the copper-mesh PIFA was used for testing the flexibility and bending characteristics of the hexagon PIFA. The principle was the same, just that the set-up was slightly modified. Namely, the distance between the two fixed support points was shortened from 160 mm to 137 mm, because of the different lengths of the tested antennas. Fig. 4.32 (a) shows the hexagon PIFA fixed inside the testing set-up. A comparison of measured $|S_{11}(f)|$ when bended under different radii is reported in Fig. 4.33.

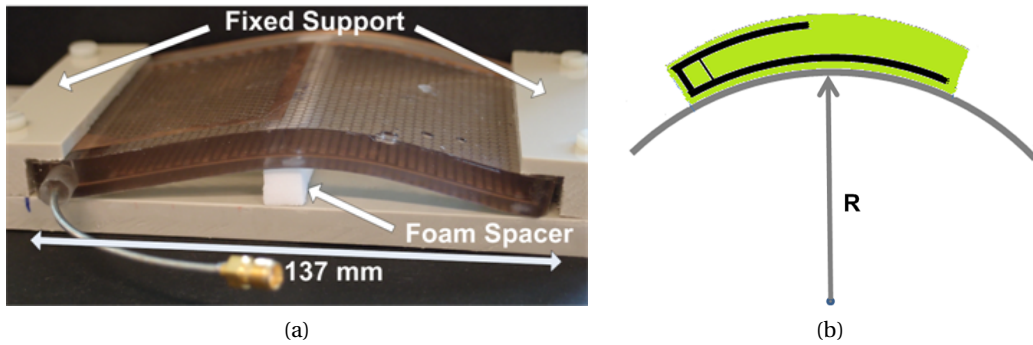


Fig. 4.32: Bending of the PIFA: (a) In-house custom designed bending set-up and (b) Bending skim for determining the radius of the bended curvature.

In this case the maximum frequency deviation is slightly larger, 3 MHz in total. Again the limit bending was performed for a radius of $R=230$ mm. Compared to the copper-mesh PIFA, the deviation of the $|S_{11}(f)|$ when bended under same radii, 230 mm, is 1 MHz larger for the hexagon PIFA. This is expected because the hexagon antenna is shorter and thicker and the same bending radius affects its performances more.

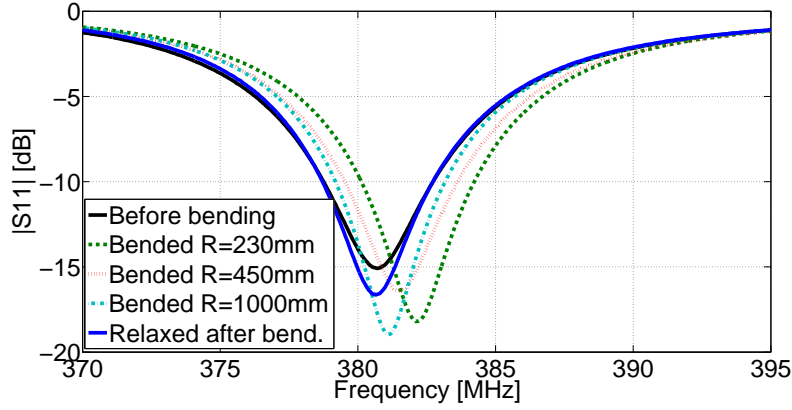


Fig. 4.33: Comparison of measured $|S_{11}(f)|$ of the hexagon PIFA when bended under different radii.

4.2.4 Radiation Pattern and Gain

The radiation patterns and gain of the hexagon PIFA are reported in a similar way like for the copper-mesh antenna, section 4.1.4. Simulations were performed with HFSS, for two different scenarios, antenna in free space and antenna placed on a phantom. Measurements of the radiation patterns were performed in the same anechoic chamber as for the previous antenna (see Fig. 4.16). Please note again that for the frequency of interest, around 383 MHz, the size of the chamber and the used absorbers is at the lower limits for characterizing the AUT. Still, the comparison between the simulated and measured patterns matched fairly. The radiation patterns were also measured for two different scenarios, AUT characterized in free space and AUT characterized when placed on the chunk of pork meat, see Fig. 4.35.

The simulated radiation patterns and the computed gain, for the antenna in free space and antenna placed on a simplified phantom are depicted in Fig. 4.34 (a) and (b), respectively. Compared to the copper-mesh PIFA, no significant differences in the shapes of the simulated radiation patterns are observed. The only remarkable difference appears in the computed gain, which is in favor of the hexagon antenna. The computed values for the gain and radiation efficiency for the antenna placed in free space and placed on the phantom, are -4.43 dBi and -8.73 dBi (gain) and 24% and 6% (efficiency), respectively. The improvement of the gain mainly comes from the modification applied in the antenna's structure. The 2 mm increase in the separation between the ground plane and the radiating patch, resulted in increased gain and radiation efficiency of the antenna.

Inside the anechoic chamber the AUTs were characterized and measured under two different scenarios. For the first scenario, the AUT is in a free space, while for the second the AUT is placed on a chunk of meat. Fig. 4.35 illustrates the described scenarios. For each scenario the antennas were characterized for two different orientations, orientation marked as a $\Phi=0^\circ$

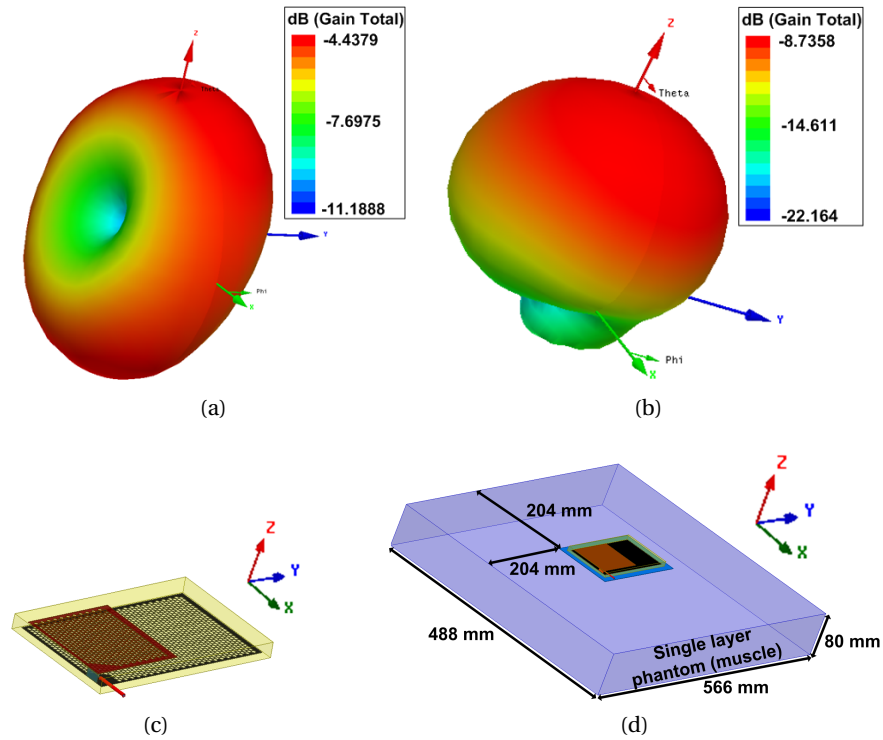


Fig. 4.34: Radiation pattern and simulated gain of the hexagon PIFA in free space and on the phantom (@383 MHz): (a) In free space, (b) On a simplified phantom, (c) Antenna orientation and (d) Orientation of the antenna when placed on the phantom.

and orientation marked as a $\Phi=90^\circ$, see for instance Fig. 4.36. For each orientation two different cuts were measured, $\Phi=0^\circ$ cut (XZ-plane) and $\Phi=90^\circ$ cut (YZ-plane). Simulated and measured radiation patterns for the hexagon PIFA are reported in Fig. 4.37.

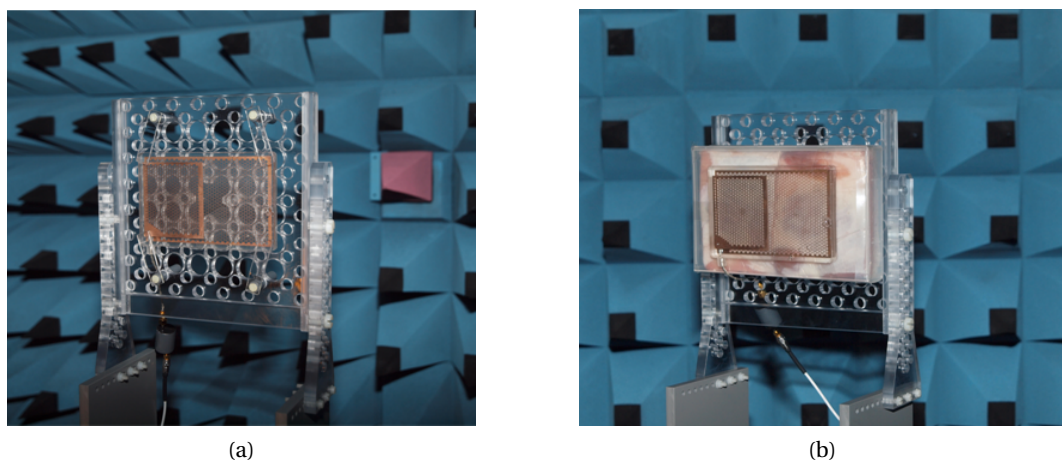


Fig. 4.35: AUT inside the anechoic chamber: (a) In free space and (b) On the chunk of pork meat.

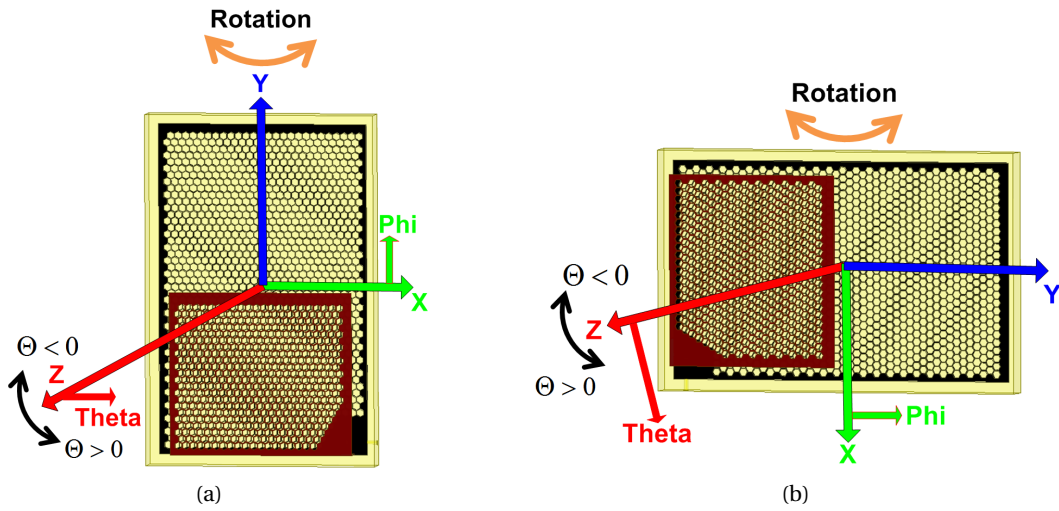


Fig. 4.36: Orientation of the AUT while measuring the radiation pattern inside the anechoic chamber:
 (a) Orientation of the antenna for the case $\Phi=0^\circ$ and (b) Orientation of the antenna for the case $\Phi=90^\circ$.

Again, as in the case of copper-mesh PIFA, due to the low directivity of the AUT, the influence of the connecting cables inside the anechoic chamber and difference in size between the phantom and used chunk of pork meat contribute to the discrepancies between the measured and simulated radiation patterns.

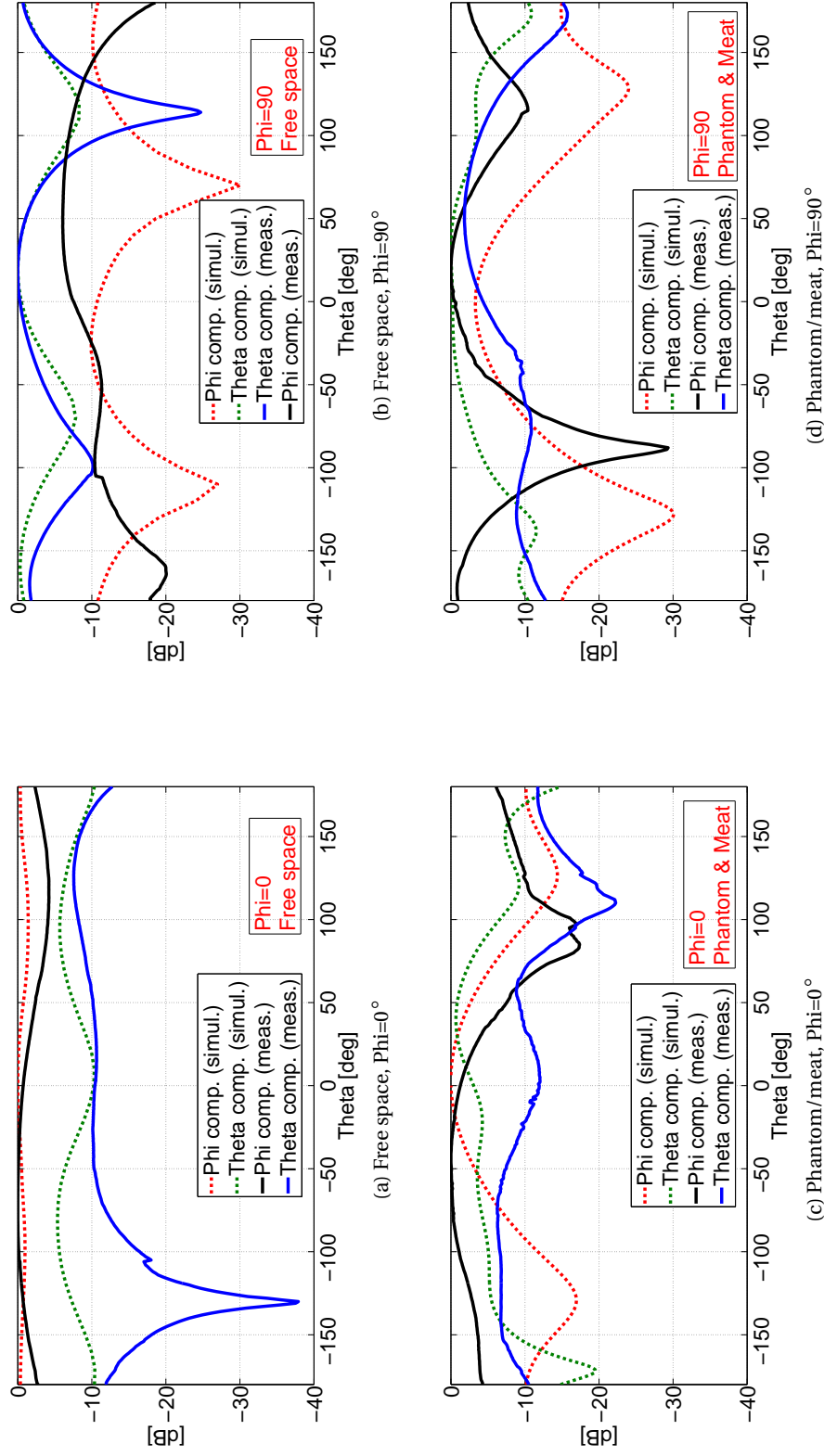


Fig. 4.37: Measured and simulated radiation patterns for the hexagon PIFA (@383 MHz): (a) AUT in free space, $\Phi=0^\circ$, (b) AUT in free space, $\Phi=90^\circ$, (c) AUT on a phantom/meat, $\Phi=0^\circ$ and (d) AUT on a phantom/meat, $\Phi=90^\circ$.

Maximum Measured Gain

The obtained gain values for both the scenarios are reported bellow:

- Antenna in free space, Gain=-1.05 dBi
- Antenna placed on a chunk of pork meat, Gain=-1.86 dBi

4.2.5 Conclusions

A combination of custom perforated conductors and pure PDMS as a substrate resulted in a successful wearable UHF PIFA design. With the proposed approach the difference between the experiment and the actually measured responses was reduced to 1 MHz. The introduction of hexagon shapes in the conductor lead to the miniaturization of the antenna. Indeed, the hexagon patterns enlarge the current path on the antenna, thus making the antenna electrically larger. The miniaturization is also caused by the use of a substrate with slightly higher permittivity compared to the loaded PDMS. On the other side, increased substrate losses were successfully compensated by enlarging the antenna's height for 2 mm. This enlargement also led to improved gain and efficiency of the hexagon antenna prototype.

From the robustness and stability point of view, the hexagon antenna had a behavior similar to the first antenna prototype. The antenna exhibited stable performance in terms of being placed on the wearer or being left in free space. Both, simulated and measured radiation patterns provided hemispherical radiation coverage, which is again desired for placing the antenna on the wearer's chest or back.

Nevertheless, we still see a potential for ameliorating the gain and radiation efficiency of the hexagon antenna and this will be the main goal while designing the next antenna prototype. In general, the proposed technology of perforating the conductors provides a good starting point for eventual serial production of such antennas.

Table 4.6 summarizes the simulated and measured gain and radiation efficiency of the AUT.

Hexagon PIFA @ 383 MHz	Free Space		Phantom/Meat	
	Gain [dBi]	η [%]	Gain [dBi]	η [%]
Simulation	-4.43	24	-8.73	6
Measurement ^a	-1.05	NA	-1.86	NA

Tab. 4.6: A summary of the simulated and measured gain and radiation efficiency of the hexagon PIFA (@383 MHz).

^aThere are no available measured values for the radiation efficiency.

4.3 PIFA with an Air Gap Operating at 380 MHz

The last reported prototype is a hexagon PIFA, but with an air gap introduced between the ground plane and the radiating patch. The role of the air gap is to create a lossless medium (air) in the near-field region of the antenna. The creation of the air-gap was inspired from [56], where a coating of the conductive parts of PIFA was performed. The presence of the air gap should enhance the overall radiation performance of the antenna like radiation efficiency and gain. The structure of this prototype is based on the design of hexagon PIFA, using hexagon perforated conductive sheets and pure PDMS for fabricating the final structure.

4.3.1 Antenna Model and Geometrical Parameters

The third fabricated PIFA prototype was also intended to operate around 385 MHz (Tetrapol band [10]). The proposed antenna was modeled and designed in HFSS in similar way to the hexagon PIFA. Solid copper conductive sheets perforated with hexagons, with a thickness of $300\text{ }\mu\text{m}$ and material properties as suggested from the HFSS materials library for copper, relative permittivity $\epsilon_r=1$ and bulk conductivity $\sigma=2\cdot 10^7\text{ S/m}$ were used as conductors. We again opted for a pure PDMS for the substrate material, defined with relative permittivity $\epsilon_r=2.8$ and loss tangent $\tan\delta=0.006$. A full 3D model and detailed 2D sketches are illustrated in Fig. 4.38 and Fig. 4.39, respectively, while Table 4.8 reports the values of all the geometrical parameters. The overall size of the final prototype is the same as for the hexagon PIFA, $134.4 \times 88 \times 10.6\text{ mm}^3$. The main difference between the two prototypes is in the presence of the air gap in the latter. Due to this, the length of the radiating patch in the case of air-gap PIFA is slightly longer.

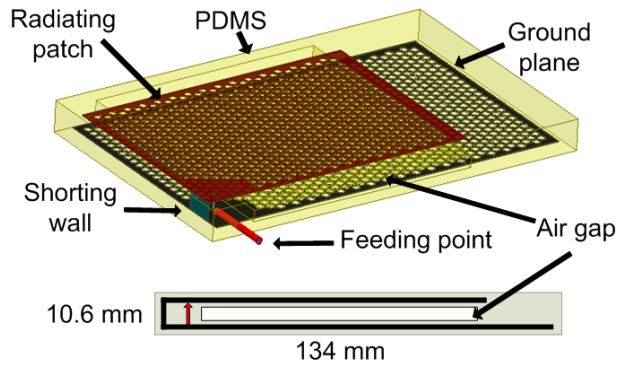


Fig. 4.38: Model of the PIFA modeled in HFSS.

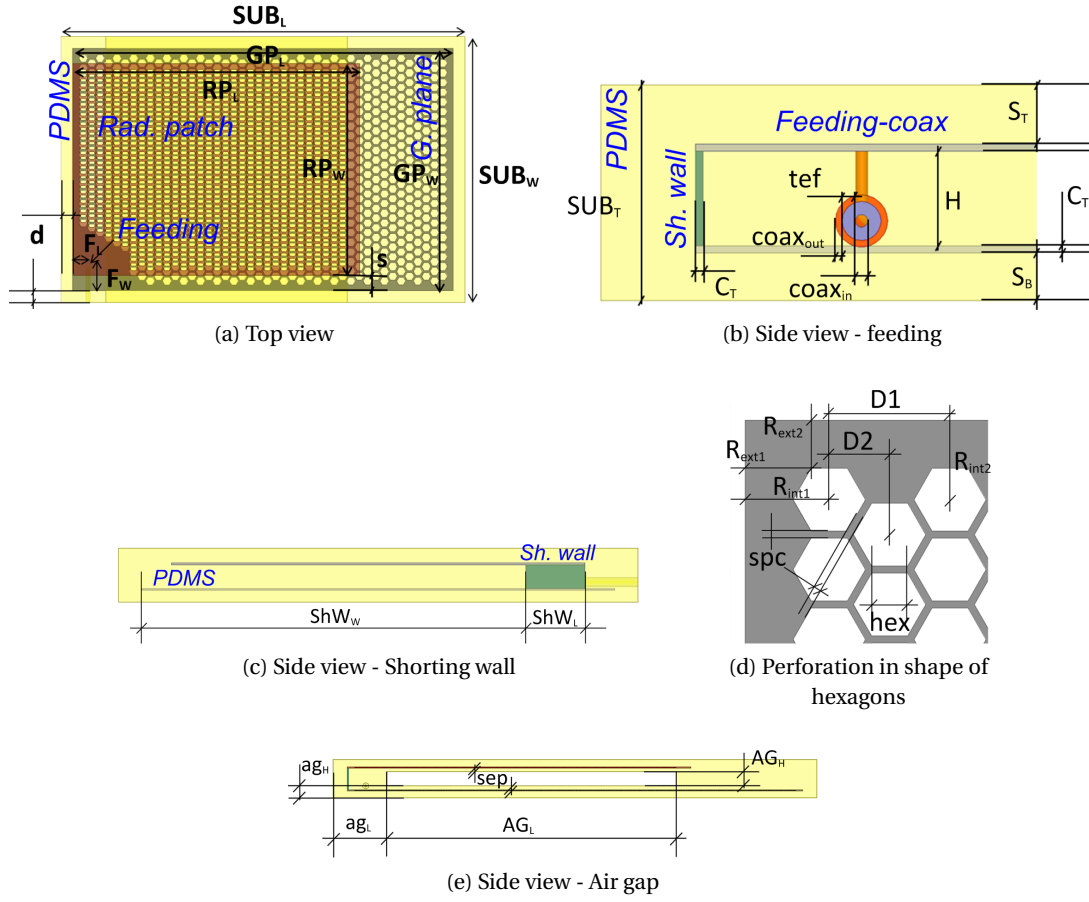


Fig. 4.39: 2D sketches of the designed antenna prototype: (a) Top view: PDMS, ground plane, patch and position of the feeding, (b) Side view - coaxial cable feeding, (c) Side view - Shorting wall, (d) Perforations applied on the ground plane and radiating patch and (e) Side view - Air gap.

Parameter	Value [mm]	Parameter	Value [mm]	Parameter	Value [mm]
GP_L	126	C_T	0.3	R_{int1}	3.5
GP_W	80	S_T	2	R_{int2}	3.3
RP_L	95	S_B	2	D_1	5.02
RP_W	70	H	4	D_2	2.51
SUB_L	134	$coax_{in}$	0.53	hex	1.5
SUB_W	88	$coax_{out}$	0.275	spc	0.3
SUB_T	10.6	tef	1.65	AG_L	80
F_L	5	ShW_L	10	AG_H	4
F_W	9.5	ShW_W	65	ag_L	11
d	4	R_{ext1}	2.75	ag_H	3.3
s	5	R_{ext2}	2	sep	1

Tab. 4.7: Values of the designed parameters indicated in Fig 4.39.

4.3.2 Fabrication of the Antenna Prototype

From the fabrication point of view, the only novelty compared to the hexagon PIFA is the way the air gap was created. For that purpose, we used a modified mold, depicted in Fig. 4.40. The main modification was performed on the frame of the mold (part marked as number 2 in Fig. 4.40 (a)). In order to introduce the plate that creates the air gap between the ground plane and the patch, a part of the frame was cut from both sides, as illustrated in Fig. 4.41 (c). The entire procedure was as follows:

1. Part 1 and part 2 were assembled and tightened with the screws.
2. All the conductive parts of the antenna and the soldered coaxial cable were placed and fixed inside the mold.
3. The coaxial cable was put through the hole drilled on the frame (please see Fig. 4.40 (b) and Fig. 4.41 (c)).
4. A rubber cap was used as a sealing device from outside, preventing the leakage of the PDMS.
5. Part 3 (see Fig. 4.40 (b)) was introduced as shown in the figure and tightened with screws.
6. Finally, parts 4 and 5 were put on the both sides of the frame and tightened with screws.
7. Everything was ready for sprinkling the PDMS inside the mold.

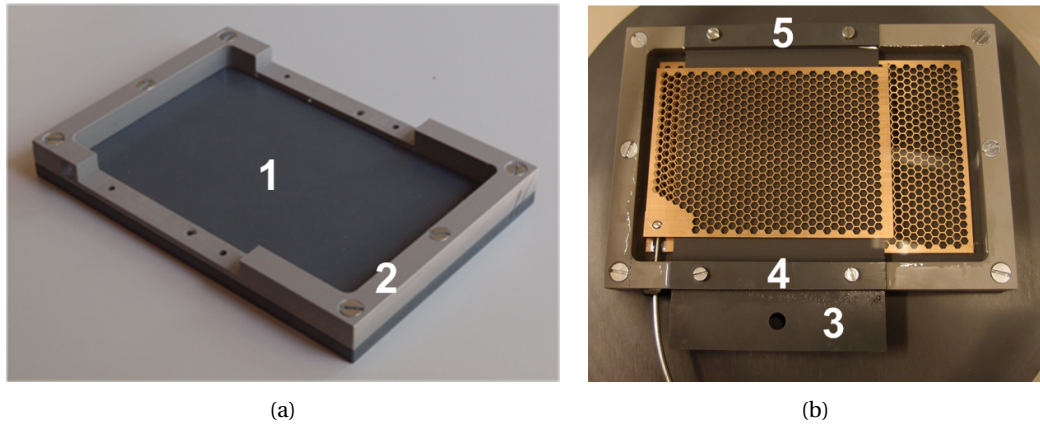


Fig. 4.40: Prototype of the mold used for air-gap PIFA: (a) Bottom plate and frame assembled and (b) Conductive parts of the antenna placed inside the mold.

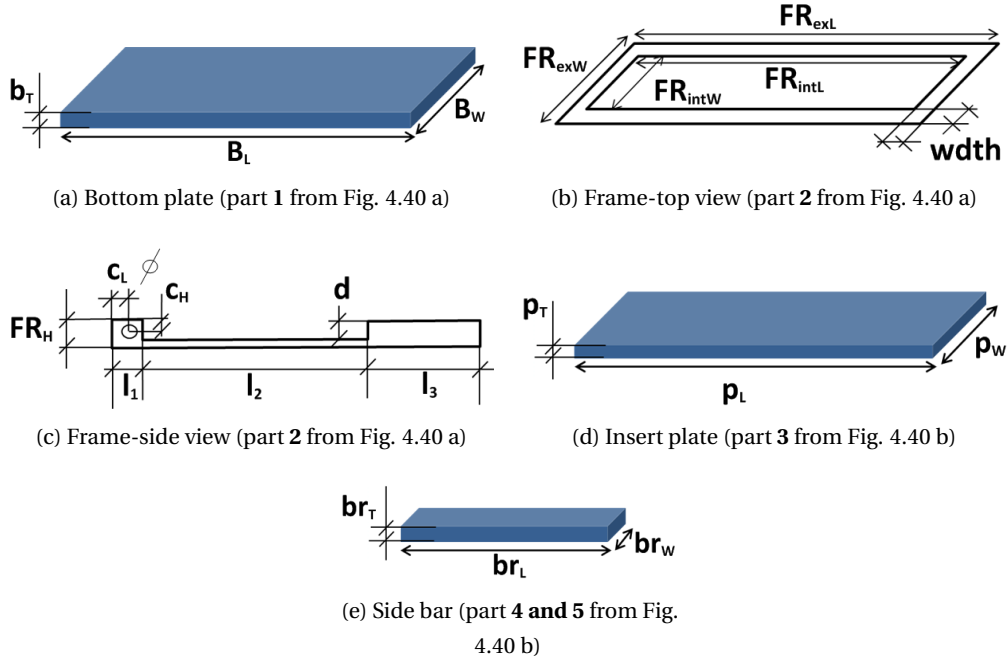


Fig. 4.41: 2D sketches of the designed mold: (a) Bottom plate, (b) Frame - top view, (c) Frame - side view, (d) Plate used for creating the air gap and (e) Side bars, mounted on the top of the plate for the air gap.

Parameter	Value [mm]	Parameter	Value [mm]	Parameter	Value [mm]
B_L	154	$width$	10	p_L	130
B_W	107	c_L	9	p_W	80
B_T	6	c_H	5	p_T	4
FR_{exW}	154	\varnothing	8	br_L	80
FR_{exL}	107	d	8	br_W	10
FR_{intL}	134	l_1	15	br_T	4
FR_{intW}	88	l_2	80		
FR_H	10.6	l_3	39		

Tab. 4.8: Values of the designed parameters indicated in Fig 4.41.

The built antenna prototype is depicted in Fig. 4.42 and it is $134.4 \times 88 \times 10.6 \text{ mm}^3$ large. Since the antenna was built with an air gap introduced between the ground plane and radiating patch in the continuation of this manuscript, it will be referred to as an air-gap PIFA. A comparison of the predictions (simul.) and experiment (meas.) of $|S_{11}(f)|$ is reported in Fig. 4.43. A disagreement between the simulated and measured response is around 5 MHz. One of the reasons for such a relatively high discrepancy lies in the increased complexity of the

overall structure. The resonant frequency is rather sensitive to the size of the air gap. If the fabrication is done in a controlled and automatized environment (and not manually), these errors can be significantly reduced.



Fig. 4.42: Manufactured PIFA prototype.

In addition, after the initial measurement, it was noticed that also slight bending of the antenna changes the shape of the air gap (mainly the distance between the ground plane and the radiating patch) which changes the resonant frequency of the antenna. In order to prevent this unwanted effect, spacers similar to those reported for maintaining the parallelism between the two plates, were used inside the air gap. These spacers have a cylindrical shape, 3 mm in diameter and 4 mm in height and they are built from pure PDMS. Of course, bringing the spacers inside the air gap and thus the near field of the antenna, affects the response of the antenna. Anyhow, we have used these spacers to finely tune the resonant frequency of the antenna, even after the PDMS was polymerized. PDMS spacers, in shape of cylinders, are introduced inside the air gap of the built air-gap PIFA and they are depicted in Fig. 4.44.

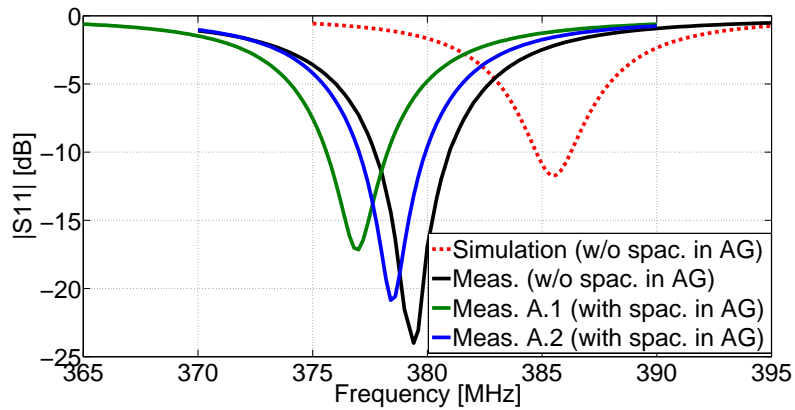


Fig. 4.43: Comparison of simulated and measured $|S_{11}(f)|$ of the air-gap PIFA.



Fig. 4.44: Spacers introduced inside the air gap.

Since we needed more than one antenna prototype for conducting different system measurements (as it will be reported in Chapter 5), a second air-gap PIFA prototype was built. The responses of the two different prototypes are reported in Fig. 4.43. The difference between the first and the second prototype with introduced spacers is less than 2 MHz. Although there is some discrepancy between the prediction (simul.) and actual antenna measurement, with the second prototype it was confirmed that the proposed technology can be easily reproduced even in a standard laboratory environment.

4.3.3 Comparison of $|S_{11}(f)|$ Responses for Different Situations

A set of $|S_{11}(f)|$ simulations and measurements were performed when the antenna was radiating in a free space (simul. & meas.), placed on the simplified phantom (simul.), placed on the chunk of pork meat (meas.), and placed on a wearer (meas.). It can be seen in Fig. 4.45 that the antenna stays tuned all the time, no matter whether it is in free space or on any part of the body, thus demonstrating again the effect of the ground plane in decoupling the antenna from the wearer.

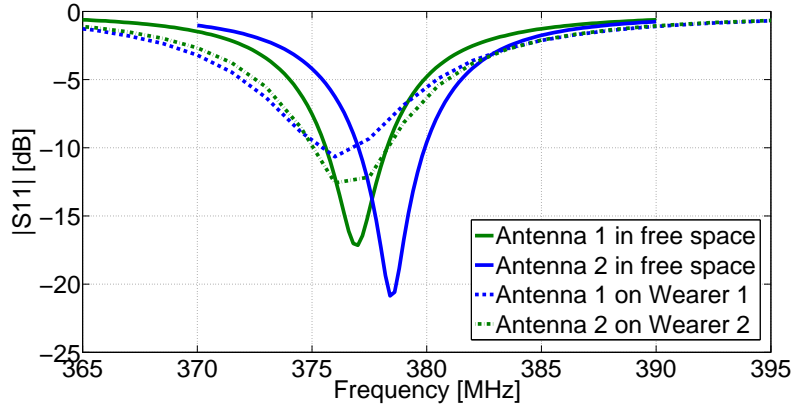


Fig. 4.45: Comparison of measured $|S_{11}(f)|$ of the air-gap PIFA in a free space and when placed on the human body.

A comparison of the simulations (free space & phantom) and measurements (Free space, chunk of pork meat and human body) of $|S_{11}(f)|$ is reported in Fig. 4.46. As can be seen, all the responses remain stable within the defined frequency band except the measurements on the chunk of pork meat, which have an identical behavior to the hexagon PIFA. Since the

air-gap antenna is similar to the hexagon antenna in terms of size and very close in terms of the operating frequency, the assumptions that were made for the hexagon antenna remained valid here, either some wave diffraction occurs due to the meat and/or box edges or simply the antenna is too close to the meat, between 1-2 mm.

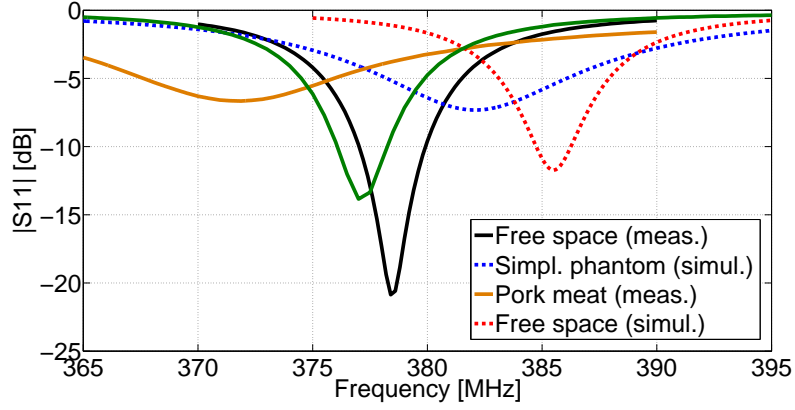


Fig. 4.46: Comparison of simulated and measured $|S_{11}(f)|$ of the air-gap PIFA in a free space, on a simplified single layer muscle phantom, on a chunk of pork meat and when placed on the human body.

4.3.4 Radiation Pattern and Gain

The radiation patterns and gain of the air-gap PIFA are reported in the same way as for the hexagon PIFA, section 4.2.4. The comparison between the simulated and measured patterns again fairly match. As in the previous case, the measured radiation patterns were also performed for two different scenarios, AUT characterized in free space and AUT characterized when placed on the chunk of pork meat, see Fig. 4.35.

The simulated radiation patterns and the computed gain, for the antenna in free space and antenna placed on a simplified phantom are depicted in Fig. 4.47 (a) and (b), respectively. The computed gain is the highest of all prototypes. The simulated values for the gain for the antenna placed in a free space and placed on the phantom, are -3.04 dBi and -7.01 dBi, while the computed values for the radiation efficiency are 37% and 9.2%, respectively.

Measured and simulated radiation patterns for the air-gap PIFA are reported in Fig. 4.50. The radiation patterns are compared for two different scenarios, antenna in free space and antenna placed on a phantom/meat (see Fig. 4.48) and for each scenario the antennas were characterized for two different orientations, $\Phi=0^\circ$ and $\Phi=90^\circ$, respectively.

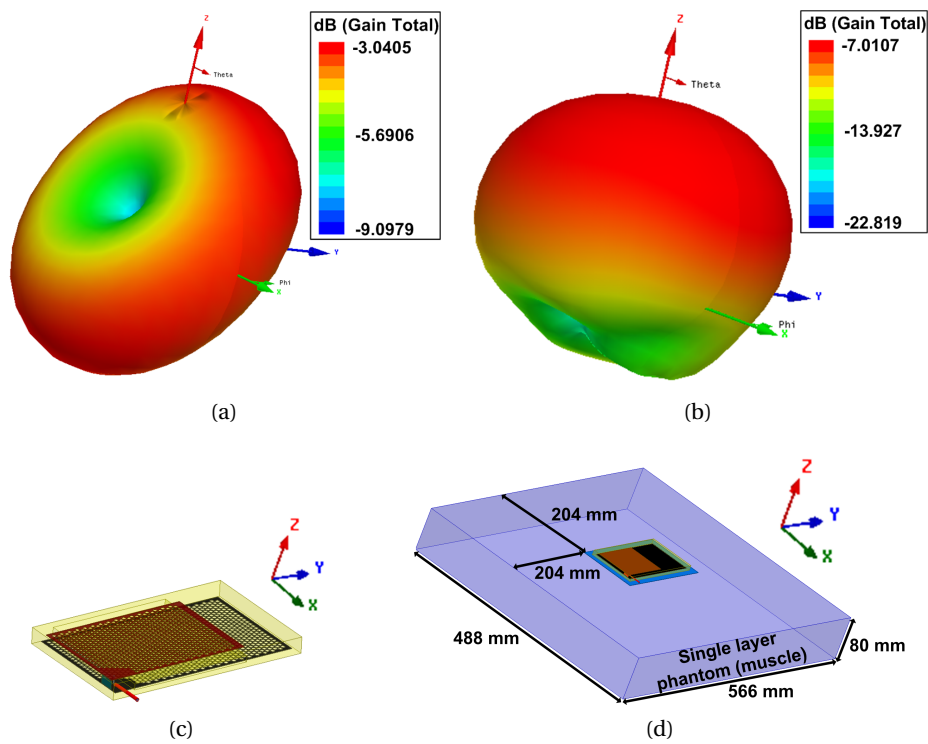


Fig. 4.47: Radiation pattern and simulated gain of the air-gap PIFA in free space and on the phantom (@380 MHz): (a) In free space, (b) On a simplified phantom, (c) Antenna orientation and (d) Orientation of the antenna when placed on the phantom.

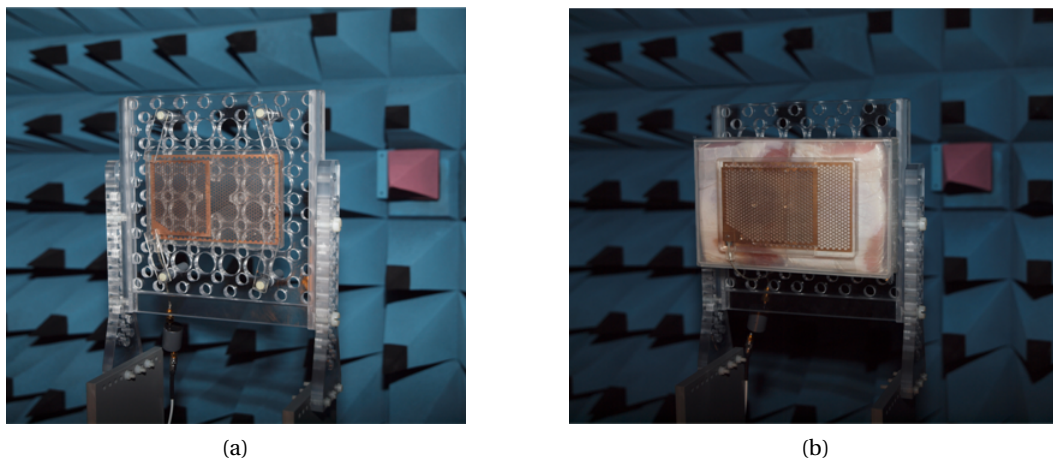


Fig. 4.48: AUT inside the anechoic chamber: (a) In free space and (b) On the chunk of pork meat.

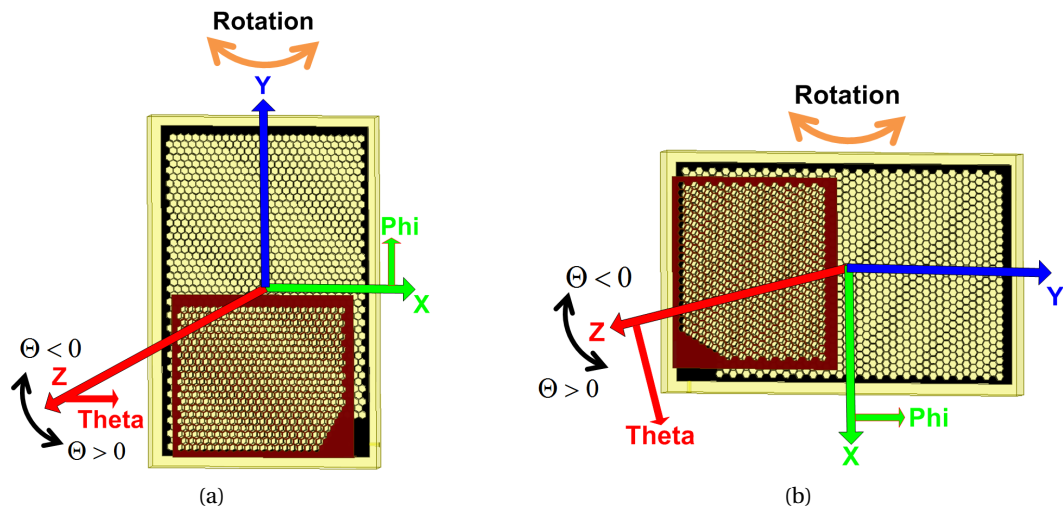


Fig. 4.49: Orientation of the AUT while measuring the radiation pattern inside the anechoic chamber:
 (a) Orientation of the antenna for the case $\Phi = 0^\circ$ and (b) Orientation of the antenna for the case $\Phi = 90^\circ$.

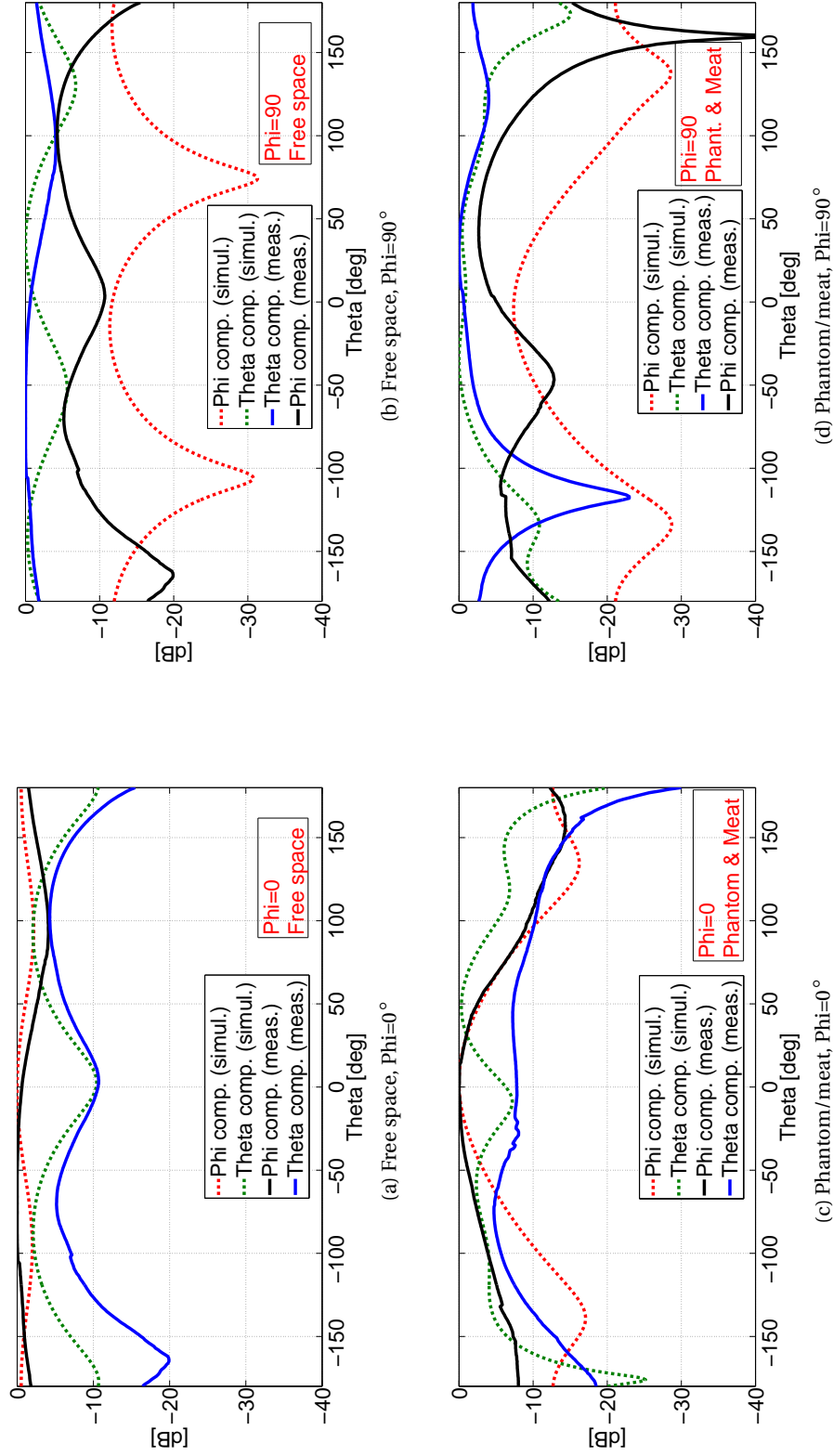


Fig. 4.50: Measured and simulated radiation patterns for the air-gap PIFA (@378 MHz): (a) AUT in free space, $\Phi=0^\circ$, (b) AUT in free space, $\Phi=90^\circ$, (c) AUT on a phantom/meat, $\Phi=0^\circ$ and (d) AUT on a phantom/meat, $\Phi=90^\circ$.

Maximum Measured Gain

The obtained gain values for both the scenarios are reported bellow:

- Antenna in free space, Gain=1.09 dBi
- Antenna placed on a chunk of pork meat, Gain=-3.11 dBi

4.3.5 Conclusions

Introducing the air-gap between the ground plane and the radiating patch improved the radiation performances of the antenna significantly. The introduced air-gap replaced the lossy substrate material with air in the near-field region of the antenna, which resulted in an improved gain and radiation efficiency (simul.). Compared to the hexagon PIFA, the radiation efficiency has been increased by 50%, for the antenna simulated in free space and when placed on the simplified phantom. Furthermore the gain was improved for both simulated scenarios for about 1 dB.

Looking at the measured gain values in free space, our assumptions are again confirmed. The maximum measured gain for the air-gap PIFA was 2 dB higher compared to the hexagon PIFA, measured under the same conditions. Yet, when we looked at the measured gain for the case when the antennas were placed on the chunk of pork meat, the obtained result showed an opposite trend. In this situation, the maximum gain of the air-gap PIFA is 1 dB lower compared to the hexagon PIFA. One of the explanations for the deterioration of the gain of the air-gap antenna is the fact that the EM fields, instead of being confined in the near-field region of the antenna, couple more to the meat. Nevertheless, these results should be taken with caution as there is some deviation of the resonant frequency measured while the antenna was placed on the chunk of meat. Unfortunately, we could not measure the gain of the antenna while being placed on a wearer.

Practically, the presence of the air-gap introduces additional uncertainties during the fabrication process. As it was seen, the discrepancy between the simulated and measured antenna responses was around 5 MHz. Still, introducing spacers inside the gap, was seen as a good solution for this problem. Moreover, the introduction of the spacers brought an additional level of fine tuning the antenna's operating frequency, even after the PDMS had polymerized. The final result is that the size of the antenna, compared to the hexagon PIFA, remained unchanged while the gain and radiation efficiency have been improved.

Although some imprecision appeared in the modeling vs. experimental process, it was shown that the proposed technology can be easily reproduced, even in a standard lab environment. A second air-gap antenna prototype was built with characteristics and responses almost

identical to the first prototype, thus confirming the repeatability of the fabrication process. The second built prototype was used for additional system measurements that will be reported in more details in Chapter 5.

Table 4.9 summarizes the simulated and measured gain and radiation efficiency of the AUT.

Air-gap PIFA @ 378 MHz	Free Space		Phantom/Meat	
	Gain [dBi]	η [%]	Gain [dBi]	η [%]
Simulation	-3.04	37	-7.01	9.2
Measurement ^a	1.09	NA	-3.11	NA

Tab. 4.9: A summary of the simulated and measured gain and radiation efficiency of the hexagon PIFA (@378 MHz).

^aThere are no available measured values for the radiation efficiency.

4.4 Summary on the Results

In order to summarize and draw some conclusions from the reported antenna prototypes, this section discusses the different aspects considered in this chapter:

- Technology - Complexity vs. Precision.
- Robustness - Free space vs. On-body.
- Radiation pattern, gain and efficiency.
- Further steps.

At the end of this section, a detailed table, Table 4.10, reports all the relevant simulated and measured parameters for all the three antenna prototypes.

Technology - Complexity vs. Precision

In general, for the three reported antenna prototypes, a new technology for fabricating robust wearable antennas was presented. The essence of the proposed technology is a combination of PDMS as a substrate (silicon based material that is liquid in its initial phase) and copper-mesh or perforated structures as conductors. Once the PDMS has polymerized, the entire structure remains encapsulated inside the silicon material, resulting in a robust and flexible antenna prototype.

However, different variations of the proposed technology raised different questions in terms of fabrication complexity and precision that can be achieved. Taking into account that all the

fabrication steps were performed in a standard lab environment, a satisfactory precision was obtained for all the reported antenna prototypes. For more details, please refer to Table 4.10 where experimental and actual measured responses are compared. If this technology would be used in serial (automatized) production, conductors perforated with hexagon or any other shape would provide sufficient precision and better control over the entire antenna's structure and thus its performance.

Robustness - Free space vs. On-body

Measured responses of the antennas, both in free space and when placed on a human body, showed a good stability in terms of frequency detuning, as no significant frequency shifts appeared due to the presence of the human body. Only the input matching levels changed, which was expected due to the increased losses.

In order to confirm this stability analysis, we looked at the Smith charts of two antenna prototypes, mesh and air-gap PIFA, for the cases when the antennas were simulated in free space and when placed on a simplified phantom. For both cases, looking at the same frequency span, we see the same trend, the antenna on a phantom tends to be under-coupled. For the concrete simulation purposes, the distance between the antenna and the phantom is rather small (1 mm) which increases the impact of the phantom on the region very close to the feed.

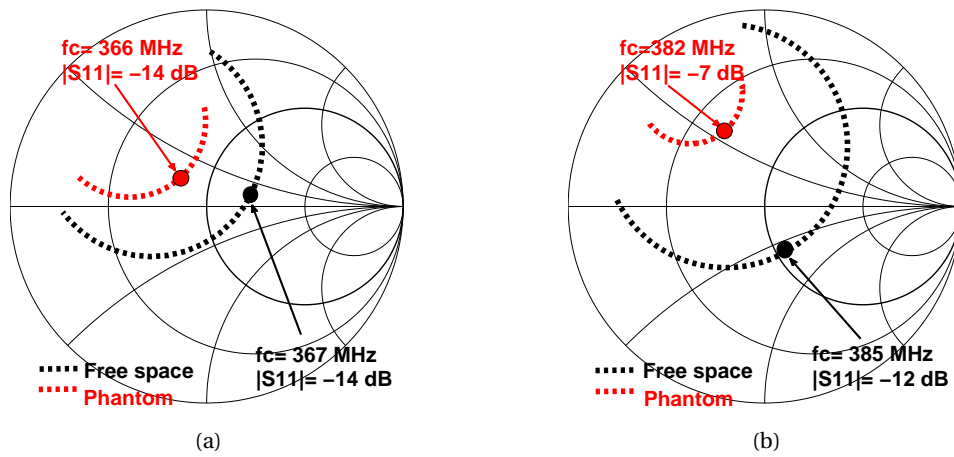


Fig. 4.51: $|S_{11}(f)|$ responses (Smith chart representation) of the AUTs when simulated in free space and on a phantom: (a) Copper-mesh PIFA and (b) Air-gap PIFA.

No broadening of the antennas' bandwidth is observed, meaning that just by wearing the antennas on everyday clothes will result in a robust antennas' performance with the respect to the body presence.

The proposed antennas have also demonstrated resilience towards different mechanical influences. Bending of the antennas was one of the conducted tests, where the flexibility and performance were tested while the antennas being bent under different radii. The obtained results, where no significant frequency shift occurred, confirmed the robustness of the proposed antennas when exposed to potential mechanical influences. Moreover, the copper-mesh PIFA was exposed to washing, showing strong resilience against the water and potential mechanical damages due to the washing machine rotations. Stability of the antenna in terms of frequency remained within 1-2 MHz shifts.

Additional robustness tests for the reported antennas, when exposed to different external environment conditions will be reported in Chapter 5.

Radiation Pattern, Gain and Efficiency

All the reported antennas have a similar behavior in terms of the radiation patterns. When the antennas are in free space, both simulated and measured patterns are close to a dipole antenna pattern. However, by placing the antenna on a phantom or on a chunk of meat, the back radiation is suppressed, while the front part radiates in a hemispherical shape. This is a desirable radiation pattern as the antennas are intended either for being placed on the back or chest on wearer, so that such patterns will provide broad coverage.

The gain and efficiency of the antennas were improved with each new built prototype. There were two approaches used in order to improve the radiation characteristics of the antenna. In the first approach, although the loaded PDMS was replaced by a pure one (it has higher relative permittivity and higher losses), the improvement was achieved by modifying the antenna's structure. Increasing the height for 2 mm only, hexagon PIFA compared to the copper-mesh PIFA, yields a significant improvement in the radiation performances: the simulated radiation efficiency for the hexagon antenna was 75% higher compared to the copper-mesh PIFA. A similar trend was observed for the measured gain, from -8.4 dBi for a copper-mesh antenna to -1.05 dBi for a hexagon antenna. For more details please refer to the Table 4.10.

In the second approach, (air-gap PIFA), the modification of the near-field region of the antenna increased the gain compared to the hexagon PIFA. For the air-gap PIFA, measured gain in free space was 1.09 dBi, which is 2 dB higher compared to the hexagon antenna.

Future Work

In general, PIFAs offer a lot of freedom in the design process and manipulation with their structures and overall performances. As already seen from the above stated characteristics and results, significant progress was achieved from the first antenna prototype, copper-mesh PIFA,

until the last one, air-gap PIFA. This indicates, that for the specified applications, voice communication inside the Tetrapol band, PIFAs are promising candidates. Additional improvements can be done in terms of the antenna size, higher gain and higher efficiency.

Measurement ^a			
On-body	$ S_{11}(f) $	[dB]	-20
	f_c	[MHz]	362
Chunk of pork meat	Gain	[dBi]	-12.7
	η	[%]	NA
	$ S_{11}(f) $	[dB]	-28
	f_c	[MHz]	363
	Gain	[dBi]	-8.4
	η	[%]	NA
Free Space	$ S_{11}(f) $	[dB]	-10
	f_c	[MHz]	364
	Gain	[dBi]	-9.1
	η	[%]	4.7
Phantom	$ S_{11}(f) $	[dB]	-14
	f_c	[MHz]	365.4
	Gain	[dBi]	-6.9
	η	[%]	15
Free Space	$ S_{11}(f) $	[dB]	-16.3
	f_c	[MHz]	367
	Gain	[dBi]	-4.43
	η	[%]	24
Antenna prototype	$ S_{11}(f) $	[dB]	-12
	f_c	[MHz]	386
	Gain	[dBi]	-3.04
	η	[%]	37

5 System Measurements and Comparison with the Commercial Antennas

Закон конкуренције, понекад тежак за појединца, је најбољи за расу, јер обезбеђује опстанак најбољих у свакој области.

And while the law of competition may be sometimes hard for the individual, it is best for the race, because it ensures the survival of the fittest in every department.

—Andrew Carnegie

All the performed measurements reported in the previous chapter provided enough information about the radiation characteristics of each of the proposed antennas within the standard laboratory conditions. Yet, since the antennas are intended to be used within the Tetrapol and Polycom voice communication systems, additional tests of the antennas at the system level are required. The system level measurements consider the performance of the antennas in terms of transferred power and quality of the established communication links, in indoor, outdoor-urban and outdoor-open field environment.

The measurements presented in this chapter can be divided into two main categories. In the first category the measurements are performed in a controlled environment, inside a large anechoic chamber, where the $|S_{11}(f)|$ and $|S_{21}(f)|$ levels are measured for the different antenna pairs. The second category of measurements encompass tests in realistic conditions. With the support from an industrial partner in this project, a Swiss based company, (RUAG [12]), which provided us with an operational communication equipment, ("POLYCOM Radio portable COVERT700" [13]), we were able to perform realistic measurements in different circumstances. Also, on their recommendation, for the purposes of the system measurements, a set of air-gap PIFAs is compared with the commercially available wearable antennas that they are using.

Unfortunately, there is not enough information about the behavior of wearable UHF antennas while working in realistic conditions, neither in literature nor for commercial antennas. In [83] the performance of UHF body-worn antennas in an indoor environment is reported for several realistic situations. However, in this scenario diversity is the main research scope and wearable antennas are used only on the receiving side, but not on the transmitting. (It is not specified what type of antenna is used on the transmitting side). A similar approach is reported in [27], but this time for an outdoor scenario. A communication link between the Geostationary-Orbit Search and Rescue (GEOSAR) satellite and a wearable antenna integrated into the inflatable life vest is reported. In both scenarios, the communication between the base station and the wearer is established. On the other hand, all the reported results in this chapter refer to a more specific scenario, the communication between two wearers, a wearer-to-wearer (Body-to-Body) communication link. Moreover, the antennas' input power is dictated by the authorities, making this scenario quite challenging.

While doing the introduced measurements, the evaluation of the different antenna pairs is done in two ways, quantitatively and qualitatively. With the first approach, the communication performances of the antennas are evaluated while measuring transmitted/received power levels. In other words, the antenna mounted on one of the wearers is always connected to a power generator, while the antenna mounted on the second wearer is connected to a portable spectrum analyzer and received power levels are measured.

The qualitative evaluation is performed with the Polycom communication equipment. Two communication sets, each for one wearer, are used so that the real voice communication can be established. For this type of evaluation sound recorded files exist. It should be mentioned that for the analysis performed in this thesis, the qualitative comparisons are of a subjective character, where judgments of the wearers are used for evaluating the quality of the established communication.

This chapter is organized as follows: the measurements conducted inside the anechoic chamber are reported in section 5.1, additional analysis on the antennas stability are reported in section 5.1.2. Measurements performed in the realistic environment conditions are reported in section 5.2, where also the used measurement and communication equipment are described. The last section of this chapter, 5.2.8 introduces a specific measurement scenario, the so-called "rotating scenario", where, by specific orientation constellations of the two wearers, the radiation patterns of the tested antennas are evaluated.

5.1 Measurements in a Controlled Environment

In continuation of the standard laboratory measurements and the initiated collaboration with RUAG, it was decided to compare the proposed air-gap PIFAs with commercially available wearable antennas, also intended for voice communication inside the UHF range. For comparison purposes, three types of commercial antennas were used: wearable dipole antennas, with and without baluns, (produced by Panorama [106]), and a wearable antenna produced by Pharad [104]. The basic idea of this test was to compare the transmitted/received levels, $|S_{21}(f)|$, in a completely anechoic environment, thus testing the communication performances of the considered antennas without being affected externally.

Two wearers, with the antennas placed on them, were positioned inside an anechoic chamber and transmission/reflection levels were measured and compared. For all the proposed scenarios, a pair of identical antennas was used. In order to assure the repeatability and equal treatment of the different antenna pairs, custom tailored vests were prepared and used during the measurements. Each of the vests had different sleeves/pocket, used for the different antennas, air-gap PIFA or dipole (Panorama) antennas, respectively. An example of the custom tailored vest is shown in Fig. 5.1.

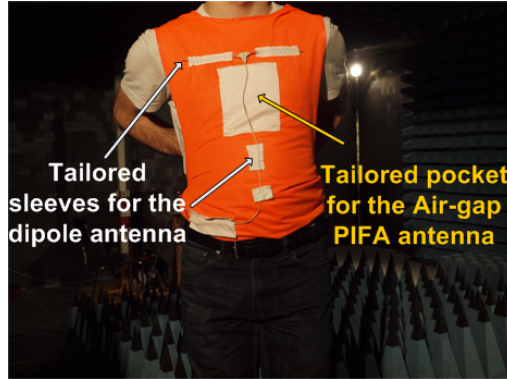


Fig. 5.1: Custom tailored vests.

A Vector Network Analyzer (VNA) was used for measuring the $|S_{21}(f)|$ levels. The anechoic chamber was large enough, $5 \times 5 \times 2 \text{ m}^3$, to ensure that the two wearers were in the far field region of each other. For all the measurement scenarios, the wearers were standing at a distance of $d=3 \text{ m}$ from each other. A scheme of the described anechoic chamber scenario is depicted in Fig. 5.2.

Four antennas were tested in this scenario: air-gap PIFAs, dipoles without baluns, dipoles with baluns, and one single wearable antenna from Pharad. Unfortunately, we had only one available antenna from this supplier (Pharad), thus we were not able to perform equal comparisons as with the other two commercial antenna pairs.

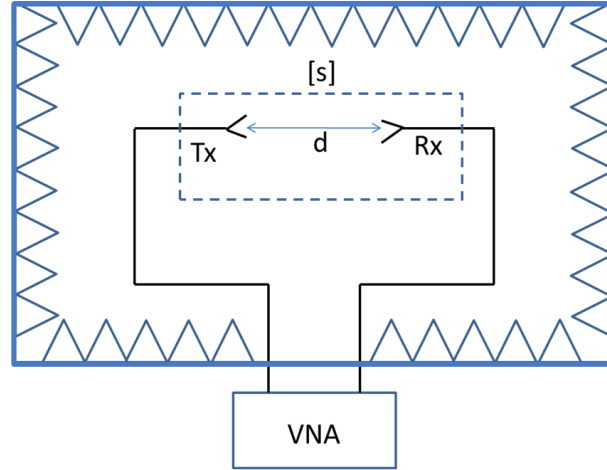
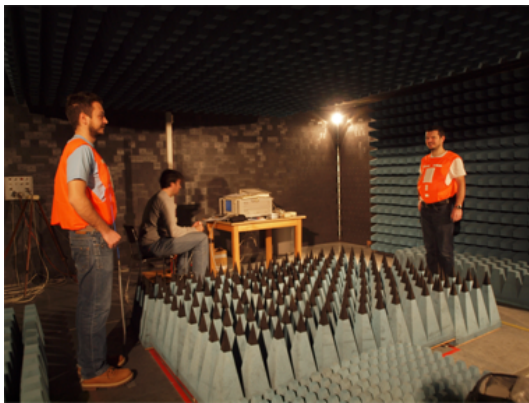


Fig. 5.2: Schematic of the measurement set-up inside the anechoic chamber.

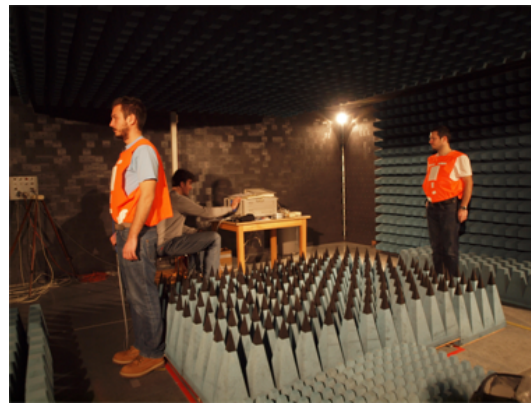
5.1.1 Measured ($|S_{21}(f)|$) in a Controlled Environment (Anechoic Chamber)

Two different situations were considered while comparing the antennas inside the anechoic chamber:

- **Front-to-front case** - The antennas are placed on the wearers' chest, the wearers and thus the antennas face each other and the direct $|S_{21}(f)|$ level was measured, (line of sight (LoS), Fig. 5.3 (a)).
- **Front-to-back case** - The placement of the antennas on the wearers is identical as in the previous case, but this time the wearers are oriented in such a way that one wearer (body) was always in between the antennas (none line of sight (NLoS), Fig. 5.3 (b)).



(a)



(b)

Fig. 5.3: Measurement scenario inside the anechoic chamber: (a) Front-to-front (LoS) and (b) Front-to-back (NLoS).

As can be seen from Fig. 5.4, the level of $|S_{21}(f)|$ for the air-gap PIFA pair is significantly higher than for the dipoles (with/without Balun), nearly 20 dB inside the desired frequency band.

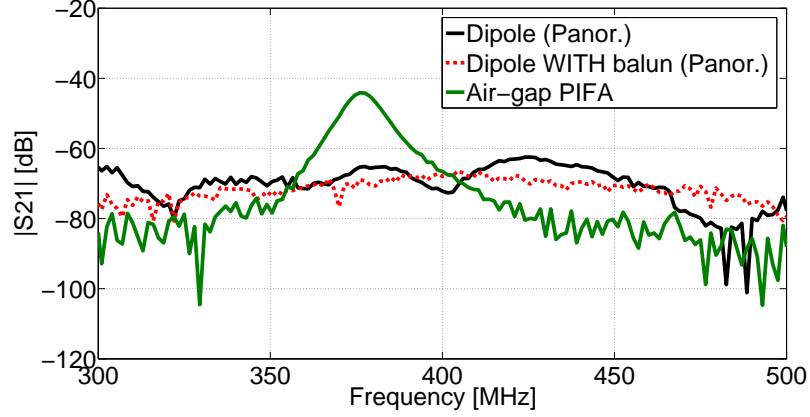


Fig. 5.4: Comparison of the measured $|S_{21}(f)|$ for the three different antenna types, front-to-front (LoS).

The second measured case, *front-to-back*, indicated the same trend between the compared antennas. The $|S_{21}(f)|$ level for PIFAs was higher for 10 dB compared to the dipoles.

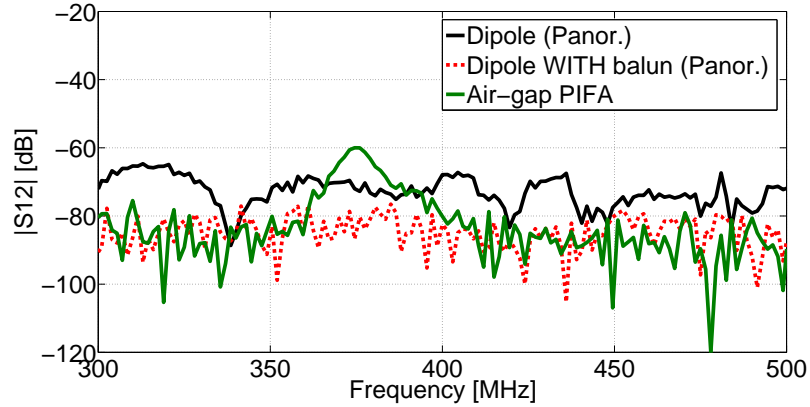


Fig. 5.5: Comparison of the measured $|S_{21}(f)|$ for the three different antenna types, front-to-back (NLoS).

For both measurement cases, the dipole antennas with baluns were exhibiting lower $|S_{21}(f)|$ levels, and were showing no resonant behavior inside the band of interest. The presence of the balun prevented the current flow on the feeding cable, thus shortening the actual antenna length, which results in an unmatched antenna and worse $|S_{21}(f)|$ performances. Therefore, we have decided for the further measurements to compare only the air-gap PIFAs and dipole (Panorama) wearable antennas without baluns.

5.1.2 Stability, Free Space vs. On-body

Because of the specific nature of the security applications, wearable antennas are supposed to work in a reliable way regardless of being worn by the wearers or left in their vicinity. Stability plays an important role in all wearable scenarios. In order to test the stability, two different cases were considered. In the first case the performance of the antennas was compared while worn on two different wearers, while the second case reports the difference in the antennas' performance when placed on a wearer or left in a free space.

Since we were using a 2 port VNA for performing the measurements, all scattering parameters $|S_{11}(f)|$, $|S_{21}(f)|$ and $|S_{22}(f)|$ were measured simultaneously. Fig. 5.6 shows the measured $|S_{11}(f)|$ and $|S_{22}(f)|$ on wearer 1 and wearer 2, respectively, for the commercial antenna and the PIFA. Responses differ when worn by different wearers. The performance of the PIFA however was not affected by the change of the wearer.

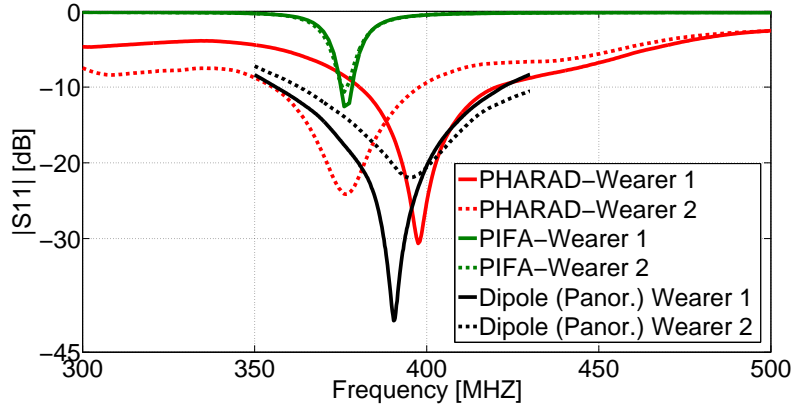


Fig. 5.6: Comparison of the $|S_{11}(f)|$ for the three different antennas when measured on two different wearers.

The second scenario compares antenna performance in free space and on a wearer. Ideally, there should be no difference in order to allow the user to take off his vest. However, most of the wearable antennas found in the literature and on the market are designed to provide reliable communication links while being mounted on the wearer [24, 84, 104, 106], but not if they are in some different situation, leading to a high probability of lost connection when the antenna is not on the wearer.

In order to test this stability aspect, we compared again the $|S_{11}(f)|$ of the same antennas, air-gap PIFAs and the commercial dipoles, measured on the wearers and in free space. As can be seen in Fig. 5.7 commercially available antennas always show a strong detuning tendency when not placed on the body.

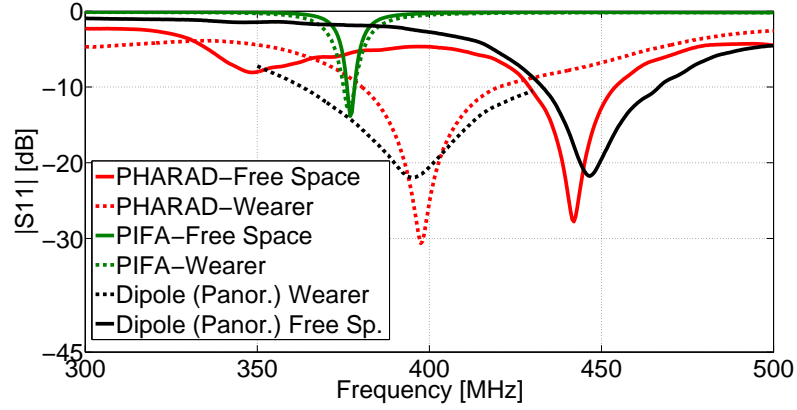


Fig. 5.7: Comparison of the $|S_{11}(f)|$ for the three different antenna types when measured in a free space and on the wearer.

These results indicate that the commercial antennas are exclusively designed for operating on the body. Once they are moved away, they change their behavior by shifting the resonant frequency and changing the input matching level. Since both commercial antennas are relatively small (overall dimensions) with the respect to the wavelength, the coaxial feeding cables contribute to the overall radiation in both cases, which adds additional uncertainties in the antennas' performances. Just by sliding the hand over the cables, the frequency can be shifted by 30-50 MHz, enough to move the antenna response out of the Tetrapol band frequencies.

For the air-gap PIFA we see that the frequency shifts are in the range of 1-2 MHz, and the antenna is completely independent from the body presence. The PIFA remains all the time inside the intended frequency band. Due to the narrow bandwidth of the antenna itself, PIFA cannot cover the entire Tetrapol bandwidth. However, this is not a problem for the most of Tetrapol communications, where no full band coverage is required. In other words, the users are always assigned to a narrower sub-band, dedicated to different services like army, police or any other rescue service. Table 5.1 summarizes the measured $|S_{21}(f)|$ levels and stability measurements for the tested antennas, which proves the suitability of the proposed PIFA for these applications.

Antenna prototype	$\max S_{21}(f) $ [dB]		Stability (f_c) [MHz]		
	LoS	NLoS	Free space	Wearer 1	Wearer 2
	-44	-60	377	377	378
	-56	-69	447	390	395
	NA	NA	443	376	396

Tab. 5.1: Summary of the transferred power levels and stability of the tested antennas.

5.2 Measurements in a Realistic Environment

In this section a set of measurement scenarios performed in realistic everyday conditions are reported. The measurements were performed in the following environments:

- Indoor - Laboratory corridor
- Indoor - University campus buildings
- Outdoor - University campus
- Outdoor - Open field area

However, before moving on to the description of the scenarios and reporting the measurement results, an overview of the used equipment will be presented. Two different sets of equipment were used, one for quantitative and another one for qualitative measurements.

5.2.1 Equipment Used for Quantitative Measurements

For the quantitative measurements a pair of power generator and hand-held spectrum analyzer were used. On the transmitting side, a *Hewlett Packard* power generator was used all the time in a continuous operating mode with a transmitting power set at +18 dBm (the maximum available power). Since the generator was always fixed in one determined position, one of the wearers was always next to it with the antenna connected to the generator's output. On the receiving side, a *Rohde & Schwarz* hand-held spectrum analyzer was used. A mobile spectrum analyzer was used so that the measurements were not limited to a certain range. Depending on the measuring mode, direct power measurement (power sensor) or extracting the power from the spectrum analyzer mode, different sensitivities were achieved. In the direct power

mode the maximum sensitivity was around -67 dBm, while in the spectrum analyzer mode, the maximum sensitivity was around -110 dBm of received power. The used measurement devices, power generator and hand-held spectrum analyzer, are depicted in Fig. 5.8.

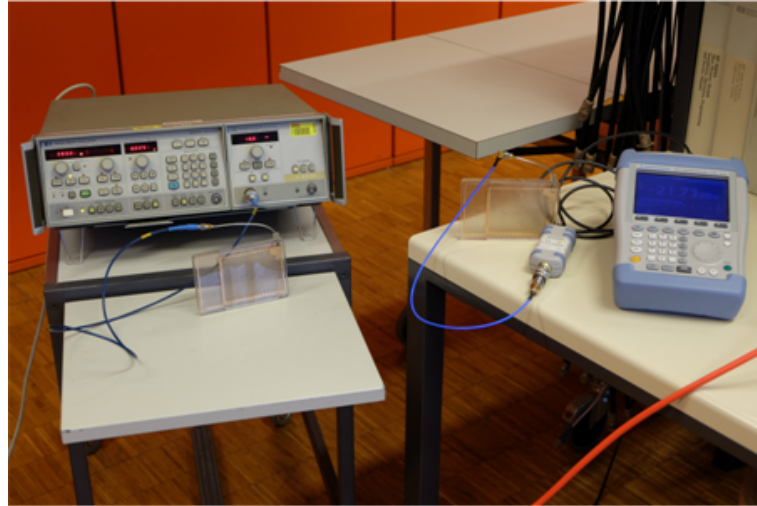


Fig. 5.8: Measurement equipment: *Hewlett Packard* power generator (left) and *Rohde & Schwarz* hand-held spectrum analyzer (right).

5.2.2 Equipment Used for Qualitative Measurements

For the qualitative measurements, the Polycom communication equipment provided by RUAG was used. It consists of a voice communication equipment developed for the purposes of the Polycom program users, military, police, rescue services etc. [151]. The equipment consists of a communication module, a battery unit, a microphone/loudspeaker and a standard Sub-Miniature version A (SMA) connector, so that different antennas can be connected. Different transmitting power levels can be set on this system, but for the purposes of the performed tests the transmitting power was set to 33 dBm (2 W), with a Frequency Division Multiple Access (FDMA) modulation. The full specification of the *POLYCOM Radio portable COVERT700* can be found in [13]. The Polycom communication set with the antenna (air-gap PIFA) attached to it is shown in Fig. 5.9.

Specially custom tailored vests, with sleeves that allowed a vertical orientation of the dipole legs (shoulder-hip), were provided by RUAG for measurement purposes. The vests have special pockets where the complete Polycom set can fit, Fig. 5.10. A vertical orientation of the dipoles was indicated as the best possible constellation, based on previous measurements and experiences from RUAG's customers (Saint Gallen police department).

The position of the dipole (Panorama) antenna, when mounted inside the vest, is indicated in Fig. 5.11 (a). Due to the specific shape and the materials they are made of, like leather or

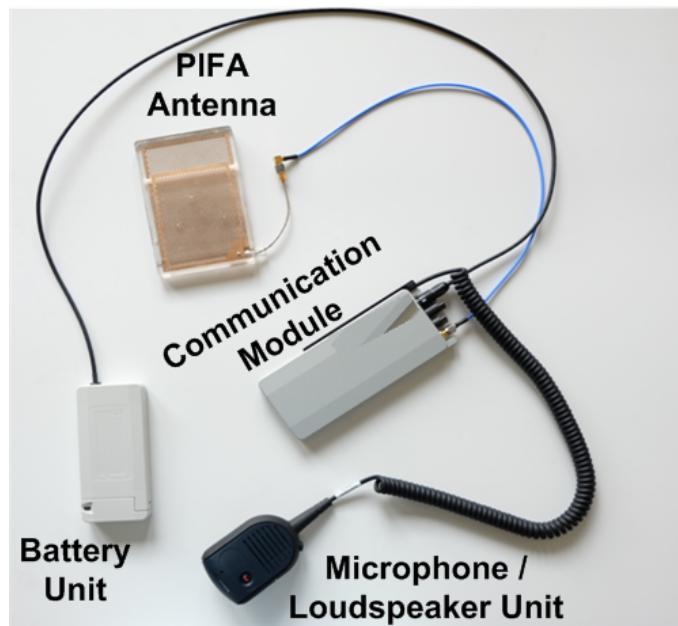


Fig. 5.9: Polycom communication set, provided by RUAG.

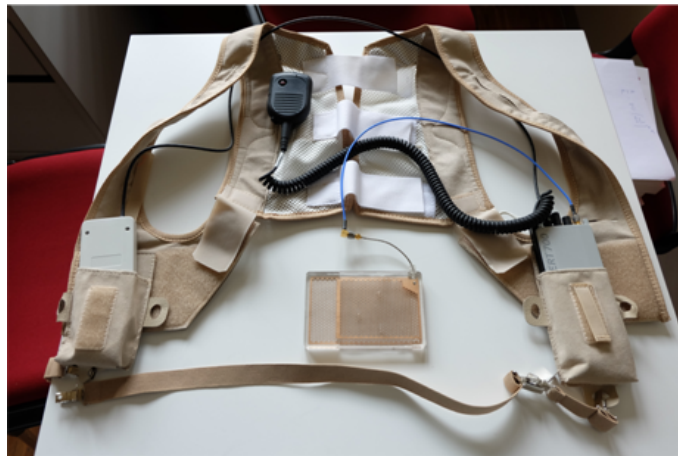


Fig. 5.10: Customized vests for Polycom purposes.

cordura, we were also using them while doing measurements with the air-gap PIFAs, in order to ensure identical conditions, mainly equal separation from the body. The tailored orange vests (Fig. 5.1) were always put over the Polycom vests, Fig. 5.11 (b).

5.2.3 Measurements Inside the Laboratory (Corridors+Offices)

Laboratory environment was chosen first for testing the antennas performances. The diversity created by the different offices, corridors and various objects represents a typical indoor environment. The plan of the laboratory unit corridors and offices is depicted in Fig. 5.12.

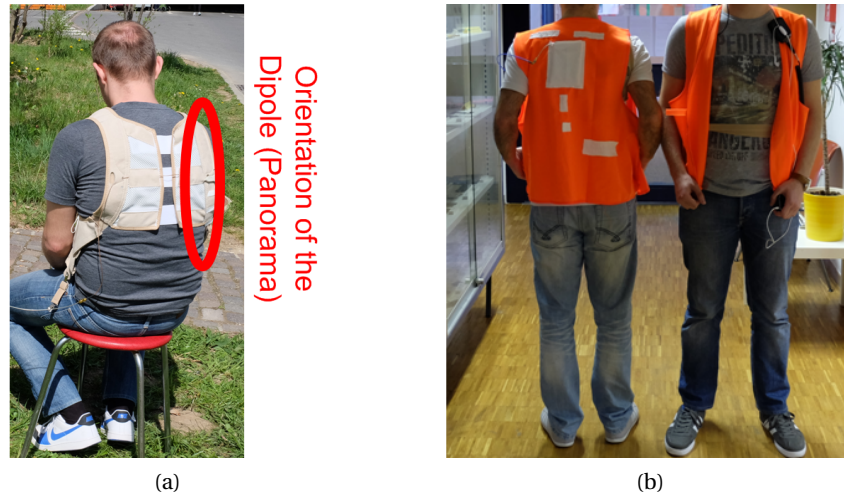


Fig. 5.11: Wearers in action: (a) Dipole (Panorama) antenna introduced inside the vest's sleeves and (b) Custom tailored vests for air-gap PIFAs put over the Polycom vests.

White parts correspond to corridors, while the gray zones are the offices and different rooms within the laboratory. The whole unit is 50 m in length and 20 m in width. Two different measurement campaigns were conducted.

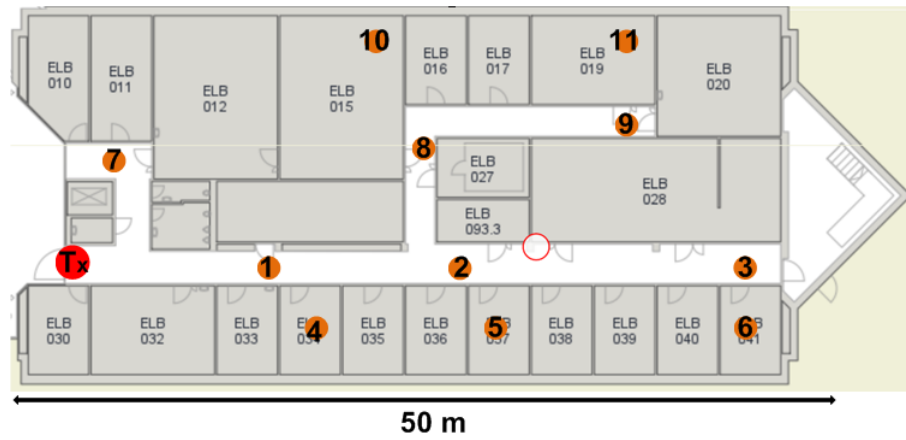


Fig. 5.12: Laboratory plan (LEMA).

In the first campaign, the Polycom communication units were used and a quality of the established voice communication was evaluated. Two wearers, equipped with the indicated sets, were going around the laboratory corridors and rooms while trying to establish comprehensive communication. For all the possible situations, for both antenna pairs, air-gap PIFAs and dipoles (Panorama), satisfactory coverage was achieved. No differences were observed in the quality of communication. Still, it should be mentioned that this was a subjective judgment of the wearers, while the recorded audio files exist as an evidence. There are mainly two reasons for such an outcome. The transmitting power set at the Polycom devices was +33 dBm (2

W), fairly large for such a small environment. The second reason was the environment of the laboratory itself. The metal ceilings and many lining metal cupboards (please refer to Fig. 5.13 (a)), create metallic waveguides that produce many reflections while performing the tests.

For the second measurement campaign, instead of qualitative and subjective evaluation, quantitative measurements were performed using a power generator on the transmitting side and a hand-held spectrum analyzer on the receiving side. One of the wearers, the so-called T_x wearer, had a fixed position at the entrance of the laboratory corridor (red spot in Fig. 5.12), while the second wearer, the so-called R_x wearer, was going around the corridors and rooms with the spectrum analyzer and measuring the levels of the received power. For all the reported cases, the antennas are worn on the wearers' back. The antenna of the T_x wearer was connected to the output of the power generator (continuous wave mode, transmitting +18 dBm (63 mW) all the time), while the R_x wearer was going around and stopping at each of the pre-determined 11 points, (points 1-11 as indicated in Fig. 5.12). For each point two measurements were done, one while the antennas were facing each other, and the second while the R_x wearer was randomly turned in some direction, mainly trying to have the body in the link. One measurement situation is shown in Fig. 5.13 (b), a T_x - R_{x1} LoS case.

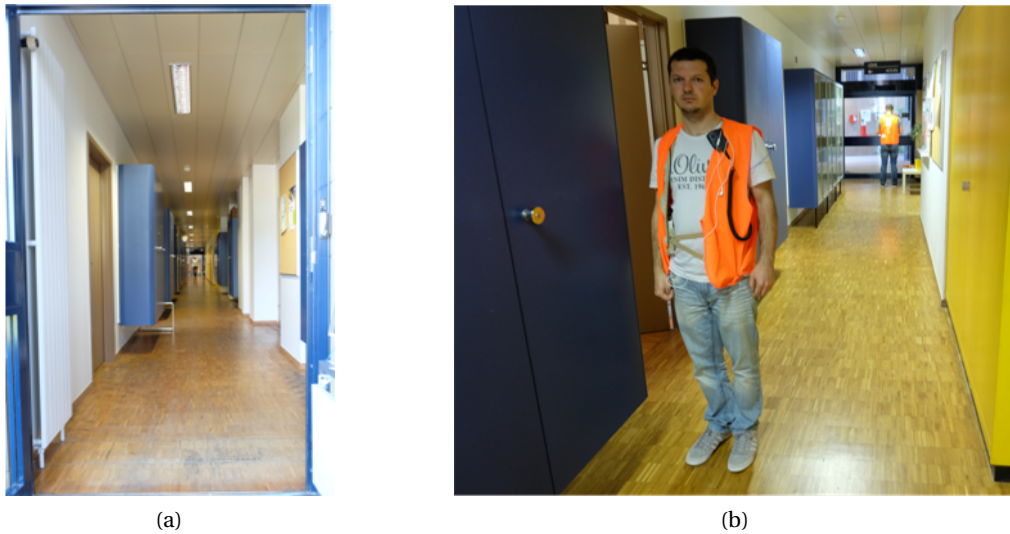


Fig. 5.13: Measurements inside the laboratory corridor and offices: (a) Interior of the corridor and (b) One of the performed measurements.

The measured power levels for all the cases are reported in Table 5.2. Looking at the values for both antenna pairs, they do not differ significantly, so the only way to compare them quantitatively was to make a geometrical averaging of all the received power levels for a given antenna pair for a given orientation (e.g. LoS or NLoS). For both cases, LoS and NLoS, the average received power for PIFAs was higher by 3 dB and 1 dB, respectively.

5.2. Measurements in a Realistic Environment

Taking into account the specific environment and conditions under which the measurements were performed, we have found that the geometric mean provides a realistic picture about the performance of the antennas in such scenarios. Namely, with this type of averaging, all the considered values are treated with equal weight. If linear averaging were used, the dominant contribution would originate from the highest received power level, thus neglecting all the lower ones, giving a too large importance to the path loss and potential multiple reflections occurring in the considered environment.

Position of the R_x wearer	Air-gap PIFAs		Dipole (Panorama) antennas	
	P_{rcvd} [dBm] (LoS)	P_{rcvd} [dBm] (NLoS)	P_{rcvd} [dBm] (LoS)	P_{rcvd} [dBm] (NLoS)
R_{x1}	-35	-48	-35	-43
R_{x2}	-52	-52	-50	-52
R_{x3}	-65	-67	-62	-55
R_{x4}	-45	-49	-55	-60
R_{x5}	-64	-70	-68	-68
R_{x6}	-80	-90	-78	-78
R_{x7}	-45	-50	-40	-50
R_{x8}	-62	-62	-74	-68
R_{x9}	-73	-73	-78	-88
R_{x10}	-63	-63	-72	-68
R_{x11}	-82	-85	-80	-93
Averaged received power	-60	-64	-63	-65

Tab. 5.2: Received measured power levels inside the laboratory (LEMA).

5.2.4 Measurements Inside the University Building

For the second measurement campaign, the area of interest was extended to several neighboring buildings next to the LEMA laboratory. Again, qualitative and quantitative measurements were performed. Fig. 5.14 (a) depicts the plan of the buildings where the measurements were performed. The dark parts are the buildings, while the light zones are outdoor space between them.

In the first part, the evaluation of the established voice communication was performed by using the Polycom communication sets. Again, no significant differences were observed between the two antenna pairs in terms of the quality and comprehension of the voice communication. Recorded audio files exist as an evidence.

Chapter 5. System Measurements and Comparison with the Commercial Antennas

For the second part, the T_x wearer had a fixed position at the entrance of the LEMA laboratory (Position marked as T_x in Fig. 5.14 (a)), while the R_x wearer was moving around the buildings, 1-4, as marked in the Fig. 5.14 (a). The antenna of the T_x wearer was connected to the output of the power generator (continuous wave mode with +18 dBm output power). Since, the measurements were in different buildings, and with many obstacles in between, orientations of the T_x and the R_x wearers were randomly defined and for each position one measurement was done.

Fig. 5.14 (b), shows the typical interior of the buildings, where combination of different structures and materials like metal, concrete, tiles, etc., are present.

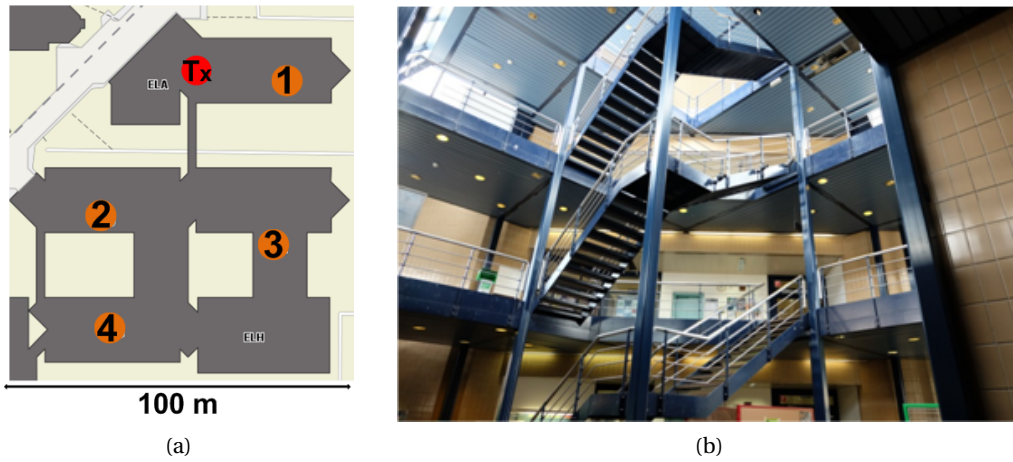


Fig. 5.14: Measurements inside the campus buildings: (a) Building plan and (b) Interior of the buildings.

Table 5.3 summarizes the measured results, reporting the geometrical averaging of the measured power levels as a quantitative comparison between the two antenna pairs.

Position of the R_x wearer	Air-gap PIFAs	Dipole (Panorama) antennas
	P_{rcvd} [dBm]	P_{rcvd} [dBm]
R_{x1}	-55	-57
R_{x2}	-59	-66
R_{x3}	-68	-70
R_{x4}	-65	-65
Averaged received power	-61.75	-64.5

Tab. 5.3: Received measured power levels inside the department buildings (EL).

The air-gap PIFA on average had for 3 dB higher received power level, results similar to the laboratory measurements.

5.2.5 Measurements on the Campus (Outdoor)

In this scenario the measurements were performed in the wider area of the EPFL university campus, mainly outdoor. Since the sensitivity of the used spectrum analyzer was not sufficient anymore, the measurements were done only with the Polycom communication sets. The idea was to check the quality and comprehension of the established voice communication while the wearers were walking across the campus. As can be seen from the aerial picture in Fig. 5.15, the campus consists of various types of buildings distributed in a different way, thus mimicking a realistic urban environment. The wearers were moving mainly at level 0 and level 1, in accordance with the terrain configuration.

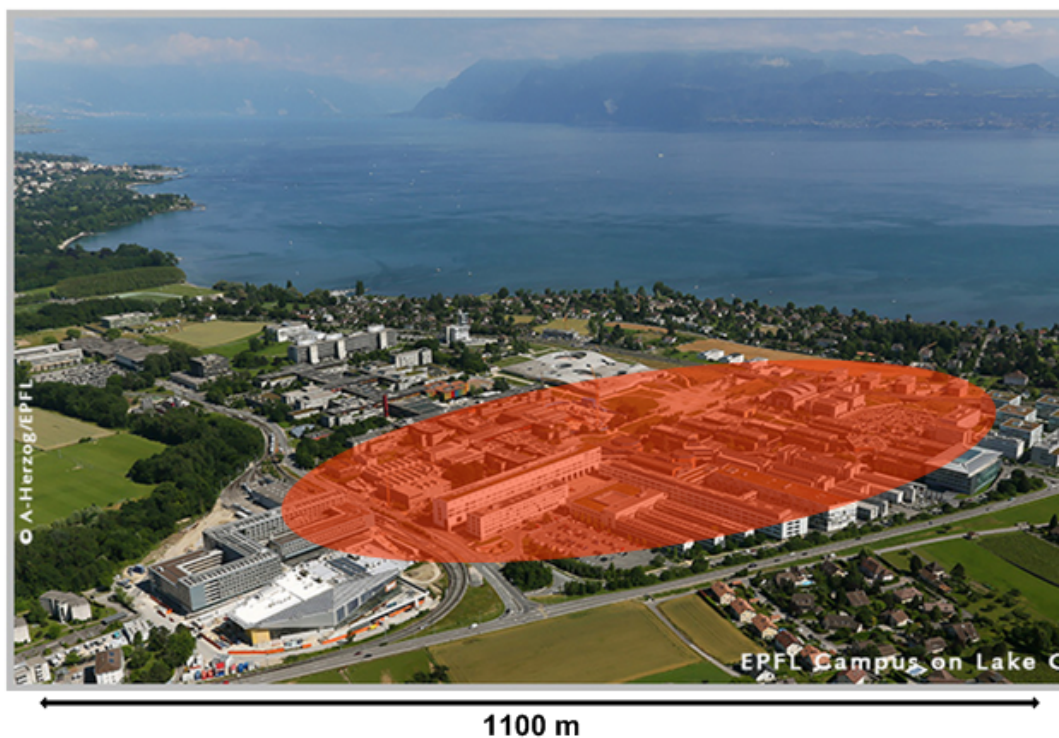


Fig. 5.15: EPFL Campus. Shaded part is the area where successful coverage was established.

The trajectory of the movement of the two wearers is depicted in Fig. 5.16. Both wearers started from the same point, marked as "*START FINISH*" in the figure, and moved in opposite directions, as indicated with the arrows. The quality of the established voice communication was comprehensive all the time, apart from the two spots (marked as blind spot 1 and 2 in Fig. 5.16). At these points, no communication was established because of the underground passages depicted in Fig. 5.17. Both antenna pairs, PIFAs and dipoles, performed equally in the given scenario.

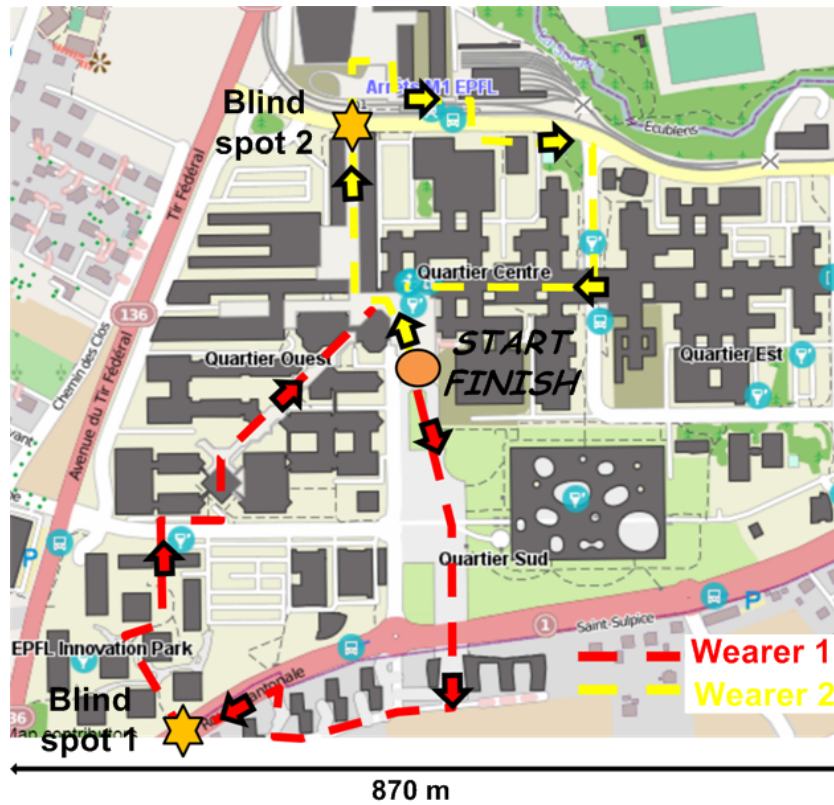


Fig. 5.16: EPFL plan with the trajectories of the two wearers.



(a)



(b)

Fig. 5.17: Blind spots marked with the stars in Fig. 5.16: (a) Under the road (1) and (b) Underground passage (2).

The performed scenario has shown that the proposed antennas are able to provide stable and comprehensive communication in an urban environment.

5.2.6 Extended Outdoor Scenario (on the Campus)

A more challenging scenario was considered in order to test the communication limits of the investigated antennas. Since the previous scenario did not report any particular difficulties and/or differences in the established communication over the entire campus area, we have decided to perform a more challenging scenario. The map of the whole EPFL campus is depicted in Fig. 5.18. This time, one of the wearers (wearer 1) was located at the 0 level (black spot in Fig. 5.18), inside the office, while the second wearer was going across and along the campus, going at different levels, 0-3, inside and outside the buildings. A moving trajectory of the wearer 2 was partially predefined, so that the wearer 1 knew how it should be oriented, pointing the antenna roughly in a direction where the wearer 2 was at that moment. The same scenario was repeated for the two antenna pairs, dipoles (Panorama) and air-gap PIFAs.

Fig. 5.19, (a)-(d), shows the coverage per level and per antenna pair. For all the cases, (a)-(d), the non-shaded areas represent the parts where no access was allowed, red shaded are the areas where both antennas performed equally well, whereas black shaded areas are the regions where no coverage was established neither with PIFAs or dipoles. Finally, the blue shaded area is the difference in favor of PIFAs, where understandable and comprehensive communication was established by using the air-gap PIFAs but not the commercial dipoles (Panorama).

Analyzing level by level, it can be seen that for each case PIFAs were providing a wider coverage, sometimes more emphasized sometimes less. The most remarkable difference is for the level 0, where PIFAs coverage was almost twice as large (in terms of covered area/surface) compared to the dipoles. Similar trends are observed for levels 2 and 3. Both antenna pairs perform almost equally only at level 1, with slight advantage for the PIFAs. As the PIFAs have a hemispherical radiation pattern, they provide better coverage in both azimuthal and elevation plane, thus resulting in better overall communication links. The coupling to the wearer is also lower in the case of PIFAs, enabling higher radiation efficiency, resulting in a wider communication area coverage.

Overall, PIFAs provide better communication links, in the sense that for the same measurement constellation and the same transmitted power, a comprehensive communication is achieved for larger area with PIFAs than with dipoles.

In order to have a better insight in the campus environment, several different areas are depicted in Fig. 5.20. As can be seen from the pictures, in different areas, buildings and floors different materials are used for construction purposes, thus giving a very diverse environment with metal, glass, concrete, wooden surfaces etc.



Fig. 5.18: Map of the EPFL campus.

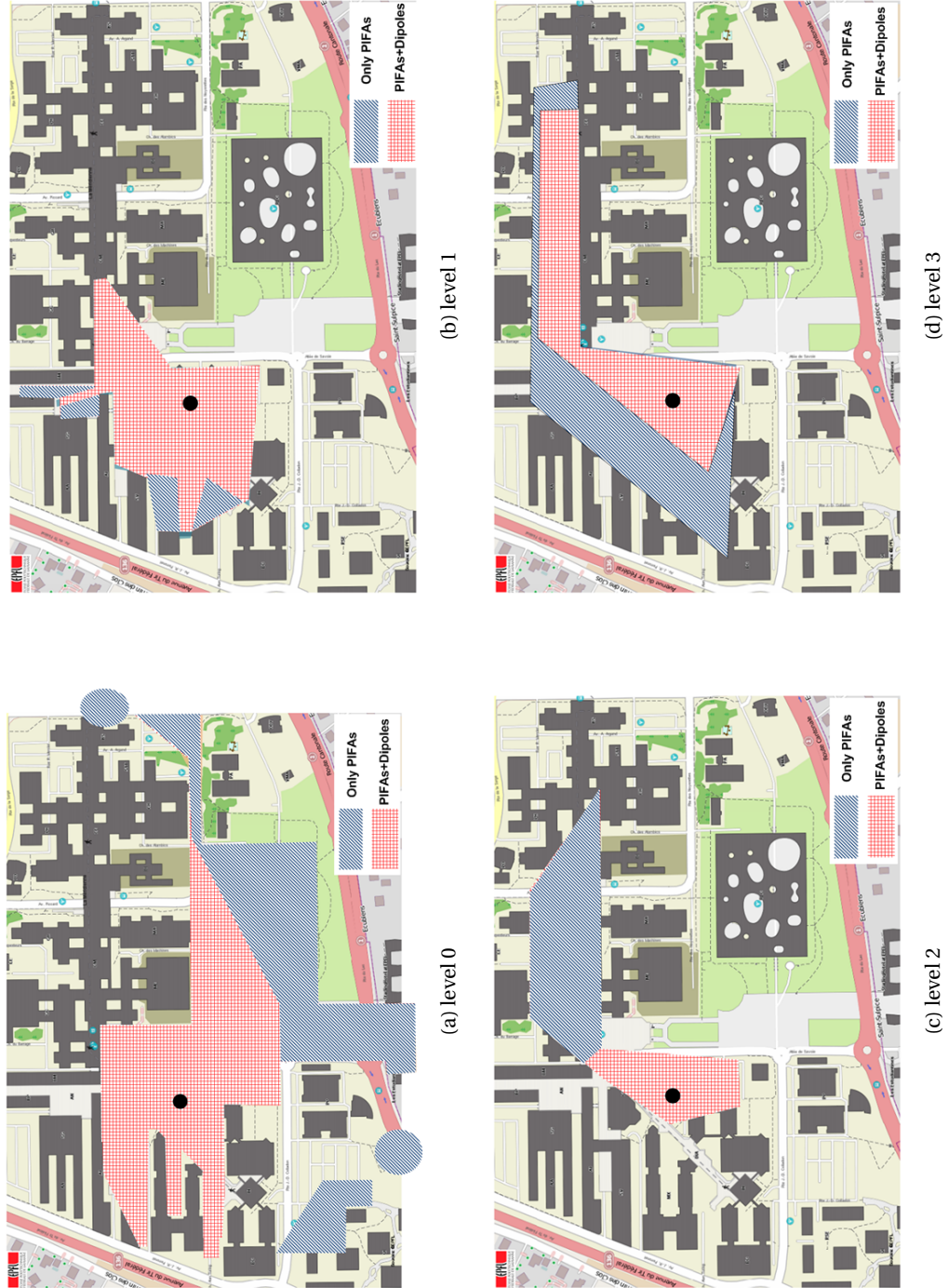


Fig. 5.19: Communication coverage at different levels with PIFAs and Dipoles: (a) level 0, (b) level 1, (c) level 2 and (d) level 3.



(a) Level -1



(b) Level 0



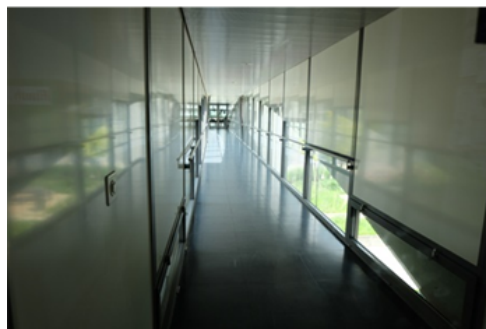
(c) Level 0



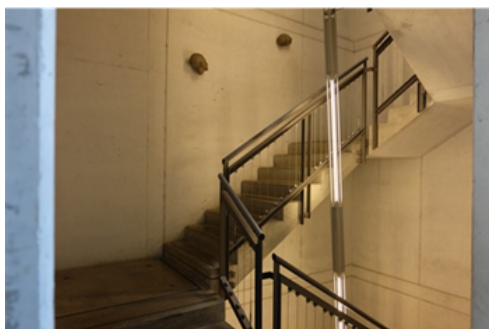
(d) Level 1



(e) Level 1



(f) Level 2



(g) Level 3



(h) From level 5

Fig. 5.20: Different buildings and levels across the EPFL campus.

5.2.7 Outdoor, Open-Field Scenario (Aarberg Area)

With the exhaustive extended campus measurement campaign, most of the aspects of performance and communication in urban environment were exploited. Nonetheless, since the proposed antennas are supposed also to be used in different rural and outdoor conditions, additional tests were needed to assess the performance of the antennas in such surroundings. For that reason, we have found an area with rather flat terrain configuration, where for almost 8 km there was no significant change in elevation (max elevation 3 m).

Polycom sets served the purpose for the qualitative measurements. Wearer 1 was fixed in one point (red spot in Fig. 5.21) while the wearer 2 was moving away and the evaluation of the established voice communication was tested. Since the distances were in the range of several kilometers (km), a bicycle was used as a means of transportation ☺. Some of the measurements were done in motion (10-15 km/h bicycle speed), while others statically (going off the bicycle each time the measurement was performed). Same scenario was repeated for both antenna pairs. The maximum distance between the two wearers and thus antennas, where still understandable communication was achieved, was around 7.3 km for both antenna pairs.



Fig. 5.21: Outdoor field measurements in Aarberg-Worben area, Switzerland, (OpenStreetMap^a).

^a<http://www.openstreetmap.org/>

Chapter 5. System Measurements and Comparison with the Commercial Antennas

Here, one important remark should be pointed out. For the specified measurements, a special permissions were issued by the Swiss regulatory office, Swiss Federal Office of Communication [11], strictly defining the frequency band for the outdoor test measurements. The dedicated frequency was 384.245 MHz. Looking back at the $|S_{11}(f)|$ responses of the air-gap PIFAs and the dipole (Panorama) commercial antennas when placed on a wearer (shown in Fig. 5.6), one can see that the PIFAs for the specified frequency range were fairly out of their matched region, which was not the case with the dipoles. Our assumption was that by having the PIFAs well-matched ($|S_{11}(f)| < -10$ dB) the range of the potential communication distance could have been extended further.

Fig. 5.22 shows the area where the measurements were performed, nearby Aarberg, the so-called "three lakes region" in the north-western part of Switzerland.



(a) Measurement equipment



(b) Terrain config.



(c) Terrain config.



(d) Terrain config.

Fig. 5.22: Terrain configuration in Aarberg area.

Yet, since we had the opportunity to be outdoor, we also performed a set of quantitative measurements, similar to the ones described in the previous sections. The only difference here was that we could not use the power generator (no convenient electrical supply), but the Polycom unit was used as a transmitter instead. The transmitting power of the unit (+33 dBm

5.2. Measurements in a Realistic Environment

(2 W)), although modulated, was sufficiently large to evaluate the performance of the antennas at larger distances. At the distance of 2.3 km the sensitivity of the hand-held spectrum analyzer was still enough (around -110 dBm) to measure the received power levels. Table 5.4 reports the measured received power levels for both antenna pairs.

T_x - R_x wearer distance [m]	Air-gap PIFAs		Dipole (Panorama) antennas	
	P_{rcvd} [dBm] (LoS)	P_{rcvd} [dBm] (NLoS)	P_{rcvd} [dBm] (LoS)	P_{rcvd} [dBm] (NLoS)
T_x - R_{x1} =170	-71	-71	-68	-75
T_x - R_{x2} =350	-81	-79	-81	-85
T_x - R_{x3} =550	-88	-99	-88	-90
T_x - R_{x4} =750	-79	-81	-90	-88
T_x - R_{x5} =1400	-96	-101	-100	-100
T_x - R_{x6} =2000	-96	-101	-105	-107
T_x - R_{x7} =2300	-96	-101	-110	-105
Averaged received power	-86.7	-90.4	-93.75	-94.75

Tab. 5.4: Received measured power levels in outdoor conditions (Aarberg).

Graphical representation of the received measured power levels is shown in Fig. 5.23.

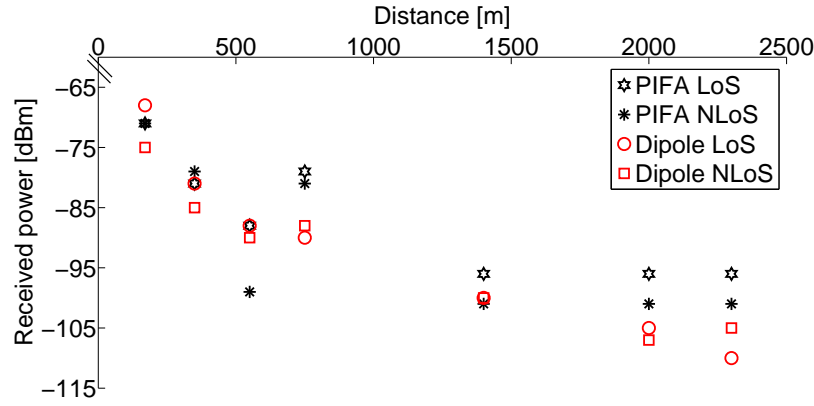


Fig. 5.23: Received measured power levels in outdoor conditions (Aarberg).

For both evaluated orientations, LoS and NLoS, air-gap PIFAs received for 7 dB and 4 dB, higher power compared to the dipole (Panorama) antennas, respectively. This leads to the conclusion that the air-gap PIFAs are more favorable candidate for a realistic outdoor communication. In order to further strengthen this statement we introduced an additional rotating scenario, described in the next section.

5.2.8 Rotating Scenario (Outdoor)

In the rotating scenario the two tested antenna pairs were measured while being fixed in a controlled outdoor environment with pre-determined positions and orientations. The T_x wearer was connected to the power generator (continuous mode with +18 dBm output power), staying all the time at a fixed position, just rotating by 90° in the azimuthal plane. The R_x wearer is located first at a 30 m then at a 100 m distance from the T_x wearer. For both distances, the R_x wearer, having the antenna in one fixed position on the body, was also turning by 90° steps in the azimuthal plane. In each of the rotating positions and combinations (32 in total for one antenna pair) received power levels were measured. Fig. 5.24 illustrates the overall constellation and the measurement set-up.

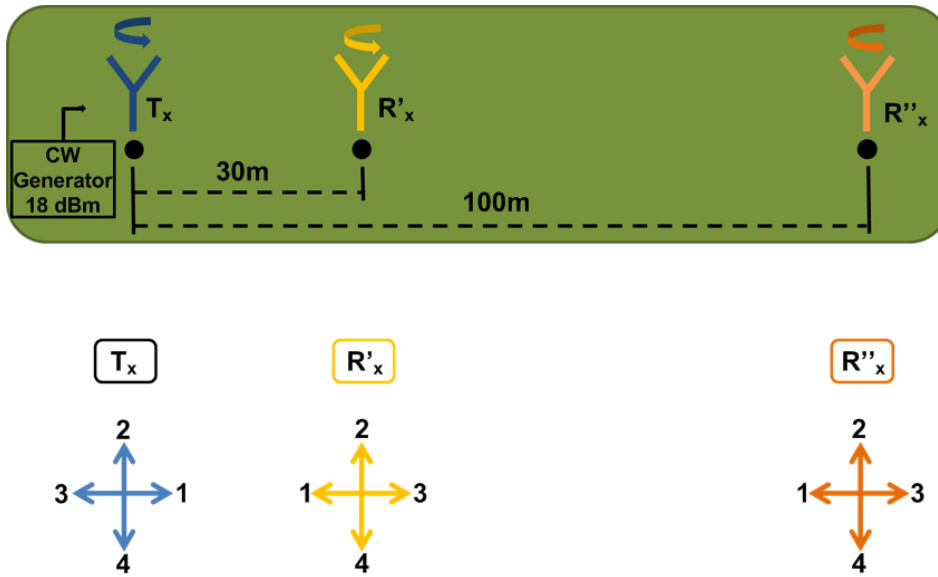


Fig. 5.24: Rotating scenario.

In order to clarify the described measurements, two measurement constellation will be described. For example, $T_{x1} - R_{x1}$ combination shows the scenario when the wearers, and thus the antennas, are turned in such a way so that the antennas are facing each other (LoS), Fig. 5.25 (a). Another example, the $T_{x1} - R_{x3}$ combination represents the orientation of the antennas so that always one wearer (body) is in between, while the antennas are oriented in opposite directions, Fig. 5.25 (b).

Table 5.5 reports the measured received power for all the combinations for both antenna pairs, at 30 m and 100 m distance, respectively. As in the previous cases, the averaged received power is used as a quantitative parameter for comparing the performance of the tested antennas. By analyzing the measured power levels, one can see that the differences between the obtained values for one antenna pair for a given scenario can significantly differ. Therefore, it was

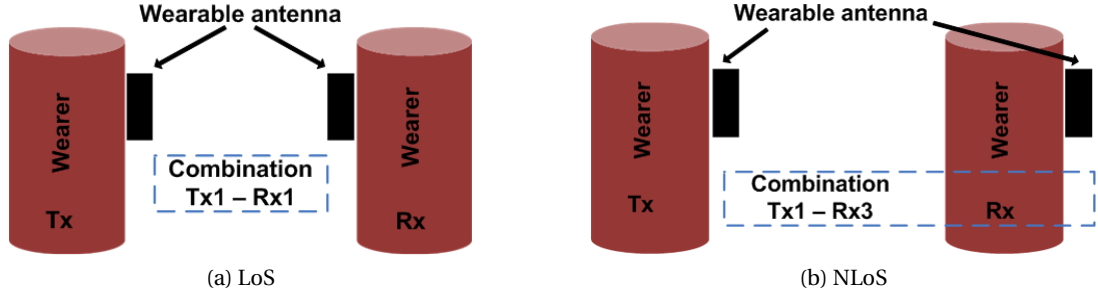


Fig. 5.25: Graphical representation of the measurement combinations.

decided that an additional parameter will be introduced: the maximum difference between any two values for a given antenna pair in a given scenario, in order to supplementary compare the performance of the tested antennas.

Rotating scenario	d [m]	30 m				100 m			
	[dBm]	R'_{x1}	R'_{x2}	R'_{x3}	R'_{x4}	R''_{x1}	R''_{x2}	R''_{x3}	R''_{x4}
Air-gap PIFA	T_{x1}	-62	-62	-67	-64	-84	-82	-84	-83
	T_{x2}	-70	-65	-70	-63	-84	-85	-88	-85
	T_{x3}	-62	-65	-65	-61	-85	-82	-90	-87
	T_{x4}	-60	-65	-64	-60	-78	-80	-82	-85
Dipole (Panorama)	T_{x1}	-60	-59	-63	-77	-88	-87	-86	-90
	T_{x2}	-78	-71	-73	-82	-88	-87	-90	-91
	T_{x3}	-80	-79	-77	-84	-90	-88	-85	-90
	T_{x4}	-62	-67	-72	-77	-88	-93	-90	-95


Tab. 5.5: Received measured power levels from the rotating scenario.

Table 5.6 summarizes the measured power levels by reporting the average received power and maximum power deviation. For both scenarios air-gap PIFAs exhibited higher received average power and lower received power differences, thus showing a better radiation behavior in the azimuthal plane.

Rotating scenario	30 m		100 m	
	AVG P_{rcvd} [dBm]	Max diff. [dB]	AVG P_{rcvd} [dBm]	Max diff. [dB]
Air-gap PIFA	-64	10	-84	12
Dipole (Panorama)	-72	25	-89	15

Tab. 5.6: Received measured power levels from the rotating scenario.

A summary of all the measurements performed in realistic conditions is reported in Table 5.7.

Scenario	Lab. corridors		Univ. campus	Open field		Rotat. scen.			
	AVG P_{rcvd} [dBm]	(NLoS)	AVG P_{rcvd} [dBm]	AVG P_{rcvd} [dBm]	(LoS)	AVG P_{rcvd} [dBm]	Max diff. [dB]	AVG P_{rcvd}	Max diff.
AUT			Random orient.			30 m	30 m	100 m	100 m
				(LoS)	(NLoS)				
	-60	-64	-61.75	-86.7	-90.4	-64	10	-84	12
									
	-63	-65	-64.5	-93.75	-94.75	-72	25	-89	15

Tab. 5.7: Summary of the received power levels in realistic conditions.

5.3 Conclusions

This chapter presented comprehensive measurements conducted at a system level and under different circumstances. In the first part, the performance of the antennas was tested in a controlled environment, inside the anechoic chamber, where $|S_{21}(f)|$ levels were measured and stability of the antennas evaluated. The second part of the chapter reports the operation of the antennas in realistic everyday conditions. In all situations we have compared the proposed air-gap PIFAs with the currently available commercial antennas found on the market.

The measurements inside the anechoic chamber reported better performance of the air-gap PIFAs vs. the dipole (Panorama) commercial antennas. The measured $|S_{21}(f)|$ levels for both cases, LoS and NLoS, were for 10 dB higher for PIFAs. Moreover, during the $|S_{21}(f)|$ evaluations, the stability of the wearable antennas when placed on the wearer and/or when left to radiate in free space was observed. Stability of the antennas was evaluated by comparing the $|S_{11}(f)|$ responses. Again, air-gap PIFAs remained stable, within 1-2 MHz frequency shift, while the commercial ones were significantly changing their responses, clearly indicating a high dependence on the body presence. Furthermore, it was observed that they are exclusively designed for on-body performance, while in any other circumstances they cannot provide reliable operation.

The communication equipment provided by RUAG, offered us wide opportunities for testing the antennas in different urban and rural conditions. A set of quantitative (measuring received power levels) and qualitative (estimating the comprehensiveness of the established voice communication) tests were performed in order to assess the behavior of the air-gap PIFAs and wearable dipoles (Panorama) while being exposed in indoor, dense urban and open field non-populated environment. On average, air-gap PIFAs were always receiving between 3 and 6 dB more power for the same transmitted power. Moreover, the PIFA proved to have a more omnidirectional behavior when mounted on a wearer, as it was less sensitive to the rotation of the wearers.

All these results lead to the conclusion that PIFAs and their intrinsic structure are less dependent on the wearer than the commercially available antennas and they provide more favorable radiation pattern and better coverage.

6 Specific Absorption Rate (SAR), Near-field Effects and Radiation Efficiency

In Chapters 4 and 5, much of attention was drawn to the antenna-human body interactions. All the analysis was carried out to determine how the presence of the human body affects the wearable antenna performance. However, this interaction is actually bi-directional. Therefore, in this chapter it will be considered how the antenna affects the hosting body. Indeed, the electromagnetic (EM) fields from the wearable antenna will couple into the tissues and energy will be absorbed and deposited in a certain region or over the entire body.

Human body exposure to the EM radiation is monitored through several parameters like the increase of the temperature, the exposure to time-varying electric and magnetic fields or the commonly established Specific Absorption Rate (SAR). SAR is defined as the ratio between the transferred power and the mass of the body where the SAR values are evaluated [17]. Depending on the frequency range of interest, different parameters are observed with respect to the human body exposure to a uniform (plane-wave) electromagnetic field. Our main focus will be on the frequencies in the range between 300 MHz to several GHz, at which significant local, non-uniform absorption occurs and is evaluated through the SAR [169].

The wide use of wearable antennas in different applications requires precise regulations for the human body exposures to the EM radiation. There are mainly two standardization guidelines regulating this issue, one proposed by the Institute of Electrical and Electronics Engineers (IEEE) [170], and the International Commission on Non-Ionizing Radiation Protection (IC-NIRP) [169], and the second one proposed by the US regulatory Federal Communications Commission (FCC) [171].

The evaluated SAR values depend on several parameters: operating frequency, intensity of the field, polarization of the field, source-object configuration (whether the object is in the near or far radiation field), and the characteristics of the exposed body and ground and reflect effects. In the range between 100 kHz to 10 GHz, restrictions on the SAR are provided in

Chapter 6. Specific Absorption Rate (SAR), Near-field Effects and Radiation Efficiency

order to prevent entire body heat stress and excessive local tissue heating [169]. Two different exposures have been defined, occupational and general public exposure. The occupational exposure refers to population groups (adults) who are aware of the EM exposures and potential risks and trained to take adequate precautions. By contrast, the general public comprises all the other groups of people of all ages and different health statuses. In many cases, the wider public is not aware of their exposure to the EM radiation and it is not expected that they will take precautions to minimize or avoid the exposure. Therefore, stricter regulations are required for public as compared to occupational exposure [169].

The two different standards, IEEE/ICNIRP and FCC, have different definitions for the occupational and general public exposure. The provided definitions might refer to two different spatial averaged values, over the entire body, whole-body average SAR and localized SAR, e.g. head and trunk. Also, when evaluating SAR values, an important aspect is the averaging mass where the SAR is calculated. According to the ICNIRP/IEEE standard, the averaging mass is 10 g of tissue, while the FCC does the averaging over 1g of tissue. Table 6.1 presents all the defined values for both standards for different occupations, and different averaging (whole body or head/trunk) for the frequencies between 100 kHz and 6 GHz.

[W/kg]	Averaging mass	General exposure		Occupational exposure	
		Whole body	head/trunk	Whole body	head/trunk
IEEE/ICNIRP	10 g	0.08	2	0.4	10
FCC	1 g	0.08	1.6	0.4	8

Tab. 6.1: An overview of the defined SAR values for both standards, IEEE/ICNIRP and FCC for the frequencies between 100 kHz and 6 GHz^a.

^aIn the case of IEEE/ICNIRP standard, the upper limit is 10 GHz.

For the frequency ranges bellow 100 kHz and above 6 GHz (10 GHz for the IEEE/ICNIRP standards), different scientific bases are used for the basic exposure restrictions. At lower frequencies basic restrictions are provided on current density, in order to prevent effects on nervous system functions, while at the higher frequencies, up to 300 GHz, power density is taken as a basic restriction, in order to prevent the excessive heating in tissues near the body surface.

In our case, since the antennas are worn by professionals, occupational localized (trunk) averaged SAR values are considered. In all the SAR analysis performed for our research purposes a 10 g averaging mass is used, since the fields used in our simulations are considered to be with slow variation. Therefore, we will be referring to the IEEE/ICNIRP standard.

SAR limitations are particularly stringent in applications with a relatively high transmitting power like in the case of security applications. For these applications, the robustness and the

range of the communication link are important aspects, leading to the choice of a rather low frequency band to achieve the range and the use of a high transmitting power, leading to a potentially high SAR.

We will focus in our study on antennas operating between 360-370 MHz, with an intention to shift towards a transmission link between 380-400 MHz and high transmitted powers. There are two reasons why 360-370 MHz band has been selected for the SAR analysis: (1) lower frequencies are more challenging and demanding to remain within the defined SAR regulations and (2) compared to the hexagon PIFA models, the copper-mesh PIFA (solid conductors in simul.) is time wise a better option, as the time needed for the simulation is shorter compared to the hexagon models. Yet, our goal was not to calculate precisely the SAR values for the specific antenna types, but to analyze the general trends and ideas that have been proposed in this thesis. A solid conductor PIFA model is sufficiently good for these purposes.

Before presenting the performed analysis, an overview of relevant research work related to SAR in the frame of wearable antenna will be presented. Reduction of the SAR has been an ongoing topic for some time and it is of particular interest for implantable and wearable antennas.

A simple SAR investigation is presented in [172], where a dipole antenna at 400 MHz is used for observation of the induced SAR in a non-homogeneous model of human body. A set of simulations and measurements where different materials are used in order to assess the SAR values are presented in [173]. Fractal Planar Inverted F Antennas (F-PIFAs) designed for dual-band operation (2.45 and 5.2 GHz) are used to assess the influence of different materials on the SAR levels. The same antenna prototype is built using three different materials as conductors, copper foil, Shieldt and Plain Copper Polyester Taffeta Fabric (PCPTF) and felt (in all cases) as a substrate material. No significant differences in the simulated/measured SAR values are observed between the use of different conductive materials.

Material aspects are also considered in [174] where the SAR is reduced by using polymeric ferrite sheets as a shielding between the human body and wearable antenna. Reduction of the SAR can be observed from other perspectives as well. In [175] different insulating layers are introduced in order to improve the radiating efficiency of implantable antennas intended for telemetry applications. Although the SAR is not directly mentioned, the presented study clearly shows that if the antenna is well isolated from the vicinity tissues, the efficiency is higher. Higher efficiency is due to the reduced coupling to the human tissues, which on the other hand results in reduced SAR.

Since the human body is all the time in the near-field zone of the wearable UHF antenna, a special emphasize is put on the importance of the antenna-body interaction. A thorough study on this topic is presented in [169]. Reactive near-fields produce the majority of the energy in the lossy dielectric objects, in our case human body. Therefore, the near region of

wearable antennas should always be considered when SAR evaluations are required. Similar conclusions have been drawn in [176] for UWB antennas. Despite the fact that UWB antennas operate at higher frequencies compared to UHF antennas, thus having a smaller near field region than the latter, the reactive near field is still a significant contributor to the SAR in this case.

A thorough research of the EM field exposure analysis mainly for low frequencies (up to 100 kHz) has been reported in [177]. In this work, the author has analyzed separately the interaction of the electric and magnetic fields and their influence on the wearer. Indeed, at low frequencies where the wavelength is several orders of magnitude longer than the object (body) itself, the interactions inside the body become more quasi-static, while the electric and magnetic field components become decoupled [178].

From all the reported research on the topic of SAR, one can conclude that SAR is closely correlated to the near-field distribution. On the other hand, near-field effects also affect the overall radiation performances of the wearable antenna, more concretely the radiation efficiency. The less the wearable antenna is coupled to the body, the higher radiation efficiency can be achieved. Therefore, the near field region will be one of the pervading topics of this chapter around which the research hypothesis are built.

This chapter is organized as follows: section 6.1 presents the methods and models used for SAR and radiation efficiency analysis. In the second section, the role of the ground plane in the SAR reduction will be investigated. A comparison between the wearable dipole antenna and proposed PIFA will be used for demonstrating purposes. All the results regarding SAR reduction for PIFA are shown in section 6.3. The first part of this section presents the SAR dependence on the near fields triggered by the dense current distribution in the shorting wall region of the antenna, while the second part shows that the SAR reduction is also achievable if certain dielectrics are used. For both cases, some solutions have been proposed in order to overcome this problem. Finally, section 6.4 gives the conclusions and some future steps.

6.1 Models and Methods

All the following studies done regarding the SAR are based on simulations performed by a 3D EM software, HFSS. All simulations are performed in an identical environment for all the considered antenna models in terms of input matching, feeding structure, phantom size and structure and position of the observed antennas with respect to the phantom. Considering the group of applications we are interested in, we will be focusing our efforts on the analysis and SAR reduction for antennas operating between 360-370 MHz.

Two antennas have been used for the investigation purposes, (a) a proposed copper-mesh PIFA model and (b) a commercially available wearable dipole (Panorama) antenna [106]. The structure of the PIFA was already explained in section 4.1.1, and is summarized here. The model used for the simulation is a PIFA, built using solid copper conductive sheets encapsulated inside PDMS ($\epsilon_r = 2.15$ and $\tan \delta = 0.01$). The overall dimensions of the PIFA are $157.5 \times 88 \times 9.1 \text{ mm}^3$, Fig. 6.1 (a).

The model used for the dipole wearable antenna was designed in HFSS, based on the data provided from the datasheet [108]. The dipole has length of 256 mm and a feeding coaxial cable of 300 mm (in the simulation model), with conductors isolated with a PVC material, see Fig. 6.1 (b). For both antenna models the feeding structure is a coaxial cable with a wave port assigned on one end, and the defined input power at the port is 1 W. SAR values are calculated for a 10 g tissue averaging.

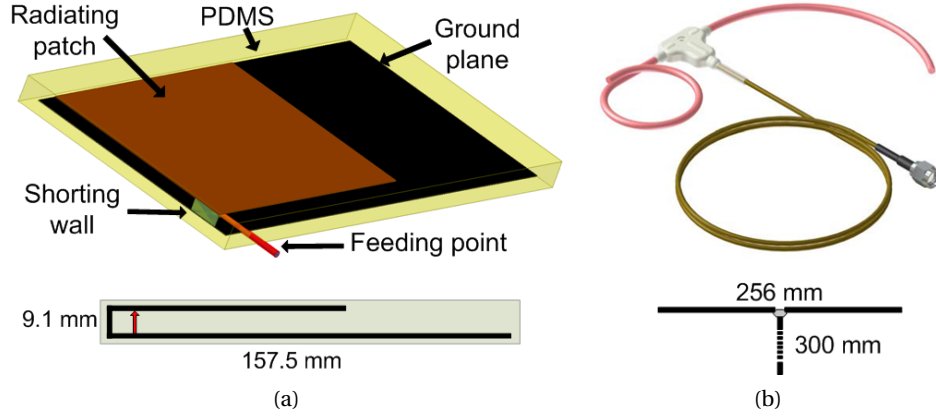


Fig. 6.1: Considered antenna models: (a) PIFA and (b) Dipole (Panorama) [106].

For simulation purposes, a simplified single layer phantom is used, mimicking the muscle characteristics at 400 MHz, $\epsilon_r = 56$ and $\tan \delta = 0.6$ [167]. The size of the phantom is $490 \times 560 \times 80 \text{ mm}^3$, large enough to ensure a quarter-wave length margin between the antenna and the phantom edges. Both antennas are simulated with 1 mm textile material, $\epsilon_r = 1$ and $\tan \delta = 0$ separating the antennas from the phantom. A SAR observation plane is introduced across the phantom thickness, below the feed, Fig. 6.2, as this is the hottest region for the SAR.

It should be noted that since the difference of magnitude between the different plots is large, the figures show different dynamic ranges. Each of the plots are averaged in accordance with the analyzed case.

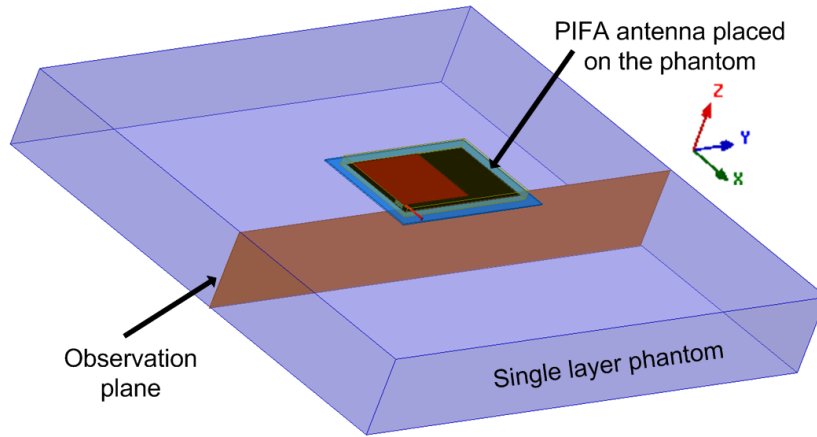


Fig. 6.2: Single layer phantom and the PIFA mounted on the top of it.

6.2 SAR Comparison, PIFA vs. Dipole

A starting point for the analysis was the comparison in performance between the commercial wearable dipoles and the proposed PIFAs. Indeed, since the dipoles have no ground plane in their structure, they are expected to have larger SAR, and thus higher peak SAR values compared to the PIFAs. Nevertheless, this comparison triggered some interesting observation aspects for the SAR for PIFAs.

The introduced antennas, PIFA and dipole (Panorama), are simulated and compared under the same conditions (phantom, power, averaging), with both antennas well matched, $|S_{11}(f)| = -15$ dB. The SAR distribution is presented in Fig. 6.3 (a) and (b), for the PIFA and for dipole antenna, respectively.

SAR distribution of the PIFAs is confined close to a region of the feeding point, indicating that the SAR is mainly due to the reactive near-field components. The near-field effects can be caused from the feeding structure or from some high density current regions. The advantage of the PIFA is that the structure of the antenna itself offers several degrees of freedom to diminish the near-field effects. This can be done either by introducing some specific feeding structure or relaxing the high density current regions. More details will be shown in the section 6.3.

The considered dipole antenna due to its shape and length allows a placement of the antenna on the wearer only in a way that the dipole's legs are parallel to the body. This way of placement will result in increased SAR both from the feeding point and the currents that flow along the dipole's legs. The main reason for this observation is that dipole feed produce high current and magnetic field, and it is closer to the tissue block, thus coupling the field energy more effectively because of feed orientation (electrical fields vectors parallel to the tissue block). Unfortunately, the dipole's structure does not offer many alternatives to overcome this issue,

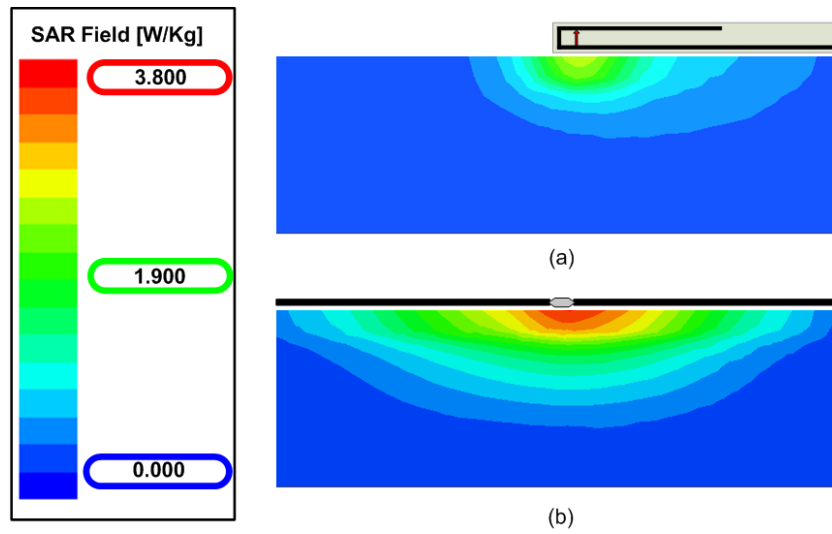


Fig. 6.3: SAR evaluation comparison between: (a) PIFA wearable antenna and (b) Dipole wearable antenna (Panorama) (all the plots are averaged to the maximum value of 3.8 [W/kg])

especially as the SAR originates not only from the near fields but also from the orientation of the field's vectors. The feed is set by the dipole's structure and there is no ground plane allowing to decouple the antenna from the wearer.

Table 6.2 reports the simulated values for the SAR and radiation efficiency for both antennas, as computed by HFSS.

<i>AUT</i>	SAR (peak value) [W/kg]	Radiation efficiency [%]
PIFA	2.68	4.7
Dipole	3.8	1.1

Tab. 6.2: Simulated values for the SAR and radiation efficiency as computed by HFSS.

The peak SAR value of the dipole is by 30% higher than the peak value of the PIFA. The difference in the computed efficiencies is even larger as the radiation efficiency of the dipole antenna (1.1%) is 80% lower than the efficiency of the PIFA, which is 4.7%. This result matches the assumption we have done based on the study performed in [175], that the SAR of the antenna is directly related to the antenna radiation efficiency. The conclusion is that whenever it is possible and when the application allows for it, antennas with ground planes should be used.

Both antennas exhibited rather low radiation efficiencies due to the strong coupling to the phantom. This was partially caused by the small separation between the antenna and the phantom.

6.3 Results

6.3.1 Near-fields Triggered by the High Density Current Regions

High density current regions are often present in places where miniaturization is applied on antennas. The proposed PIFA can be also considered in a similar manner. Since the antenna has a low profile, strong near-fields appear in the region between the feeding and the shorting wall, which are 7 mm apart. The shorting wall, $10 \times 4 \times 0.3 \text{ mm}^3$, and the ground plane area where it is connected generate a concentration of near-fields. In order to assess their effects, surface currents are observed in XZ plane parallel with the shorting wall, spread along the x-length (88 mm) of the ground plane, Fig. 6.4. A strong current concentration is detected in this plane which needs to be reduced to lower the SAR.

The spreading of the current region is achieved by enlarging slightly this part of the ground, extending it beyond the shorting wall, as shown in Fig. 6.4 (a), thus providing an extended current path. The surface currents are compared for three different situations: (1) no extension of the ground plane, (2) 4 mm extension and (3) 8 mm extension, Fig. 6.4 (b).

As can be seen from the field distribution, the extension of the ground plane reduces the fields in the lower region and redirects them mainly in the upper part. This is a desirable outcome for wearable antennas because the overall level of coupling is reduced and so is the SAR.

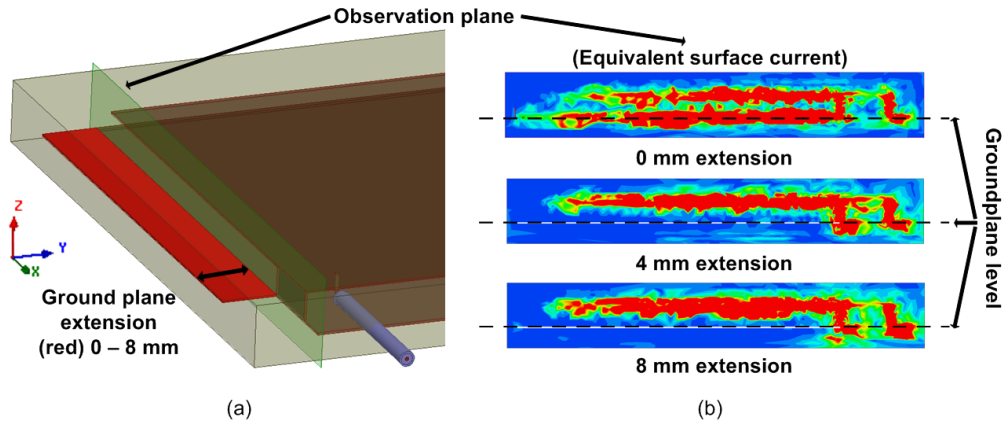


Fig. 6.4: (a) PIFA model with a ground plane extension and (b) Equivalent surface current in the XZ plane parallel with the shorting wall (all the plots are averaged to the maximum value (red) of 2.92 [A/m]).

The plotted SAR values depicted in Fig. 6.5 clearly show this tendency. The overall SAR distribution is reduced for the case of 8 mm ground plane extension compared to the case where no extension is applied. Looking on the concrete numbers, calculated peak SAR values, a 8 mm ground plane extension results in SAR reduction by 37% compared to the initial case.

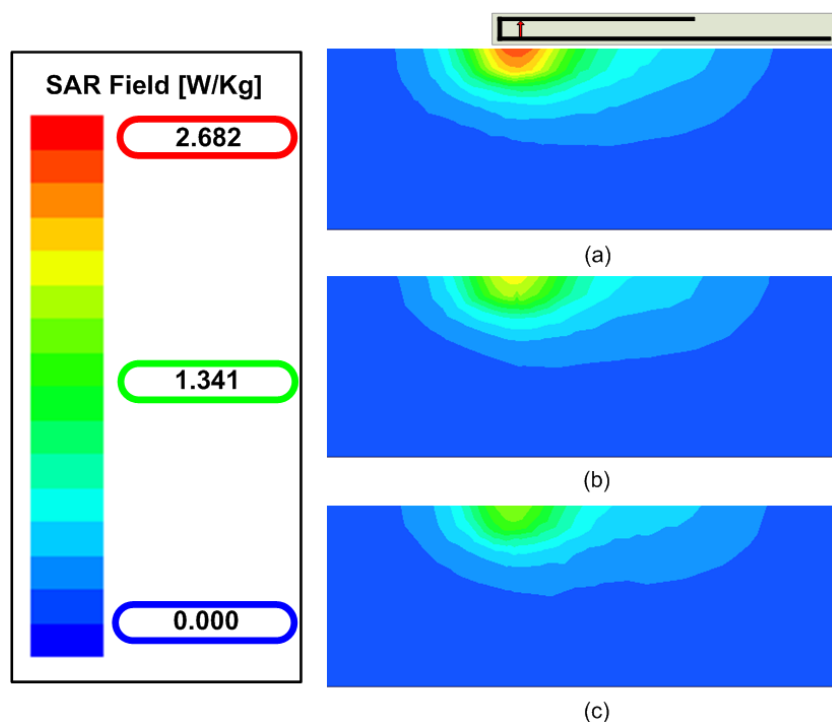


Fig. 6.5: SAR evaluation comparison for the PIFA: (a) With no extension of the ground plane, (b) with the 4 mm ground plane extension and (c) with the 8 mm ground plane extension (all the plots are averaged to the maximum value of 2.68 [W/kg]).

Near-field effects can also appear due to the feeding structure of the antenna. For instance, in our case the antenna is fed by a coaxial cable which introduces an inductance related to the length of the protruding inner pin of the cable. The higher this inductance is, the higher the related near fields and SAR will be. In the presented case, this effect is smaller than the effect of the shorting wall as the pin has been shortened to only 3 mm. Furthermore, the feed of the PIFA is vertical to the phantom and positioned behind the ground plane, thus additionally reducing the coupling to the body. Strong near-field effects can cause significant SAR increase, and deteriorate the overall antenna performances. It is thus very important to control the near field as much as possible, in order to reduce the SAR values in the wearer's body.

As expected, due to the changes in the structure of the PIFA, some changes occurred in the antenna's performances in the $|S_{11}(f)|$ response, Fig. 6.6, and in the radiation efficiency. There are no significant changes in the radiation patterns of the three different cases.

Table 6.3 summarizes the calculated values of the SAR, radiation efficiency and shifts of the $|S_{11}(f)|$ due to the modifications in the ground plane.

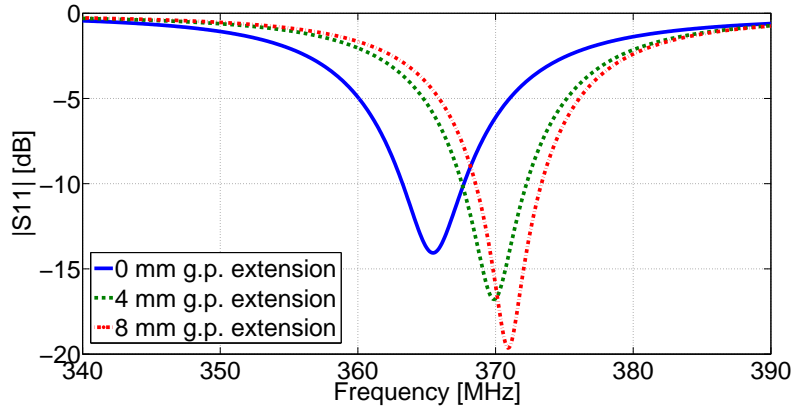


Fig. 6.6: Influence of the ground plane extension on the $|S_{11}(f)|$ response for the PIFA.

<i>AUT</i>	SAR (peak value) [W/kg]	Radiation efficiency [%]	$ S_{11}(f) $	
			[MHz]	[dB]
0 mm g.p. ext.	2.68	4.7	365	-14
4 mm g.p. ext.	2.04	5.6	370	-17
8 mm g.p. ext.	1.71	6	371	-19

Tab. 6.3: Simulated values for the SAR, radiation efficiency and $|S_{11}(f)|$, while extending the ground plane, as computed by HFSS.

6.3.2 Role of the Substrate Material in SAR Evaluation

The near-field impact on SAR can be partially diminished if substrates with higher permittivities are used. Higher permittivity substrates are able to confine the fields inside the material, thus reducing the near field coupling to the body. On the other hand, substrates with very high permittivities might lead to extremely low radiation efficiency, resulting in a non-operational antenna.

In order to check the role of the substrate in reducing the SAR, we simulated the proposed PIFA model, maintaining the same dimensions for the conductive parts, while changing the characteristics of the substrate. Three different cases were analyzed: (1) PDMS as defined in the initial simulation model, $\epsilon_r=2.15$ and $\tan \delta=0.01$, (2) PDMS without losses, $\epsilon_r=2.15$ and $\tan \delta=0$ and (3) no substrate (PDMS) at all. Since the losses of the used PDMS are not negligible, a part of the SAR reduction occurs due to the dielectric losses, which is unavoidable when PDMS is used. In order to separate the SAR reduction initiated by the field confinement due to the dielectric from the SAR reduction caused by the losses of the material, an additional check has been performed, using an ideal dielectric having the same permittivity as the PDMS but no losses, case (2). The obtained result presents how much reduction of SAR is due to the dielectric only. The three cases are presented in Fig. 6.7.

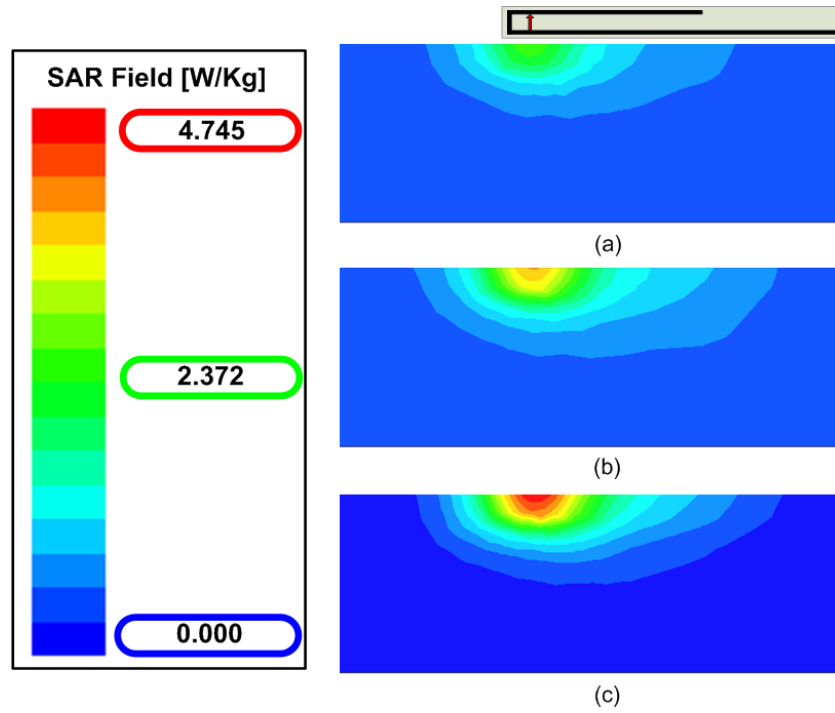


Fig. 6.7: SAR evaluation of the PIFA for the three different cases: (1)-(a) PDMS as defined in the initial simulation model, $\epsilon_r=2.15$ and $\tan \delta=0.01$, (2)-(b) PDMS without losses, $\epsilon_r=2.15$ and $\tan \delta=0$ and (3)-(c) no substrate (PDMS) at all (all the plots are averaged to the maximum value of 4.745 [W/kg])

Table 6.4 summarizes the calculated values of the SAR, radiation efficiency and shifts of the $|S_{11}(f)|$ due to the modifications in the ground plane.

<i>AUT</i>	Case	SAR (peak value) [W/kg]	Radiation efficiency [%]	$ S_{11}(f) $	
				[MHz]	[dB]
PDMS ($\epsilon_r=2.15$, $\tan \delta=0.01$)	(1)	2.68	4.7	365	-14
PDMS ($\epsilon_r=2.15$, $\tan \delta=0$)	(2)	4.12	7.2	366	-14
WITHOUT PDMS	(3)	4.7	17	523	-12

Tab. 6.4: Simulated values for the SAR, radiation efficiency and $|S_{11}(f)|$, while changing the substrate's characteristics, as computed by HFSS.

Dielectric properties of the substrate materials also affect the antenna's radiation characteristics. The three analyzed cases, (1) PDMS with losses, (2) PDMS without losses and (3) antenna without PDMS reported interesting results: cases (1) and (2) show similar behavior in terms of radiation pattern, frequency and matching level, while the efficiency is improved in (2) by 53%. In case (3), all the radiation parameters have changed significantly : $f_c=523$ MHz, $|S_{11}(f)|=-12$ dB and the radiation pattern has been modified. This behavior is expected since, by removing the substrate, the configuration of the antenna is changed.

Chapter 6. Specific Absorption Rate (SAR), Near-field Effects and Radiation Efficiency

Although case (3) shows an improvement in the efficiency by 25%, compared to the case (1), looking at the SAR we observe an opposite trend, case (1) for 40% lower peak SAR value compared to the case (3).

The above study shows that the contribution of the dielectric to the SAR reduction is significant, even if it is masked by the effect of the losses in the case of PDMS. The market of the elastomers used in electronics, and thus in antennas, is in constant progress and different flexible materials are appearing [179]. These polymers have similar characteristics to PDMS, they are transparent and elastic and used in different microfluidic chip production. Substrate materials with good dielectric properties can still significantly contribute to the SAR reduction for wearable antennas.

6.4 Conclusions

In this chapter we pointed out to the importance of the near-field effects while assessing the performance of wearable antennas. A strong correlation between the near-field region and radiation efficiency and SAR was demonstrated on the observed examples. For the wearable antennas that operate at lower frequencies, for instance in UHF band, the influence of the near-field effects is even more emphasized since the hosting body is located in the antenna's near field region. A PIFA model was used for the demonstration purposes, while at the same time modifications in its structure were proposed in order to ameliorate the overall antenna's performances.

The PIFA is a good candidate for wearable antennas in security scenarios, where high SAR values might be an issue, as its structure inherently gives the possibility to diminish the obtained SAR values by careful design. In particular, the presence of the ground plane is of paramount importance, as it greatly reduces the coupling of the antenna to the wearer's body. This lowers the SAR, and enhances the overall antenna radiation efficiency.

In the particular example of the PIFA used in this case, extending the ground plane gives additional freedom for spreading high density current regions (shorting wall). Specifically, an extension of ground plane of only 5% compared to the initial size, reduces the overall SAR by more than 35%.

The confinement of the near field regions of the wearer is another strategy to reduce the SAR and enhance the efficiency. This can, for instance, be achieved by using a dielectric substrate to manufacture the antenna or by carefully designing the feed region. Moreover, a combination of ground plane extension along with some higher permittivity substrate materials will inherently lead towards SAR reduction.

7 Conclusions and Perspectives

*Сунце ће једном престати да сија и његова
топлота која нам живот даје повући ће се и
наша властита Земља постаће грумен леда
који јури кроз вечну ноћ ... У међувремену
охрабрујућа светлост науке и уметности, увек
све јача по интензитету, осветљава нам пут
...*

*The suns bright light will have ceased to shine and its life
giving heat will have ebbed away, and our own earth
will be a lump of ice, hurrying on through the eternal
night. But do not let us despair... Meanwhile the
cheering lights of science and art, ever increasing in
intensity, illuminate our path ...*

—Nikola Tesla, in *Century* 1900

7.1 Conclusions

Wearable applications and, thus, wearable antennas are becoming an unavoidable part of nowadays wireless communication. Various activities can be accomplished and many of them can be significantly accelerated with the help of wearable applications. For instance, in modern health care, data collected from different sensors (e.g. blood pressure, temperature, etc.) worn by a patient can be transferred to peripheral units (smart phones, tablet) and sent to a hospital or a medical doctor, who can in turn provide feed-back within a couple of minutes [180].

Chapter 7. Conclusions and Perspectives

Many wearable antennas have been reported in the literature, covering different applications and various frequency bands. Nevertheless, there is still no clear overview or guideline on how to tackle the design of wearable antenna for a particular application. A classification of wearable antennas according to different categories was actually the starting point of this thesis and it was addressed in Chapter 2. A detailed overview of the various antenna types found in different applications, built with different technologies and materials were presented.

The aim of this thesis was to provide an appropriate wearable antenna design suitable for security applications, more specifically for voice communication inside the commercially used Tetrapol band. In this context and specified project requirements, we defined two main challenges addressed in this thesis: (A) **Coupling** - Antenna \leftrightarrow Human body interactions and (B) **Robustness** - communication, mechanical and environmental robustness. Several sub-challenges were derived from the initial two.

In Chapter 3 a combination of substrate and conductive materials was investigated and proposed for fabricating robust wearable antennas. We proposed substrate materials whose EM properties can be adjusted (for instance reducing their relative permittivity and/or loss angle) while the materials preserve their flexible, bio-compatible and waterproof characteristics. For the purposes of this thesis research, we opted for a silicone based elastomer, PDMS. However, the proposed solution can be extended to any other material whose dielectric and mechanical properties satisfy the specified criteria.

A widely present problem with the use of silicon based materials, the adherence to conductive sheets, was overcome by proposing mesh or perforated conductive structures. Apart from being flexible, their mesh and/or perforated structure in a combination with the initial liquid state of PDMS allowed complete immersion of the conductors inside the silicon, resulting in a robust, flexible and waterproof structure.

In parallel with the exploration of the technology, we analyzed the potential antenna candidates that would respond to the defined requirements. The overview performed in Chapter 2 helped us to select an appropriate antenna type. A Planar Inverted F Antenna (PIFA) was selected as an adequate candidate. The PIFA's overall size with respect to the wavelength allowed an easy integration into the wearer's uniform, without affecting its daily activities.

The detailed antenna designs and the measured antenna characteristics were reported in Chapter 4. With the three proposed PIFA prototypes we tackled the defined challenges. With the first prototype we showed the sustainability of using PDMS as a substrate and copper-mesh structures as conductor, thus mitigating the problem of adherence. An imprecision issue that appeared due to the mesh fraying was overcome by introducing perforated conductive sheets, using hexagon shapes for perforation, which also contributed to the overall miniaturization of the antenna. Finally, the third prototype, an air-gap PIFA, maintained all the technological

aspects from the previous prototype, but this time the near-field zone of the antenna was modified, with an introduced air-gap between the ground plane and the radiating part. The presence of the air-gap improved the radiation characteristics of the antenna, resulting in higher gain and higher radiation efficiency.

In the next stage, the PIFA was compared to a commercially available antenna. A communication equipment (Polycom, developed by RUAG) was used to perform the system measurements and comparisons. All the comparisons and system level measurements were performed in realistic everyday situations, thus providing a wide picture for the PIFAs' behavior in different practical scenarios. All the performed tests were reported in Chapter 5.

In all the performed test scenarios, the air-gap PIFA exhibited robust and reliable communication links, at the same time showing better results than the commercial antennas. A hemispherical radiation pattern and higher gain and radiation efficiency contributed to a better performance of PIFAs compared to dipoles.

Finally, in Chapter 6, the near field and SAR performances of the PIFA were analyzed. We could conclude that both SAR and radiation efficiency depend critically on the near-field distribution around the antenna and its coupling to the wearer. Ways to mitigate this coupling, and thus enhance the antenna's performance were suggested, e.g. relaxation of the high current density regions, by modifying the structure of the antenna or the use of substrate materials whose EM properties can influence the SAR levels.

In conclusion, with the proposed solutions and strategies we suggest an A-Z guideline for the design and development of robust wearable antennas. In our case, the antennas were intended for voice communication inside the existing UHF bands (Polycom), but the proposed technology can be easily adapted for other wearable applications, where the robustness and stability of the wearable antenna come in first place.

7.2 Perspectives

In this thesis, several aspects related to wearable antennas were addressed. However, there are still open issues and improvements that should be investigated. As a constantly growing field, wearable antennas will remain in the scope of the research for some time. Regardless of the type of application they are intended for, some requirements will remain present:

- Size reduction - miniaturization
- Improvement of the wearability aspects
- Diversity
- Improvement of the radiation characteristics
- SAR reduction

Chapter 7. Conclusions and Perspectives

Miniaturization of the devices is always welcome, especially when it comes to wearable antennas, where space for their placement is rather limited (human body) with more and more devices present. Therefore, size reduction of wearable antennas is one of the desired directions. Wearable antennas operating at UHF are in particular interesting for miniaturization, as their initial size is rather large. From the proposed PIFAs we see an open possibility in the overall size reduction, and notably the thickness of the antenna.

The wearability comes in line with the miniaturization of the antennas. The smaller the antenna is, the better placement can be obtained, thus providing an optimal performance of the wearable antenna. Wearable antennas intended for security applications require even a more discreet approach, especially for undercover applications, where the integration of the antennas within the wearer's uniform is highly desirable.

In applications where the robustness of the communication link is an important aspect, the use of more than one antenna can significantly improve the overall performance. Therefore, space diversity becomes a logical solution, which in turn requires miniaturization of the antennas. Small antennas are easier to place around the body. For the UHF bands the use of two wearable antennas, for instance one on the chest and a second one on the back, can assure almost omnidirectional communication coverage.

Miniaturization always leads to a trade-off between the antenna's size and its performances. One would like a higher radiation efficiency, more favorable radiation pattern or higher gain while keeping the antenna size constant. These improvements can be achieved either by modifying the antenna's structure or by using adequate substrate and conductive materials. In the case of the proposed PIFAs and materials that have been used, both approaches can be applied.

A PIFA offers many possibilities, where some slight modifications (e.g. ground plane extension, shorting wall or feeding position), can improve the radiation characteristics of the antenna. Moreover, using materials presenting less losses (e.g. new polymers) will also improve the antenna's performances.

While considering the perspectives of the proposed PIFAs, an important aspect is also the potential mass production of these antennas. Therefore, it should be borne in mind that all the potentially selected materials and technologies should also fulfill some industrial requirements so that the whole process can be easily conducted in an industrial environment. Moreover, controlled and automatized environment will improve several aspects that were found as weak points while fabricating the antennas in standard lab environment.

Bibliography

- [1] M. Patel and J. Wang, “Applications, challenges, and prospective in emerging body area networking technologies,” *IEEE Wireless Communications*, vol. 17, no. 1, pp. 80–88, February 2010.
- [2] “Samsung Gear S™,” 2014. [Online]. Available: <http://www.samsung.com/us/mobile/wearable-tech/SM-R750PZKASPR>
- [3] “IEEE 802.15 WPAN™ Task Group 6 (TG6) Body Area Networks,” p. 1, 2014. [Online]. Available: <http://www.ieee802.org/15/pub/TG6.html>
- [4] W. Scanlon, “Narrow band channel characterization & system issues for body-centric communications,” in *European School of Antennas*, 2009.
- [5] P. S. Hall and Y. Hao, *Antennas and Propagation for Body-Centric Wireless Communications*, 2nd ed. Norwood, MA, USA: Artech House, Inc., 2012.
- [6] M. Grimm and D. Manteuffel, “Antennas and Propagation for On-, Off- In-Body Communications,” in *Antennas and Propagation for On-, Off- In-Body Communications, Ultra-Wideband Radio Technologies for Communications, Localization and Sensor Applications*, R. S. Tomä, Ed. InTech, 2013.
- [7] R. Chandra, “Antennas, wave propagation, and localization in wireless body area networks,” Ph.D. dissertation, Lund university, Lund, Sweden, 2014.
- [8] M. S. Wegmuller, “Intra-body communication for biomedical sensor networks,” Ph.D. dissertation, Swiss Federal Institute of Technology, Zurich, Switzerland, 2007.
- [9] H. Higgins, “Implanted Wireless Communication Making a Real Difference,” in *Wireless Body Area Networks-Technology, Implementation and Applications*, M. Yuce and J. Khan, Eds. Pan Stanford, 2012.
- [10] Tetrapol, “Tetrapol factsheet,” pp. 1–10, 2014. [Online]. Available: <http://www.bakom.admin.ch/themen/technologie/01220/index.html?lang>
- [11] Federal Office of Communications (OFCOM), “Swiss national frequency allocation plan and specific assignments,” pp. 2–194, 2014. [Online]. Available: <http://www.bakom.admin.ch/themen/frequenzen/00652/00653/index.html?lang=en>
- [12] “RUAG Network Enabled Operations - NEO Services,” 2014. [Online]. Available: <http://www.ruag.com/defence/network-enabled-operation-services/>

Bibliography

- [13] —, “POLYCOM Radio portable COVERT700 Communication camouflée et sûre,” RUAG Defence | Centre POLYCOM, Case Postale | 3000 Berne 22 | Suisse, Tech. Rep., Dec 2014. [Online]. Available: http://www.ruag.com/fileadmin/ruag/Defence/Network_Enabled_Operations_Services/Security_Radio_Network_-_POLYCOM/PDF/FS_Covert_fr_low-pdf.pdf
- [14] —, “TETRA, critical communication for all professional users,” 2014. [Online]. Available: http://www.tandcca.com/Library/Documents/About_TETRA/TETRA_Fact_sheet_09-12_Final_2.pdf
- [15] —, “Customer cases, TETRAPOL references,” 2014. [Online]. Available: <http://www.tetrapol.com/community/references/>
- [16] —, “Brief TETRA fact sheet,” 2014. [Online]. Available: http://www.tandcca.com/Library/Documents/About_TETRA/TETRA_Fact_sheet_09-12_Final_2.pdf
- [17] C. Furse, D. A. Christensen, and C. H. Durney, *Basic Introduction to Bioelectromagnetics*, 2nd ed. Taylor & Francis Group, 2005.
- [18] J. Trajkovikj, J.-F. Zurcher, and A. Skrivervik, “Soft and flexible antennas on permittivity adjustable PDMS substrates,” in *Loughborough Antennas and Propagation Conference (LAPC)*, Nov 2012, pp. 1–4.
- [19] J. Trajkovikj, J.-F. Zurcher, and A. K. Skrivervik, “PDMS, A Robust Casing for Flexible W-BAN Antennas [EurAAP Corner],” *IEEE Antennas and Propagation Magazine*, vol. 55, no. 5, pp. 287–297, Oct 2013.
- [20] J. Trajkovikj, J.-F. Zurcher, and A. Skrivervik, “Soft and flexible UHF antennas for W-BAN applications,” in *IEEE Antennas and Propagation Society International Symposium (APSURSI)*, July 2014, pp. 305–306.
- [21] —, “Performance of UHF W-BAN antennas in a real environment scenario,” in *Loughborough Antennas and Propagation Conference (LAPC)*, Nov 2014, pp. 18–21.
- [22] J. Trajkovikj, T. Debgovic, and A. Skrivervik, “UHF W-BAN Antennas in Indoor and Outdoor Environment,” in *Proceedings of the 9th European Conference on Antennas and Propagation (EuCAP)*, Apr 2015, pp. 1–4, accepted.
- [23] J. Trajkovikj and A. Skrivervik, “Diminishing SAR for Wearable UHF Antennas,” *IEEE Antennas and Wireless Propagation Letters*, vol. PP, no. 99, pp. 1–4, Dec 2014.
- [24] D. Psychoudakis, G. Lee, C. Chen, and J. Volakis, “Military UHF body-worn antennas for armored vests,” in *Proceedings of the 6th European Conference on Antennas and Propagation (EuCAP)*. IEEE, 2010, pp. 1–4.
- [25] C. Hertleer, H. Rogier, L. Vallozzi, and L. Van Langenhove, “A Textile Antenna for Off-Body Communication Integrated Into Protective Clothing for Firefighters,” *IEEE Transactions on Antennas and Propagation*, vol. 57, no. 4, pp. 919–925, April 2009.
- [26] A. Serra, P. Nepa, and G. Manara, “A wearable multi antenna system on a life jacket for Cospas Sarsat rescue applications,” in *IEEE International Symposium on Antennas and Propagation (APSURSI)*, July 2011, pp. 1319–1322.

- [27] J. Lilja, V. Pynttari, T. Kaija, R. Makinen, E. Halonen, H. Sillanpaa, J. Heikkinen, M. Mantysalo, P. Salonen, and P. De Maagt, "Body-Worn Antennas Making a Splash : Lifejacket-Integrated Antennas for Global Search and Rescue Satellite System," *IEEE Antennas Propagation Magazine*, vol. 55, no. 2, pp. 324–341, 2013.
- [28] International Telecommunication Union (ITU), "Frequency Bands allocated to Terrestrial Broadcasting Services," 2014. [Online]. Available: <http://www.itu.int/en/ITU-R/terrestrial/broadcast/Pages/Bands.aspx>
- [29] D. Psychoudakis and J. Volakis, "Conformal Asymmetric Meandered Flare (AMF) Antenna for Body-Worn Applications," *IEEE Antennas Wireless Propagation Letters*, vol. 8, pp. 931–934, 2009.
- [30] J. Matthews and G. Pettitt, "Development of flexible, wearable antennas," in *Proceedings of the 3rd European Conference on Antennas and Propagation (EuCAP)*, March 2009, pp. 273–277.
- [31] L. Vallozzi, W. Vandendriessche, H. Rogier, C. Hertleer, and M. Scarpello, "Wearable textile GPS antenna for integration in protective garments," in *Proceedings of the 4th European Conference on Antennas and Propagation (EuCAP)*, April 2010, pp. 1–4.
- [32] A. Dierck, H. Rogier, and F. Declercq, "A Wearable Active Antenna for Global Positioning System and Satellite Phone," *IEEE Transactions on Antennas and Propagation*, vol. 61, no. 2, pp. 532–538, Feb 2013.
- [33] D. Curone, G. Dudnik, G. Loriga, J. Luprano, G. Magenes, R. Paradiso, A. Tognetti, and A. Bonfiglio, "Smart Garments for Safety Improvement of Emergency/Disaster Operators," in *Proceedings of the 29th Annual International Conference of the IEEE Engineering in Medicine and Biology Society (EMBS)*, Aug 2007, pp. 3962–3965.
- [34] D. Tobon, T. Falk, and M. Maier, "Context awareness in WBANs: a survey on medical and non-medical applications," *IEEE Wireless Communications*, vol. 20, no. 4, pp. 30–37, August 2013.
- [35] Z. Popovic, P. Momenroodaki, and R. Scheeler, "Toward wearable wireless thermometers for internal body temperature measurements," *IEEE Communications Magazine*, vol. 52, no. 10, pp. 118–125, October 2014.
- [36] F. Axisa, P. Schmitt, C. Gehin, G. Delhomme, E. McAdams, and A. Dittmar, "Flexible technologies and smart clothing for citizen medicine, home healthcare, and disease prevention," *IEEE Transactions on Information Technology in Biomedicine*, vol. 9, no. 3, pp. 325–336, Sept 2005.
- [37] S. Park and S. Jayaraman, "Enhancing the quality of life through wearable technology," *IEEE Engineering in Medicine and Biology Magazine*, vol. 22, no. 3, pp. 41–48, May 2003.
- [38] Ullah, S., "Wireless body area network for ubiquitous health monitoring," 2010. [Online]. Available: <http://www.koreaittimes.com/story/10133/wireless-body-area-network-ubiquitous-health-monitoring>
- [39] "Federal Communications Commission (FCC)," 2014. [Online]. Available: www.fcc.gov

Bibliography

- [40] “European Telecommunications Standards Institute (ETSI),” 2014. [Online]. Available: www.etsi.org
- [41] “Medical Device Radiocommunications Service (MedRadio),” 2009. [Online]. Available: www.fcc.gov
- [42] Federal Communications Commission (FCC), “Revision of Part 15 of the Commission’s Rules Regarding Ultra-Wideband Transmission Systems,” 2002. [Online]. Available: http://transition.fcc.gov/Bureaus/Engineering_Technology/Orders/2002/fcc02048.pdf
- [43] R. Fisher, “60 GHz WPAN Standardization within IEEE 802.15.3c,” in *International Symposium on Signals, Systems and Electronics, (ISSSE '07)*, July 2007, pp. 103–105.
- [44] S. Alipour, F. Parvaresh, H. Ghajari, and F. Donald, “Propagation characteristics for a 60 GHz Wireless body area network (WBAN),” in *Military Communications Conference (MILCOM 2010)*, Oct 2010, pp. 719–723.
- [45] C. Constantinou, Y. Nechayev, X. Wu, and P. Hall, “Body-area propagation at 60 GHz,” in *Loughborough Antennas and Propagation Conference (LAPC)*, Nov 2012, pp. 1–4.
- [46] A. Pellegrini, A. Brizzi, L. Zhang, K. Ali, Y. Hao, X. Wu, C. Constantinou, Y. Nechayev, P. Hall, N. Chahat, M. Zhadobov, and R. Sauleau, “Antennas and propagation for body-centric wireless communications at millimeter-wave frequencies: A review [wireless corner],” *IEEE Antennas and Propagation Magazine*, vol. 55, no. 4, pp. 262–287, Aug 2013.
- [47] X. Wu, L. Akhoondzadeh-Asl, Z. Wang, and P. Hall, “Novel Yagi-Uda antennas for on-body communication at 60GHz,” in *Loughborough Antennas and Propagation Conference (LAPC)*, Nov 2010, pp. 153–156.
- [48] A. Skriversvik and F. Merli, “Design strategies for implantable antennas,” in *Loughborough Antennas and Propagation Conference (LAPC)*, Nov 2011, pp. 1–5.
- [49] F. Merli, “Implantable antennas for biomedical applications,” Ph.D. dissertation, Swiss Federal Institute of Technology, Lausanne, Switzerland, 2011.
- [50] J. Kim and Y. Rahmat-Samii, “Implanted antennas inside a human body: simulations, designs, and characterizations,” *IEEE Transactions on Microwave Theory and Techniques*, vol. 52, no. 8, pp. 1934–1943, Aug 2004.
- [51] W. Xia, K. Saito, M. Takahashi, and K. Ito, “Performances of an implanted cavity slot antenna embedded in the human arm,” *IEEE Transactions on Antennas and Propagation*, vol. 57, no. 4, pp. 894–899, April 2009.
- [52] A. Kiourti, J. Costa, C. Fernandes, A. Santiago, and K. Nikita, “Miniature implantable antennas for biomedical telemetry: From simulation to realization,” *IEEE Transactions on Biomedical Engineering*, vol. 59, no. 11, pp. 3140–3147, Nov 2012.
- [53] S. Curto, P. McEvoy, X. Bao, and M. Ammann, “Compact Patch Antenna for Electromagnetic Interaction With Human Tissue at 434 MHz,” *IEEE Transactions on Antennas and Propagation*, vol. 57, no. 9, pp. 2564–2571, Sept 2009.

- [54] A. Chandran, G. Conway, and W. Scanlon, "Compact low-profile patch antenna for medical body area networks at 868 MHz," in *IEEE Antennas and Propagation Society International Symposium*, July 2008, pp. 1–4.
- [55] L. Ma, R. Edwards, and S. Bashir, "A wearable monopole antenna for ultra wideband with notching function," in *IET Seminar on Wideband and Ultrawideband Systems and Technologies: Evaluating current Research and Development*, Nov 2008, pp. 1–5.
- [56] C. Lin, Z. Li, K. Ito, M. Takahashi, and K. Saito, "A small tunable and wearable planar inverted-F antenna (PIFA)," in *Proceedings of the 6th European Conference on Antennas and Propagation (EuCAP)*, March 2012, pp. 742–745.
- [57] A. Alomainy, "Antenna Design and Channel Characterization for Ultra Wideband Body-Centric Wireless Communications," in *European School of Antennas*, 2009.
- [58] A. Alomainy, Y. Hao, and F. Pasveer, "Numerical and experimental evaluation of a compact sensor antenna for healthcare devices," *IEEE Transactions on Biomedical Circuits and Systems*, vol. 1, no. 4, pp. 242–249, Dec 2007.
- [59] Y. Rahmat-Samii, "Wearable and implantable antennas in body-centric communications," in *Proceedings of the 2nd European Conference on Antennas and Propagation (EuCAP)*, Nov 2007, pp. 1–5.
- [60] "Running GPS Watches," 2014. [Online]. Available: http://sports.tomtom.com/en_us/
- [61] "Micoach," 2014. [Online]. Available: <http://micoach.adidas.com/>
- [62] X. L. Chen, N. Kuster, Y. C. Tan, and N. Chavannes, "Body effects on the GPS antenna of a wearable tracking device," in *Proceedings of the 6th European Conference on Antennas and Propagation (EuCAP)*, March 2012, pp. 3313–3316.
- [63] J.-F. Zürcher, O. Staub, and A. K. Skrivervik, "SMILA: A compact and efficient antenna for mobile communications," *Microwave and Optical Technology Letters*, vol. 27, no. 3, pp. 155–157, 2000.
- [64] A. Skrivervik and J.-F. Zürcher, "Miniature antenna design at LEMA," in *19th International Conference on Applied Electromagnetics and Communications (ICECom)*, Sept 2007, pp. 1–4.
- [65] M. Lapinski, M. Feldmeier, and J. Paradiso, "Wearable wireless sensing for sports and ubiquitous interactivity," in *IEEE Sensors*, Oct 2011, pp. 1425–1428.
- [66] D. Gaetano, P. McEvoy, M. Ammann, J. Browne, L. Keating, and F. Horgan, "Footwear Antennas for Body Area Telemetry," *IEEE Transactions on Antennas and Propagation*, vol. 61, no. 10, pp. 4908–4916, Oct 2013.
- [67] D. Gaetano, P. McEvoy, M. J. Ammann, C. Brannigan, L. Keating, and F. Horgan, "Footwear and Wrist Communication Links using 2.4 GHz and UWB Antennas," *Electronics*, vol. 3, no. 2, pp. 339–350, 2014. [Online]. Available: <http://www.mdpi.com/2079-9292/3/2/339>

Bibliography

- [68] "Snow flaik tracks skiers," 2011. [Online]. Available: <http://news.discovery.com/tech/snow-flaik-tracks-skiers.htm>
- [69] "Verb for shoe - very intelligent shoes," 2004. [Online]. Available: <http://www.gizmag.com/go/3565/picture/7504/>
- [70] "Zegna Sport Bluetooth iJacket incorporates smart fabric," 2007. [Online]. Available: <http://www.gizmag.com/go/7856/>
- [71] J. Ranck, "The wearable computing market: a global analysis," 2012. [Online]. Available: <http://go.gigaom.com/rs/gigaom/images/wearable-computing-the-next-big-thing-in-tech.pdf>
- [72] C. A. Balanis, *Antenna Theory Analysis and Design*, 3rd ed. John Wiley Sons, Inc., 2005, vol. 28.
- [73] A. Skrivervik, J.-F. Zürcher, O. Staub, and J. Mosig, "PCS antenna design: the challenge of miniaturization," *IEEE Antennas and Propagation Magazine*, vol. 43, no. 4, pp. 12–27, Aug 2001.
- [74] H. Wheeler, "Small antennas," *IEEE Transactions on Antennas and Propagation*, vol. 23, no. 4, pp. 462–469, Jul 1975.
- [75] L. J. Chu, "Small antennas," *Journal of Applied Physics*, vol. 19, no. 12, pp. 1163–1175, Dec 1948.
- [76] F. R. Harrington, "Effect of Antenna Size on Gain, Bandwidth, and Efficiency," *Journal of Research of the National Bureau of Standards-D. Radio Propagation*, vol. 64D, no. 1, pp. 1–12, Jan-Feb 1960.
- [77] J. McLean, "A re-examination of the fundamental limits on the radiation Q of electrically small antennas," *IEEE Transactions on Antennas and Propagation*, vol. 44, no. 5, pp. 672–, May 1996.
- [78] M. Gustafsson, C. Sohl, and G. Kristensson, "Physical limitations on antennas of arbitrary shape," *Proceedings of the Royal Society of London A: Mathematical, Physical and Engineering Sciences*, vol. 463, no. 2086, pp. 2589–2607, Aug 2007.
- [79] K. Fujimoto, *Mobile Antenna Systems Handbook*, 3rd ed. Boston /London: Artech House, Inc., 2008.
- [80] O. Staub, J.-F. Zürcher, and A. Skrivervik, "Some considerations on the correct measurement of the gain and bandwidth of electrically small antennas," *Microwave and Optical Technology Letters*, vol. 17, no. 3, pp. 156–160, 1998.
- [81] S. Bokhari, J.-F. Zurcher, J. Mosig, and F. Gardiol, "A small microstrip patch antenna with a convenient tuning option," *IEEE Transactions on Antennas and Propagation*, vol. 44, no. 11, pp. 1521–1528, Nov 1996.
- [82] J.-F. Zurcher, A. Skrivervik, and O. Staub, "SMILA: a miniaturized antenna for PCS applications," in *IEEE Antennas and Propagation Society International Symposium*, vol. 3, July 2000, pp. 1646–1649 vol.3.

-
- [83] G.-Y. Lee, D. Psychoudakis, C.-C. Chen, and J. Volakis, "Omnidirectional Vest-Mounted Body-Worn Antenna System for UHF Operation," *IEEE Antennas and Wireless Propagation Letters*, vol. 10, pp. 581–583, 2011.
 - [84] D. Psychoudakis and J. Volakis, "Conformal Asymmetric Meandered Flare (AMF) Antenna for Body-Worn Applications," *Antennas and Wireless Propagation Letters*, vol. 8, pp. 931–934, 2009.
 - [85] J. Trajkovikj, B. Fuchs, and A. Skrivervik, "LEMA internal report," 2011.
 - [86] M. M. Weiner, *Monopole Antennas*, 1st ed. Taylor and Francis, 2003.
 - [87] L. Ma, R. Edwards, and W. Whittow, "A multi-band printed monopole antenna," in *Proceedings of the 3rd European Conference on Antennas and Propagation (EuCAP)*, March 2009, pp. 962–964.
 - [88] B. Sanz-Izquierdo, J. Miller, J. Batchelor, and M. Sobhy, "Dual-band wearable metallic button antennas and transmission in body area networks," *IET Microwaves, Antennas Propagation*, vol. 4, no. 2, pp. 182–190, Feb 2010.
 - [89] M. Koohestani, J.-F. Zurcher, A. Moreira, and A. Skrivervik, "A Novel, Low-Profile, Vertically-Polarized UWB Antenna for WBAN," *IEEE Transactions on Antennas and Propagation*, vol. 62, no. 4, pp. 1888–1894, April 2014.
 - [90] L. Salman and L. Talbi, "G-shaped wearable cuff button antenna for 2.45 GHZ ISM band applications," in *14th International Symposium on Antenna Technology and Applied Electromagnetics the American Electromagnetics Conference (ANTEM-AMEREM)*, July 2010, pp. 1–4.
 - [91] L. Vallozzi, P. Van Torre, C. Hertleer, H. Rogier, M. Moeneclaey, and J. Verhaevert, "Wireless Communication for Firefighters Using Dual-Polarized Textile Antennas Integrated in Their Garment," *IEEE Transactions on Antennas and Propagation*, vol. 58, no. 4, pp. 1357–1368, April 2010.
 - [92] S. Sankaralingam and B. Gupta, "A Circular Disk Microstrip WLAN Antenna for Wearable Applications," in *Annual IEEE India Conference (INDICON)*, Dec 2009, pp. 1–4.
 - [93] J. Carter, J. Saberlin, T. Shah, P. Sai Ananthanarayanan, and C. Furse, "Inexpensive fabric antenna for off-body wireless sensor communication," in *IEEE Antennas and Propagation Society International Symposium (APSURSI)*, July 2010, pp. 1–4.
 - [94] P. Salonen, L. Sydanheimo, M. Keskilammi, and M. Kivikoski, "A small planar inverted-F antenna for wearable applications," in *The 3rd International Symposium on Wearable Computers*, Oct 1999, pp. 95–100.
 - [95] K. Fujimoto, *Small Antennas*. John Wiley & Sons, Inc., 2005.
 - [96] Z. N. Chen, Ed., *Antennas for Portable Devices*, 1st ed. Wiley-VCH, 2007.
 - [97] K.-L. Wong, Ed., *Compact and Broadband Microstrip Antennas*, 1st ed. Wiley-VCH, 2002.

Bibliography

- [98] N. Firoozy and M. Shirazi, "Planar Inverted-F Antenna (PIFA) Design Dissection for Cellular Communication Application," *Journal of Electromagnetic Analysis and Applications*, vol. 03, no. 406-412, pp. 379–384, Aug 2011.
- [99] P. Soh, G. Vandenbosch, V. Volski, and H. Nurul, "Characterization of a simple broadband textile planar inverted-F antenna (PIFA) for on body communications," in *22nd International Conference on Applied Electromagnetics and Communications (ICECom)*, Sept 2010, pp. 1–4.
- [100] P. Soh, S. Boyes, G. Vandenbosch, Y. Huang, and Z. Ma, "Dual-band Sierpinski textile PIFA efficiency measurements," in *Proceedings of the 6th European Conference on Antennas and Propagation (EuCAP)*, March 2012, pp. 3322–3326.
- [101] P. Soh, G. Vandenbosch, S. L. Ooi, and N. H. M. Rais, "Design of a Broadband All-Textile Slotted PIFA," *IEEE Transactions on Antennas and Propagation*, vol. 60, no. 1, pp. 379–384, Jan 2012.
- [102] C.-H. Lin, K. Saito, M. Takahashi, and K. Ito, "A Compact Planar Inverted-F Antenna for 2.45 GHz On-Body Communications," *IEEE Transactions on Antennas and Propagation*, vol. 60, no. 9, pp. 4422–4426, Sept 2012.
- [103] C. Cibir, P. Leuchtmann, M. Gimersky, R. Vahldieck, and S. Mosciroda, "Modified E-shaped PIFA antenna for wearable systems," in *Submitted to URSI International Symposium and Electromagnetic Theory*, 2004, pp. 23–27.
- [104] "Pharad wearable antennas," 2014. [Online]. Available: <http://www.pharad.com/tetra-wearable-antenna.html>
- [105] "British aerospace and defence (BAE)," 2014. [Online]. Available: <http://www.baesystems.com/>
- [106] "Panorama wearable antennas," 2014. [Online]. Available: http://www.panorama-antennas.com/index.php?route=product/product&path=84_87&product_id=112
- [107] Data-sheet, "Tetra Wearable Antenna, model BW-380-430," 2014. [Online]. Available: <http://www.pharad.com/pdf/Tetra-Wearable-Antenna-Datasheet.pdf>
- [108] —, "Body Worn 380-400 MHz Tetra Antenna," 2014. [Online]. Available: [http://www.panorama-antennas.com/datasheets/BWDT-S1\[OLD\].pdf](http://www.panorama-antennas.com/datasheets/BWDT-S1[OLD].pdf)
- [109] I. report (police), "Messtechnische Erfassung der horizontalen Abstrahleigenschaften von Tarnantennen," 2011.
- [110] Salvado, Rita and Loss, Caroline and Gonçalves, Ricardo and Pinho, Pedro, "Textile materials for the design of wearable antennas: A survey," *Sensors*, vol. 12, no. 11, pp. 15 841–15 857, 2012. [Online]. Available: <http://www.mdpi.com/1424-8220/12/11/15841>
- [111] P. Salonen, Y. Rahmat-Samii, M. Schaffrath, and M. Kivikoski, "Effect of textile materials on wearable antenna performance: a case study of GPS antennas," in *IEEE Antennas and Propagation Society International Symposium*, vol. 1, June 2004, pp. 459–462 Vol.1.

- [112] P. Salonen, Y. Rahmat-Samii, H. Hurme, and M. Kivikoski, "Effect of conductive material on wearable antenna performance: a case study of WLAN antennas," in *IEEE Antennas and Propagation Society International Symposium*, vol. 1, June 2004, pp. 455–458 Vol.1.
- [113] J. Santas, A. Alomainy, and Y. Hao, "Textile Antennas for On-Body Communications: Techniques and Properties," in *Proceedings of the 2nd European Conference on Antennas and Propagation (EuCAP)*, Nov 2007, pp. 1–4.
- [114] N. Rais, P. Soh, F. Malek, S. Ahmad, N. Hashim, and P. Hall, "A review of wearable antenna," in *Loughborough Antennas and Propagation Conference (LAPC)*, Nov 2009, pp. 225–228.
- [115] T. Kaija, J. Lilja, and P. Salonen, "Exposing textile antennas for harsh environment," in *Military Communications Conference (MILCOM 2010)*, Oct 2010, pp. 737–742.
- [116] Y. Ouyang and W. Chappell, "High Frequency Properties of Electro-Textiles for Wearable Antenna Applications," *IEEE Transactions on Antennas and Propagation*, vol. 56, no. 2, pp. 381–389, Feb 2008.
- [117] Q. Bai and R. Langley, "Bending of a small coplanar textile antenna," in *Loughborough Antennas and Propagation Conference (LAPC)*, Nov 2010, pp. 329–332.
- [118] I. Locher, M. Klemm, T. Kirstein, and G. Troster, "Design and Characterization of Purely Textile Patch Antennas," *IEEE Transactions on Advanced Packaging*, vol. 29, no. 4, pp. 777–788, Nov 2006.
- [119] K. Koski, L. Sydanheimo, Y. Rahmat-Samii, and L. Ukkonen, "Fundamental Characteristics of Electro-Textiles in Wearable UHF RFID Patch Antennas for Body-Centric Sensing Systems," *IEEE Transactions on Antennas and Propagation*, vol. PP, no. 99, pp. 1–1, 2014.
- [120] A. Rida, L. Yang, R. Vyas, and M. Tentzeris, "Conductive Inkjet-Printed Antennas on Flexible Low-Cost Paper-Based Substrates for RFID and WSN Applications," *IEEE Antennas and Propagation Magazine*, vol. 51, no. 3, pp. 13–23, June 2009.
- [121] W. Whittow, A. Chauraya, J. Vardaxoglou, Y. Li, R. Torah, K. Yang, S. Beeby, and J. Tudor, "Inkjet-printed microstrip patch antennas realized on textile for wearable applications," *IEEE Antennas and Wireless Propagation Letters*, vol. 13, pp. 71–74, 2014.
- [122] A. Chauraya, W. Whittow, J. Vardaxoglou, Y. Li, R. Torah, K. Yang, S. Beeby, and J. Tudor, "Inkjet printed dipole antennas on textiles for wearable communications," *IET Microwaves, Antennas Propagation*, vol. 7, no. 9, pp. 760–767, June 2013.
- [123] V. K. Palukuru, K. Sanoda, V. Pynttäre, T. Hu, R. Mäkinen, M. Mäntysalo, J. Hagberg, and H. Jantunen, "Inkjet-Printed RF Structures on BST-Polymer Composites: An Application of a Monopole Antenna for 2.4 GHz Wireless Local Area Network Operation," *International Journal of Applied Ceramic Technology*, vol. 8, no. 4, pp. 940–946, 2011.
- [124] K. Kirschenmann, K. Whites, and S. Woessner, "Inkjet printed microwave frequency multilayer antennas," in *IEEE Antennas and Propagation Society International Symposium*, June 2007, pp. 924–927.

Bibliography

- [125] Q. Liu, K. Ford, R. Langley, A. Robinson, and S. Lacour, "A stretchable PIFA antenna," in *Loughborough Antennas and Propagation Conference (LAPC)*, Nov 2011, pp. 1–4.
- [126] K. Wu, "Integration and interconnect techniques of planar and non-planar structures for microwave and millimeter-wave circuits - current status and future trend," in *Asia-Pacific Microwave Conference (APMC)*, vol. 2, Dec 2001, pp. 411–416 vol.2.
- [127] M. Esquius Morote, "Horn Antennas and Dual-Polarized Circuits in Substrate Integrated Waveguide (SIW) Technology," Ph.D. dissertation, Swiss Federal Institute of Technology, Lausanne, Switzerland, 2014.
- [128] F. Ghanem, R. Langley, and L. Ford, "Propagation control using SIW technology," in *IEEE Antennas and Propagation Society International Symposium (APSURSI)*, July 2010, pp. 1–4.
- [129] S. Agneessens, S. Lemey, R. Moro, M. Bozzi, and H. Rogier, "The next generation textile antennas based on substrate integrated waveguide technology," in *31st General Assembly and Scientific Symposium (URSI GASS)*, Aug 2014, pp. 1–4.
- [130] R. Moro, M. Bozzi, A. Collado, A. Georgiadis, and S. Via, "Plastic-based Substrate Integrated Waveguide (SIW) components and antennas," in *42nd European Microwave Conference (EuMC)*, Oct 2012, pp. 1007–1010.
- [131] R. Moro, M. Bozzi, S. Kim, and M. Tentzeris, "Novel inkjet-printed substrate integrated waveguide (SIW) structures on low-cost materials for wearable applications," in *Microwave Conference (EuMC)*, Oct 2012, pp. 72–75.
- [132] T. Kaufmann and C. Fumeaux, "Wearable Textile Half-Mode Substrate-Integrated Cavity Antenna Using Embroidered Vias," *Antennas and Wireless Propagation Letters*, vol. 12, pp. 805–808, 2013.
- [133] S. Lemey and H. Rogier, "SIW textile antennas as a novel technology for UWB RFID tags," in *IEEE RFID Technology and Applications Conference (RFID-TA)*, Sept 2014, pp. 256–260.
- [134] S. Agneessens and H. Rogier, "Compact Half Diamond Dual-Band Textile HMSIW On-Body Antenna," *IEEE Transactions on Antennas and Propagation*, vol. 62, no. 5, pp. 2374–2381, May 2014.
- [135] T. Someya, Ed., *Stretchable Electronics*, 1st ed. Wiley-VCH, 2013.
- [136] C.-P. Lin, C.-H. Chang, Y. Cheng, and C. Jou, "Development of a Flexible SU-8/PDMS-Based Antenna," *Antennas and Wireless Propagation Letters*, vol. 10, pp. 1108–1111, 2011.
- [137] J. E. Mark, "Overview of Siloxane Polymers," in *Silicones and Silicone-Modified Materials*, C. S. J., F. J. J., O. M. J., and S. S. D., Eds. Washington, DC: American Chemical Society, 2000, ch. 2, pp. 1–10.
- [138] Data-sheet, "SYLGARD® 184 SILICONE ELASTOMER KIT," 2014. [Online]. Available: <http://www.dowcorning.com/applications/search/products/details.aspx?prod=01064291>

- [139] A. Mata, A. Fleischman, and S. Roy, "Characterization of polydimethylsiloxane (PDMS) properties for biomedical micro/nanosystems," *Biomedical Microdevices*, vol. 7, pp. 281–293, December 2005.
- [140] Data-sheet, "X-34-4184-A/B Liquid Silicone Rubber UV Cure Type (PDMS)," 2014. [Online]. Available: https://www.silicone.jp/j/news/2014/images/Plas_06_j.pdf
- [141] J.-H. So, J. Thelen, A. Qusba, G. J. Hayes, G. Lazzi, and M. D. Dickey, "Reversibly Deformable and Mechanically Tunable Fluidic Antennas," *Advanced Functional Materials*, vol. 19, no. 22, pp. 3632–3637, 2009. [Online]. Available: <http://dx.doi.org/10.1002/adfm.200900604>
- [142] M. Kubo, X. Li, C. Kim, M. Hashimoto, B. J. Wiley, D. Ham, and G. M. Whitesides, "Stretchable Microfluidic Radiofrequency Antennas," *Advanced Materials*, vol. 22, no. 25, pp. 2749–2752, 2010. [Online]. Available: <http://dx.doi.org/10.1002/adma.200904201>
- [143] S. Cheng and Z. Wu, "A Microfluidic, Reversibly Stretchable, Large-Area Wireless Strain Sensor," *Advanced Functional Materials*, vol. 21, no. 12, pp. 2282–2290, 2011. [Online]. Available: <http://dx.doi.org/10.1002/adfm.201002508>
- [144] N. Tiercelin, P. Coquet, R. Sauleau, V. Senez, and H. Fujita, "Polydimethylsiloxane membranes for millimeter-wave planar ultra flexible antennas," *Journal of Micromechanics and Microengineering*, vol. 16, pp. 2389–2395, 2006.
- [145] S. Hage-Ali, N. Tiercelin, P. Coquet, R. Sauleau, H. Fujita, V. Preobrazhensky, and P. Pernod, "A Millimeter-Wave Microstrip Antenna Array on Ultra-Flexible Micromachined Polydimethylsiloxane (PDMS) Polymer," *IEEE Antennas and Wireless Propagation Letters*, vol. 8, pp. 1306–1309, 2009.
- [146] Z. Wang, L. Zhang, Y. Bayram, and J. Volakis, "Embroidered Conductive Fibers on Polymer Composite for Conformal Antennas," *IEEE Transactions on Antennas and Propagation*, vol. 60, no. 9, pp. 4141–4147, Sept 2012.
- [147] United Nations specialized agency for information and communication technologies – ICTs, "International Telecommunication Union (ITU)," 2014. [Online]. Available: <http://www.itu.int/en>
- [148] Radiocommunication sector of ITU, "Recommendation ITU-R P.676-9 - Attenuation by atmospheric gases," *Radiowave propagation, P Series*, no. 4, pp. 1–24, 2012.
- [149] P. Zheng, L. L. Peterson, B. S. Davie, and A. Farrel, *Wireless Networking Complete*. San Francisco, CA, USA: Morgan Kaufmann Publishers Inc., 2009.
- [150] J. Shi, "Ultra-wideband Impulse Radio System for Medical Implant Communications," Ph.D. dissertation, Nagoya Institute of Technology, Nagoya, Japan, 2013.
- [151] Federal Office for the Protection of the Population, "Polycom - le réseau radio suisse de sécurité," 2014. [Online]. Available: <http://www.bevoelkerungsschutz.admin.ch/internet/bs/fr/home/themen/polycom.html>

Bibliography

- [152] B. Walke, D. Kuypers, P. Seidenberg, P. Sievering, M. Steppler, and V. Obradovic, "Eignung der Standards ETSI/TETRA und TETRAPOL zur Erfüllung der betrieblich-taktischen Forderungen der Behörden und Organisationen mit Sicherheitsaufgaben (BOS)," Lehrstuhl für Kommunikationsnetze, RWTH-Aachen, Kopernikusstr. 16, 52074, Tech. Rep., Dec 2000. [Online]. Available: <http://www.comnets.rwth-aachen.de>
- [153] J. R. Fried, Ed., *Polymer Science and Technology*, 3rd ed. Prentice Hall, 2003.
- [154] E. Apaydin, "Microfabrication techniques for printing on pdms elastomers for antenna and biomedical applications," Ph.D. dissertation, The Ohio State University, Ohio, US, 2009.
- [155] "SYLGARD (R) 184 SILICONE ELASTOMER CURING AGENT," pp. 1–8, 2011, data-sheet. [Online]. Available: <http://www.dowcorning.com/DataFiles/0902770180655d5b.pdf>
- [156] N. Farcich, J. Salonen, and P. Asbeck, "Single-Length Method Used to Determine the Dielectric Constant of Polydimethylsiloxane," *IEEE Transactions on Microwave Theory and Techniques*, vol. 56, no. 12, pp. 2963–2971, Dec 2008.
- [157] "Faserverbundwerkstoffe / Matériaux composites / Composite materials," p. , 2013. [Online]. Available: <http://www.suterkunststoffe.ch/pdf/produkteuebersicht.pdf>
- [158] J.-F. Zurcher, "Low permittivity substrates based on Silgard-184 RTV (LEMA internal report)," 2012.
- [159] Agilent, *Basics of Measuring the Dielectric Properties of Materials*, 2014, Application Note. [Online]. Available: <http://www3.imperial.ac.uk/pls/portallive/docs/1/11949698.PDF>
- [160] Laboratory of Electromagnetic and Acoustics (EPFL), *Permittivity measurements*, 2014, Tutorial. [Online]. Available: http://lema.epfl.ch/files/Teaching/HFLaboratories/Lab5_2014.pdf
- [161] Data-sheet, "100 mesh copper .0045" wire dia. 36 inches wide," 2014. [Online]. Available: http://www.twpinc.com/tcpdf/pdf/create.php?prod_id=3769
- [162] —, "22 Mesh Copper .015 36" Wide," 2014. [Online]. Available: http://www.twpinc.com/tcpdf/pdf/create.php?prod_id=2885
- [163] "ANSYS HFSS," 2014. [Online]. Available: <http://www.ansys.com/Products/Simulation+Technology/Electronics/Signal+Integrity/ANSYS+HFSS>
- [164] —, "Solidworks," 2014. [Online]. Available: <http://www.solidworks.com/>
- [165] M. Cabedo-Fabres, E. Antonino-Daviu, A. Valero-Nogueira, and M. Bataller, "The Theory of Characteristic Modes Revisited: A Contribution to the Design of Antennas for Modern Applications," *IEEE Antennas and Propagation Magazine*, vol. 49, no. 5, pp. 52–68, Oct 2007.
- [166] B. Ivsic, J. Bartolic, D. Bonefacic, A. Skrивervik, and J. Trajkovikj, "Design and analysis of planar UHF wearable antenna," in *Proceedings of the 6th European Conference on Antennas and Propagation (EuCAP)*, March 2012, pp. 1–4.

-
- [167] "Calculation of the Dielectric Properties of Body Tissues in the frequency range 10 Hz - 100 GHz," 2014. [Online]. Available: <http://niremf.ifac.cnr.it/tissprop/htmlclie/htmlclie.htm#stsftag>
 - [168] D. Psychoudakis, C.-C. Chen, and J. Volakis, "Wearable UHF antenna for squad area networks (SAN)," in *IEEE Antennas and Propagation Society International Symposium*, July 2008, pp. 1–4.
 - [169] G. Ziegelberger, "ICNIRP GUIDELINES for limiting exposure to time-varying electric, magnetic and electromagnetic fields (up to 300 GHz)," *Health Phys.*, vol. 74, no. 4, pp. 494–522, 1998.
 - [170] IEEE-SA Standards Board, "IEEE Recommended Practice for Measurements and Computations of Radio Frequency Electromagnetic Fields With Respect to Human Exposure to Such Fields, 100 kHz–300 GHz," *IEEE Std C95.3-2002 (Revision of IEEE Std C95.3-1991)*, no. 4, pp. 1–126, 2002.
 - [171] Federal Communications Commission Office of Engineering and Technology, "Evaluating Compliance with FCC Guidelines for Human Exposure to Radiofrequency Electromagnetic Fields," *Supplement C*, pp. 1–42, 2001.
 - [172] A. Hirata, T. Fujino, and T. Shiozawa, "SAR in the human body due to EM waves emitted from a dipole antenna at 400 MHz band," in *IEEE International Symposium on Electromagnetic Compatibility, EMC '03*, vol. 1, May 2003, pp. 17–20.
 - [173] P. Soh, G. Vandenbosch, F. Wee, A. van den Bosch, M. Martinez-Vazquez, and D.-P. Schreurs, "Specific Absorption Rate (SAR) evaluation of biomedical telemetry textile antennas," in *IEEE MTT-S International Microwave Symposium Digest (IMS)*, June 2013, pp. 1–3.
 - [174] R. Augustine, T. Alves, M. Zhadobov, B. Poussot, T. Sarrebourg, R. Sauleau, M. Thomas, and J.-M. Laheurte, "SAR reduction of wearable antennas using polymeric ferrite sheets," in *Proceedings of the 4th European Conference on Antennas and Propagation (EuCAP)*, April 2010, pp. 1–3.
 - [175] F. Merli, B. Fuchs, J. Mosig, and A. Skrivervik, "The Effect of Insulating Layers on the Performance of Implanted Antennas," *IEEE Transactions on Antennas and Propagation*, vol. 59, no. 1, pp. 21–31, Jan 2011.
 - [176] T. Tuovinen, M. Berg, K. Yazdandoost, E. Salonen, and J. Iinatti, "Reactive near-field region radiation of planar UWB antennas close to a dispersive tissue model," in *Loughborough Antennas and Propagation Conference (LAPC)*, Nov 2012, pp. 1–4.
 - [177] X. L. Chen, "Computational Analysis and Methods for Electromagnetic Exposure Limits, Antenna Optimization and Cell Phone Design," Ph.D. dissertation, Swiss Federal Institute of Technology, Lausanne, Switzerland, 2013.
 - [178] J. C. Lin, *Electromagnetic Fields in Biological Systems*, 1st ed. Taylor & Francis Group, 2011, p. 458.

Bibliography

- [179] Carlborg, Carl Fredrik and Haraldsson, Tommy and Öberg, Kim and Malkoch, Michael and van der Wijngaart, Wouter, "Beyond PDMS : off-stoichiometry thiol-ene (OSTE) based soft lithography for rapid prototyping of microfluidic devices," *Lab on a Chip*, vol. 11, no. 18, pp. 3136–3147, 2011.
- [180] D. Panescu, "Emerging Technologies [wireless communication systems for implantable medical devices]," *IEEE Engineering in Medicine and Biology Magazine*, vol. 27, no. 2, pp. 96–101, March 2008.

Jovanche Trajkovikj

*Electronics and Telecommunication
Engineer*

Rue du Simplon 35, Lausanne
1006, Switzerland

+41 (0)774058765

✉ jovance.trajkovic@gmail.com

Nationality: Serbian

Date of birth: 20.01.1984



Education

03/2011 **PhD at the Laboratory of Electromagnetics and Acoustics (LEMA),**
05/2015 *EPFL*, Lausanne, Switzerland..

- Design and realization of wearable antennas intended for security applications
- Collaboration in a Nano-Tera project on a study and design of implantable antennas intended for telemetry applications

09/2009 **Graduate Engineer of Electrical Engineering and Computer Science -**
07/2010 **Master, FTN**, Novi Sad, Serbia.

Applied Electronics.

Master thesis in Passive Microwave Circuits in CMOS Technology.

09/2002 **Graduate Engineer of Electrical Engineering and Information Tech-**
01/2007 **nologies, FEIT**, Skopje, Macedonia.

Electronics, Communication theory and Telecommunications.

Professional experiences

08/2003 **Service departments in tourism, I spent seven seasons around Greek islands,**
08/2010 *working all the time in tourism business, food & beverages and sales.*, Corfu,
Rhodes, Skiathos, Crete, Greece.

Professional Trainings and Courses

03/2011 **Antenna Project Management, European School of Antennas, EPFL, Lau-**
sanne, Switzerland.

06/2011 **Body Area Wireless sensoR nEtnetwork (B-AWaRE) Summer School,**
École Polytechnique Fédérale de Lausanne, EPFL, Lausanne, Switzerland.

04/2012 **Ultra Wideband Antennas, European School of Antennas, KIT, Karlsruhe,**
Germany.

02/2014 **Venture lab entrepreneurship course - the essentials on the creation of**
06/2014 **a start up, venturElab**, College of Management of Technology - EPFL, Lausanne,
Switzerland.

———— Languages

Serbian	Native language
Macedonian	Native language
English	Fluent
French	Intermediate
Greek	Intermediate
Russian	Intermediate
German	Basic

———— Social skills and competences

<i>Teamwork</i>	Wide experience in coordination and teamwork acquired as a member of different research and working teams and student associations.
<i>Mediating skills</i>	Oral presentations in academic conferences and to industrial partners were common activities during my research period.

———— Organizational skills and competences

- Experience in planning and organizing international events at university level.

———— Computer skills and competences

- Fully competent in full-wave electromagnetic solvers Ansys HFSS and CST Microwave Studio.
- Knowledge of Matlab, Solidworks, L^AT_EX.

———— Hobbies

- Various sport activities: football, basketball, volleyball, skiing, etc.
- Reading, interested in politics and economy, **The Economist** preferred magazine.

List of Publications

Refereed Journal Papers

- [J01] **J. Trajkovikj**, J.-F. Zürcher and A. K. Skrivervik, "PDMS, A Robust Casing for Flexible W-BAN Antennas [EurAAP Corner]", *IEEE Antennas and Propagation Magazine*, vol. 55, no. 5, pp. 287-297, October 2013.
- [J02] **J. Trajkovikj** and A. K. Skrivervik, "Diminishing SAR for Wearable UHF Antennas", *IEEE Antennas and Wireless Propagation Letters*, vol. PP, no. 99, pp. 1-4, December 2014.

Refereed International Conference Papers

- [C01] B. Ivsic, J. Bartolic, D. Bonefacic, A. K. Skrivervik and **J. Trajkovikj**, "Design and analysis of planar UHF wearable antenna", *Proc. 6th European Conf. Antennas Propag. (EuCAP)*, Prague, Czech Republic, March 2012.
- [C02] **J. Trajkovikj**, J.-F. Zürcher and A.K. Skrivervik, "Soft and flexible antennas on permittivity adjustable PDMS substrates", *Proc. Loughborough Antennas and Propag. Conf. (LAPC)*, Loughborough, UK, November 2012.
- [C03] D. D. Cara, **J. Trajkovikj**, R. Torres-Sanchez, J.-F. Zürcher and A.K. Skrivervik, "A low profile UWB antenna for wearable applications: The tripod kettle antenna (TKA)", *Proc. 7th European Conf. Antennas Propag. (EuCAP)*, pp. 3257-3260, Gothenburg, Sweden, April 2013.
- [C04] A.K. Skrivervik and **J. Trajkovikj**, "Some considerations on wearable antennas", *21st Int. Conf. on Applied Electromag. and Commun. (ICECom)*, Dubrovnik, Croatia, October 2013.

List of Publications

- [C05] **J. Trajkovikj**, J.-F. Zürcher and A.K. Skrivervik, "PDMS, a safe shelter for flexible W-BAN antennas", *Proc. 8th German Microwave Conference (GeMiC)*, Aachen, Germany, March 2014.
- [C06] **J. Trajkovikj**, "Robust and Flexible Antennas: Good Candidates for Wearable Applications", *11th Int. Conf. on Wearable and Implantable Body Sensor Networks*, Zurich, Switzerland, June 2014. (**Best Doctoral Colloquium Paper Award**)
- [C07] **J. Trajkovikj**, J.-F. Zürcher and A.K. Skrivervik, "Soft and flexible UHF antennas for W-BAN applications", *Proc. IEEE Antennas Propag. Society Int. Symp. (APSURSI)*, pp. 305-306, Memphis, Tennessee, US, July 2014.
- [C08] A.K. Skrivervik, D. D. Cara, **J. Trajkovikj** and J.-F. Zürcher, "Compact UWB antennas for Wireless Body Area Networks (W-BANs)", *IEEE-APS Topical Conf. on Antennas and Propag. in Wireless Commun. (APWC)*, pp. 125-128, Palm Beach, Aruba, August 2014.
- [C09] **J. Trajkovikj**, J.-F. Zürcher and A.K. Skrivervik, "Performance of UHF W-BAN antennas in a real environment scenario", *Proc. Loughborough Antennas and Propag. Conf. (LAPC)*, pp. 18-21, Loughborough, UK, November 2014. (**First prize for the IET Antennas and Propagation Network, "Best Student Paper"**)
- [C10] **J. Trajkovikj**, T. Debogovic and A.K. Skrivervik, "UHF W-BAN Antennas Operating in Indoor and Outdoor Environment", *Proc. 9th European Conf. Antennas Propag. (EuCAP)*, pp., Lisbon, Portugal, April 2015. (*Accepted*)
- [C11] A.K. Skrivervik, **J. Trajkovikj**, M. Koohestani and N. Pires, "Considerations on SAR and Efficiency for W-BAN Antennas", *Proc. 9th European Conf. Antennas Propag. (EuCAP)*, pp., Lisbon, Portugal, April 2015. (*Accepted*)

Workshop Presentations

- [WS01] **J. Trajkovikj**, J.-F. Zürcher and A.K. Skrivervik, "Soft & Flexible Antennas: Good Candidates for Wearable Applications", *Joint COST IC1004/VISTA Meeting*, Ghent, Belgium, September 2013. (**VISTA ESR best presentation award**)